

The sorption characteristics of inorganic and organic compounds found in hydraulic fracturing
flowback and produced water: Implications for fate and transport

by

Sean Philip Funk

A thesis submitted in partial fulfillment of the requirements for the degree of

Doctor of Philosophy

Department of Earth and Atmospheric Sciences
University of Alberta

© Sean Philip Funk, 2019

Abstract

In recent years, due to increasing energy demands, hydraulic fracturing operations for recovering unconventional hydrocarbon resources has increased. Wastewater recovered is referred to as flowback and produced water (FPW), and is often saline, contains numerous organic and inorganic constituents, and may pose threats to groundwater resources. Hundreds of spills of FPW have been reported to the Alberta Energy Regulator each year. As such, the environmental risk that FPW may pose to shallow groundwater environments has emerged as a major concern in several jurisdictions. Recently, samples of FPW derived from hydraulic fracturing of the Duvernay Formation, near the Fox Creek, AB region, were characterized and found to contain a previously unidentified class of aryl phosphates (including diphenyl phosphate (DPP), triphenyl phosphate (TPP), among others). As an emerging contaminant in soil and groundwater systems, as well as being potentially harmful to aquatic ecosystems, it is important to determine the environmental fate of these aryl phosphates if spilled in near-surface environments. Batch sorption experiments and bioassay toxicological studies were conducted on DPP, with the aim of determining: 1) the sorption behavior of DPP onto various surficial sediments collected within the Fox Creek, AB region; and 2) the toxicity of DPP toward aquatic ecosystems. We report that the sorption of DPP onto both clay-rich soils and sandy sediment was low compared to that of other aryl phosphates, with an average $\log K_{OC}$ value of 2.30 ± 0.42 (1σ). Therefore, the transport of DPP in groundwater would be rapid due to its low degree of sorption on surficial materials. We also determined the acute 96 h-LC₅₀ of DPP on zebrafish embryos to be 50.0 ± 7.1 mg/L. From the results of our study, we infer that DPP may pose an environmental risk to aquatic ecosystems if released into the environment.

FPW is a highly complex fluid, containing numerous inorganic and organic constituents. Contaminants within this complex fluid may interact with each other, either synergistically or antagonistically, resulting in varied sorption behavior. Groundwater flow may also have an influence on how these contaminants sorb onto porous media. To quantify these impacts, batch and column experiments were conducted using FPW collected from hydraulic fracturing operations in the Duvernay Formation with soils collected from Fox Creek, AB. In our batch experiments, we found that for many of the dissolved inorganics (e.g. Sr, Cu, Ni), sorption was depressed relative to published literature values, likely a result of competition with other constituents within the fluid and the high ionic strength of the FPW. Differential sorption of polyethylene glycols (PEGs) was observed, with sorption increasing with increasing ethylene oxide numbers. Column experiments were also conducted to address how groundwater flow may influence sorption. Some dissolved inorganic constituents (e.g. Sr, Li, B) and PEGs were observed to exhibit depressed sorption compared to the batch experiments. We argue that sorption is non-instantaneous, characterized by two stages: a fast adsorption phase onto external sorption sites, followed by a slow absorption phase into internal sorption sites. Flow likely negated the latter process. However, the heavy metals (e.g. Cu) were observed to exhibit enhanced retention in the presence of flow. We argue that because the column experiments were conducted under anaerobic conditions, precipitation of heavy metal-bearing solids (possibly sulphides) may have acted to sequester these elements.

Modeling how contaminants are transported in the subsurface is a major problem that faces many hydrogeologists. To aid with this, we developed HYDROSCAPE, a MATLAB[®]-based software program that uses an analytical solution to the advection-dispersion equation to solve solute transport problems. The solution is heuristically modified in two important, novel

ways, allowing the user to: 1) customize the source region; and 2) implement horizontal geological units within the domain (“simple geology”). Using HYDROSCAPE, three simple spill scenarios were simulated. The first two scenarios involved the introduction of FPW into an alluvial aquifer, the first with a source that is active for only 96 h, the second with a source that is continuous. The third scenario involved the downward percolation of FPW through an organic-rich, clay-rich soil horizon. Our results demonstrate the importance of considering source region history, the impact groundwater flow has on contaminant residence time, and how co-contaminant interactions affect the arrival order of contaminants in the subsurface.

Preface

Some of the research conducted in this thesis forms part of a research collaboration, led by Dr. Daniel Alessi at the Department of Earth & Atmospheric Sciences, University of Alberta, with Dr. Jonathan Martin at the Department of Environmental Science and Analytical Chemistry, Stockholm University, Dr. Greg Goss at the Department of Biological Sciences, University of Alberta, and Dr. Nicolas Utting at CanmetENERGY, Natural Resources Canada being the lead collaborators. The experiments in **Chapters 2 and 3** were designed and conducted by myself. Analytical work in **Chapter 2** was conducted by L. Duffin, C. McMullen, C. Sun, and A. Harms, whereas toxicological bioassays were conducted by Y. He. Analytical work in **Chapter 3** was conducted by C. Sun and K. Snihur. XRD results were conducted by D. Caird; other soil analyses were conducted by C. McMullen and K. von Gunten. The computer program described in **Chapter 4** was designed by both myself and D. Hnatyshin. Derivation of the mathematical framework was by me, whereas much of the graphical user interface was designed by D. Hnatyshin. Simulations run in **Chapter 4** were my original work, as well as the literature review in **Chapter 1**.

Chapter 2 of this thesis has been published as Funk S, Duffin L, He Y, McMullen C, Sun C, Utting N, Martin JW, Goss GG, Alessi DS (2019) Assessment of impacts of diphenyl phosphate on groundwater and near-surface environments: Sorption and toxicity. *Journal of Contaminant Hydrology* **221**: 50 – 57. I was responsible for designing and conducting the experiments and contributed to the interpretations and writing of the manuscript. D.S. Alessi was the supervisory author, contributing manuscript edits, with N. Utting, J.W. Martin, and G.G. Goss also contributing manuscript edits.

Chapter 4 of this thesis has been published as Funk S, Hnatyshin D, Alessi DS (2017)

HYDROSCAPE: A new versatile software program for evaluating contaminant transport in groundwater. *SoftwareX* **6**: 261 – 266. I was responsible for concept formation, mathematical derivation, running of simulations, and writing of the manuscript. D.S. Alessi was the supervisory author, contributing manuscript edits. D. Hnatyshin also contributed manuscript edits.

To my parents, Paul and Doris, and my fiancée, Rebecca

Acknowledgements

I would like to thank Dr. Daniel Alessi, my supervisor, for his guidance, support, insight, and funding he provided through his Natural Science and Engineering Research Council of Canada (NSERC) Discovery Grant. He afforded me many opportunities to demonstrate my work at conferences, and more importantly, to meet and talk to others working in hydrogeology and environmental sciences. These experiences, as well as the lessons taught, were invaluable in the pursuit of a career in environmental sciences and are much appreciated. I have experienced many unique things during my degree and have many memories from this time in my life that will be cherished for a lifetime. I would also like to thank Dr. Carl Mendoza and Dr. Ben Rostron for being on my supervisory committee, for their guidance, and for many helpful discussions that resulted in a stronger dissertation. Many others also invested their time and efforts into the furtherment of my career, including my former Master's supervisor, Dr. Robert Luth, and my former Bachelor's supervisor, Dr. Thomas Chacko. Early in my degree, I approached both when I was at a crossroads, switching fields, and without their support and guidance, I would not be where I am now. For that, I am grateful. Lastly, I would like to extend my appreciation and gratitude to my fellow graduate students, Danny Hnatyshin, Dan Skoreyko, Judit Deri-Takacs, Konstantin Von Gunten, Md Samrat Alam, Katherine Snihur, Pamela Twerdy, among many others, as well as former post-doctorate students, Shannon Flynn and Max Lukenbach, for their support.

I am grateful for the additional financial support I received over the course of my degree, including an NSERC Postgraduate Scholarship, Queen Elizabeth II Scholarships, and President's Doctoral Prizes of Distinctions granted to me, along with numerous teaching and research assistantships over the years. This support allowed me to concentrate on my studies and my

research without worries from external factors. That contribution was huge, and most appreciated.

Table of Contents

Chapter 1 – Introduction	1
1.1. Hydraulic Fracturing.....	1
1.2. Hydraulic Fracturing in the Duvernay Formation	3
1.3. Toxicity of FPW on aquatic ecosystems	7
1.4. Mechanisms for Soil Retention	9
1.5. Limitations of the K_d model	12
1.6. Background, Aims, and Goals for this Study	14
References	19
Chapter 2 – Assessment of impacts of diphenyl phosphate on groundwater and near-surface environments: Sorption and toxicity	29
2.1. Introduction.....	29
2.2. Materials	31
2.2.1. Aqueous Solutions.....	31
2.2.2. Sediments.....	32
2.3. Methods.....	33
2.3.1. Experimental Methods	33
2.3.1.1. Batch Sorption Experiments.....	33
2.3.1.2. Zebrafish Embryo Toxicity Assays	33
2.3.2. Analytical Methods	34
2.3.2.1. Soil Analyses	34
2.3.2.2. Solution Analyses:	35
2.4. Results & Discussion.....	36
2.4.1. Sorption behavior of DPP	36
2.4.2. Groundwater Transport.....	42
2.4.3. Toxicity of DPP	44
2.5. Summary & Conclusions.....	48
Acknowledgements	49
References	49
Chapter 3 – The sorption characteristics of metals, metalloids, and organic compounds in hydraulic fracturing flowback and produced water	57

3.1. Introduction	57
3.2 Materials	61
3.2.1 Aqueous Solutions	61
3.2.2 Sediments	64
3.3 Methods	66
3.3.1 Experimental Methods	66
3.3.1.1 Batch Sorption Experiments	66
3.3.1.2 Column Transport Experiments	66
3.3.2 Analytical Methods	68
3.3.2.1 Soil Analyses	68
3.3.2.1 Solution Analyses	70
3.4 Results & Discussion	71
3.4.1 Batch sorption of inorganic components	71
3.4.1.1 Strontium	74
3.4.1.2 Boron	78
3.4.1.3 Lithium	81
3.4.1.4 Barium	81
3.4.1.5 Nickel and Copper	82
3.4.2 Batch sorption of organic components	85
3.4.3 Column sorption of inorganic components	89
3.4.3.1 Strontium, lithium, boron, sodium, and potassium	90
3.4.3.2 Calcium, magnesium, manganese, and barium	92
3.4.3.3 Trace metals	94
3.4.4 Column sorption of organic components	98
3.5 Summary & Conclusions	100
Acknowledgements	103
References	103
Chapter 4 – HYDROSCAPE: A new versatile software program for evaluating contaminant transport in groundwater	119
4.1. Introduction	119
4.2. Comparison with Related Programs	120

4.3. HYDROSCAPE Architecture	122
4.4. Implementation	124
4.4.1. Advanced Features	124
4.4.1.1. User-Defined Sources	125
4.4.1.2. Simple Geology	127
4.4.2. Parameter Estimation and Sensitivity Analysis	127
4.5. Comparison with Numerical Simulations	129
4.6. Transport of FPW contaminants	133
4.7. Conclusions	141
Acknowledgements	148
References	148
Chapter 5 – Conclusions & Future Directions	153
5.1. Conclusions	153
5.2. Future Directions	158
References	163
Appendix A	169
Appendix B	189
Appendix C	215

List of Tables:

Table 2.1: Tabulated values for K_d and $\log K_{OC}$ for each sediment type at each pH condition...	41
Table 2.2: List of minimum, median and maximum retardation factors (R) for DPP, and TPP..	44
Table 2.3: 96 h-LC ₅₀ (mg/L) values for various aryl phosphate compounds on various fish species.	47
Table 3.1: Table of chemical analyses for FPW samples 1 and 2.....	63
Table 3.2: Elemental composition of the three different soil types used in this study.....	65
Table 3.3: Exchangeable cations, acidity and total CEC in cmol charge per kg dry sample (equal to cmol(+)/kg).	65
Table 3.4: Porosity and dry bulk density of FLUV in column A and B.	66
Table 3.5: Linear K_d (L/kg) values for each corresponding sediment type used in this study, for each element analyzed.	73
Table 3.6: Freundlich and Langmuir parameters for Sr for Samples 1 and 2, including R^2 values of fit.....	73
Table 3.7: Linear K_d (L/kg) values for PEGs for the three tested soil types for FPW Sample 1.	88
Table 3.8: Retardation factors (R) and effective distribution coefficients (K_d') for select metals, for both columns A and B.	92
Table 3.9: Retardation factors (R) and the calculated effective linear distribution coefficients (K_d') for the PEGs in the column experiments.....	100
Table 4.1: List of commonly used notation and symbols, along with their units, for the three-dimensional advection-dispersion equation (ADE).	143
Table 4.2: Comparison of some key features of HYDROSCAPE to other programs that use analytical solutions to the ADE.	144
Table 4.3: The list of the parameters that can be estimated in HYDROSCAPE.	145
Table 4.4: List of inputs for each patch source	146
Table 4.5: List of parameters used in HYDROSCAPE (“HYD”) and MODFLOW (“MOD”) simulations.	146
Table 4.6: List of model parameters for both the 1D and 3D (pseudo-2D) simulations.....	147

List of Figures:

Figure 1.1: A map of the areal extent of the Duvernay Formation within Alberta, Canada.....	6
Figure 1.2: Schematic cross-section showing the informal Duvernay lithostratigraphic units as defined by the Alberta Energy Regulator (AER).	6
Figure 2.1: Partitioning coefficients (K_d) vs. pH for A) moraine; B) glaciolacustrine clay; C) stagnant moraine; D) HFO-coated sand; and E) fluvial sand.	40
Figure 2.2: Zebrafish (ZF) embryo survival (%) vs. concentration of DPP (mg/L).	47

Figure 3.1: Sorption isotherms for A) strontium; B) boron; C) lithium, for MOR (blue), GLC (red), and FLUV (green).....	77
Figure 3.2: Linear sorption isotherms for A) PEG-6; B) PEG-7; C) PEG-9; and D) PEG-11....	89
Figure 3.3: Breakthrough curves of some inorganics for A) column A; and B) column B.....	92
Figure 3.4: Breakthrough curves of some inorganics for A) column A; and B) column B.....	94
Figure 3.5: Breakthrough curves of some heavy metals for A) Ni (purple) and Cu (blue) for column A; B) Ni (purple) and Cu (blue) for column B; and C) Zn for column A (black) and B (grey).....	97
Figure 3.6: Breakthrough curves of PEGs for A) column A; and B) column B.....	100
Figure 4.1: HYDROSCAPE’s graphical user interface (GUI) showcasing a user-defined source region and simple geology (left side) with a Google Maps™ output (right side).....	124
Figure 4.2: Schematic diagram illustrating how HYDROSCAPE constructs a source region of arbitrary shape and arbitrary concentration distribution.....	126
Figure 4.3: Schematic diagram illustrating how HYDROSCAPE implements simple geology.....	127
Figure 4.4: A) Source region geometry and concentration distribution. Inputs for the source regions are given in Table 4.4. B) The source function used.	131
Figure 4.5: Comparison of HYDROSCAPE (top) and MODFLOW (bottom) in cross-section through the centerline after A) 3 years; B) 6 years; and C) 10 years.	132
Figure 4.6: Comparison of breakthrough curves; A) within the aquitard screened at a depth of 2.5 m; B) within the aquifer screened at 52.5 m.....	133
Figure 4.7: Comparison of breakthrough curves for discrete 3-D simulations taken 50 m away through fluvial sediment from the source with Cl (green), Sr (blue), Cu (orange), PEG-6 (grey), and PEG-11 (yellow) using K_d values from: A) column experiments; B) batch experiments; and C) literature values.....	139
Figure 4.8: Comparison of breakthrough curves for 3-D simulations taken 200 m away through fluvial sediment from the source with Cl (green), Sr (blue), Cu (orange), PEG-6 (grey), and PEG-11 (yellow) using K_d values from: A) column experiments; B) batch experiments; and C) literature values.....	140
Figure 4.9: Comparison of breakthrough curves for 1-D simulations taken 5 m down through moraine soil with Cl (green), Sr (blue), DPP (purples), and PEGs (yellows). Light and dark variations of colors denote a range of K_d values used in the simulations; shaded area represents the time window whereby the compound may breakthrough. K_d values taken from batch experiments. Simulations: A) using an $\alpha_L = 5$ m; and B) using an $\alpha_L = 0.5$ m.....	141

List of Symbols & Abbreviations:

\sim	Approximately
\approx	Approximately equal to
\neq	Not equal to
$<$	Less than
\leq	Less than, or equal to
$>$	Greater than
\geq	Greater than, or equal to
\pm	Plus, or minus
∂	Partial derivative
∇h	Hydraulic gradient
α_L	Longitudinal dispersivity
α_{TH}	Transverse horizontal dispersivity
α_{TV}	Transverse vertical dispersivity
λ	First-order decay constant
ρ_b	Dry bulk density
σ	Standard deviation
θ	Theta
Φ	Porosity
τ	Tortuosity
2-BE	2-butoxyethanol

A	Cross-sectional area
ADE	Advection-dispersion equation
AE	Alcohol ethoxylates
AEO	Alkyl ethoxylates
BAC	Benzalkonium chlorides
BCF	Bioconcentration factor
C	Concentration
C_0	Source concentration
CEC	Cation exchange capacity
CDP	Cresyl diphenyl phosphate
ChV	Chronic value
CID	Collision-induced dissociation
C_s	Solid concentration
D^*	Effective diffusion coefficient
D_0	Free-solution diffusion coefficient
DEM	Digital elevation map
D_L	Longitudinal dispersion coefficient
DPP	Diphenyl phosphate
D_{TH}	Transverse horizontal dispersion coefficient
D_{TV}	Transverse vertical dispersion coefficient
EHDP	2-ethylhexyl diphenyl phosphate

EO	Ethylene oxide
EROD	Ethoxyresorufin-O-deethylase
ESI	Electrospray ionization
exp	Exponential
f _{OC}	Organic carbon fraction
FLUV	Fluvial sand
FPW	Flowback and produced water
GA	Glutaraldehyde
GAC	Granulated activated carbon
GLC	Glaciolacustrine clay
GUI	Graphical user interface
H	Source thickness
HAO	Hydrous aluminum oxide
HCD	Higher-energy collision dissociation
HFF	Hydraulic fracturing fluid
HFO	Hydrous ferrous oxide
HPLC	High-performance liquid chromatography
IC	Inorganic carbon
ICP-MS/MS	Inductively coupled plasma-tandem mass spectrometry
IDDP	Isodecyl diphenyl phosphate
IPDP	Isopropylphenyl diphenyl phosphate

K	Hydraulic conductivity
K_d	Distribution coefficient
K_d'	Effective distribution coefficient
K_F	Freundlich coefficient
K_{OC}	Organic carbon partitioning coefficient
K_{OW}	Octanol-water partitioning coefficient
k_s	Source decay constant
LC_{50}	Half lethal concentration
$L(t - t_0)$	Logistic function
MCI	Molecular connectivity index
MD	Measured depth
MOR	Moraine
MRM	Multiple reaction monitoring
MS/MS	Tandem mass spectrometry
n	Porosity
n	Freundlich exponent
NORMs	Naturally occurring radioactive materials
NPOC	Non-purgeable organic carbon
PAH	Polycyclic aromatic hydrocarbons
PAM	Polyacrylamide
PEG	Polyethylene glycols

Pe _x	Peclet number
POC	Purgeable organic carbon
PV	Pore volume
PZC	Point of zero charge
Q	Volumetric flow rate or volumetric flux
R	Retardation factor
R ²	Coefficient of determination
SOM	Soil organic matter
SPE	Solid phase extraction
STGM	Stagnant moraine
Sw	Water solubility limit
TBDP	Tertbutylphenyl diphenyl phosphate
TC	Total carbon
Tcf	Trillion cubic feet
TDS	Total dissolved solids
TN	Total nitrogen
TOC	Total organic carbon
TP	Total phosphorous
TPP	Triphenyl phosphate
TVD	Total vertical depth
UFD	Upstream finite difference

v Average linear groundwater velocity

W Source width

XRD X-ray Diffraction

Chapter 1 – Introduction

1.1. Hydraulic Fracturing

In recent years, due to increasing energy demands, combined hydraulic fracturing and horizontal drilling techniques for unconventional hydrocarbon resources have increased (Vengosh et al. 2013; Rivard et al. 2014). Hydraulic fracturing is a stimulation or enhancement process targeted at tight geological formations (e.g. shales, siltstones, etc.) whereby hydraulic fracturing fluid (HFF), an engineered fluid that is typically comprised of 90 to 97% fluid (typically water, by volume), ~2-10% proppants (by volume), and up to 2% chemical additives, is injected into a well at pressures sufficient enough to fracture, or stimulate, the hydrocarbon producing formation (Vidic et al. 2013; US EPA 2016). Shut-in or “soak times” vary between wells, and allow for HFF to imbibe the tight rock, releasing the trapped hydrocarbons (King 2012). The proppants, often composed of quartz sand or ceramic beads, are used to “prop open” the fractures, allowing hydrocarbons from the formation to flow freely into the wellbore (Brannon and Pearson 2007; Gupta and Valko 2007; Hyne 2012). Although the chemical additives in HFF make up only a small fraction of the fluid itself, it may still comprise of tens of thousands of liters of the injected volume for some wells (Sjolander et al. 2011; US EPA 2015). These additives include a variety of chemicals engineered to improve the performance of a fracturing job, such as friction reducers, gelling agents, biocides, surfactants, among others (Carter et al. 2013; Rogers et al. 2015).

Wastewater recovered is referred to as flowback and produced water (FPW), and is often brackish to briny, contains numerous organic compounds (including hydrocarbons and others from the formation), inorganic constituents (metals, metalloids), naturally occurring radioactive

materials (NORMs), and the chemical additives injected as well as their reaction, degradation, or breakdown products (Colborn et al. 2011 Warner et al. 2012, 2014; Drollette et al. 2015; DiGiulio and Jackson 2016; Alessi et al. 2017; He et al. 2017b). Typically, flowback water refers to the fluid produced immediately after opening the well, and is dominated by returned HFF, but before the well starts producing significant quantities of hydrocarbons; produced water is defined as the fluid produced in conjunction with hydrocarbons (US EPA 2015). For the purposes of our research, because these definitions are somewhat arbitrary, we consider both to be essentially wastewater, and make no distinction between them. In Alberta, FPW from the Duvernay Formation is often stored on-site in large storage tanks, after which the vast majority of the wastewater is transported to deep-well injection sites for disposal via tanker trucks (Alessi et al. 2017). However, some (e.g. Encana Corporation 2013) have adopted the practice of recycling some of their wastewater in an attempt to reduce their dependence on freshwater resources. In the United States, disposal practices are many and varied, depending on the jurisdiction, and can include underground injection (US GAO 2012), reuse for subsequent fracturing operations (Gregory et al. 2011; Rassenfoss 2011; Boschee 2012, 2014), treatment at either a central wastewater treatment facility or at publicly owned treatment works (Lutz et al. 2013; Easton 2014; PA DEP 2015), land application such as irrigation of agricultural land or road spreading (Hammer and VanBriesen 2012; Tiemann et al. 2014), or held within lined pits for evaporation (Clark and Veil 2009; CDOC 2015). Recently, the environmental risk that FPW may pose to shallow groundwater environments and surface water bodies has emerged as a major concern in several jurisdictions (Llewellyn et al. 2015; Gehman et al. 2016). Due to the complexity of the chemicals added to the injected HFF, and the potential for downhole reaction by-products to be

produced during stimulation, evaluating the potential risks that FPW may pose on the near-surface environment is challenging.

1.2. Hydraulic Fracturing in the Duvernay Formation

To begin to assess the risks that FPW spills may pose to near-surface environments, such as shallow groundwater resources, we studied samples of FPW collected from hydraulic fracturing operations conducted in the Duvernay Formation. The FPW samples were collected from wells in the Fox Creek area, solely within the Duvernay Formation (**Figure 1.1**). The Duvernay Formation is of upper Devonian age, approximately 372 Ma (Rokosh et al. 2012), located within the province of Alberta (near the provincial border between British Columbia and Alberta), covering an estimated area of approximately 130,000 km² (roughly 20% of the area of the province) (Preston et al. 2016). The depth to the Duvernay Formation from the surface varies from approximately 1,000 m towards the eastern edge of the formation, down to approximately 5,500 m at the western border (Rokosh et al. 2012), a depth that is considerably more than most other shale targets found within the Western Canadian Sedimentary Basin (WCSB). The lithology of the Duvernay Formation is variable across the unit. Towards the east, the lithology is dominated by an organic-rich lime-mudstone (i.e. limestone), transitioning towards a less calcareous and more shale-rich lithology towards the west (Rokosh et al. 2012). The Alberta Energy Regulator (AER) breaks the Duvernay Formation into three informal lithostratigraphic members, simply defined as: A shale, B carbonate, C shale (**Figure 1.2**), reflecting this transition in lithology. For simplicity, this thesis will employ that nomenclature. The overall thickness of the Duvernay can range from as little as 2 m to as thick as 99 m, with the carbonate package ranging from 0 m to 66 m thick, and the combined shale thickness (i.e. A and C shale) ranging from 0 m to 62 m thick (Preston et al. 2016) (**Figure 1.2**).

Current estimates for the unconventional hydrocarbon resource found within the Duvernay is quite extensive. Shale-hosted natural gas in the Duvernay may range from 353 to 540 trillion cubic feet (Tcf) (Rokosh et al. 2012). Shale-hosted gas condensates have been estimated to be between approximately 7.5 billion barrels to as high as 16.3 billion barrels (Rokosh et al. 2012). Lastly, the estimated shale-hosted oil in the Duvernay is between 44 billion barrels and 82.9 billion barrels (Rokosh et al. 2012). In addition to being the primary focus for unconventional hydrocarbon development in Alberta, the Duvernay is also the source rock for much of the conventional hydrocarbons found in Alberta, including the famous Leduc reefs, but also those located in the Swan Hills formation, the Nisku and Grosmont carbonate platforms, as well as numerous other clastic reservoirs (e.g. Gilwood and Granite Wash sands) (Preston et al. 2016). Unlike other shale plays in Alberta, the Duvernay contains significant quantities of liquid hydrocarbons, including free condensate and oil. Thermal maturity also changes across the formation, increasing towards the west, corresponding with the increase in depth (Rokosh et al. 2012). This leads to a transition in the type of hydrocarbons present within the Duvernay itself. Towards the west, it is expected that a larger portion of the formation would be dry-gas generating, transitioning toward more condensate-dominated and oil generating rocks toward the eastern border (Rokosh et al. 2012).

As noted above, hydraulic fracturing operations in North America have seen rapid growth and development in the 21st century (Rivard et al. 2014). In the Duvernay, development and commencement of hydraulic fracturing operations combined with horizontal drilling and multistage fracturing started in 2011 and has steadily increased with each year thereafter (Preston et al. 2016). Hydraulic fracturing operations typically utilize local freshwater resources. Alessi et al. (2017) conducted a comprehensive comparative analysis of hydraulic fracturing-related

wastewater management and practices in four North American plays, including the Duvernay. They found that some companies with operations in the Duvernay Formation are aiming to reduce freshwater consumption by accessing alternative water sources, such as sourcing municipal wastewater and recycling hydraulic fracturing-derived wastewater. Alessi et al. (2017) further state that the extent to which those practices will be employed in the future is unclear, because access to freshwater remains inexpensive and convenient. According to CSUR (2013), anywhere from 10,000 to 60,000 m³ of water was used per well for hydraulic fracturing operations conducted within the Duvernay. However, the survey Alessi et al. (2017) conducted between November 2011 and March 2014 indicated that for most unconventional wells in the region, the average amount of water used was slightly less than 10,000 m³. Although wastewater handling, treatment and disposal practices for the Duvernay is not well documented, government regulation prevents produced water from being treated by municipal wastewater treatment plants (Rokosh et al. 2012). If this wastewater (flowback and produced water) is unable to be reused/recycled or treated, then it is normally disposed of in an approved disposal well, the fate for the majority of oil and gas wastewaters in western Canada (Rokosh et al. 2012; Rivard et al. 2014).

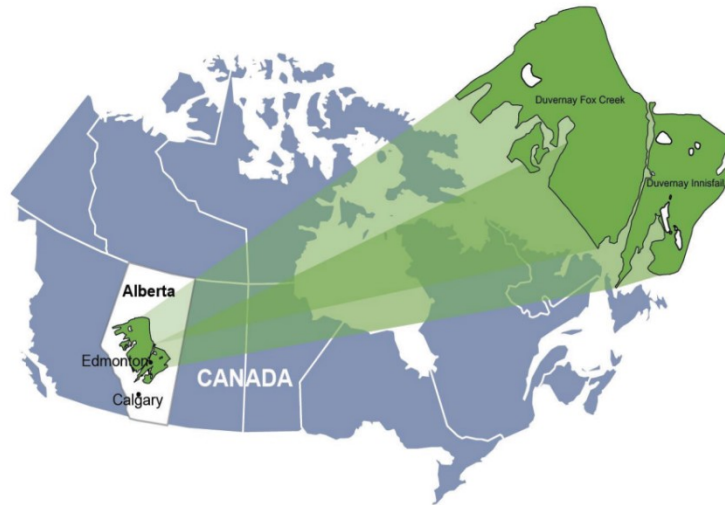


Figure 1.1: A map of the areal extent of the Duvernay Formation within Alberta, Canada. Figure from Preston et al. (2016). Permission to reproduce the figure given by the Alberta Energy Regulator (AER).

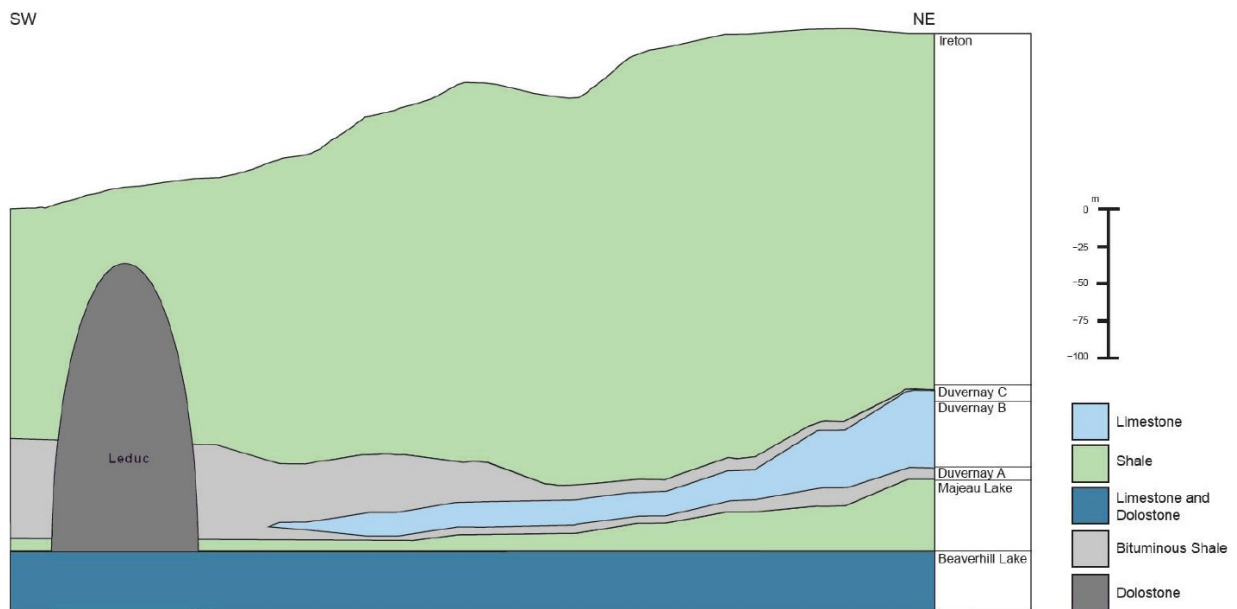


Figure 1.2: Schematic cross-section showing the informal Duvernay lithostratigraphic units as defined by the AER. Figure from Preston et al. (2016). Permission to reproduce the figure given by the AER.

1.3. Toxicity of FPW on aquatic ecosystems

The potential impact and toxicity of FPW derived from hydraulic fracturing operations conducted within the Duvernay Formation on aquatic ecosystems has been recently studied. These studies conducted exposures of representative fish and invertebrate aquatic species to FPW collected from the region to quantify the potential adverse effects that may have occurred. For example, He et al. (2017a) studied the biotransformation, oxidative stress, and potential endocrine disruption on rainbow trout exposed to Duvernay-derived FPW. They found that exposure to the FPW resulted in significant induction of EROD (ethoxyresorufin-O-deethylase) activity, a biomarker of chemical exposure in fish induced by compounds such as polycyclic aromatic hydrocarbons (PAHs), in both the liver and gills. They also detected an increased lipid peroxidation induced by oxidative stress. Using gene analyses, they also observed evidence of biotransformation, oxidative stress, and endocrine disruption. Similarly, Blewett et al. (2017b) studied the effects of FPW exposure to the gill morphology of rainbow trout. In their study, juvenile rainbow trout was exposed to FPW (2.5% or 7.5%) for 48 h. They found that gill morphology displayed a decrease in interlamellar cell mass and mean lamellar length, indicative of hyperosmotic stress.

Folkerts et al. (2017a) studied the cardiotoxic and respirometric disruption in zebrafish embryos exposed to FPW and found that those exposed to FPW between 24 and 72 h post-fertilization showed an increased frequency of pericardial edema, yolk-sac edema, and tail-spine curvature. They also observed that select cardiac genes were significantly altered, suggesting that the cardiovascular systems in the embryos were compromised, resulting in a reduction in embryonic respiration/ metabolic rates (MO_2). They concluded that organics found within the

tested FPW significantly contributed to the cardiac and respiratory responses found in the zebrafish embryos. Folkerts et al. (2017b) further studied the swim performance on juvenile zebrafish after acute exposure to FPW. In their study, zebrafish embryos (24 h post-fertilization) were exposed to either 2.5% or 5% FPW solutions for either 24 or 48 h, and then returned to freshwater. Any surviving embryos were then placed in freshwater and allowed to grow for up to 60 d (juvenile phase). The fish exposed to FPW showed a marked decrease in swim performance when compared to the controls. Similar to the study with embryos, the authors suggest that the organics found in the FPW were largely responsible for these significant negative effects on the zebrafish swim performance. These studies on both rainbow trout and zebrafish strongly suggest that exposure, both acute and chronic, to FPW have adverse effects on fish species and have the potential to negatively impact aquatic ecosystems.

Water fleas, *Daphnia magna*, are small crustaceans/arthropods that can be found in many freshwater lakes and shallow ponds and play an important role in aquatic ecosystems (Lari et al. 2016), and as such, are commonly used as model invertebrates in many ecotoxicological studies (OECD 2008; Tatarazako and Oda 2007). Blewett et al. (2017a) studied the sublethal and reproductive effects of both acute and chronic exposure to FPW on daphnia, monitoring the total neonates produced and the average number of neonates produced per daphnid, and found that chronic (21 d) exposure to the FPW resulted in a significant decrease in brood size and neonates per daphnid when compared to the controls. They also found that neonates were more susceptible than full grown adults, with an acute (48 h) half lethal concentration (LC₅₀) of 0.19% of the undiluted FPW, as compared to 0.75% for adults. Ultimately, they concluded that FPW could significantly negatively impact freshwater crustaceans in aquatic ecosystems.

These studies, taken together, strongly suggest that FPW has the potential to negatively impact aquatic ecosystems if accidentally released into the environment, specifically surface water bodies. The data support the organic fraction contained within the FPW to be a significant contributing factor in these adverse effects (Folkerts et al. 2017a, b; He et al. 2017a), although the high salinity is also a contributing factor. Because FPW has the potential to impact aquatic ecosystems, understanding the transport of FPW through soil and saturated unconsolidated materials is critical to assessing the overall risk the FPW may have on the surrounding environment. Therefore, investigating the sorptive behavior of compounds found within FPW is critical in this evaluation.

1.4. Mechanisms for Soil Retention

A brief overview of the various mechanisms by which dissolved constituents may be retained by porous media will be presented. For a more detailed discussion on the various sorption mechanisms that influence metal mobility, refer to Smith (1997). There are several mechanisms by which contaminants, or more generally, dissolved constituents, in aqueous solution may be retained or sequestered by the solid medium (i.e. soil) that they pass through. Common soil constituents that are known to retain contaminants from solution include clay particles, organic matter, Fe- and Mn-oxides (or (oxy)hydroxides), carbonates, and to a lesser extent, other silicate minerals. Adsorption is a common mechanism whereby a dissolved constituent in aqueous solution adheres to the outside surface of the soil particles, either by a physical mechanism (e.g. electrostatic attraction), or by a chemical reaction (e.g. ligand exchange). Adsorption is therefore a surface phenomenon.

Adsorption may be described as specific or non-specific. Non-specific adsorption, sometimes referred to as outer-sphere complexation, refers to a mechanism whereby ions in

solution are surrounded by water molecules (due to their polarity; called a hydration sphere), and are attracted to the charged surfaces of the solid particles due to electrostatic attraction. Clay minerals, for example, have typically negative charges, either permanent due to isomorphous substitutions of elements within the crystal structure of the minerals themselves, or non-permanent caused by protonation-deprotonation reactions on the clay surface. The latter process results in a pH-dependance on the surface charge of the mineral surfaces. Cations, which have a net positive charge, are therefore generally attracted to the surface of clay minerals due to Coulombic electrostatic attraction. Some mineral surfaces may exhibit a net positive charge, which in turn could attract anions in solution. These types of reactions are generally known as ion exchange reactions and can either be cation exchange or anion exchange reactions, whereby a cation (or anion) is adsorbed onto the surface of the mineral, which subsequently releases cations (or anions) into solution. Typically, the ions released into solution are not of interest, but sometimes they are (e.g. if the released ions were heavy metals).

Specific sorption, sometimes referred to as inner-sphere complexation, refers to a mechanism whereby a constituent interacts with a specific functional group (i.e. site) on the mineral surface. Mechanisms by which specific sorption may occur can include ligand exchange and chemisorption. A ligand, generally, is any ion, molecule, or functional group in solution that has a central metal atom to form a coordination complex. These ligands may interact with other functional groups on the mineral surfaces, bonding to the surface, releasing other ligands into solution. Chemisorption is any adsorption process whereby retention is achieved through the formation of a chemical bond, usually covalent, between the molecule or compound and the surface of the solid medium. Some ligand exchange reactions are also chemisorption reactions.

Absorption differs from adsorption, as the dissolved constituent is either incorporated into the crystal structure of the mineral itself or is retained within internal sites within the soil particle. Intraparticle diffusion is a common mechanism by which absorption occurs. By its nature, absorption is generally a kinetically slower process compared to adsorption (e.g. van Beinum et al. 2005). Because of the difficult nature of separating the processes of adsorption and absorption, no distinction is usually made between them, and therefore an umbrella term, sorption, is used to describe both processes.

By its nature, many of the abovementioned processes are applicable to dissolved metals, which typically form cations or cation complexes in solution. Polar organic compounds may also be influenced by the same mechanisms outlined above. However, nonpolar organic compounds can also sorb onto solid surfaces. Generally, non-polar organic compounds cannot effectively bond with polar water molecules. As a result, minimizing the interfacial area between the non-polar organic compound and polar water would be considered thermodynamically favorable (Piwoni and Keeley 1990). Thus, the segregation of non-polar organics from water is known as the hydrophobic effect, or hydrophobic sorption. As organic matter is a common constituent in most soils, non-polar organic compounds dissolved in solution are attracted to these hydrophobic sites in the soil organic matter (SOM). This model suggests a strong correlation between sorption and the organic carbon fraction (f_{OC}) of the soil.

Although not typically incorporated into the definition of sorption, precipitation of insoluble solids is yet another mechanism for removal of contaminants from aqueous solution. Here, the more general term of soil retention will be used to describe all mechanisms, including sorption and precipitation, that act to remove contaminants from aqueous solution. Constituents within the solution may interact with each other and may form solid materials that are

insoluble. Precipitation reactions usually involve dissolved metals (e.g. heavy metals) but can also include organic compounds. Common insoluble materials include carbonates, sulphides, oxides, hydroxides, or oxyhydroxides. If said precipitates do not redissolve back into solution, these solid materials are therefore incorporated into the solid matrix itself.

Any or all these processes may occur simultaneously in the subsurface, and each act to reduce the mobility (i.e. enhance soil retention) of the dissolved constituents in aqueous solution, whether it be organic or inorganic. Understanding the magnitude as well as the mechanisms for which these constituents are retained within the subsurface is critical for evaluating their long-term transport potential, and potential re-release if environmental conditions change.

1.5. Limitations of the K_d model

A linear distribution coefficient (K_d ; sometimes referred to as a partitioning coefficient), is a common and simple mathematical model, defined as the ratio of the mass of solute sorbed per unit mass of sediment, to the mass of solute remaining in solution per unit volume of solution (equation 1.1).

$$K_d = \frac{c_s}{c} \quad (1.1)$$

where C_s is the solid concentration [M/M], and C is the aqueous concentration [M/L³].

K_d values for many inorganic and organic compounds are ubiquitous in the literature due to its simplicity and applicability (in terms of a retardation coefficient, R) in contaminant transport modeling. However, due to this simplicity, there are certain limitations to the applicability of the K_d model to real-world systems, and limitations when comparing K_d values to others published in the literature. Not all these limitations will be touched on in this section.

Inherent in the K_d model is the assumption that the solid material (i.e. the sorbent) has an infinite capacity to retain or sorb the solute of interest. This is unrealistic, as each particle of soil has both a finite surface area, and finite volume, and therefore, finite capacity to sorb the dissolved constituent. As such, at high concentrations, a plateau is often observed, and therefore, the simple linear model breaks down. Other mathematical models, such as the Freundlich or Langmuir models, may be employed instead in these cases (see **Appendix B**). The K_d model also assumes that equilibrium has been reached, and that the reaction is reversible. In dynamic, transient systems, such as those found in flowing groundwater systems, this assumption must be evaluated further. In cases where the kinetics of the sorption reaction are significantly faster than the residence time of the groundwater, a K_d model may be applicable. However, if the kinetics of sorption, such as when sorption is rate-limited, the K_d model may no longer be valid (Brusseau 1994).

K_d values are typically experimentally determined for either specific soils (e.g. Tehervand and Jalali 2017) or for individual soil components (e.g. Covelo et al. 2007). As such, K_d values can vary dramatically for a single constituent, sometimes by orders of magnitudes, and cannot be extrapolated beyond the tested range of concentrations or environmental conditions (e.g. pH, ionic strength, temperature, etc.) of the experiments. Comparisons of K_d values between differing soils must be done carefully, noting the influence of certain soil properties that may affect the magnitude of sorption, such as the grain size distribution, SOM content, the mineralogy, the percentage of clay minerals present, and presence of other minerals, such as carbonates or Fe- or Mn-oxides, among others. As such, although comparisons of K_d values from a number of experiments and publications are common, one must always consider the variables or mechanisms that influence the sorption process. If incorrectly applied, one could grossly

overestimate or underestimate the mobility of the dissolved constituent of interest, leading to erroneous results.

1.6. Background, Aims, and Goals for this Study

Since 2013, 830 incidents involving FPW were reported to AER (AER 2019), and similarly occur in other North American jurisdictions where fracturing occurs (US EPA 2015). Therefore, it is imperative that the potential impacts FPW spills have on the environment, including aquatic ecosystems, are characterized. This study is broken up into three distinct sections, each addressing a different facet of characterizing the potential environmental impact hydraulic fracturing-derived FPW may have in near-surface soil and groundwater environments. The first study (**Chapter 2**) aimed to characterize the sorption behavior and toxicity of diphenyl phosphate (DPP), an aryl phosphate contaminant identified in a sample of FPW from hydraulic fracturing of the Duvernay Formation. The second project (**Chapter 3**) aimed to characterize the sorption behavior of several dissolved inorganic species and major organic compounds found within the FPW samples collected from hydraulic fracturing operations near Fox Creek, AB. In both **Chapter 2 and Chapter 3**, surficial materials collected from around the Fox Creek area were used in both studies. The third project (**Chapter 4**) aimed to develop a new tool that hydrogeologists can use to evaluate contaminant transport in porous media. This new tool was developed to simulate simple transport scenarios quickly, such as those from FPW spills, among others. Using the results from **Chapter 2 and Chapter 3** as a guide, some FPW spill scenarios were simulated. These projects are briefly outlined below.

Chapter 2 focuses on the sorption of DPP onto a variety of surficial sediment found near the Fox Creek region. Recently, samples of FPW derived from fracturing the Duvernay Formation, AB, were found to contain a previously unidentified class of aryl phosphates

(including DPP, triphenyl phosphate (TPP), among others) (He et al. 2017b). Aryl phosphates are also used in a variety of other industries, and their constituents can be found in flame retardants, plasticizers, lubricants, hydraulic fluids, and oxidizers. While little is known about these aryl phosphates, studies on zebrafish indicate that TPP may result in developmental toxicity (Isales et al. 2015), cardiotoxicity (Du et al. 2015), and be an endocrine disruptor (Liu et al. 2012). TPP is also known to have a high log organic carbon partitioning coefficient (K_{OC}) value, suggesting that if introduced into the soil environment, TPP would undergo strong sorption to the organic matter within the soil (Anderson et al. 1993). Unfortunately, neither the sorption behavior nor toxicity of DPP is well known. Therefore, as an emerging contaminant in soil and groundwater systems, it is important to determine the environmental fate of these aryl phosphates if spilled in near-surface environments. To constrain the sorption behavior of DPP and its potential for aquatic toxicity, batch sorption experiments and zebrafish embryo toxicity assays were conducted, respectively. For the batch sorption experiments, four surficial sediment samples from the Fox Creek area, AB, representing the dominant soil types in the region (>50% by area), were tested. Sorption of DPP onto these materials were determined as a function of pH. For the zebrafish embryo toxicity assays, the LC_{50} for DPP was determined. Together, the resulting data sheds light and constrains the sorption behavior and potential transport behavior of a potential emerging contaminant in the near-surface environment and quantifies its potential impact on aquatic ecosystems. Characterizations of the surficial materials used in this study, and results from kinetic and degradation experiments are provided in **Appendix A**.

Chapter 3 builds on the work of **Chapter 2**, using FPW collected from the Fox Creek area to quantify and constrain the potential competitive or synergistic interactions that may occur in such a complex mixture. There are few studies aimed at determining the sorption potential of

compounds found in hydraulic fracturing-derived FPW, and in those few, the FPW used was prepared in a laboratory and thus have chemical compositions far simpler than field-collected FPW. Ye and Prigiobbe (2018) studied the sorption of Ba under briny conditions, mimicking the high total dissolved solids (TDS) commonly found in FPW, while Chen et al. (2017) studied the sorption of As(V) and Se(VI) in various synthetically made produced water samples. Both studies found that the high ionic strength of the FPW samples inhibited sorption of these metals. Manz et al. (2016) studied the sorption of two organic compounds typically found in FPW samples, 2-butoxyethanol (2-BE), a surfactant often found in hydraulic fracturing fluids, and furfural, a non-surfactant also found in hydraulic fracturing fluids, onto granular activated carbon and shale rock. Interestingly, 2-BE exhibited the strongest sorption at the highest salt concentration tested, whereas salt concentration had little effect on sorption of furfural. They found that when the two compounds were mixed together in the same aqueous solution, they found that sorption of both compounds was reduced, with furfural sorbing more strongly relative to 2-BE. Oetjen et al. (2018) marked the first sorption-based study to use authentic hydraulic fracturing-derived FPW from within the Denver-Julesburg basin in Colorado. They found that metals (e.g. Cu, Zn) were mobilized from the agricultural soil they used, likely because of the brackish salt concentration of the FPW. They also found that the agricultural soil used strongly sorbed and sequestered the organics (including polyethylene glycols, benzalkonium chlorides, and alkyl ethoxylates) found in the FPW, with none of the organics or their metabolites detected in the leachate. Thus, it is critical to consider the co-contaminant effects, whether synergistic or antagonistic, when evaluating the potential risk and impact FPW poses on the environment (McLaughlin et al. 2016).

This research project aimed to characterize the sorption behavior of numerous inorganic and organic compounds found in FPW samples collected from Duvernay Formation hydraulic fracturing operations. Using the same surficial sediment from Fox Creek, AB, as discussed above, batch sorption and column transport experiments were conducted to determine the equilibrium co-contaminant sorption of the FPW and the influence flow has on sorption, respectively. Inductively coupled plasma-mass spectrometry (ICP-MS/MS) and high-performance liquid chromatography (HPLC) Orbitrap mass spectrometry were used to detect and quantify the complex mixture of inorganic and organic compounds, respectively, within the FPW samples. The raw data from these chemical analyses are provided in **Appendix B**. This project marks one of the first extensive studies of the contaminant sorption behavior using a real FPW sample and characterizes the potential impact the Duvernay Formation-derived FPW may have if released into adjacent soil and groundwater environments.

Chapter 4 focuses on the development of an analytical groundwater transport model to simulate spill scenarios. Understanding contaminant transport mechanisms and behavior in the subsurface is a major problem in hydrogeology. To help resolve the uncertainties associated with groundwater transport, complex numerical models are often used to predict how a contaminant plume evolves through time. However, numerical simulations can be costly to develop and time consuming. Analytical solutions to the advection-dispersion equation (ADE), a partial differential equation that governs solute movement in groundwater, are invaluable for rapid and inexpensive assessments of contaminant scenarios and for verifying numerical models. These solutions often require simplified representations of the aquifer (homogeneous) and source region (constant concentration throughout time), which restrict their applicability to real-world systems. To circumnavigate some of these limitations, HYDROSCAPE was created, a new easy-

to-use software package that uses the three-dimensional analytical solutions of Karanovic et al. (2007) to solve contaminant transport problems. Unlike other programs that use analytical solutions, HYDROSCAPE utilizes novel mathematical techniques to circumnavigate some of the limitations of the solutions. These new features allow the user to: 1) build a fully customized source region, and 2) implement horizontal layers, with different hydraulic conductivities, within the domain. By allowing the domain to be heterogeneous and the source region to vary in shape, concentration, and time, more complexity is possible in these models and they are then more applicable to real-world settings. While some limitations still exist within the models, HYDROSCAPE represents a bridge between simple models using analytical solutions and complex numerical simulations, and may be a valuable tool for hydrogeologists in the future. Additional comparisons between HYDROSCAPE and numerical simulations are provided in **Appendix C**.

Using HYDROSCAPE, various spill scenarios were simulated. These spill scenarios included the short-term release of FPW into an aquifer from a point source, the continuous leakage of FPW into an aquifer from a point source, as well as the downward percolation of FPW through an organic-rich soil horizon. Results from the DPP sorption study from **Chapter 2** and the FPW sorption and transport study in **Chapter 3** were utilized in these spill simulations. We compared how flow could impact the distribution and breakthrough of different classes of contaminants found within FPW, and how simulation predictions could be impacted due to using different linear distribution coefficients (K_d) values taken from batch sorption experiments or from column transport experiments. We also demonstrated how certain contaminants may distribute and separate from others due to their affinity to sorb onto the porous medium they flow through, something noted by McLaughlin et al. (2016). Taken together, these three studies mark

a significant step forward in determining and characterizing the potential environmental interactions, fate, and impact of the chemical constituents of FPW may have if accidentally released into the shallow subsurface environment.

References

Alberta Energy Regulator. AER Compliance Dashboard, Reportable Releases, February, 2019;

<http://www1.aer.ca/compliancedashboard/incidents.html>

Alessi DS, Zolfaghari A, Kletke S, Gehman J, Allen DM, Goss GG (2017) Comparative analysis of hydraulic fracturing wastewater practices in unconventional shale development: Water sourcing, treatment and disposal practices. *Canadian Water Resources Journal* **42**: 105 – 121.

Anderson C, Wischer D, Schmieder A, Spiteller M (1993) Fate of triphenyl phosphate in soil. *Chemosphere* **27**: 869 – 879.

Blewett TA, Delompre PLM, He Y, Folkerts EJ, Flynn SL, Alessi DS, Goss GG (2017a) Sublethal and reproductive effects of acute and chronic exposure to flowback and produced water from hydraulic fracturing on the water flea *Daphnia magna*. *Environmental Science & Technology* **51**: 3032 – 3039.

Blewett TA, Weinrauch AM, Delompre PLM, Goss GG (2017b) The effects of hydraulic flowback and produced water on gill morphology, oxidative stress and antioxidant response in rainbow trout (*Oncorhynchus mykiss*). *Scientific Reports* **7**: 46582; doi: 10.1038/srep46582

Boschee P (2012) Handling produced water from hydraulic fracturing. *Oil and Gas Facilities* **1**: 23 – 26.

Boschee P (2014) Produced and flowback water recycling and reuse: Economics, limitations, and technology. *Oil and Gas Facilities* **3**: 16 – 22.

- Brannon HD, Pearson CM (2007) Proppants and fracture conductivity. In: Modern Fracturing: Enhancing Natural Gas Production (1st Ed.). Houston, TX: Energy Tribune Publishing, Inc.
- Brusseau ML (1994) Transport of reactive contaminants in heterogenous porous media. *Reviews of Geophysics* **32**: 285 – 313.
- California Department of Conservation (CDOC) (2015) Monthly production and injection databases. Statewide production and injection data. Sacramento, CA: California Department of Conservation, Division of Oil, Gas & Geothermal Resources. Retrieved from:
http://www.conservation.ca.gov/dog/prod_injection_db/Pages/Index.aspx
- Canadian Society for Unconventional Resources (CSUR) (2013) Hydraulic fracturing and oil and gas development. <http://www.csur.com/images/YukonCofCOctober2013RevisedFinal.pdf> (accessed March, 2016).
- Carter KE, Hakala JA, Hammack RW (2013) Hydraulic fracturing and organic compounds: Uses, disposal and challenges. In: SPE Eastern Regional Meeting; Society of Petroleum Engineers: Pittsburgh, PA. DOI: <http://dx.doi.org/10.2118/165692-MS>.
- Chen SS, Sun Y, Tsang DCW, Graham NJD, Ok YS, Feng Y, Li X-D (2017) Insights into subsurface transport of As(V) and Se(VI) in produced water from hydraulic fracturing using soil samples from Qingshankou Formation, Songliao Basin, China. *Environmental Pollution* **223**: 449 – 456.
- Clark CE, Veil JA (2009) Produced water volumes and management practices in the United States. Argonne National Laboratory, Argonne, IL. ANL/EVS/R-09/1. pp. 64.
- Colborn T, Kwiatkowski C, Schultz K, Bachran M (2011) Natural gas operations from a public health perspective. *Human and Ecological Risk Assessment* **17**: 1039 – 1056.

- Covelo EF, Vega FA, Andrade ML (2007) Competitive sorption and desorption of heavy metals by individual soil components. *Journal of Hazardous Materials* **140**: 308 – 315.
- DiGiulio DC, Jackson RB (2016) Impact to underground sources of drinking water and domestic wells from production well stimulation and completion practices in the pavilion, Wyoming, Field. *Environmental Science & Technology* **50**: 4524 – 4536.
- Drollette BD, Hoelzer K, Warner NR, Darrah TH, Karatum O, O'Connor MP, Nelson RK, Fernandez LA, Reddy CM, Vengosh A, Jackson RB, Elsner M, Plata DL (2015) Elevated levels of diesel range organic compounds in groundwater near Marcellus gas operations are derived from surface activities. *Proceedings of the National Academy of Sciences of the United States of America* **112**: 13184 – 13189.
- Du Z, Wang G, Gao S, Wang Z (2015) Aryl organophosphate flame retardants induced cardiotoxicity during zebrafish embryogenesis: By disturbing expression of the transcriptional regulators. *Aquatic Toxicology* **161**: 25 – 32.
- Easton J (2014) Optimizing fracking wastewater management. *Pollution Engineering* January 13.
- Encana Corporation (2013) Sustainability report, 47. Calgary, AB: Encana Corporation.
- Folkerts EJ, Blewett TA, He Y, Goss GG (2017a) Cardio-respirometry disruption in zebrafish (*Danio rerio*) embryos exposed to hydraulic fracturing flowback and produced water. *Environmental Pollution* **231**: 1477 – 1487.
- Folkerts EJ, Blewett TA, He Y, Goss GG (2017b) Alterations to juvenile zebrafish (*Danio rerio*) swim performance after acute embryonic exposure to sub-lethal exposures of hydraulic fracturing flowback and produced water. *Aquatic Toxicology* **193**: 50 – 59.

- Gehman J, Thompson DY, Alessi DS, Allen DM, Goss GG (2016) Comparative analysis of hydraulic fracturing wastewater practices in unconventional shale development: Newspaper coverage of stakeholder concerns and social license to operate. *Sustainability* **8**: 1 – 23; doi:10.3390/su8090912
- Gregory KB, Vidic RD, Dzombak DA (2011) Water management challenges associated with the production of shale gas by hydraulic fracturing. *Elements* **7**: 181 – 186.
- Gupta DVS, Valko P (2007) Fracturing fluids and formation damage. In: M Economides; T Martin (Eds.), *Modern Fracturing: Enhancing Natural Gas Production* (pp. 227 – 279). Houston, TX: Energy Tribune Publishing, Inc.
- Hammer R, VanBriesen J (2012) *In frackings wake: New rules are needed to protect our health and environment from contaminated wastewater*. New York, NY: Natural Resources Defense Council.
<http://www.nrdc.org/energy/files/fracking-wastewater-fullreport.pdf>
- He Y, Folkerts EJ, Zhang Y, Martin JW, Alessi DS, Goss GG (2017a) Effects on biotransformation, oxidative stress, and endocrine disruption on rainbow trout (*Oncorhynchus mykiss*) exposed to hydraulic fracturing flowback and produced water. *Environmental Science & Technology* **51**: 940 – 947.
- He Y, Flynn SL, Folkerts EJ, Zhang Y, Ruan D, Alessi DS, Martin JW, Goss GG (2017b) Chemical and toxicological characterization of hydraulic fracturing flowback and produced water. *Water Research* **114**: 78 – 87.
- Hyne NJ (2012) *Nontechnical Guide to Petroleum Geology, Exploration, Drilling and Production* (3rd Edition). Tulsa, OK: PennWell Corporation.
- Isales GM, Hipszer RA, Raftery TD, Chen A, Stapleton HM, Volz DC (2015) Triphenyl phosphate-induced developmental toxicity in zebrafish: Potential role of the retinoic acid receptor. *Aquatic Toxicology* **161**: 221 – 230.

- Karanovic M, Neville CJ, Andrews CB (2007) BIOSCREEN-AT: BIOSCREEN with an exact analytical solution. *Ground Water* **45**: 242 – 245.
- King GE (2012) Hydraulic fracturing 101: What every representative, environmentalist, regulator, reporter, investor, university researcher, neighbor and engineer should know about estimating frac risk and improving frac performance in unconventional gas and oil wells. Society of Petroleum Engineers Annual Technical Conference and Exhibition, February 6-8, 2012, The Woodlands, TX. Document: SPE-152596-MS, 80.
- Lari E, Wiseman S, Mohaddes E, Morandi G, Alharbi H, Pyle GG (2016) Determining the effect of oil sands process-affected water on grazing behaviour of *Daphnia magna*, long-term consequences, and mechanism. *Chemosphere* **146**: 362 – 370.
- Liu X, Ji K, Choi K (2012) Endocrine disruption potentials of organophosphate flame retardants and related mechanisms in H295R and MVLN cell lines and in zebrafish. *Aquatic Toxicology* **114**: 173 – 181.
- Llewellyn GT, Dorman F, Westland JL, Yoxtheimer D, Grieve P, Sowers T, Humston-Fulmer E, Brantley SL (2015) Evaluating the groundwater supply contamination incident attributed to Marcellus shale gas development. *Proceedings of the National Academy of Sciences of the United States of America* **112**: 6325 – 6330.
- Lutz BD, Lewis AN, Doyle MW (2013) Generation, transport, and disposal of wastewater associated with Marcellus shale gas development. *Water Resources Research* **49**: 647 – 656.
- Manz KE, Haerr G, Lucchesi J, Cater KE (2016) Adsorption of hydraulic fracturing fluid components 2-butoxyethanol and furfural onto granulated activated carbon and shale rock. *Chemosphere* **164**: 585 – 592.

- McLaughlin MC, Borch T, Blotevogel J (2016) Spills of hydraulic fracturing chemicals on agricultural topsoil: Biodegradation, sorption, and co-contaminant interactions. *Environmental Science & Technology* **50**: 6071 – 6078.
- OECD (Organisation for Economic Cooperation and Development) (2008) Guideline for testing chemicals; No. 211, *Daphnia magna* reproduction test. OECD: Paris.
- Oetjen K, Blotevogel J, Borch T, Ranville JF, Higgins CP (2018) Simulation of a hydraulic fracturing wastewater surface spill on agricultural soil. *Science of the Total Environment* **645**: 229 – 234.
- PA DEP (Pennsylvania Department of Environmental Protection) (2015) PA DEP oil & gas reporting website, statewide data downloads by reporting period. waste and production files downloaded for Marcellus/unconventional wells, July 2009 December 2014. Harrisburg, PA. Retrieved from <https://www.paoilandgasreporting.state.pa.us/publicreports/Modules/DataExports/DataExports.aspx>
- Piwoni MD, Keeley JW (1990) Basic concepts of contaminant sorption at hazardous waste sites. United States Environmental Protection Agency, Office of Research and Development, Office of Solid Waste and Emergency Response, EPA/540/4-90/053.
- Preston A, Garner G, Beavis K, Sadiq O, Stricker S (2016) Duvernay reserves and resources report: A comprehensive analysis of Alberta's foremost liquid-rich shale resource. Alberta Energy Regulator, Suite 1000, 250 – 5 Street SW, Calgary, AB.
- Rassenfoss S (2011) From flowback to fracturing: Water recycling grows in the Marcellus Shale. *Journal of Petroleum Technology* **63**: 48 – 51.
- Rivard C, Lavoie D, Lefebvre R, Séjourné S, Lamontagne C, Duchesne M (2014) An overview of Canadian shale gas production and environmental concerns. *International Journal of Coal Geology* **126**: 64 – 76.

Rogers JD, Burke TL, Osborn SG, Ryan JN (2015) A framework for identifying organic compounds of concern in hydraulic fracturing fluids based on their mobility and persistence in groundwater. *Environmental Science & Technology Letters* **2**: 158 – 164.

Rokosh CD, Lyster S, Anderson SDA, Beaton AP, Berhane H, Brazzoni T, Chen D, Cheng Y, Mack T, Pana C, Pawlowicz JG (2012) Summary of Alberta's shale- and siltstone-hosted hydrocarbon resource potential. Energy Resources Conservation Board and Alberta Geological Survey, ERCB/AGS Open File Report 2012-06, 327.

Sjolander SA, Clark J, Rizzo D, Turack J (2011) Water facts #31: Introduction to hydrofracturing. University Park, PA: Penn State College of Agricultural Sciences – Cooperative Extension. http://www.shale-gas-information-platform.org/fileadmin/ship/dokumente/introduction_to_hydrofracturing-2.pdf

Smith KS (1997) Metal sorption on mineral surfaces: An overview with examples relating to mineral deposits. *The Environmental Geochemistry of Mineral Deposits: Part A: Processes, Techniques, and Health Issues Part B: Case Studies and Research Topics, Reviews in Economic Geology, Volumes 6A and 6B, Chapter 7*, Society of Economic Geologists, GS Plumlee, MJ Logsdon, LF Filipek.

Tahervand S, Jalali M (2017) Sorption and desorption of potentially toxic metals (Cd, Cu, Ni and Zn) by soil amended with bentonite, calcite and zeolite as a function of pH. *Journal of Geochemical Exploration* **181**: 148 – 159.

Tatarazako N, Oda S (2007) The water flea *Daphnia magna* (Crustacea, Cladocera) as a test species for screening and evaluation of chemicals with endocrine disrupting effects on crustaceans. *Ecotoxicology* **16**: 197 – 203.

Tiemann M, Folger P, Carter NT (2014) Shale energy technology assessment: Current and emerging water practices. Washington, DC: Congressional Research Service.

<http://nationalaglawcenter.org/wp-content/uploads/assets/crs/R43635.pdf>

United States Environmental Protection Agency (2015). Review of state and industrial spill data: Characterization of hydraulic fracturing-related spills. Office of Research and Development, Washington, D.C., EPA/601/R-14/001.

United States Environmental Protection Agency (2016). Hydraulic fracturing for oil and gas: Impacts from the hydraulic fracturing water cycle on drinking water resources in the United States. Office of Research and Development, Washington, D.C., EPA/600/R-16/236Fa.

United States Government Accountability Office (US GAO) (2012) Energy-water nexus: Information on the quality, quantity, and management of water produced during oil and gas production.

GAO0120156. Washington, DC. <http://www.gao.gov/products/GAO-12-156>

van Beinum W, Hofmann A, Meeussen JCL, Kretzschmar R (2005) Sorption kinetics of strontium in porous hydrous ferric oxide aggregates I. The Donnan diffusion model. *Journal of Colloid and Interface Science* **283**: 18 – 28.

Vengosh A, Warner N, Jackson R, Darrah T (2013) The effects of shale gas exploration and hydraulic fracturing on the quality of water resources in the United States. *Procedia Earth and Planetary Sciences* **7**: 863 – 866.

Vidic RD, Brantley SL, Vandenbossche JM, Yoxtheimer D, Abad JD (2013) Impact of shale gas development on regional water quality. *Science* **340**: 826.

Warner NR, Jackson RB, Darrah TH, Osborn SG, Down A, Zhao K, White A, Vengosh A (2012) Geochemical evidence for possible natural migration of Marcellus Formation brine to shallow

aquifers in Pennsylvania. Proceedings of the National Academy of Sciences of the United States of America **109**: 11961 – 11966.

Warner NR, Jackson RB, Darrah TH, Millot R, Kloppmann W, Vengosh A (2014) New tracers identify hydraulic fracturing fluids and accidental releases from oil and gas operations. Environmental Science & Technology **48**: 12552 – 12560.

Ye Z, Prigiobbe V (2018) Effect of ionic strength on barium transport in porous media. Journal of Contaminant Hydrology **209**: 24 – 32.

Chapter 2 – Assessment of impacts of diphenyl phosphate on groundwater and near-surface environments: Sorption and toxicity¹

2.1. Introduction

Diphenyl phosphate (DPP; $C_{12}H_{11}PO_4$; **Figure A1**) is a major environmental degradation product and metabolite of several aryl phosphate esters, including triphenyl phosphate (TPP), 2-ethylhexyl diphenyl phosphate (EHDP) and others that include the DPP-moiety (Howard and Deo 1979; Muir and Grift 1981; David and Seiber 1999a; Su et al. 2014; Wang et al. 2016). Aryl phosphate esters are used in the manufacture of a variety of products including, but not limited to, flame retardants (Reemtsma et al. 2008; van der Veen and de Boer 2012), plasticizers (Reemtsma et al. 2008; Wei et al. 2015), lubricants (Andresen et al. 2004), and hydraulic fluids (Williams and LeBel 1981; David and Seiber 1999b). Therefore, it is important to study the environmental fate and transport of aryl phosphates due to their wide-spread use and potential for toxicity in the environment.

Aryl phosphates have been found to contaminate soil and water at a number of locales worldwide, especially those near major industrialized sites (e.g. Sheldon and Hites 1979; Williams et al. 1982; Ishikawa et al. 1985; Fukushima et al. 1992; Martínez-Carballo et al. 2007). Rodil et al. (2012), studying the northwest region of Spain between November 2007 and September 2008, monitored the presence of 53 compounds, including some aryl phosphate esters, in wastewater, surface water, and drinking water. It was found that DPP was widespread, being present in many of the studied samples, whereas TPP was found in only one sample (Rodil et al. 2012). More recently, He et al. (2017) analyzed the organic and inorganic chemistry of

¹ A version of this chapter was submitted to and published in *Journal of Contaminant Hydrology* as Funk S, Duffin L, He Y, McMullen C, Sun C, Utting N, Martin JW, Goss GG, Alessi DS (2019) Assessment of impacts of diphenyl phosphate on groundwater and near-surface environments: Sorption and toxicity.

flowback and produced water (FPW) collected from hydraulic fracturing operations in the region of Fox Creek, Alberta, Canada. Of the numerous chemical compounds identified in this FPW, a group of aryl phosphates, including TPP and DPP, were identified. The authors did not conclude that there was a purpose for adding aryl phosphates to the injected hydraulic fracturing fluids. However, they did identify an additive known as Irgafos 168, a triphenyl phosphite that is sometimes added to hydraulic fracturing fluids as a processing stabilizer and secondary antioxidant; the aryl phosphates in these samples were presumed to be downhole oxidation products of this additive. Hundreds of spills of FPW are reported to the Alberta Energy Regulator (AER) each year (AER 2016); similarly, the US Environmental Protection Agency (EPA) conducted an extensive study of hydraulic fracturing related spills in 11 states, and out of the 464 spills studied (over a 6-year period), approximately 48% of the spilled materials were FPW (US EPA 2016). Clearly, there is a possibility of introducing aryl phosphates from hydraulic fracturing operations, including DPP, into the environment.

The environmental fate of many aryl phosphates has not been extensively studied. Some work has been done to determine their sorption behavior and environmental fate. Studies by Saeger et al. (1979), Renberg et al. (1980), Muir and Grift (1981), Huckins et al. (1991), and Anderson et al. (1993) all concluded that the aryl phosphates studied, including TPP and others that had the DPP-moiety, exhibited low water solubility and high partitioning to the organic matter or sediment fraction. Muir and Grift (1981) and Anderson et al. (1993) both concluded that TPP degraded to DPP over the course of their experiments and that DPP was the main degradation product.

Studies on the toxicity of aryl phosphates are also limited. Su et al. (2014) has conducted the only known study on the cytotoxic effects of DPP using chicken embryonic hepatocytes,

wherein the authors found that DPP had less cytotoxic effects than its parent TPP. However, the toxicity to common aquatic organisms, representative of those likely to be found in regions where, for example, hydraulic fracturing wastewater handling occurs, is unknown.

Currently, it is unclear how changes in soil (e.g. mineralogy, fraction of organic carbon (foc)) or solution chemistry (e.g. pH) impact the sorption behavior of DPP. The goals of the present study were two-fold. First, we investigated how DPP would interact in near-surface environments, characterizing the sorption characteristics and modeling transport of DPP in a variety of natural soils collected from the region. We also used synthetic hydrous ferrous oxide (HFO)-coated sand across a wide-range of pH (~5 to ~9) and solid-to-DPP concentration ratios to understand the sorption behavior and transport potential of DPP in groundwater and soil environments. Second, we investigated the potential for adverse effects of DPP, a major environmental degradation product of commonly used aryl phosphates (Muir and Grift 1981; Su et al. 2014), on zebrafish embryo acute toxicity.

2.2. Materials

2.2.1. Aqueous Solutions

For the simulated groundwater used in the batch sorption experiments, an electrolyte solution containing approximately 1,000 mg/L Cl^- and 500 mg/L HCO_3^- , was made by adding NaCl and NaHCO_3 to Milli-Q distilled water. The simulated groundwater composition was based on a representative groundwater sample collected in the Fox Creek area (~500 mg/L HCO_3^-) (Table A2), as well as representative FPW samples (>100,000 mg/L Cl^-) collected in the same region (Table S1 in Supplementary Materials of He et al. 2017). We assumed an approximate 100:1 Cl^- dilution of FPW with groundwater. To simplify the experiments, no other cations or

anions were considered because they were not in high abundance in either sample. Stock solutions were made just prior to use in each experiment. The presence of HCO_3^- serves a dual purpose; bicarbonate is both a common anion found in many shallow groundwater samples and acts as a pH buffer for the experiments. A portion of the electrolyte solution was then segregated, after which DPP was added such that the concentration of the stock solution was approximately 500 mg/L. Measurements of the stock and electrolyte solutions were made gravimetrically.

2.2.2. Sediments

Two broad classes of unconsolidated sediment were used in this study: 1) synthetic hydrous ferric oxide (HFO)-coated sand and 2) representative surficial sediments collected in the Fox Creek area, AB, Canada. The procedure for making the HFO-coated sand is outlined in the **Appendix A**. The surficial sediments were collected at locations around the Fox Creek area, corresponding with major soil types found in the region (Pawley and Atkinson 2013; Utting 2013). Collected sediment types studied included glaciolacustrine clay (GLC), moraine (MOR), stagnant moraine (STGM), and fluvial sand (FLUV). Grain-size distributions of these collected soil types are given in **Tables A3 and A4**.

Samples of moraine are dark-brown to black in color; samples of glaciolacustrine clay and stagnant moraine are a beige color (**Figure A2**). X-ray diffraction (XRD) and TN/TC/TOC (total nitrogen/total carbon/total organic carbon) results for the surficial sediment collected are given in **Table A5**. The results show that the moraine soil has the highest TOC content (8.92%) and is mostly comprised of clay minerals (muscovite and kaolinite). The glaciolacustrine clay and stagnant moraine are composed of more feldspars (albite and orthoclase) and less clay minerals (predominantly muscovite), with a lower TOC content (GLC: 1.64%; STGM: 0.66%) compared to the moraine samples. The fluvial sand was dominantly comprised of quartz, with

minor amounts of feldspar, clay minerals (muscovite and kaolinite), some carbonates, and pyrite. Not surprisingly, analyses of the fluvial sand indicate that it has the lowest TOC (0.23%) and TN (0.02%) of all the collected samples.

2.3. Methods

2.3.1. Experimental Methods

2.3.1.1. Batch Sorption Experiments

Batch sorption experiments on the five sediments studied here closely followed the methods reported in Roy et al. (1992) and Zachara and Streile (1991). A constant solids-to-solution (simulated groundwater spiked with DPP) ratio of 1:4 (~2.5 g sand) was applied to HFO-coated sand and fluvial sand, and 1:50 (0.2 g sediment) was used for clay-dominated sediment types. Experiments were conducted in polypropylene vials. The pH of each vial was adjusted by adding small volumes of either concentrated HCl or NaOH (from 0.1 M to 5 M) to the solution, until the pH of the solution was within ± 0.05 of the desired target. Additionally, the mass of each vial was measured before and after the pH probe was placed into solution to record any solution losses due to pH measurements. Each tube was then placed on a rotator for approximately 24 h. Our kinetics data indicate that DPP sorption reached equilibrium before 8 h for all sediment types (see **Appendix A**). After this equilibration time, the pH of each tube was measured and recorded, and the sample was then centrifuged for 40 min at 10,000 g. The supernatant was then extracted from each vial using a plastic pipette tip (unfiltered) to be analyzed for DPP, total organic carbon (TOC), and total phosphorous (TP) in solution.

2.3.1.2. Zebrafish Embryo Toxicity Assays

Zebrafish embryo toxicity tests were conducted to assess the potential for adverse effects of DPP on aquatic organisms, such as fish. Exposures were conducted under semi-static

conditions in 50 mL glass beakers at $25 \pm 1^\circ\text{C}$ under a 16 h/8 h light/dark cycle. Seven concentrations of DPP (3.1, 6.3, 12.5, 25, 50, 100, 200 mg/L) and one control water group using dilution water were tested. Exposure solutions were prepared by dissolving DPP powder into dilution water prior to exposure. The dilution water was moderately hard water (see **Appendix A**). Each exposure beaker contained 30 mL of exposure solution/control water, and half of the exposure solution was changed daily. To begin an experiment, 10 fertilized embryos (1 h post fertilization, hpf) were randomly selected and placed into each exposure beaker. During the 96 h exposure period, any dead embryos observed were removed immediately. All the exposures were repeated for three replications; in total, 30 embryos were tested for each exposure/control group. At the end of exposure, the half-lethal concentration (LC_{50}) was calculated using the Toxicity Relationship Analysis Program (TRAP v1.21; Erickson 2010).

2.3.2. Analytical Methods

2.3.2.1. Soil Analyses

We conducted XRD analyses to determine the mineralogical makeup of the soil samples. Samples were run in a Rigaku Ultima IV with a cobalt source with data collected from a 2θ range from 5° to 90° . The JADE 9.5 analysis package (KS Analytical Systems) was used to fit the resultant diffraction patterns.

Soil analyses for TN (total nitrogen), TC (total carbon), and TOC (total organic carbon) were determined using dry flash combustion following the method outlined by Nelson and Sommers (1996) and Bremner (1996), using a Costech Model EA 4010 Elemental Analyzer. A known mass of soil was placed in a combustion chamber containing Cr (III) oxide and cobaltous/ic oxide silver catalysts. Upon the addition of oxygen into the combustion chamber, the temperature was increased from approximately $1,020^\circ\text{C}$ to between $1,800$ and $2,000^\circ\text{C}$.

During combustion, the nitrogen (N) and carbon (C) in the sample is converted into N₂ or NO_x (which is later reduced to N₂) and CO₂, respectively. The N₂ and CO₂ gases are then collected, separated, run through a chromatographic column and detected quantitatively using a thermal conductivity detector.

2.3.2.2. Solution Analyses:

Aliquots of solution taken from the batch sorption experiments were analyzed using three methods. Samples (~30-40 mL total) were diluted (~1/8) with Milli-Q water and kept at 4°C in a refrigerator before they were analyzed for TOC using a Shimadzu TOC V_{CPH} instrument. Fresh dilution and rinse water were obtained each day from an Elix 5 water system with Milli-Q filtration to minimize CO₂ absorption from the atmosphere. Standard solutions were prepared from dried and desiccated reagents (potassium hydrogen phthalate for TC/NPOC (non-purgeable organic carbon) and sodium bicarbonate/sodium carbonate for IC/POC (inorganic carbon/purgeable organic carbon)) and were analyzed before each sample set. Acid reagents (phosphoric and hydrochloric acids) were monitored and replenished or replaced as necessary. Samples were analyzed in sets of 12 to 15 using an auto-sampler, and each sample was subsampled 3 to 5 times for each of the following analyses: TC, IC, NPOC, and POC before the analysis results were compiled.

Total phosphorous (TP) concentrations of water samples were determined by inductively coupled plasma-optical emission spectroscopy (ICP-OES) using a Thermo iCAP6300 Duo ICP-OES instrument. As with the TOC method, samples were diluted (1/8) with Milli-Q water and kept at 4°C in a refrigerator before they were analyzed for TP. Yttrium (Y) was used during the analyses as an internal standard to correct for matrix effects.

The quantitation of DPP in solution was performed using a 3200 QTRAP tandem mass spectrometer in multiple reaction monitoring (MRM) mode. An Agilent 1260 auto-sampler injected 40 μL of sample and an Agilent 1200 binary pump set to flow 700 $\mu\text{L}/\text{min}$ of 1:1 water:methanol was used to carry the sample to the mass spectrometer. Samples were introduced to the mass spectrometer via electrospray ionization (ESI) in negative ion mode.

Two reactions were monitored. Quantitation was done using the transition 249.1/93.1 ($[\text{DPP-H}]^- \rightarrow [\text{OPh}]^-$) and confirmed with the transition 249.1/65.0 ($[\text{DPP-H}]^- \rightarrow [\text{OPHOH}]^-$). External standards were prepared the day of analysis. Samples under 100 ppm were quantitated using a calibration curve with six points covering 0 to 100 ppm, and samples over 100 ppm were quantitated using a separate calibration curve with six points covering 0 to 800 ppm.

2.4. Results & Discussion

2.4.1. Sorption behavior of DPP

Most aryl phosphates are characterized by high $\log K_{\text{OW}}$ (water-octanol partitioning coefficient) and $\log K_{\text{OC}}$ values, indicating that they are highly hydrophobic and lipophilic, prone to partition onto organic matter in sediment and likely to accumulate in fatty tissue (Boethling and Cooper 1985). Saeger et al. (1979) conducted the most extensive study and found that aryl phosphates generally exhibited very low water solubility (S_{w} ; for TPP = 1.9 mg/L) and high log octanol-water partitioning coefficients ($\log K_{\text{OW}}$; for TPP $\log K_{\text{OW}} = 4.63$). Other aryl phosphates with the DPP-moiety, including isodecyl diphenyl phosphate (IDDP), tertbutylphenyl diphenyl phosphate (TBDP), 2-ethylhexyl diphenyl phosphate (EHDP), isopropylphenyl diphenyl phosphate (IPDP), and cresyl diphenyl phosphate (CDP), exhibited comparable results (Saeger et al. 1979), which were in good agreement with a similar study conducted by Renberg et al.

(1980). Muir et al. (1980) reported the log organic carbon partitioning coefficient ($\log K_{OC}$) for TPP to be 4.17. Huckins et al. (1991) investigated the sorption of TPP onto topsoil (5% sand, 77% silt, 18% clay; organic carbon fraction $f_{OC} = 1.12\%$) and measured $\log K_{OC}$ to be 3.93. Muir and Grift (1981) reported the linear distribution coefficient (K_d) for suspended matter within river water was 12,389 L/kg for EHDP. However, based on the pK_a (3.88; Christ et al. 2011) and molecular structure of DPP, it was unclear to us whether the sorption of DPP would be dominated by protonation-deprotonation processes and therefore exhibit a pH-dependence on sorption, or be similar to other aryl phosphates and be dominated by hydrophobicity and correlate with f_{OC} . To that end, we tested whether the sorption of DPP onto sediment or soil has a pH-dependence within an environmentally relevant range between pH ~ 5 and ~ 9 .

The three independent analytical techniques used to determine the concentration of DPP in solution (MS/MS, TOC, and TP) were consistent with each other. The simplistic composition of the aqueous solution allowed for the use of TOC and TP methods to a high degree of confidence. Blanks consisting of surficial sediment suspended in the electrolyte solution were observed to exhibit low concentrations of phosphorous (<0.05 mg/L), but significantly higher concentrations of organic carbon (>1 mg/L). However, normalization of solution TP and TOC concentrations in our experiments with the blank were largely consistent with each other and with direct quantification using MS/MS. Factoring in the difficulties in quantifying DPP using the MS/MS method, and DPP likely to be the sole phosphorous source in the aqueous solution, we argue that TP is likely the most reliable. However, because the TP method only measures phosphorous and not DPP specifically, we caution the use of this method for more complex mixtures with multiple phosphorous compounds.

Quality control tests were conducted to ascertain the degree to which DPP may sorb onto the polypropylene vials and pipette tips. We observed no measureable degree of sorption of DPP onto the polypropylene items. Within the experimentally tested range of solution concentrations and pH, DPP exhibits a low degree of sorption onto organic-rich, clay-dominated sediment (MOR, STGM, GLC), with K_d values ranging from ~ 2.0 to ~ 12.0 L/kg (**Figure 2.1A to C**), to very low degrees of sorption onto predominantly sandy material (HFO, FLUV), with K_d values almost an order of magnitude lower (~ 0.1 to ~ 0.5 L/kg; **Figure 2.1D and E**). The ratio of the mass of DPP sorbed onto the solid material, dubbed the solid concentrations (C_s), to the concentration of DPP remaining in solution (C) after equilibrium remained constant as a function of increasing total DPP concentration, and the linear K_d method was therefore used to model our sorption data (**Figure A5**). This is consistent with the high solubility of DPP in water relative to other aryl phosphates. Uncertainties for C_s were estimated by propagating the errors associated with the measurements of the mass of sediment and volume of solution put into each vial, the mass of DPP powder dissolved into the original stock solution, and errors associated with the quantification of DPP in the supernate after the experiment (see **Appendix A**). These uncertainties were then incorporated into the errors for K_d values.

The K_d for most of the sediments (GLC, STGM, HFO, and FLUV) tested do not appear to be affected by changes in pH, remaining constant (within the uncertainties calculated for the experiments) within the tested pH range of approximately 5 to 9.1 (**Figure 2.1B to E**). Because of the uncertainties in the calculated K_d values, it is not possible to determine with certainty whether there is a pH-dependence on sorption using the three analytical techniques used in this study. This is also consistent with the reported pK_a of DPP (~ 3.88 ; Christ et al. 2011), suggesting that the proton-active phosphoryl functional DPP would remain largely deprotonated within the

tested pH range. Rather, based on our experimental results, sorption of DPP onto these sediments appears to be dominated by hydrophobicity, and therefore controlled by the f_{OC} of the soil. Using our sorption data, a consistent $\log K_{OC}$ value of 2.30 ± 0.42 (1σ) was calculated (**Table 2.1**); our calculated values of $\log K_{OC}$ are also consistent with estimates derived from K_{OW} and MCI determinations (US EPA 2012).

Despite the past research outlined above, the sorption behavior of diphenyl phosphate onto sediments has not been studied extensively. Muir and Grift (1981) found that the K_d value for suspended matter within river water for DPP was 337 L/kg. A reported value for the $\log K_{OC}$ of DPP of 2.292 using a calculated K_{OW} ($\log K_{OW} = 2.88$) method or 2.426 using the molecular connectivity index (MCI) method came from a software program called EPI Suite (US EPA 2012). These estimates are consistent with the estimated higher water solubility limit ($S_w = 513.03$ mg/L). All methods of estimation indicate that DPP will have a low sorption potential, approximately two orders of magnitude lower K_{OC} values compared to other aryl phosphates, and thus is likely to be mobile in near-surface environments.

Unlike the other sediments, the moraine sediment does appear to exhibit some pH-dependence on the calculated K_d values within the tested range of pH from 5.6 to 7.9. There appears to be a decrease in sorption with increasing pH (**Figure 2.1A**). This trend is seen most readily in the MS/MS data (**Figure 2.1A**). It is unclear why the moraine appears to exhibit this pH-dependence, but we hypothesize it may have to do with the mineralogy of the clay in this soil type. Kaolinite is the dominant clay mineral in the moraine soil. As pH increases, the clays in the soil become increasingly negative, thus repelling the deprotonated and negatively-charged functional group in DPP.

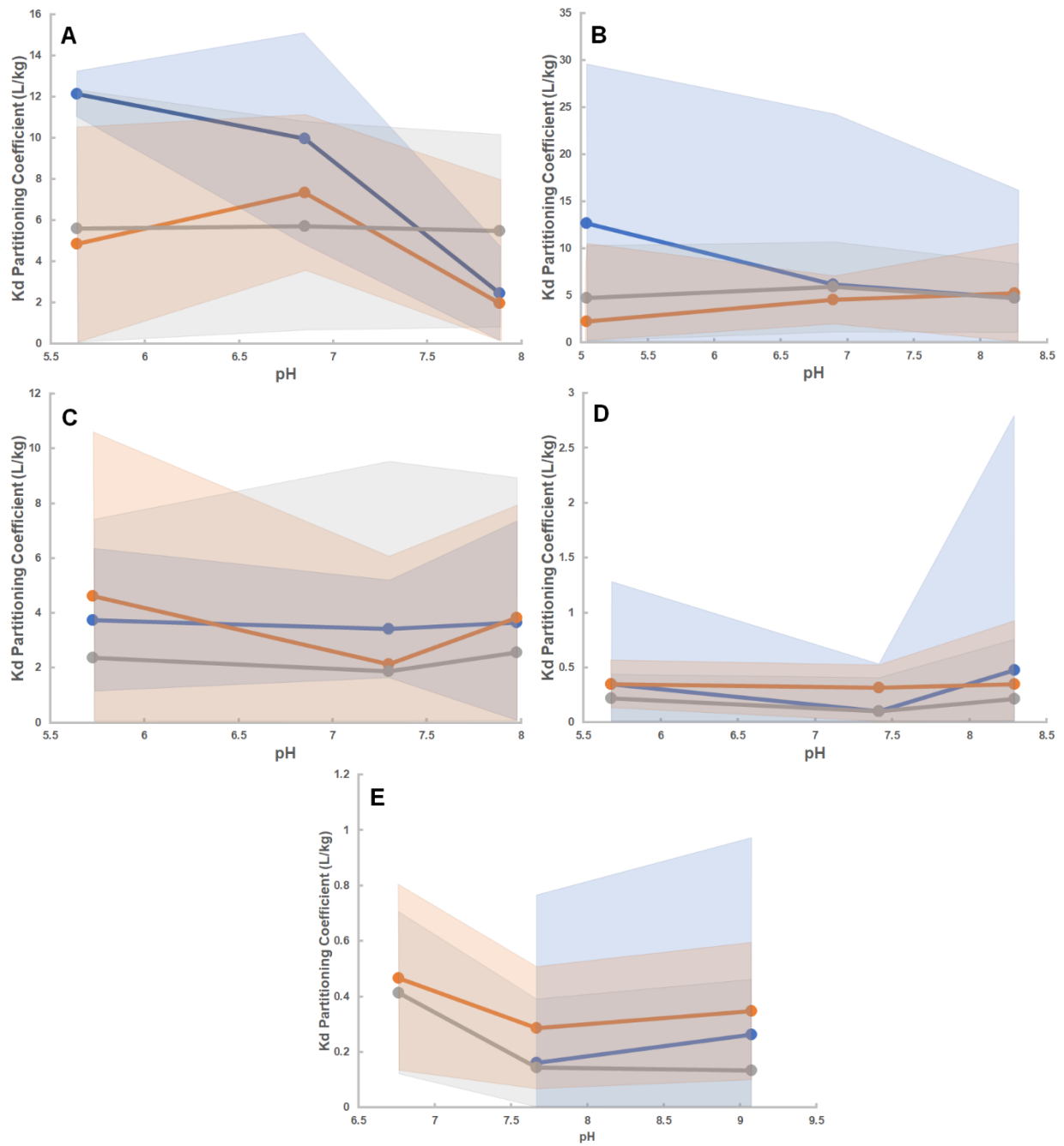


Figure 2.1: Partitioning coefficients (K_d) vs. pH for **A)** moraine; **B)** glaciolacustrine clay; **C)** stagnant moraine; **D)** HFO-coated sand; and **E)** fluvial sand. Blue = MS/MS; Orange = TOC; Grey = TP. Shaded area represents the approximate errors for the K_D . Errors were calculated by propagating both measurement and analytical errors.

Sediment	pH	pH Error	MS/MS			TOC			TP		
			K _d [§] (L/kg)	K _d Error [§]	log K _{OC} [§]	K _d [‡] (L/kg)	K _d Error [‡]	log K _{OC} [‡]	K _d [*] (L/kg)	K _d Error [*]	log K _{OC} [*]
MOR	5.64	0.06	12.14	1.09	2.13	4.86	5.61	1.74	5.60	6.70	1.80
MOR	6.85	0.12	9.96	5.12	2.05	7.32	3.78	1.91	5.71	5.07	1.81
MOR	7.88	0.075	2.44	2.28	1.44	1.95	6.00	1.34	5.49	4.67	1.79
GLC	5.04	0.135	12.70	16.82	2.88	2.21	8.26	2.12	4.73	5.52	2.45
GLC	6.89	0.11	6.16	18.03	2.57	4.53	2.59	2.43	5.91	4.79	2.55
GLC	8.25	0.19	4.71	11.48	2.45	5.23	5.27	2.50	4.76	3.63	2.46
HFO	5.68	0.08	0.35	0.93	---	0.35	0.22	---	0.22	0.21	---
HFO	7.41	0.04	0.10	0.43	---	0.31	0.21	---	0.10	0.31	---
HFO	8.29	0.06	0.48	2.32	---	0.35	0.58	---	0.22	0.54	---
STGM	5.73	0.07	3.72	2.60	2.75	4.61	5.94	2.84	2.37	5.03	2.56
STGM	7.30	0.08	3.41	1.78	2.71	2.12	3.95	2.51	1.86	7.66	2.45
STGM	7.98	0.15	3.64	3.72	2.74	3.83	4.09	2.76	2.55	6.38	2.59
FLUV	6.76	0.145	N.D	N.D	N.D	0.47	0.34	2.31	0.41	0.29	2.25
FLUV	7.67	0.06	0.16	0.61	1.84	0.29	0.22	2.09	0.14	0.25	1.80
FLUV	9.07	0.085	0.26	0.71	2.06	0.35	0.25	2.18	0.13	0.33	1.76
Average log K _{OC}					2.33±0.46			2.23±0.43			2.19±0.36

Table 2.1: Tabulated values for K_d and log K_{OC} for each sediment type at each pH condition. K_d and log K_{OC} values were calculated using either the MS/MS, TOC or TP data. Errors reported from the average log K_{OC} values are to one sigma. log K_{OC} values for HFO were not calculated because f_{OC} was assumed to be zero. N.D. = not determined.

§ = calculated from MS/MS data

‡ = calculated from TOC data

* = calculated from TP data

2.4.2. Groundwater Transport

A variety of aryl phosphates have been found in soil and water samples, especially those near major industrialized sites (e.g. Sheldon and Hites 1979; Williams et al. 1982; Ishikawa et al. 1985; Fukushima et al. 1992; Martínez-Carballo et al. 2007). With recent findings of DPP in wastewater in Spain (Rodil et al. 2012) and in flowback water from Alberta (He et al. 2017), there is potential for DPP to be introduced into the environment. To assess the potential environmental impacts of a DPP release at or into the near-subsurface, an analysis of retardation factors (equation 2.1) was conducted. We assumed that a linear sorption model was valid for DPP concentrations up to 500 mg/L. The retardation factor (equation 2.1) was calculated using the following:

$$R = 1 + \frac{\rho_b}{n} K_d \quad (2.1)$$

where R is the retardation factor [-], ρ_b is the dry bulk density [M/L³], n is the total porosity [-], and K_d is the distribution coefficient [L³/M] determined from our DPP sorption experiments.

To assess the impact to groundwater systems DPP may pose, we calculated a number of retardation factors for each type of soil observed and collected from the Fox Creek area by varying certain soil parameters. For this analysis, we assumed that organic-rich clay soils had a dry bulk density of 1.3 g/cm³ (Arshad et al. 1996) and a range of porosities between 0.5 and 0.8 (Freeze and Cherry 1979; Terzaghi et al. 1996; Obrzud and Truty 2018). The range of K_d values was taken from our experiments with MOR, GLC, and STGM, and ranged from 1.86 and 12.70 L/kg. We constructed an array of porosities between 0.5 and 0.8, testing every 0.01 value in between; similarly, we constructed an array of K_d values between 1.86 and 12.70 L/kg, testing

every 0.01 value in between. In total, 31 porosities and 1,085 K_d values were tested, resulting in 33,635 different retardation factors for high-organics, clay-dominated soils. We found that retardation factors for these clay-dominated soils varied dramatically, ranging from between 4.02 and 34.02. However, the stagnant moraine soil exhibited less of a range, varying only between 4.02 and 12.99. For more sandy material, we assumed that the dry bulk density was 1.7 g/cm^3 (Das 2008) and had a range of porosities between 0.25 and 0.45 (Das 2008). The range of K_d values was taken from our experiments with HFO and FLUV and ranged from 0.1 and 0.48 L/kg. Using a similar frequency of values above, 21 porosities and 39 K_d values were tested, resulting in 819 different retardation factors for sandy materials. We found that the retardation factors for more sandy-rich materials varied less than clay-dominated soils, varying between 1.38 and 4.26.

For comparison, we conducted a similar analysis on retardation factors for other aryl phosphates, including TPP. For TPP, $\log K_{OC}$ values ranged from 3.40 to 4.17 L/kg (Huckins et al. 1991; Anderson et al. 1993; Brooke et al. 2009). Other aryl phosphates with the DPP-moiety, such as EHDP ($\log K_{OC} = 3.98$), CDP ($\log K_{OC} = 3.94$), IDDP ($\log K_{OC} = 3.84$), IPDP ($\log K_{OC} = 3.77$), and TBDP ($\log K_{OC} = 3.68$), were not tested due to their similarity to TPP (Brooke et al. 2009). To calculate retardation factors from K_{OC} , we used the following equivalence equation (equation 2.2):

$$K_d = f_{OC} \times K_{OC} \quad (2.2)$$

where K_d is the distribution coefficient [L^3/M], f_{OC} is the fraction of organic carbon in the soil [-], and K_{OC} is the organic carbon partitioning coefficient [L^3/M]. Equation 2.2 was then substituted into equation 2.1 to calculate R .

We found that for TPP, the retardation factors for each soil varied greatly, but was consistently one or more orders of magnitude higher than for DPP (**Table 2.2**). This is consistent with the greater hydrophobic nature of TPP, compared to DPP (Brooke et al. 2009). Comparing the log K_{OC} values for the other aryl phosphates, this analysis suggests that the other aryl phosphates with the DPP-moiety would exhibit retardation factors near the median value of TPP, still suggesting stronger sorption when compared to DPP.

Soil	R (for DPP)			R (for TPP)		
	Min	Median	Max	Min	Median	Max
MOR	4.17	15.1	32.6	365.1	1,099.8	3,431.3
GLC	4.59	15.9	34.0	67.9	203.0	631.7
STGM	4.02	7.5	13.0	27.9	82.3	254.8
FLUV	1.49	2.5	4.20	10.4	29.3	89.5
HFO	1.38	2.4	4.26	---	---	---

Table 2.2: List of minimum, median and maximum retardation factors (R) for DPP, and TPP. For MOR, GLC, and STGM, porosities ranged from 0.5 to 0.8; for FLUV and HFO, porosities ranged from 0.25 to 0.45. Dry bulk density was assumed to be 1.3 and 1.7 g/cm³ for clay and sand, respectively. f_{oc} for soils taken from **Table A5**.

2.4.3. Toxicity of DPP

The toxicities of a variety of aryl phosphates, including DPP, have not been extensively studied. Toxicity data for these compounds are limited in terms of both number and quality. This study focuses mainly on acute toxicity of aryl phosphates to fish embryos. Due to the lack of available toxicological data or information on DPP, we conducted 96 h-LC₅₀ experiments with DPP for zebrafish embryos and determined the value to be 49.98 ± 7.06 mg/L (**Figure 2.2**). Using the US EPA ECOSAR (v2.0) software program, we estimated a fish 96 h-LC₅₀ of 33.5

mg/L, and a chronic value (ChV) of 3.6 mg/L (Mayo-Bean et al. 2017). These values are far higher than those found in FPW samples from the Fox Creek area, AB, Canada, which were estimated to be approximately 0.0037 mg/L (3.7 µg/L), and above those found by Rodil et al. (2012) in their wastewater samples (<0.01 mg/L). Direct comparison of our reported LC₅₀ on zebrafish embryos with values reported above is difficult; however, it may shed light on the relative magnitude of its toxicity.

Triphenyl phosphate (TPP) is among the most extensively studied, with studies on zebrafish indicating that TPP may result in developmental toxicity (Oliveri et al. 2015; Isales et al. 2015; Jarema et al. 2015), cardiotoxicity (McGee et al. 2013; Du et al. 2015), endocrine disruption (Liu et al. 2012), and bioaccumulation in tissues and organs (Wang et al. 2017). **Table 2.3** lists some 96 h-LC₅₀ values for various aryl phosphates on various fish species. Our results suggest that DPP is significantly less toxic than TPP, but its toxicity is comparable to some of the experimentally determined values for other aryl phosphates, such as IDDP and IPDP (**Table 2.3**).

Su et al. (2014) studied the cytotoxic effects of TPP and DPP on chicken embryonic hepatocytes. It has been found that DPP had less cytotoxic effect on chicken embryonic hepatocytes than its parent product TPP, but had a stronger ability to alter gene expression. Among the gene expression alterations that were significantly down-regulated were those associated with thyroid hormone regulation, glucose and fatty acid metabolism, and lipid/cholesterol metabolism (Su et al. 2014). Wang et al. (2016) detected amounts of DPP at significantly higher concentrations in the liver and intestine (up to 3 to 3.5 times) than its parent TPP in adult zebrafish. Muir and Grift (1981) studied the uptake and bioaccumulation of DPP in rainbow trout. They found that the bioconcentration factor (BCF) for DPP was between 0.29 and 2.5 (Muir and Grift 1981), indicating that it weakly bioaccumulates. Calculated BCF determined

by BCFBAF (v3.01) was 5.501 L/kg, somewhat consistent with the Muir and Grift (1981) study results. Van den Eede et al. (2016) speculated that because DPP is highly polar, it is likely to be cleared from the human body rapidly and has less potential to penetrate tissues by passive diffusion.

Our discussion above has focused mainly on short-term (acute) effects on fish, but long-term (chronic) effects may also be present. Using the US EPA ECOSAR (v2.0) program, we can estimate a ChV of ~3.6 mg/L that may result in significant toxic potential for a longer-term exposure. For other aquatic species, a daphnid 48 h-LC₅₀ and ChV were estimated to be 20.6 and 2.5 mg/L, respectively, whereas a 96 h-LC₅₀ and ChV for green algae as a representative aquatic plant can be estimated to be 21.5 and 6.7 mg/L, respectively. These LC₅₀'s and ChV's are both lower than those estimated for fish. This may indicate that DPP is less acutely toxic to aquatic ecosystems than other aryl phosphates, although longer-term studies, species sensitivity distribution studies, and the effects of sub-lethal longer-term exposures remain to be investigated. Therefore, the toxic potential of DPP on aquatic ecosystems remains unclear and requires further study.

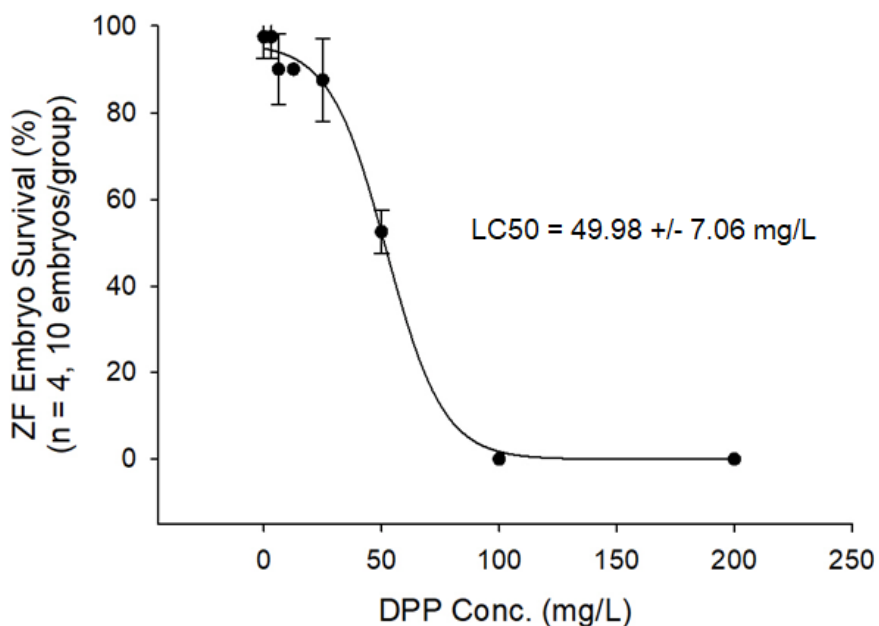


Figure 2.2: Zebrafish (ZF) embryo survival (%) vs. concentration of DPP (mg/L). The LC₅₀ determined was 49.98 ± 7.06 mg/L.

Compound	Rainbow Trout	Bluegill sunfish	Goldfish	Channel catfish	Killifish	Fathead Minnow	Sheepshead minnows
	<i>Oncorhynchus mykiss</i>	<i>Lepomis macrochirus</i>	<i>Carassius auratus</i>	<i>Ictalurus punctatus</i>	<i>Oryzias latipes</i>	<i>Pimephales promelas</i>	<i>Cyprinodon variegatus</i>
TPP	~0.26 to 0.85 ^[1,2,3,4,5,6]	0.78 ^[7]	0.7 ^[8]	0.42 ^[4]	1.2 ^[8]	~0.66 to 1.0 ^[2,4,9,10]	>0.32 ^[2]
CDP	---	---	---	---	1.3 ^[11]	---	---
IDDP	26 ^[12]	72 ^[12]	---	---	---	---	---
IPDP	~0.9 to 4.5 ^[12] ~0.59 to 1.7 ^[13]	29 ^[12] 12 ^[13]	---	>15	---	1.7 ^[12] ~8.5 to 35 ^[13]	---
TBDP	2.0 ^[12]	3.1 ^[12]	---	0.8 ^[12]	---	2.3 ^[12]	---

Table 2.3: 96 h-LC₅₀ (mg/L) values for various aryl phosphate compounds on various fish species. Only those values deemed valid are included.

1 Sitthichaikasem (1978), 2 Mayer et al. (1981), 3 Palawski et al. (1983), 4 Mayer and Ellersieck (1986), 5 IUCLID (2001), 6 OECD (2002), 7 Huckins et al. (1991), 8 Sasaki et al. (1981), 9 Admans et al. (2001), 10 Sinks and Schultz (2001), 11 UNEP (2002), 12 Cleveland et al. (1986), 13 Nevins and Johnson (1978)

2.5. Summary & Conclusions

This study aimed to determine the sorption behavior of diphenyl phosphate (DPP), an emerging contaminant, under a variety of environmentally relevant pH conditions and with both synthetic and natural sediment samples. Also evaluated was the potential environmental impact DPP may have if released into the groundwater. Batch sorption experiments, using a synthetic representative groundwater composition and five different sediment types, were conducted to determine the distribution coefficients (K_d) of DPP for each soil. Little toxicity data exists for DPP, so the 96 h-LC₅₀ for DPP on zebrafish embryos was determined to assess if DPP may be toxic to aquatic ecosystems.

Our results show that DPP has a low to very low degree of sorption, with K_d ranging from approximately 2 to 12 L/kg for clay-rich soil types (moraine, glaciolacustrine clay, stagnant moraine) and down to approximately 0.1 to 0.4 L/kg for sand-rich materials (HFO-coated sand, fluvial sand). Within the tested pH range (~5 to 9), most of the materials tested showed no significant pH-dependence on sorption and neither the Freundlich nor Langmuir equations were used or required to fit the data. Normalized to f_{OC} , the log K_{OC} value for DPP in this study was 2.30 ± 0.43 (1σ). We reason that the sorption of DPP onto the sediment type is dominated and controlled by its f_{OC} . The one exception, the clay-rich moraine, showed a decreasing trend of sorption with increasing pH. We hypothesize that because the moraine was dominated by clays, which become increasingly negative with increasing pH, the resulting repulsion of the deprotonated DPP molecule may have reduced sorption at the higher pH. Analysis of the retardation factors of DPP, compared to other TPP (and other aryl phosphates), showed that transport of DPP for various soil types is consistently lower than other aryl phosphates. For more sandy soils, the transport of DPP is near conservative (R is between 1.38 and 4.26) in some

cases. For more clay- and organic-rich soils, retardation factors range from approximately 4 to 34, which is at least an order of magnitude less than other aryl phosphates for the same soil type. By conducting DPP toxicity assays, we determined that the 96 h-LC₅₀ for zebrafish embryos was ~50 mg/L. Taken together with the cytotoxicity study of Su et al. (2014) on chicken embryonic hepatocytes, this suggests that DPP has the potential to impact aquatic ecosystems and possibly other non-aquatic organisms. Future studies should expand and focus on characterizing the toxicity of DPP on other organisms, including aquatic, avian, and mammalian species. They should also address both chronic and acute effects. Because of its low sorption potential, coupled with its known toxicity, DPP may pose a threat to groundwater aquifers and aquatic ecosystems in the event of a surface spill.

Acknowledgements

This research was funded by a Collaborative Research and Development Grant from the Natural Sciences and Engineering Research Council of Canada (NSERC) (CRDPJ 469308-14) to D. Alessi, G. Goss, and J. Martin, support from the Encana Corporation, and a Queen Elizabeth II Graduate Scholarship to S. Funk. We would like to thank K. Kasperski and X. Wang for their helpful comments during the writing of this manuscript, and A. Harms for his technical expertise. We would also like to thank two anonymous reviewers for improving the manuscript.

References

- Admans G, Takahashi Y, Ban S, Kato H, Abe H, Hanai S (2001) Artificial neural network for predicting the toxicity of organic molecules. *Bulletin of the Chemical Society of Japan* **74**: 2451 – 2461.
- Alberta Energy Regulator (n.d.) *Compliance Dashboard*. AER, Suite 1000, 250 – 5 Street SW, Calgary, Alberta, T2P 0R4, retrieved 06 February 2016 from:
<http://www1.aer.ca/compliancedashboard/index.html>

- Anderson C, Wischer D, Schmieder A, Spiteller M (1993) Fate of triphenyl phosphate in soil. *Chemosphere* **27**: 869 – 879.
- Andresen JA, Grundmann A, Bester K (2004) Organophosphorus flame retardants and plasticizers in surface waters. *Science of the Total Environment* **332**: 155 – 166.
- Arshad MA, Lowery B, Grossman B (1996) Physical Tests for Monitoring Soil Quality. In: Doran JW, Jones AJ, editors. *Methods for assessing soil quality*. Madison, WI. p. 123 – 141.
- Boethling RS, Cooper JC (1985) Environmental fate and effects of triaryl and tri-alkyl/aryl phosphates esters. *Residue Reviews* **94**: 49 – 99.
- Bremner JM (1996) Nitrogen Total. In: Sparks (ed.) *Method of soil analysis. Part 3: Chemical methods*. SSSA Book Ser. 5. SSSA, Madison, WI, p. 1085 – 1122.
- Brooke DN, Crookes MJ, Quarteman P, Burns J (2009) An overview of the environmental risk evaluation reports for aryl phosphate esters. Environment Agency, Rio House, Waterside Drive, Aztec West, Almondsbury, Bristol, UK.
- Christ P, Lindsay AG, Vormittag SS, Neudörfel JM, Berkessel A, O'Donoghue AC (2011) pK_a values of chiral Brønsted acid catalysts: Phosphoric acids/amides, sulfonyl/sulfonyl imides, and perfluorinated TADDOLs (TEFDDOLs). *Chemistry A European Journal* **17**: 8524 – 8528.
- Cleveland L, Mayer FL, Buckler DR, Palawski DU (1986) Toxicity of five alkyl-aryl phosphate ester chemicals to four species of freshwater fish. *Environmental Toxicology and Chemistry* **5**: 273 – 282.
- Das BM (2008) *Advanced Soil Mechanics*. Taylor & Francis, London, UK and New York, NY.
- David MD, Seiber JN (1999a) Accelerated hydrolysis of industrial organophosphates in water and soil using sodium perborate. *Environmental Pollution* **105**: 121 – 128.

- David MD, Seiber JN (1999b) Analysis of organophosphate hydraulic fluids in U.S. Air Force base soils. *Archives of Environmental Contamination and Toxicology* **36**: 235 – 241.
- Du Z, Wang G, Gao S, Wang Z (2015) Aryl organophosphate flame retardants induced cardiotoxicity during zebrafish embryogenesis: By disturbing expression of the transcriptional regulators. *Aquatic Toxicology* **161**: 25 – 32.
- Erickson RJ (2010) Toxicity Relationship Analysis Program (TRAP) Version 1.21. US Environmental Protection Agency, Washington DC, EPA/600/C-11/002.
- Freeze RA, Cherry JA (1979) *Groundwater*. Prentice Hall, Englewood Cliffs, NJ.
- Fukushima M, Kawai S, Yamaguchi Y (1992) Behavior of organophosphoric acid triesters in Japanese riverine and coastal environment. *Water Science & Technology* **25**: 271 – 278.
- He Y, Flynn SL, Folkerts EJ, Zhang Y, Ruan D, Alessi DS, Martin JW, Goss GG (2017) Chemical and toxicological characterization of hydraulic fracturing flowback and produced water. *Water Research* **114**: 78 – 87.
- Howard PH, Deo PG (1979) Degradation of aryl phosphates in aquatic environments. *Bulletin of Environmental Contamination and Toxicology* **22**: 337 – 344.
- Huckins JN, Fairchild JF, Boyle TP (1991) Role of exposure mode in the bioavailability of triphenyl phosphate to aquatic organisms. *Archives of Environmental Contamination and Toxicology* **21**: 481 – 485.
- Isales GM, Hipszer RA, Raftery TD, Chen A, Stapleton HM, Volz DC (2015) Triphenyl phosphate-induced developmental toxicity in zebrafish: Potential role of the retinoic acid receptor. *Aquatic Toxicology* **161**: 221 – 230.

- Ishikawa S, Taketomi M, Shinohara R (1985) Determination of trialkyl and triaryl phosphates in environmental samples. *Water Research* **19**: 119 – 125.
- IUCLID (2001) IUCLID Dataset for triphenyl phosphate. European Chemicals Bureau, European Commission.
- Jarema KA, Hunter DL, Shaffer RM, Behl M, Padlla S (2015) Acute and developmental behavioral effects of flame retardants and related chemicals in zebrafish. *Neurotoxicology and Teratology* **52**: 194 – 209.
- Liu X, Ji K, Choi K (2012) Endocrine disruption potentials of organophosphate flame retardants and related mechanisms in H295R and MVLN cell lines and in zebrafish. *Aquatic Toxicology* **114**: 173 – 181.
- Martínez-Carballo E, González-Barreiro C, Sitka A, Scharf S, Gans O (2007) Determination of selected organophosphate esters in the aquatic environment of Austria. *Science of the Total Environment* **388**: 290 – 299.
- Mayer FL, Adams WJ, Finley MT, Michael PR, Mehrle PM, Saeger VW (1981) Phosphate ester hydraulic fluids: An aquatic environmental assessment of Pydrauls 50E and 115E. *Aquatic Toxicology and Hazard Assessment: 4th Conference, ASTM STP 737, American Society for Testing and Materials*: 103 – 123.
- Mayer Jr, FL, Ellersieck MR (1986) Manual of acute toxicity interpretation and database for 410 chemicals and 66 species of freshwater animals. US Fish and Wildlife Service, Resource Publication 160, Washington DC.
- Mayo-Bean K, Moran-Bruce K, Meylan W, Ranslow P, Lock M, Nabholz JV, Von Runnen J, Cassidy LM, Tunkel J (2017) Ecological Structure Activity Relationship Model (ECOSAR): Estimating toxicity of industrial chemicals to aquatic organisms using the EROSAR class program.

- McGee SP, Konstantinov A, Stapleton HM, Volz DC (2013) Aryl phosphate esters within a major PentaBDE replacement product induce cardiotoxicity in developing zebrafish embryos: Potential role of the aryl hydrocarbon receptor. *Toxicological Sciences* **133**: 144 – 156.
- Muir DCG, Grift NP, Blouw AP, Lockhart WL (1980) Environmental dynamics of phosphate esters I: Uptake and bioaccumulation of triphenyl phosphate by rainbow trout. *Chemosphere* **9**: 525 – 532.
- Muir DCG, Grift NP (1981) Environmental dynamics of phosphate esters II: Uptake and bioaccumulation of 2-ethylhexyl phosphate and diphenyl phosphate by fish. *Chemosphere* **10**: 847 – 855.
- Nelson DW, Sommers LE (1996) Total carbon, organic carbon and organic matter. *In*: Sparks (ed.) Method of soil analysis. Part 3: Chemical methods. SSSA Book Ser. 5. SSSA, Madison, WI, p. 961 – 1010.
- Nevins MJ, Johnson WW (1978) Acute toxicity of phosphate ester mixtures to invertebrates and fish. *Bulletin of Environmental Contamination and Toxicology* **19**: 250 – 256.
- Obrzud RF, Truty A (2018) The hardening soil model – A practical guidebook. Z_soil.PC 100701 report, revised 8.04.2018. Zace Services Ltd.
- Oliveri AN, Bailey JM, Levin ED (2015) Developmental exposure to organophosphate flame retardants causes behavioral effects in larval and adult zebrafish. *Neurotoxicology and Teratology* **52**: 220 – 227.
- Organization for Economic Cooperation and Development (OECD)(2002) Triphenyl phosphate. SIDS Initial Assessment Report prepared for SIAM 15. Available from:
<http://www.inchem.org/documents/sids/sids/115866.pdf>.

- Palawski D, Buckler DR, Mayer FL (1983) Survival and condition of rainbow trout (*Salmo gairdneri*) after acute exposures to methyl parathion, triphenyl phosphate, and DEF. *Bulletin of Environmental Contamination and Toxicology* **30**: 614 – 620.
- Pawley SM, Atkinson N (2013) Surficial geology of the Little Smoky area (NTS 83K/NW). Energy Resources Conservation Board, ERCB/AGS Map 564, scale 1:100 000.
- Reemtsma T, Quintana JB, Rodil R, García-López M, Rodríguez I (2008) Organophosphorus flame retardants and plasticizers in water and air I: Occurrence and fate. *Trends in Analytical Chemistry* **27**: 727 – 737.
- Renberg L, Sundström G, Sundh-Nygård K (1980) Partition coefficients of organic chemicals derived from reversed phase thin layer chromatography: Evaluation of methods and application on phosphate esters, polychlorinated paraffins and some PCB-substitutes. *Chemosphere* **9**: 683 – 691.
- Rodil R, Quintana JB, Concha-Graña E, López-Mahía P, Muniategui-Lorenzo S, Prada-Rodríguez D (2012) Emerging pollutants in sewage, surface and drinking water in Galicia (NW Spain). *Chemosphere* **86**: 1040 – 1049.
- Roy WR, Krapac IG, Chou SFJ, Griffin RA (1992) Batch-type procedures for estimating soil adsorption of chemicals. EPA/530/SW-87/006-F, April 1992.
- Saeger VW, Hicks O, Kaley RG, Michael PR, Mieux JP, Tucker ES (1979) Environmental fate of selected phosphate esters. *Environmental Science & Technology* **13**: 840 – 844.
- Sasaki K, Takeda M, Uchiyama M (1981) Toxicity, absorption and elimination of phosphoric acid triesters by killifish and goldfish. *Bulletin of Environmental Contamination and Toxicity* **27**: 775 – 782.

- Sheldon LS, Hites RA (1979) Organic compounds in the Delaware River. *Environmental Science & Technology* **12**: 1188 – 1194.
- Sinks GD, Schultz TW (2001) Correlation of tetrahymena and pimpephales toxicity: Evaluation of 100 additional compounds. *Environmental Toxicology and Chemistry* **20**: 917 – 921.
- Sitthichaikasem S (1978) Some toxicological effects of phosphate esters on rainbow trout and bluegill. Iowa State University Dissertation.
- Su G, Crump D, Letcher RJ, Kennedy SW (2014) Rapid in vitro metabolism of the flame retardant triphenyl phosphate and effects on cytotoxicity and mRNA expression in chicken embryonic hepatocytes. *Environmental Science & Technology* **48**: 13511 – 13519.
- Terzaghi K, Peck RB, Mesri G (1996) *Soil Mechanics in Engineering Practice*. Wiley, New York, NY.
- United Nations Environment Programme (UNEP)(2002) SIDS dossier on diphenyl cresyl phosphate. Available from <http://www.inchem.org/pages/sids.html>.
- US Environmental Protection Agency (2012) Estimation Program Interface Suite™ for Microsoft® Windows, v4.11. United States Environmental Protection Agency, Washington, DC, USA.
- US Environmental Protection Agency (2016) Hydraulic fracturing for oil and gas: Impacts from the hydraulic fracturing water cycle on drinking water resources in the United States. EPA-600-R-16-236Fa.
- Utting DJ (2013) Surficial geology of the Fox Creek area (NTS 83K/SE). Energy Resources Conservation Board, ERCB/AGS Map 562, scale 1:100 000.
- van den Eede N, Ballesteros-Gómez A, Neels H, Covaci A (2016) Does biotransformation of aryl phosphate flame retardants in blood cast a new perspective on their debated biomarkers? *Environmental Science & Technology* **50**: 12439 – 12445.

- van der Veen I, de Boer J (2012) Phosphorus flame retardants: Properties, production, environmental occurrence, toxicity and analysis. *Chemosphere* **88**: 1119 – 1153.
- Wang G, Du Z, Chen H, Su Y, Gao S, Mao L (2016) Tissue-specific accumulation, depuration, and transformation of triphenyl phosphate (TPHP) in adult zebrafish (*Danio rerio*). *Environmental Science & Technology* **50**: 13555 – 13564.
- Wang G, Shi H, Du Z, Chen H, Peng J, Gao S (2017) Bioaccumulation mechanism of organophosphate esters in adult zebrafish (*Danio rerio*). *Environmental Pollution* **229**: 177 – 187.
- Wei G-L, Li D-Q, Zhuo M-N, Liao Y-S, Xie Z-Y, Guo T-L, Li J-J, Zhang S-Y, Liang Z-Q (2015) Organophosphorous flame retardants and plasticizers: Sources, occurrence, toxicity and human exposure. *Environmental Pollution* **196**: 29 – 46.
- Williams DT, LeBel GL (1981) A national survey of tri(haloalkyl)-, trialkyl- and triarylphosphates in Canadian drinking water. *Bulletin of Environmental Contamination and Toxicology* **27**: 450 – 457.
- Williams DT, Nestmann ER, LeBel GL, Benoit FM, Otson R (1982) Determination of mutagenic potential and organic contaminants of Great Lakes drinking water. *Chemosphere* **11**: 263 – 276.
- Zachara JM, Streile GP (1991) Use of batch and column methodologies to assess utility waste leaching and subsurface chemical attenuation. ERPI EN-7313, Project 2485-8 Interim Report, May 1991.

Chapter 3 – The sorption characteristics of metals, metalloids, and organic compounds in hydraulic fracturing flowback and produced water²

3.1. Introduction

With increasing demands on the energy sector, and the use of combined multi-stage and horizontal hydraulic fracturing techniques, there has been a recent surge in the development of unconventional hydrocarbon resources (Vengosh et al. 2013; Rivard et al. 2014). Hydraulic fracturing is a well stimulation technique aimed at enhancing the recovery of hydrocarbons from typically tight formations (e.g. shales, siltstones, etc.). The process involves injecting hydraulic fracturing fluid (HFF), an engineered fluid that is typically comprised of 90 to 97% water (by volume), ~2-10% proppants (by volume), and up to 2% chemical additives, into a well at pressures sufficient to fracture the hydrocarbon producing formation (Vidic et al. 2013; US EPA 2016). Although chemical additives in the HFF are only a small percentage of the fluid itself, they may still comprise of tens of thousands of liters for certain wells (Sjolander et al. 2011; US EPA 2015). The additives are typically a variety of chemicals mixed together, engineered to have specific characteristics to allow for the recovery of hydrocarbons, and can include friction reducers, gelling agents, biocides, surfactants, and others (Carter et al. 2013; Rogers et al. 2015). Once the formation of interest has been stimulated and the permeability has been enhanced, the well is shut-in, allowing for the HFF to imbibe the tight rock, releasing the trapped hydrocarbons (King 2012). The resulting fractures are held open by the proppant, which allows hydrocarbons locked within the formation to flow freely to the wellbore, and ultimately to the surface.

² This chapter includes contributions from Sean Funk, Chenxing Sun, Katherine Snihur, Konstantin von Gunten, Jonathan Martin, and Daniel S Alessi.

After the shut-in time, wastewater, called flowback and produced water (FPW), is then allowed to flow to the surface. FPW recovered from these operations is often briny, and contain numerous organic compounds, inorganic constituents, naturally occurring radioactive materials (NORMs), and the chemical additives injected or their downhole reaction, degradation, or breakdown products (Colborn et al. 2011; Warner et al. 2012, 2014; Drollette et al. 2015; DiGiulio and Jackson 2016; Alessi et al. 2017; He et al. 2017b). Typically, flowback water refers to the fluid produced immediately after opening the well, and is dominated by the HFF, but before the well starts producing significant quantities of hydrocarbons; produced water is defined as the fluid produced in conjunction with hydrocarbons (US EPA 2016). For the purposes of this study, we will consider both to be wastewater and make no distinction between them. Recently, the environmental risks that FPW may pose to shallow groundwater environments and surface water bodies has been discussed (e.g. Gehman et al. 2016). Due to the complexity of the chemicals added to the HFF, and the potential for reaction by-products to be produced during the stimulation process, evaluating the potential risks that FPW may pose to the environment is challenging.

There are few studies aimed at determining the sorption potential of compounds found in hydraulic fracturing related FPW to natural sediment or to soils. Manz et al. (2016) studied the sorption of 2-butoxyethanol (2-BE), a surfactant commonly found in hydraulic fracturing fluids, and furfural, a non-surfactant also found in hydraulic fracturing fluids, to shale and granulated activated carbon (GAC). The authors found that neither 2-BE nor furfural measurably sorbed onto the shale, but that they did sorb onto the GAC. For the latter, when the two compounds were mixed, 2-BE and furfural competed for sorption sites, resulting in a reduction of sorption for both compounds when compared to their mono-compound results, with furfural exhibiting

stronger sorption compared to 2-BE. The authors also found that sorption of these two compounds were influenced by temperature (between 20 and 65°C). For furfural, they found that at lower temperatures, there was greater sorption onto GAC, whereas for 2-BE, the opposite was observed (Manz et al. 2016). Salt concentration of the solution also impacted the sorption behavior of both compounds. The maximum furfural removal, at room temperature, was found to occur when there was no sodium chloride in solution, with the percentage of removal decreasing with increasing ionic strength (Manz et al. 2016). 2-BE was found to have the greatest percentage removal from a solution containing 0.1 mol/L sodium chloride, with increasing ionic strength having little effect on sorption (Manz et al. 2016). They concluded that the effect of sodium chloride concentration on sorption varied depending on the compound, with sorption enhanced for anionic compounds and having negligible effect for non-ionized compounds (Manz et al. 2016), consistent with previous findings for fulvic acids (Randtke and Jepsen 1982).

Ye and Prigiobbe (2018) studied the effect of ionic strength on the sorption of Ba in porous media. Barium was chosen because of its normally elevated concentration in hydraulic fracturing FPW and as an analogue for Ra, a radionuclide commonly found in hydraulic fracturing-derived wastewater. Although the sorption of Ba has been studied before (e.g. Zhang et al. 2001; Sajih et al. 2014), it had not been studied at the elevated ionic strengths typical of FPW. Both batch sorption experiments and column transport experiments were carried out, with goethite used as the porous medium. Ye and Prigiobbe (2018) found that in the batch experiments, sorption was measurable at a pH >5 at a temperature of 25°C, and a pH of 6 at 65°C, with sorption increasing with increasing pH. Below a pH of 5, there was negligible sorption of Ba onto the goethite. The ionic strength of the solution was shown to systematically decrease sorption, and at a concentration of 3 mol/kg NaCl, sorption was almost negligible.

Following the batch sorption experiments, the authors conducted column transport experiments at pH between 7 and 8. Unlike the results of the batch experiments, there was negligible sorption observed in the columns. Based on their observations, they speculated that if congeners of Ba (such as Ra, Ca, Mg, and Sr) were introduced into a soil environment where goethite was the dominant soil mineral, under similar pH conditions, these metals may not be retarded by the soil.

Chen et al. (2017) studied the co-sorption of As(V) and Se(VI) in various produced water from hydraulic fracturing in column transport experiments. To do so, columns were packed with soil collected from the Qingshankou formation, Songliao basin, China. Synthetic produced water, using chemistry replicated at 1, 14, and 90 days after well flowback, were flowed through the columns. The Day 90 synthetic produced water sample had the greatest ionic strength (and therefore total dissolved solids, TDS), and the lowest pH of the three solutions used. They found that for experiments using the Day 1 and Day 14 produced water, there were rapid breakthroughs and long tailings for both As and Se, but this was reduced for the Day 90 solution, likely due to the elevated ionic strength (Chen et al. 2017). They suggested that the extremely high ionic strength in the Day 90 solution reduced the likelihood of non-equilibrium transport (Chen et al. 2017). Chen et al. (2017) also found that solution chemistry, specifically pH and ionic strength, significantly affected the sorption and desorption of As and Se. They found that sorption of As(V) onto soil was markedly less for their Day 14 solution, whereas the sorption of Se(VI) increased with increasing ionic strength (Chen et al. 2017).

McLaughlin et al. (2016) studied the biodegradation, sorption, and potential co-contaminant interactions of several commonly used hydraulic fracturing fluid chemicals, including glutaraldehyde (GA), polyethylene glycol (PEG) 400 and polyacrylamide (PAM). They conducted aerobic batch experiments on Julesburg sandy loam. They found in their co-

contaminant batch sorption experiments, with the addition of salt, the presence of a surfactant (such as PEG) substantially increased the mobility of other contaminants via co-solvent effects (McLaughlin et al. 2016). Microbial biodegradation was hindered by the presence of a biocide. However, they found that sorption of biocides (such as GA) onto soil may decrease its concentration in solution to below toxic levels, allowing microbes to biodegrade the organics in solution. As such, the authors found that there was a “lag period” whereby microbes were ineffective, due to the presence of biocides and/or high salt concentrations in solution, to degrade any organics in solution. This has the result of potentially increasing contaminant travel distances and times. They stress that future work must be directed toward studying mixtures and their co-contaminant interactions rather than individual compounds.

All the abovementioned studies conducted experiments using synthetic, laboratory-mixed flowback and produced water. Therefore, the full sorption potential of all the metals, metalloids, and organic compounds found in a complex, field-collected FPW sample, is not fully understood. Characterizing either the antagonistic or synergistic sorption reactions in the complex matrix of a real FPW sample is an important step forward in assessing the potential risk FPW may pose on the environment. In this study, we investigated for the first time the sorption behavior of several metals, metalloids, and organic compounds, simultaneously, using samples of FPW collected from fractured wells drilled into the Duvernay Formation, near Fox Creek, Alberta, Canada.

3.2 Materials

3.2.1 Aqueous Solutions

Two flowback and produced water (FPW) samples from different wells conducting hydraulic fracturing operations within the Duvernay Formation around the Fox Creek area, AB, were used in this study. The first FPW sample, referred to as Sample 1, was collected on

December 2016, from Pad 16-18-63-21W5, Well ID 100/12-30-063-21W5. This well was drilled to a true vertical depth (TVD) of approximately 3,200 m and a measured depth (MD) of approximately 6,600 m, yielding a horizontal section >3 km. The second sample, referred to as Sample 2, was collected on September 2016, from Pad 8-14-63-21W5, Well ID 103/01-12-063-21W5. The second well was drilled to a TVD of approximately 3,200 m and a MD of approximately 5,700 m, yielding a horizontal section >2.5 km. The two FPW samples were collected at different points in in the flowback cycle. Sample 1 was taken 1 h after flowback was initiated; Sample 2 was taken 8 h after flowback was initiated. Sample 1 was untreated and unfiltered, containing suspended solids, whereas Sample 2 was filtered and aerated to remove much of the dissolved iron in solution. Samples from each well were collected and stored in either large volume plastic pails or amber glass containers, the latter for organics characterization. FPW used in our experiments were taken from the large volume plastic pails. The basic chemistry of each FPW solution appears in **Table 3.1**.

To conduct column transport experiments, FPW samples were diluted with simulated groundwater. For the simulated groundwater used in the experiments, an electrolyte solution containing approximately 500 mg/L HCO_3^- , was made by adding NaHCO_3 to Milli-Q distilled water. The composition of the simulated groundwater was based on groundwater samples collected around the Fox Creek area, AB (see **Table A2** in **Appendix A**).

	Sample 1 (mg/L)	Sample 2 (mg/ L)
Time after flowback	1 hour	8 hours
Cl	83,800	115,300
Na	47,900 ± 534	50,524 ± 214
Ca	7,170 ± 48.6	8,224 ± 54
Ba	5.41 ± 0.0428	8.80 ± 0.10
K	1,340 ± 9.23	2,003 ± 15
Sr	661 ± 3.46	873 ± 2.9
Mg	558 ± 3.84	752 ± 3.4
Mn	8.77 ± 0.224	6.07 ± 0.11
Br	164 ± 0.610	224 ± 3.6
B	69.1 ± 0.375	91.1 ± 2.1
Li	34.2 ± 0.285	44.8 ± 0.23
Fe	6.75 ± 0.0312	3.75 ± 0.070
Ni	< d.l.	2.18 ± 0.02
S	75.5 ± 3.29	73.4 ± 2.6
Pb	1.35 ± 0.0154	0.0978 ± 0.0031
Cu	2.61 ± 0.0228	< d.l.
Zn	3.70 ± 0.0972	< d.l.
TOC	4,712.2	402.0
TN	334.3	399.1

Table 3.1: Table of chemical analyses for FPW samples 1 and 2. Except for Cl, inorganic analyses were determined by ICP-MS/MS; Cl was determined with an ion chromatograph (IC). TOC and TN analyses were done with a TOC/TN analyzer. Additional analyses for Na, Mg, K, Ba, B, Sr and Li were done with an ICP-OES. Al, Si, P, Cr, Cu, Zn, As, Mo, and Cd were analyzed for, and were all below detection limits (unless otherwise stated).

3.2.2 Sediments

Three different sediment samples, each collected from around the Fox Creek, AB, area, were used in the batch experiments. These included a glaciolacustrine clay (GLC), moraine sediment (MOR), and a fluvial sand (FLUV). **Table 3.2** gives the elemental composition for each sediment sample used, while grain-size distributions, determined by using sieves, of these collected soil types are given in **Tables A3 and A4**. Images of the sediment used are provided in **Figure A2**. X-ray diffraction (XRD) and TN/TC/TOC (total nitrogen/total carbon/total organic carbon) results for each sediment collected are given in **Table A5**. Briefly, the results show that the moraine soil has the highest TOC content (8.92%) and is mostly comprised of clay minerals (muscovite and kaolinite). The glaciolacustrine clay is composed of more feldspars (albite and orthoclase) and lesser amounts of clay minerals (predominantly muscovite and chlorite), with a lower TOC content (GLC: 1.64%) compared to the moraine. The fluvial sand was dominantly comprised of quartz, with minor amounts of feldspar, clay minerals (muscovite and kaolinite), and some carbonates and pyrite. Not surprisingly, analyses of the fluvial sand indicate that it has the lowest TOC (0.23%) and TN (0.02%) of all the collected samples. MOR has the largest cation exchange capacity (CEC), dominated by Ca^{2+} , followed by GLC, and FLUV has the lowest CEC (**Table 3.3**).

For FLUV, additional physical soil parameters were determined for the column experiments. Two cylindrical columns were packed with FLUV, and the porosity and dry bulk density were determined for both columns (**Table 3.4**). With the use of a constant-head permeameter, the hydraulic conductivity of the columns was estimated to be approximately 1×10^{-6} m/s.

Element	GLC	MOR	FLUV
Li	37.8	27.0	24.0
B	46.9	51.6	38.7
Na	5,439	1,557	5,166
Mg	1,927.8	858.8	220.0
Al	19,926	19,485	10,159
Si	301,357	298,073	231,972
K	13,375	6,333	1,1104
P	586.3	640.3	364.7
S	141.9	485.6	68.0
Ca	501.0	2,229.8	51.9
V	86.3	56.5	50.0
Cr	46.3	24.0	27.7
Mn	168.1	138.6	80.6
Fe	23,324	15,385	9,885
Co	4.8	4.4	2.2
Ni	14.1	36.8	6.4
Cu	8.9	10.5	2.5
Zn	45.9	48.0	33.6
Sr	13.9	71.4	5.6
As	7.0	8.2	3.4
Mo	1.6	2.2	0.7
Se	0.4	1.1	0.2
Cd	0.2	0.4	0.2
Ba	246.1	510.7	214.7
Ce	2.0	23.7	0.4
Pb	14.4	13.8	10.0
Th	1.6	2.9	0.4
U	2.0	3.4	1.7

Table 3.2: Elemental composition of the three different soil types used in this study. Units are in mg/kg.

	GLC	MOR	FLUV
Na ⁺ (cmolc/kg)	0.00 ± 0.00	0.00 ± 0.00	0.00 ± 0.00
Mg ²⁺ (cmolc/kg)	3.66 ± 0.16	4.77 ± 0.43	0.53 ± 0.00
Al ³⁺ (cmolc/kg)	1.51 ± 0.12	0.08 ± 0.01	0.00 ± 0.00
K ⁺ (cmolc/kg)	0.23 ± 0.03	0.36 ± 0.05	0.07 ± 0.02
Ca ²⁺ (cmolc/kg)	10.92 ± 0.61	52.02 ± 4.54	4.80 ± 0.15
Mn ²⁺ (cmolc/kg)	0.16 ± 0.01	0.16 ± 0.00	0.00 ± 0.00
Fe ²⁺ (cmolc/kg)	0.09 ± 0.00	0.01 ± 0.00	0.00 ± 0.00
H ⁺ (cmolc/kg)	0.48 ± 0.04	0.10 ± 0.01	0.00 ± 0.00
pH _{BaCl₂}	3.99 ± 0.02	4.68 ± 0.05	6.98 ± 0.01
pH _{H₂O}	5.24	6.26	7.59
CEC _{BaCl₂} (cmolc/kg)	17.05 ± 0.88	57.49 ± 5.01	5.40 ± 0.16

Table 3.3: Exchangeable cations, acidity and total CEC in cmol charge per kg dry sample (equal to cmol(+)/kg). Results expressed as average ± 1 standard deviation (n=3), where available.

Parameter	Column A	Column B
Porosity (-)	0.36	0.36
Dry Bulk Density (g/cm ³)	1.56	1.53

Table 3.4: Porosity and dry bulk density of FLUV in column A and B.

3.3 Methods

3.3.1 Experimental Methods

3.3.1.1 Batch Sorption Experiments

Batch sorption experiments on the three sediments studied here closely followed the methods reported in Roy et al. (1992) and Zachara and Streile (1991). A constant solids-to-solution (FPW diluted with simulated groundwater) ratio of 1:12 (~1 g clay to 12 mL solution) was applied to both the moraine and glaciolacustrine clay, and approximately 1:5 (~2.5 g sand to 12 mL solution) was used for the fluvial sand. Experiments were conducted in polypropylene vials. The pH of each vial was adjusted by adding small volumes of either concentrated HCl or NaOH (ranging from 1 M to 5 M) to the solution, until the pH of the solution was within ± 0.05 of the desired target. Additionally, the mass of each vial was measured before and after the pH probe was placed into solution to record any solution losses due to pH measurements. After the last pH adjustment, the vials were placed on a rotator for approximately 72 h to reach equilibrium. After this equilibration time, the pH of each tube was measured and recorded, and the sample was then centrifuged for 40 min at 10,000 g. The supernatant was then extracted from each vial using a plastic pipette tip to be analyzed for inorganic metals and organics.

3.3.1.2 Column Transport Experiments

Column transport experiments followed closely the guidelines set out by Zachara and Streile (1991) and Lewis and Sjöström (2010). Fluvial sand was the only sediment type used in the column transport experiments, and the experiment was performed in duplicate. The fluvial sand was packed into a 15 cm long, 2.5 cm diameter cylindrical glass column, adding approximately 1 to 5 mm at a time until full; this was done to better ensure a homogeneous

distribution of sand within the column (Oliveira et al. 1996; Bergström 2000; Lewis and Sjöström 2010). Before the experiment, the dry bulk density, porosity, and hydraulic conductivity of each column was measured. Dry bulk density of each column was determined gravimetrically by comparing the mass of the column filled with sand to the column empty. By comparing the mass of sand in each column to the total volume of the column, the dry bulk density could be calculated. Similarly, the pore volume, and by extension the porosity, of each column was determined gravimetrically by comparing the mass of the column before and after saturation. A constant-head permeameter test was conducted on each column to measure the hydraulic conductivity. To do so, a constant supply of water was allowed to fill a reservoir connected to each column, and a constant head difference was set up to drive the flow of water through the column. The volume of water that flowed out of the effluent end of the column was determined gravimetrically. By rearranging Darcy's Law, the hydraulic conductivity (K) can be estimated by using equation 3.1:

$$K = \frac{q}{A\nabla h} \quad (3.1)$$

where Q is the volumetric flux [L^3/T], A is the cross-sectional area of the column [L^2], and ∇h is the hydraulic gradient [-].

After the necessary hydraulic parameters were determined for each column, both columns were connected to a high-precision peristaltic pump (Ismatec IP-12). The fluid flowed through polyethylene vacuum tubing and into the columns, and columns were bottom-fed such that the average linear groundwater velocity would be approximately 1 m/d. The column was allowed to saturate and equilibrate with simulated groundwater for several weeks in a closed system, after which the influent reservoir was switched to a 1:5 diluted FPW stock solution. The reservoir

containing the diluted FPW stock, the columns, and all the tubing were wrapped in aluminum foil to prevent potential photodegradation of organic constituents of the FPW. The total duration of the experiment was 21.8 days. Halfway during the experiment, the influent diluted FPW reservoir was changed. Effluent from each column was then collected for both inorganic and organic analyses. For the inorganic analyses, approximately 1 mL was collected and filtered through a 0.20 μm Nylon membrane. For the first two days, effluent was collected approximately every hour, after which, the sampling schedule was reduced to three times a day for the following two days, which was further reduced to once a day for the duration of the experiment. The aliquots were immediately acidified with 6 μL of 70% nitric acid to prevent metal sorption onto the polypropylene vials used to store them. For the organic analyses, approximately 5-6 mL of effluent was collected and stored in glass vials. Between one and three samples of effluent were collected each day for organic analysis. No filtering or acidification were done to these samples. All samples collected were stored in a 4°C refrigerator until analysis.

3.3.2 Analytical Methods

3.3.2.1 Soil Analyses

We conducted X-ray diffraction (XRD) analyses to determine the mineralogical makeup of the studied soil samples. XRD was conducted using a Rigaku Ultima IV with a cobalt source with data collected from a 2θ range from 5° to 90°. The JADE 9.5 analysis package (KS Analytical Systems) was used to fit the resultant diffraction patterns.

Soil analyses for TN (total nitrogen), TC (total carbon), and TOC (total organic carbon) were determined using dry flash combustion following the method outlined by Nelson and Sommers (1996) and Bremner (1996), using a Costech Model EA 4010 Elemental Analyzer. A known mass of soil was placed in a combustion chamber containing Cr-(III) oxide and

cobaltous/ic oxide silver catalysts. Upon the addition of oxygen into the combustion chamber, the temperature was increased from approximately 1020°C to between 1800 and 2000°C. During combustion, the nitrogen (N) and carbon (C) in the sample are converted into N₂ or NO_x (which is later reduced to N₂) and CO₂, respectively. The N₂ and CO₂ gases are then collected, separated, run through a chromatographic column and detected quantitatively using a thermal conductivity detector.

To determine the elemental composition of each soil studied, air-dried samples were digested by a method described in detail in von Gunten et al. (2017). For each sample, 0.1 g of sample was pre-treated with concentrated H₂O₂ and HNO₃ (1 h at 25°C, followed by 1 h at 130°C) to digest organic matter and then further treated with concentrated HF (overnight, 130°C). The residual material was then treated with a 3:1 mixture of concentrated HCl and HNO₃ (4 h at 175°C). The sample was then diluted to 2% HNO₃ and 0.5% HCl, filtered (0.2 µm) and analyzed using an Agilent 8800 Triple Quadrupole inductively coupled mass spectrometer (ICP-MS/MS).

Air-dried samples (10 g) were mixed with ultrapure water at a ratio of 1:2 mass:volume and mixed for 30 min to determine the pH (Kalra 1995). The cation exchange capacity (CEC) was determined by the exchangeable cation addition method (Hendershot and Duquette 1986). For this purpose, 1 g of air-dried sample was suspended in 50 mL of 0.1 M BaCl₂ for 2 h. The sample was then centrifuged (2000 g, 10 min) and the supernatant filtered (0.2 µm) and analyzed for Na, Mg, Al, K, Ca, Mn, and Fe by ICP-MS/MS. Exchangeable acidity was determined by the measurement of pH of the supernatant. The CEC was then calculated according to $CEC = [H^+] + [Na^+] + [K^+] + [Mg^{2+}] + [Ca^{2+}] + [Mn^{2+}] + [Fe^{2+}] + [Al^{3+}]$ (Stuanes et al. 1984).

3.3.2.1 Solution Analyses

Dissolved metals in aqueous solution were analyzed by ICP-MS/MS. Samples were diluted into 10 mL subsamples and refrigerated until analysis. For quantification of sodium and chloride, samples and standards were prepared in a matrix of 2% HNO₃, and samples were diluted to a ratio of 1:160 of sample to matrix. Standards covered a range of 0.1-150 ppm. For all other elements, samples and standards were prepared in a matrix of 2% HNO₃; 2,000 ppm NaCl was added to the standards to create a matrix similar to the diluted seawater and FPW samples. In this case, samples were diluted to a 1:16 ratio of sample to matrix, and standards covered a range of 0.0005-120 ppm in three tiers to accommodate varying concentration levels within the samples. The ICP-MS/MS measurements were made using various collision/reaction gases. **Table B1** indicates the measured masses in Quadrupole 1 (Q1) and Quadrupole 2 (Q2) and the used collision or reaction gases to eliminate isobaric interferences. Indium was used as an internal standard to account for instrumentation drift for each analysis across all collision/reaction gases used.

For analysis of dissolved organics, all water samples and laboratory blanks (~10 mL) were filtered using a 0.45 µm polytetrafluoroethylene filters (Millipore, Billerica, MA), and then immediately transferred to a 10 mL glass auto-sampler bottle. 1 mL of water from each sample or blank was directly injected to an in-line solid phase extraction (SPE) coupled with high performance liquid chromatography (HPLC) (ARIA MX, Thermo Fisher Scientific, San Jose, CA) and an Orbitrap Elite hybrid mass spectrometer (MS) (Thermo Fisher Scientific) instrument package. A Hypersil Gold aQ C18 column (20 × 2.1 mm, 12 µm particle size, Thermo Fisher Scientific) was used as the in-line SPE column. Trapped analytes were eluted from the SPE directly to the C18 analytical column (Poroshell 120 EC-C18, 3.0 × 50 mm, particle size 2.7 µm,

Agilent Technologies) through a six port, two-position valve. The mobile phase was composed of 25 mM ammonium acetate in water and methanol. The total analytical time was 35 min, and the valve switched at 3.00 min from the “loading” to “eluting” position (see **Table B2**). The Orbitrap MS was operated in electrospray positive ion mode. Ionization potential was set at 3.8 kV, while the sheath, aux, and sweep gas flows were set to 40, 28, and 2 (arbitrary units), respectively. Vaporizer and capillary temperatures were at 350°C and 325°C, respectively. Acquisition was performed in full scan mode (m/z 100 to 1000) at 2.3 Hz with resolving power set to a nominal value of 120,000 at full width half-maximum at m/z 400. Within the same analysis, tandem mass spectrometry (MS/MS) was performed using collision-induced dissociation at two energies (CID 28 and 35 eV) and higher-energy collision dissociation (HCD 60 eV) with a nominal resolving power of 60,000.

3.4 Results & Discussion

3.4.1 Batch sorption of inorganic components

Overall, with all the tested soil types, sorption of the inorganic constituents was low, with linear distribution coefficient (K_d) values for most inorganic constituents <2.5 L/kg. The majority of the inorganic constituents that were measured exhibited linear sorption trends (**Figure 3.1; Figure B1**), most having a high (>0.90) coefficient of determination (R^2) (**Table 3.5**). However, some variation in the data was observed, possibly due to uncertainties in the analytical measurements, or due to variations in ionic strength caused by diluting the FPW with a low TDS electrolyte solution. A few elements, notably Sr, exhibited non-linear sorption behavior. In these cases, Freundlich and Langmuir equations were fit to the data (**Figure 3.1; Table 3.6; Appendix B**). Distribution coefficients values for all soil types typically had single digit values or lower (**Table 3.5**). Some trends can be observed comparing the soil types. The MOR usually exhibited the largest percentage of mass removal, corresponding to the largest K_d values; GLC exhibited

the second most sorption, followed lastly by the FLUV (**Table 3.5**). This trend was expected, and likely follows the percentage of clay minerals and/or organic matter in each soil type.

Further, with the exception of Na, K, and Cu in FPW Sample 1, the fluvial sand exhibited very low degrees of sorption, with K_d values below 1 for many of the metals (**Table 3.5**); for the fluvial sand experiments, FPW Sample 2 exhibited generally lower sorption as compared to Sample 1.

By comparing the same inorganic constituent between the two different FPW samples, where possible, some additional trends are shown. Generally, with some exceptions, K_d values are higher in Sample 1 compared to Sample 2. We speculate this likely has to do with the differences in TDS, with Sample 1 having a TDS of 144,500 mg/L, whereas Sample 2 has a TDS of 168,200 mg/L. Increased salinity in solution leads to lower chemical potentials for individual ions, reducing their reactivity (Hückel 1924), and thus this difference between Samples 1 and 2 is likely sufficient to cause a measurable reduction in metals sorption to each soil type.

Element	Sample 1 K_d (L/kg) [R^2]			Sample 2 K_d (L/kg) [R^2]		
	MOR	GLC	FLUV	MOR	GLC	FLUV
Sr	N.L.	1.62 [0.979]	0.91 [1.000]	N.L.	1.25 [0.7112]	0.38 [0.959]
Li	2.08 [0.976]	1.18 [0.751]	0.76 [0.975]	1.66 [0.940]	0.48	0.41 [0.982]
B	2.36 [0.934]	1.77 [0.972]	0.59 [0.892]	1.52 [0.889]	1.47	0.54 [0.906]
Na	4.94 [0.981]	6.49 [0.990]	2.66 [0.972]	---	---	0.12 [0.941]
Mg	0.95 [0.813]	0.57 [0.934]	0.89 [0.987]	---	---	0.45 [0.943]
S	1.43 [0.910]	0.91 [0.791]	0.54 [0.877]	0.75 [0.874]	0.01	0.63 [0.952]
K	1.41 [0.980]	1.31 [0.829]	1.09 [0.973]	N.L.	0.58	0.48 [0.991]
Ca	1.66 [0.985]	1.13 [0.959]	0.80 [0.987]	---	---	0.41 [0.927]
Mn	0.89 [0.656]	---	---	---	---	---
Br	0.90 [0.960]	0.95 [0.968]	0.70 [0.985]	---	---	0.40 [0.906]
Ni	---	---	---	53.5 [0.988]	29.8 [0.705]	3.70 [0.941]
Cu	---	---	2.20 [0.928]	---	---	---

Table 3.5: Linear K_d (L/kg) values for each corresponding sediment type used in this study, for each element analyzed. N.L. = Non-linear isotherm(s) were utilized; --- = indicates that a K_d value could not be calculated. R^2 values are provided in brackets.

Sr	Sample 1	Sample 2
Freundlich parameters		
K_F	181.34	127.03
n	3.88	3.25
R^2	0.7288	0.8988
Langmuir parameters		
Double-reciprocal		
K_L	0.022	0.043
M	940.23	749.27
R^2	0.9236	0.8568
Traditional		
K_L	0.055	0.0062
M	836.38	1298.87
R^2	0.9784	0.8161

Table 3.6: Freundlich and Langmuir parameters for Sr for Samples 1 and 2, including R^2 values of fit.

3.4.1.1 Strontium

Strontium is found at high concentration (>650 mg/L) in both FPW samples and the mobility of strontium in the soil environment has been the subject of a great deal of study (e.g. Juo and Barber 1970; Ames and Rai 1978; Streng and Peterson 1989). Cation exchange capacity (CEC) was found to be a primary soil parameter in determining the magnitude of Sr sorption (Ames and Rai 1978; Lefevre et al. 1993; McHenry 1958; Serne and LeGore 1996; US EPA 1999). However, other factors have been identified. Rhodes (1957) studied the effect of solution pH and ionic strength on the sorption of Sr onto soils containing carbonate minerals and montmorillonite and found that increasing the pH from 6 to 8 and finally to 10, resulted in increasing K_d values of approximately 5, 10, and 120 L/kg, respectively, whereas increasing ionic strength resulted in a dramatic reduction in sorption. For a clayey soil, Powell et al. (2015) determined K_d values of 8.05 ± 0.62 L/kg at 0.1 M NaCl, and 32.06 ± 3.62 L/kg at 0.02 M NaCl; for a sandy soil, they determined K_d values of 6.02 ± 0.14 L/kg at 0.1 M NaCl, and 5.86 ± 0.35 L/kg at 0.02 M NaCl. These results show that for clayey soils, ionic strength had a negative impact on Sr sorption, consistent with many studies (e.g. Prout 1958; Keren and O'Connor 1983; Chen and Hayes 1999; Yu et al. 2015), whereas ionic strength did not have a measurable effect on Sr sorption to the sandy soil.

Chen and Hayes (1999) studied the sorption of Sr onto various clay and sandy materials, including quartz, kaolinite, illite, hectorite, and montmorillonite as a function of pH and ionic strength. They observed that clay minerals, such as illite, sorbed Sr more strongly than quartz, consistent with the results of Bencala et al. (1983). Akiba and Hashimoto (1990) studied the sorption of Sr onto various types of rocks and minerals. For those relevant to our study, they found that muscovite and chlorite strongly sorbed Sr ($K_d > 100$ L/kg), quartz and feldspars were intermediate ($K_d \approx 10$ L/kg), and limestone exhibited low sorption ($K_d \approx 1$ L/kg). Adeleye et al.

(1994) also studied the sorption of Sr onto various clay minerals, including varieties of kaolinite and montmorillonite. They found that Ca-varieties of kaolinite sorbed Sr more strongly than Na-varieties, with montmorillonite preferred over kaolinite (Adeleye et al. 1994). Patterson and Speol (1981) found that K_d values for Sr on quartz was low (0.4 L/kg), moderate for feldspar, biotite, and muscovite (between 2.6 and 4.7 L/kg), and high for biotite altered to vermiculite (37 L/kg).

Interestingly, Chen and Hayes (1999) also found that there was a dependence on Sr sorption on the concentration of competing ions in solution. They inferred that there was weaker, outer-sphere bonding between sorbed Sr and the solid surface, and as a result, competition between ions in solution, namely Na^+ , Mg^{2+} , and Ca^{2+} , would displace sorbed Sr, resulting in enhanced metal mobility. These results were consistent with Patterson and Speol (1981), Keren and O'Connor (1983), and Liu et al. (1995), all of whom found that divalent cations competed with Sr for sorption sites more effectively than monovalent cations. Powell et al. (2015) likewise studied the sorption of radium (Ra) and Sr onto two soils collected from the Savannah River Site located near Aiken, South Carolina, a clayey soil and a sandy soil. They conducted their experiments at a pH = 5.5, and within a range of ionic strengths between 0.02 and 0.1 M NaCl, the estimated salinity of the groundwater at the site. They found competition between Ra and Sr resulted in a decrease in sorption relative to their mono-element experiments (Powell et al. 2015), consistent with the competition observed in Chen and Hayes (1999).

Many studies have also found that Sr sorption data are fit well by Freundlich and/or Langmuir isotherms (e.g. Yu et al. 2015; Berns et al. 2018) (for definitions of variables, see **Appendix B**). Yu et al. (2015) studied the sorption of the radionuclide ^{90}Sr onto Na-montmorillonite under a variety of conditions and fit the resulting sorption data with both

Freundlich and Langmuir isotherms. Comparing the Freundlich model parameters with those obtained in this study (**Table 3.6**), we observe that their K_F values are significantly lower (between 4 and 6) than those obtained here, although the values for n are comparable. The discrepancy in K_F may be due to the lower tested concentrations (<10 mg/L) of Sr in the Yu et al. (2015) study. For the Langmuir model parameters, the M values obtained in our study are considerably larger than those in Yu et al. (2015), whereas our K_L values are smaller (**Table 3.6**). This may suggest that the soils in our study have a greater capacity for sorbing Sr compared to the montmorillonite obtained from Zhejiang, China, but have diminished binding energies. Berns et al. (2018) studied the sorption of Sr onto agricultural soil, including a silty loam that was composed of illite (70%), kaolinite (12%), chlorite (9%), and smectite (9%). Comparing results, MOR exhibited a higher K_F value and lower n value compared to Berns et al. (2018) (**Table 3.6**). This may be due to the lower CEC of the silty loam (11 cmolc/kg) as compared to MOR (**Table 3.3**).

When compared to many published literature values, our results suggest that Sr sorption onto all three soil types tested was suppressed. We argue that the high salt concentrations in the FPW (effectively ionic strength) had a negative impact on the extent of Sr sorption by decreasing the extent of the electric field around the charged surfaces of sediment minerals (Rhodes 1957; Prout 1958; Chen and Hayes 1999; Powell et al. 2015; Yu et al. 2015). Additionally, high concentrations of competing cations (e.g. Na^+ , K^+ , Mg^{2+} , Ca^{2+}) in the FPW may have acted to further suppress sorption (Chen and Hayes 1999; Powell et al. 2015). The environmental implications of our study suggest that Sr is likely to be more mobile in the soil and groundwater environment in the case that high salinity FPW is spilt on the surface.

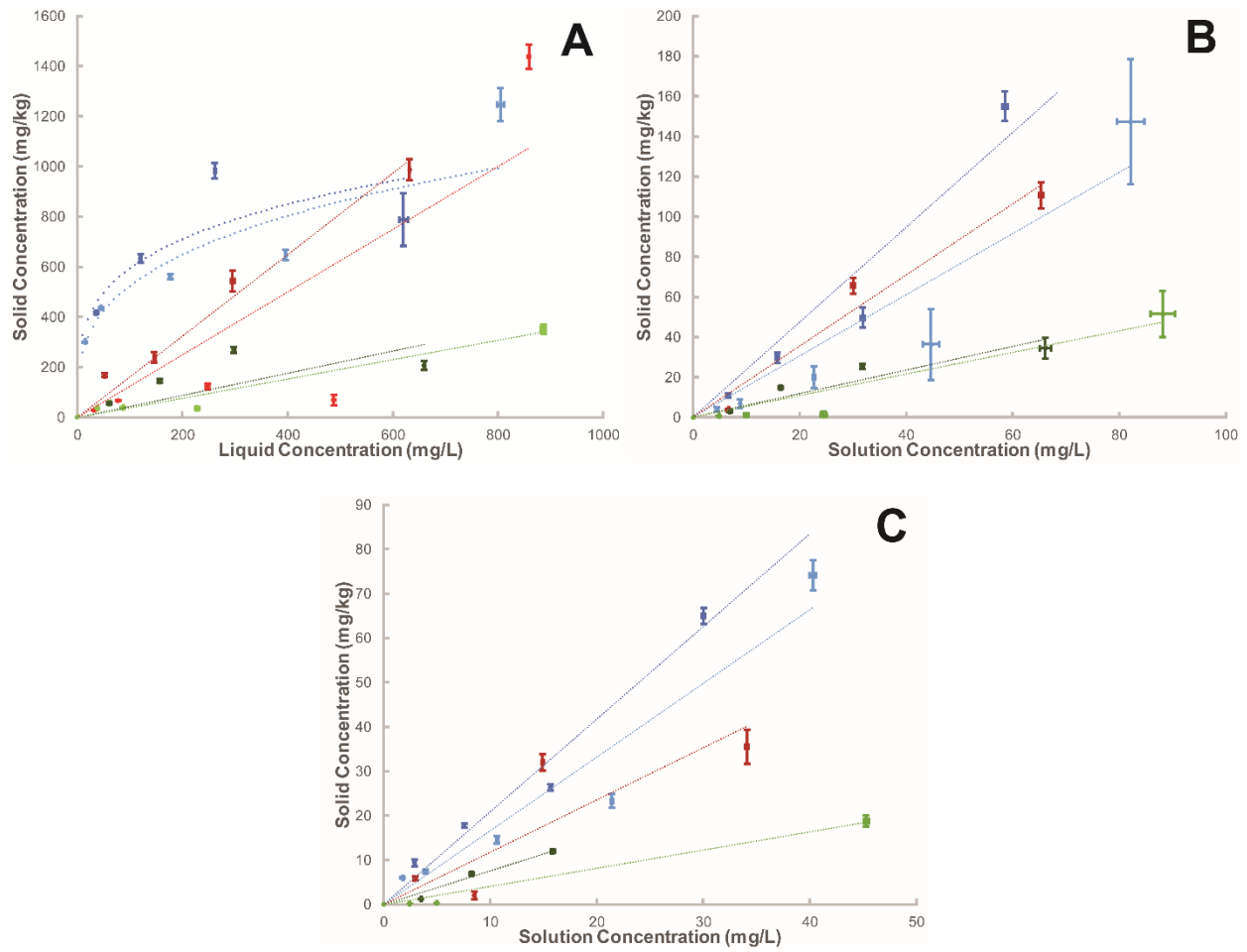


Figure 3.1: Sorption isotherms for A) strontium; B) boron; C) lithium, for MOR (blue), GLC (red), and FLUV (green). Dark variations denote Sample 1 experiments; light variations denote Sample 2 experiments. Freundlich curves are plotted for Sr MOR samples; all others are fitted with linear trends.

3.4.1.2 Boron

Boron is an essential micronutrient found naturally in the soil and groundwater environments. Boron also has many potential anthropogenic sources, including from fertilizers and herbicides, among others. Recently, the sorption of B onto soils has been raised as an important consideration, as elevated concentrations of B found in Alberta soils have been found to have adverse effects on plants and wildlife (Alberta Environment and Parks (AEP) 2015). Boron has been observed to sorb onto clay minerals through ligand exchange, i.e. chemisorption, and weakly through anion exchange (Goldberg et al. 1993; Su and Suarez 1995; Goldberg 1997, 1999). Ryan et al. (1977), Gupta et al. (1985), Mahmood-ul-Hassan et al. (2006), and Janik et al. (2015) all studied the sorption of B onto various types of soils. In many cases (e.g. Gupta et al. 1985), sorption of B was non-linear, and a Langmuir equation was used fit to the data. However, looking at the lower concentration spectrum, linear K_d values can be estimated. For a variety of soil types, ranging from clay, clay loam, silt loam, loam, and sandy loam, the values of K_d for B range from 0.39 to 5.23 L/kg, with many of the values between 1.0 and 2.0 L/kg (Ryan et al. 1977; Gupta et al. 1985; Mahmood-ul-Hassan et al. 2006; Janik et al. 2015). Typically, coarser-grained material had lower K_d values, whereas finer-grained material had higher values due to surface area effects.

Communar et al. (2004) studied the adsorption of B onto a loamy sand, where the predominant clay mineral in the soil was montmorillonite, at a variety of pH levels, ranging from 7 to 10. They found that the B sorption capacity of the soil was independent of pH (within the studied range), but that sorption of B onto the soil depended slightly on the pH. Communar et al. (2004) also found that the maximum sorption of B was at a pH of 8.5, with a pH of 7 exhibiting the lowest observed sorption, and a pH of 10 exhibiting an intermediate level of sorption. Keren et al. (1981) and Keren and Mezuman (1981) studied the pH-dependence of B sorption onto

various types of clays. These authors found that for Ca-forms of montmorillonite, illite, and kaolinite, B sorption increased with increasing pH, between approximately 7.4 and 10. Additionally, Keren and O'Connor (1982) studied the effect of exchangeable ions (Ca^{2+} and Na^+) and ionic strength (between 0.02 and 0.36 M NaCl or CaCl_2) on B sorption onto Na- and Ca-varieties of montmorillonite and illite at a pH of 9. Generally, for all clay types investigated, increasing ionic strength increased B sorption, with Ca-varieties sorbing more than their Na counterparts (Keren and O'Connor 1982). They also found that the Na-montmorillonite was more affected by changes in ionic strength than the Ca-variety (Keren and O'Connor 1982). Based on their findings, they suggested that B sorbed onto clay particles at their edges rather than on the planar surfaces, and that the negative electric field around the clay particles is a major factor in controlling B sorption (Keren and O'Connor 1982). Goldberg et al. (1993) also studied the sorption of B onto various oxides, clays, and soils as a function of pH and ionic strength. They found that B sorption onto oxides and kaolinite peaked between pH 6 and 8.5 but decreased at a pH between 8.5 and 11; for B sorption on montmorillonite and other soils, the peak was observed at a pH of 9 (Goldberg et al. 1993). Ionic strength, which varied between 0.01 and 1.0 M NaCl, was shown to increase B sorption (Goldberg et al. 1993), consistent with Keren and O'Connor 1982). Goldberg et al. (1993) suggested that the effect of ionic strength argues for an inner-sphere adsorption mechanism for goethite, gibbsite, and kaolinite, but an outer-sphere adsorption mechanism for montmorillonite and other soils.

The sorption of B onto soils from Alberta has been also been studied recently (AEP 2015). Batch sorption experiments on two different Alberta reference soils, one fine-grained, one coarse-grained, were conducted (AEP 2015). The coarse-grained soil (sandy loam) contained ~18% clay and ~3% organic matter, while the fine-grained soil (clay loam) contained ~32% clay

and 4% organic matter. Both reference soils were collected within the A horizon (10 to 20 cm depth) at two locations within Alberta. They reported K_d values for the coarse-grained soil to be 0.70 L/kg, whereas the fine-grained soil had a higher K_d value, around 1.94 L/kg. They also conducted another set of experiments wherein they washed the soils several times to remove B from the soil prior to the experiments. This pre-washing step increased the sorption of B onto each soil, resulting in K_d values for the coarse- and fine-grained soils of 1.13 L/kg and 2.36 L/kg, respectively. The AEP (2015) study found K_d values that were similar to the abovementioned studies; they argued that, with respect to B sorption properties, the Alberta reference soils used were likely similar to the soils found in the other studied regions (e.g. New Mexico, California, Arizona, Punjab).

Comparing our results to those found in the AEP (2015) study may provide some valuable insights into B sorption behavior. With K_d values approximately 0.50 L/kg for our fluvial sand, and values that range from between approximately 1.50 and 2.40 L/kg for our clay-rich soils (**Table 3.5; Figure 3.1B**), our results are consistent with the AEP (2015) study, as well as previous studies (e.g. Ryan et al. 1977; Gupta et al. 1985; Mahmood-ul-Hassan et al. 2006; Janik et al. 2015). This suggests that the sorption of B onto sediment is not significantly influenced by the high salinity of the solution, or the presence of dissolved metals and organics. This is likely due to the mechanism of sorption of B onto the various soils. Boron likely sorbs onto the clay minerals or, if present, carbonates (Goldberg 1997) via ligand exchange. This form of chemisorption is less effected by variables such as ionic strength and competition with other dissolved metals.

3.4.1.3 Lithium

Lithium is another emerging contaminant in the soil system that is worthy of investigation, although it has not been as extensively studied as other metals. Davey and Wheeler (1980) studied the sorption of Li onto fifty different soils collected from Papua New Guinea. They conducted their experiments at pH 6.8, in a solution containing 0.01 M CaCl₂, and found that Li strongly sorbed onto the soil, with mass removal percentages between 63 and 75% (Davey and Wheeler 1980). Anderson et al. (1988) reported similar findings using a MgCl₂ solution. Yalamanchali (2012) studied the uptake and sorption of Li in batch sorption studies using soil collected in New Zealand. The soil used in their study was reported to have a CEC of 12.5 cmolc/kg, which was in the low to medium range reported for New Zealand soils. They found that K_d values for Li, between a pH of 4 and 8, ranged between 0.13 and 3 L/kg, with K_d increasing with increasing pH (Yalamanchali 2012). Based on their findings, they argued that Li was highly mobile in the soil environment (Yalamanchali 2012). Our results are similar to those found by Yalamanchali (2012), suggesting that Li is not significantly influenced by the high salinity and the presence of other dissolved metals or organic compounds in solution.

3.4.1.4 Barium

The sorption behavior of barium was difficult to quantify in our experiments. In both Samples 1 and 2, the concentration of Ba in the effluent after the experiments far exceeded that of the stock FPW solution (~5-8 mg/L) (**Tables B4 and B5**). Barium concentration in the stock FPW solution and the experiments were confirmed by both ICP-MS/MS and ICP-OES. We speculate that this result may be due to either dissolution of Ba-bearing minerals within the matrix, or due to displacement of Ba²⁺ sorbed to the soil components by competing ions, with the latter being more likely. It has been speculated that sorption of Ba²⁺ on clay surfaces is non-specific, involving outer-sphere surface complexes (Zhang et al. 2001). Therefore, divalent

alkaline earth cations, such as Ba^{2+} , are assumed to be ‘exchangeable’ due to the weak bonds between the cation and the clay surface created by electrostatic forces, rather than stronger chemical bonds (Zhang et al. 2001). Zhang et al. (2001) found that sorbed Ba^{2+} could be displaced by Na^+ (or other cations) when present in high quantities in solution. This resulted in a decrease in Ba sorption as NaNO_3 concentrations (and ionic strength) increased (Zhang et al. 2001). We therefore speculate that the significant increase in Ba^{2+} concentrations observed were a result of exchange or displacement of Ba from mineral surfaces due to the high concentrations of Na^+ , K^+ , Ca^{2+} , and Mg^{2+} (and possibly Sr^{2+}) in the highly saline solution.

3.4.1.5 Nickel and Copper

The sorption of trace or heavy metals (e.g. Pb, Hg, Cr, Cd, Cu, Zn, Ni, As) has been extensively studied in either mono- or multi-element solutions. The sorption, and therefore, the K_d values, depend on several system characteristics, including pH, clay minerals, soil organic matter, the presence of Fe or Al-oxides, carbonates, as well as the ionic strength of the solution. However, sorption of trace elements is not limited to the inorganic and organic soil constituents, but also on the nature and characteristics of the element itself, as well as competition. A number of studies (e.g. Sheheen et al. 2013) have suggested many factors that influence the sorption of these trace metals in soil, including: 1) the hydrolysis constant of the metal in question; 2) the atomic weight; 3) the ionic radius; and 4) Misono softness value (Misono et al. 1967), an index determined from the ionic radius and ionization potential for a specific element that describes the tendency of the element to form covalent bonds with colloids (Sposito 1989). Competition for limited sorption sites is an important factor that negatively impacts retention of an element.

Many of the trace metals mentioned above, such as Fe, Ni, Cu, Zn, and Pb, were observed to be present in the FPW samples, but their concentrations in solution following metal

sorption were either at or below detection limits, making it difficult to quantify their sorption potential. However, some metals (Cu in Sample 1, Ni in Sample 2), yielded good results (**Table 3.5; Figures B1H and B1I**). Copper and nickel are both known to be toxic in the soil environment (Hooda 2010; Shaheen et al. 2013). Reddy and Dunn (1986) studied the sorption of Ni onto three different soils from North Carolina, including a clay-dominated soil, a silty loam, and a sandy loam, with organic matter in each soil ranging from approximately 2 to 2.5%, and CEC values between 6 and 17 meq/100 g. They found that K_d values varied between 152 and 388 L/kg. Ramachandran and D'Souza (2013) studied the sorption of Ni onto soils collected from India. They found K_d values that varied widely depending on soil parameters, with values ranging between 6.7 and 212 L/kg, and that K_d values increased with increasing pH and CEC. Similarly, Mellis et al. (2004) found that Ni sorption increased with increasing pH, noting that it was the main factor involved in Ni sorption variation. Many others (e.g. Soares et al. 2011; Tahervand and Jalali 2017; Elbana et al. 2018) have also found similar trends with respect to Ni sorption as a function of pH. Multi-element studies, either in binary or tertiary systems, involving Ni as one of its constituents have been extensively studied. Regardless of the other metals dissolved in solution (e.g. Cd, Zn), Ni sorption onto various soil and clay types in a competitive environment have always been observed to decrease (Basta and Tabatabai 1992; Antoniadis et al. 2007; Covelo et al. 2007; Usman 2008; Liao and Selim 2009).

Comparing our results with those mentioned above, we found that Ni sorption was on the lower range of what has been previously found. The K_d value was observed to be highest for MOR, with FLUV exhibiting the lowest degree of sorption (**Table 3.5**). This trend is likely related to clay content, organic matter content, and CEC of the soils. We suggest that the presence of high concentrations of salt in solution (and thereby high ionic strength), along with

competition with other dissolved metals, and possibly low pH of the FPW, depressed sorption of Ni onto soils. This is supported by the study conducted by Mattigod et al. (1979), whereby they studied the effect of ionic strength on the sorption of Ni by kaolinite, the dominant clay mineral in MOR. They found that increasing ionic strength resulted in decreasing Ni sorption (Mattigod et al. 1979). Covelo et al. (2007) reported a Ni K_d value of 1.35 L/kg for kaolinite, and Soares et al. (2011) found similar trends. Although the ionic strengths investigated by Mattigod et al. (1979) and Soares et al. (2011) were much lower than what would be expected in our FPW, the trend is consistent with our findings.

Copper is another potentially toxic metal in the soil environment if found in excess (Cameron 1992). Cerqueira et al. (2011a) reported that the sorption and retention of Cu^{2+} was most heavily influenced by pH, CEC, and total clay content, although others (e.g. Shaheen et al. 2009; Elbana et al. 2018) have also found that Cu has a strong affinity to the soil organic matter. Covelo et al. (2007) found that vermiculite sorbed Cu the strongest, with other clay minerals, such as kaolinite, mica, and Fe-oxides sorbing virtually no copper. Shaheen et al. (2009) studied the sorption of Cu onto various soils collected from Egypt and Greece. They found that sorption was very high for clay-rich soils, with K_d values $>1,000$ L/kg. Dişli (2010) conducted a series of batch experiments studying the sorption of Cu, along with Zn and Mn, on alluvial sediment collected from Turkey, and found that sorption of Cu onto the sediment depended greatly on grain-size, with finer-grained material sorbing more than coarser-grained sediment. Regardless of the soil types investigated, Dişli (2010) reported K_d values that ranged from 18,170 (for coarse-grained sediment) to 32,550 L/kg (for fine-grained sediment). Dişli (2010) suggested that the strong preference for Cu retention was due to the ionic properties of the element, namely its electronegativity and ionic radius. Many studies have shown that Cu sorption increases with

increasing pH (e.g. Usman 2008; Cerqueira et al. 2011a, b; Vega et al. 2008; Zhang et al. 2011; Saha 2012; Saha and Badruzzaman 2014; Tahervand and Jalali 2017; Elbana et al. 2018), and decreases with ionic strength (e.g. Zhu and Alva 1993; Fike 2001; Zhang et al. 2011; Saha 2012; Saha and Badruzzaman 2014). In competitive, multi-element systems, Cu is normally less influenced by the presence of other dissolved metals as compared to other elements, but a slight decrease in sorption is usually observed (e.g. Zhu and Alva 1993; Tsang and Lo 2006; Covelo et al. 2007; Seo et al. 2008; Usman 2008; Dişli 2010).

The K_d for FLUV found in our study is significantly lower than the reported range of Cu K_d values in either the mono- or multi-element systems (**Table 3.5**). We suggest that the presence of high concentrations of salt in solution (and thus high ionic strength), along with competition with other dissolved metals, the coarse-grained nature of FLUV, and possibly low pH of the fluid, all contributed to the depressed sorption of Cu onto the sediment.

3.4.2 Batch sorption of organic components

Attempts to analyze effluent from Sample 2 for organic compounds were unsuccessful, due to overall low concentrations of organic compounds. Thus, only results from Sample 1 are presented. We focused on studying the polyethylene glycols (PEGs) in the effluent due to their high concentration in the fluid. Attempts to quantify other organic classes within the Sample 1 effluent were unsuccessful due to their overall low concentration. To determine the sorption behavior of the PEGs in solution, we chose four PEGs with differing ethylene oxide (EO) numbers, denoted PEG- n , where n represents an integer in the chemical formula $C_{2n}H_{4n+2}O_{n+1}$ (**Figure B3**), which were PEG-6, PEG-7, PEG-9, and PEG-11. We also calculated a “bulk PEG” value, summing up the peak areas for all the PEGs found in solution, for comparison.

Castanho et al. (2009) studied the sorption and mobility of a PEG, with a molecular weight of 4,000, in the sandier soils of Brazil. They found that the PEG was highly mobile, exhibiting low degrees of sorption (<22% retention). K_d values ranged between 0.08 and 0.31 L/kg (Castanho et al. 2009). Clegg et al. (2014) also found that sorption of PEG with a molecular weight of 600 onto Na-bentonite was low, and that the presence of another organic molecule (polyvinyl alcohol) acted to reduce the overall extent of sorption of the PEG. Zhao et al. (1989) studied the sorption of PEGs with molecular weights between 300 and 200,000 onto five different montmorillonite clays. They observed that sorption data were best fit with a Freundlich isotherm, that the extent of sorption was low for all clays tested, and that sorption exhibited rapid kinetics, with equilibrium obtained within 30 min (Zhao et al. 1989). Montmorillonite and bentonite varieties that had Ca in the interlayer sorbed PEG more strongly than their Na-varieties, with heavier PEGs sorbing more strongly overall than lighter molecules (Zhao et al. 1989). Zhao et al. (1989) also observed that with increasing pH, sorption of the PEGs was reduced. With this, the authors suggested that PEGs sorbed onto montmorillonite mainly through van der Waal forces.

The removal of PEGs from aqueous solution by activated carbon has been studied more than for soils (Suzuki et al. 1976; Arbuckle and Osman 2000; Chang et al. 2000; Gajdos et al. 2007). Gajdos et al. (2007) found that heavier PEGs were retained more strongly relative to lighter PEGs (Gajdos et al. 2007), consistent with other work (Suzuki et al. 1976; Arbuckle and Osman 2000). Sorption was also found to be influenced by pH, with a sorption minimum found at approximately a pH of 6, with stronger sorption observed at more acidic and more alkaline conditions (Gajdos et al. 2007).

McLaughlin et al. (2016) studied the biodegradation, sorption, and co-contaminant interactions between GA, PEGs, and PAM, in a high salt, simulated hydraulic fracturing fluid. They found that abiotic processes, such as sorption, were far less pronounced for PEGs, relative to the other organic compounds that they studied, and that there was preferential sorption to organic-rich topsoil for compounds with higher numbers of ethylene glycol units. McLaughlin et al. (2016) noted that PEG removal from aqueous solution was almost exclusively due to biodegradation. With just PEG in solution, biodegradation began immediately at the onset of the experiment, but in the presence of GA and GA/PAM, there was a substantial delay in biodegradation. McLaughlin et al. (2016) also found that PEG biodegradation was completely halted in the presence of salt. Relevant to our study, they cautioned that the presence of surfactants in solution, such as PEGs, may increase the mobility of other organic constituents found in FPW of HFF, and possibly solubilize other metals found within the soil.

Within the concentration range observed in our experiments, the sorption of various PEGs onto the studied sediments appeared to be linear. We did not observe any plateauing behavior; therefore, neither Freundlich nor Langmuir isotherms were fit to the data (**Figure 3.2**). Overall, most of the K_d values calculated had high R^2 values ($R^2 > 0.70$) (**Table 3.7**). Similar to Zhao et al. (1989) and McLaughlin et al. (2016), we found that sorption, represented by the K_d value, increases with increasing EO-units. For all sediment types, PEG-6 exhibits the lowest K_d value, whereas PEG-11 exhibits the greatest value (**Table 3.7**). This suggests that one aspect of sorption of PEGs in FPW is related to hydrophobicity, likely controlled by the organic matter found within the sediment, whereby PEGs with greater numbers of EO units should have lower water solubility limits, and therefore sorb onto the organic fraction of the sediment.

However, our results suggest that organic matter within the sediment may not be the only variable that impacts sorption of PEGs in the FPW. Brownawell et al. (1997) studied the sorption of nonionic surfactants, monotridecyl ethers of PEGs known as alcohol ethoxylates (AE), as a function of pH, ionic strength, hardness (Ca^{2+} concentration), organic fraction of the sediment, and clay content. They found that variables such as pH and ionic strength had a slight impact on sorption of AE onto the sediment tested. Interestingly, Brownawell et al. (1997) did not find a strong correlation between sorption and organic carbon content of the sediment. They speculated that a secondary effect caused by expandable 2:1 clay minerals in the sediment may be masking this effect. Our XRD results used in comparing the mineralogy of MOR and GLC may suggest a similar finding (**Table A5**), wherein the dominant clay minerals in MOR was kaolinite and muscovite, and in GLC was chlorite and muscovite. Further, Zhao et al. (1989) found that sorption of PEGs onto kaolinite was significantly reduced as compared to montmorillonite clays. MOR is dominated by kaolinite, a 1:1 clay mineral, whereas GLC has chlorite, a 2:1 clay, present. Although chlorite is not expansive, the sorption interaction between the PEGs and 2:1 clays may be greater than those experienced with 1:1 clays, which may explain our findings. Verification of this hypothesis requires further investigation.

Compound	MOR [R²]	GLC [R²]	FLUV [R²]
Bulk PEG	9.41 [0.7962]	23.42 [0.8134]	14.03 [0.7359]
PEG-6	2.66 [0.7903]	6.30 [0.7521]	2.20 [0.7781]
PEG-7	3.10 [0.599]	18.00 [0.6167]	8.87 [0.6357]
PEG-9	22.22 [0.6264]	303.33 [0.909]	614.10 [0.6557]
PEG-11	130.83 [0.9212]	1554.10 [0.9132]	1644.80 [0.5985]

Table 3.7: Linear K_d (L/kg) values for PEGs for the three tested soil types for FPW Sample 1. In brackets are the R^2 values of the fitted lines through the data, passing through the origin.

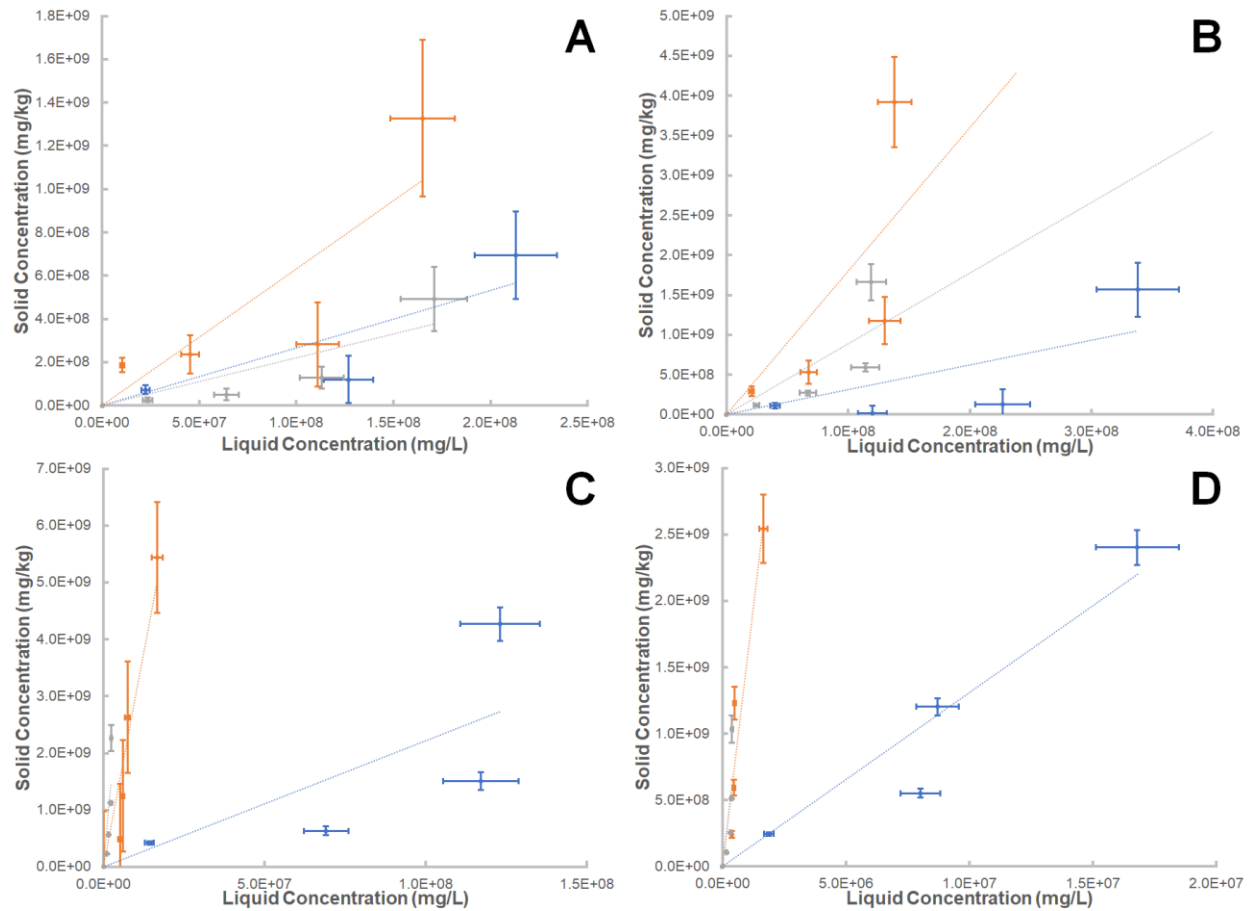


Figure 3.2: Linear sorption isotherms for A) PEG-6; B) PEG-7; C) PEG-9; and D) PEG-11. Blue denotes samples from MOR; orange denotes samples from GLC; grey denote samples from FLUV. Errors were calculated by propagating analytical and measurement errors.

3.4.3 Column sorption of inorganic components

Duplicate column experiments were conducted on solutions derived from FPW Sample 1 flowed through fluvial sand. Statistical analyses of the results between the two columns were consistent with each other, suggesting that the two columns were behaving similarly, permitting them to be used as duplicates. We found that both chloride and bromide acted conservatively during the experiment.

3.4.3.1 Strontium, lithium, boron, sodium, and potassium

Retardation factors were estimated by comparing the travel times of the sorbing solutes to the conservative solutes, and by curve fitting using the parameter estimator function in HYDROSCAPE (Funk et al. 2017; **Chapter 4**). Estimated retardation factors (R), and their associated effective linear distribution coefficients (K_d'), for strontium, lithium, boron, sodium, and potassium, are reported in **Table 3.8**. The K_d' was calculated by rearranging the formula used to calculate the retardation factor. This was done so that direct comparison of sorption results in the column experiments could be made to the above batch sorption experiments discussed above (see **Section 3.4.1**). In all cases where an R, and therefore K_d' , could be calculated, they were lower than those determined in the batch experiments (**Table 3.5**).

Column experiments with Sr were conducted by Lefevre et al. (1993) using a clayey and calcareous sandy soil. They found that precipitation of strontianite, followed by ion exchange, were the primary modes of retardation within the column. The authors found that with precipitation, the R increases, reflecting greater retention of Sr by the soil matrix. Lefevre et al. (1993) also found that precipitation was strongly governed by the concentration of dissolved Ca in solution, with greater concentrations of Ca preventing strontianite precipitation. Huo et al. (2013) studied the sorption of Sr onto a Chinese loess in both batch and column experiments. They found that the values of R in their column experiments were significantly different when compared to their batch experiments (from K_d), with R decreasing with increasing pore velocity (Huo et al. 2013), consistent with other studies (e.g. Relyea 1982; Shimojima and Sharma 1995; Costa and Prunty 2006) and consistent with our results. They argued that flow induced non-equilibrium effects (Huo et al. 2013).

Experiments designed to study the kinetics of sorption of Sr onto hydrous ferric oxide (HFO) aggregates (van Beinum et al. 2005; Hofmann et al. 2005) and soils (Liu et al. 1995) demonstrated that there was an initial stage of fast sorption as a result of adsorption onto external surfaces, followed by a slow sorption process dominated by intraparticle diffusion and sorption onto interior sites, redistribution of surface complexes, or precipitation (Sparks 2000). Similarly, B has also been observed to exhibit differing rates of sorption: an initial fast reaction dominated by chemical reactions on the outer solid surfaces, followed by a slow reaction dominated by diffusion into interior sites (Krishnasamy 1996; Arora and Chahal 2007).

We found that both Li and Na behaved near conservatively, with R values close to 1.20 (**Figure 3.3; Table 3.8**). Other metals, such as B, Sr, and K exhibited slightly greater amounts of sorption, with $K > Sr > B$; however R values were never greater than 2.30 (**Figure 3.3; Table 3.8**). The calculated K_d' values for each of these elements were less than those found in the batch sorption experiments (**Table 3.5**). The breakthrough curves for K, and possibly B and Li, appear to exhibit some tailing, possibly indicating some non-linear or rate-limited sorption processes (Brusseau 1994). Consistent with these past studies, it is likely that flow impacted the kinetics of sorption of Sr and B during our experiments. We suggest that sorption of Sr and B in a flowing system is dominated by surface processes, i.e. fast sorption, absent of slow processes dominated by diffusion and/or precipitation. A lack of diffusion of these elements into interior sites and/or precipitation of elements out of solution would decrease the overall retention, and therefore sorption, of these elements. This would explain the reduction of K_d values for Sr and B obtained from our column experiments when compared to our batch experiments. It is unclear if this could also explain the reduction in Li sorption, although it seems likely.

Element	Column A		Column B	
	R (-)	K_d' (L/kg)	R (-)	K_d' (L/kg)
Li	1.25	0.06	1.22	0.05
B	1.50	0.12	1.50	0.12
Na	1.20	0.05	1.20	0.05
K	2.30	0.30	2.10	0.26
Sr	1.90	0.21	1.80	0.19

Table 3.8: Retardation factors (R) and effective distribution coefficients (K_d') for select metals, for both columns A and B.

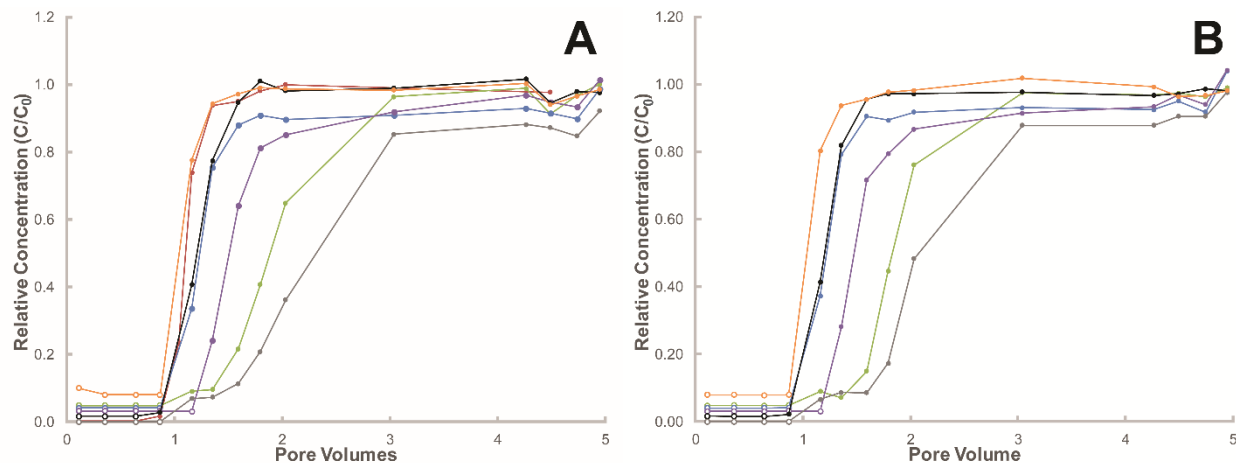


Figure 3.3: Breakthrough curves of some inorganics for A) column A; and B) column B. Colors denote different elements: red = Cl; orange = Br; green = Sr; blue = Li; purple = B; black = Na; grey = K. Empty points indicate measurement was below detection limit.

3.4.3.2 Calcium, magnesium, manganese, and barium

For elements such as Mg, Ca, Ba, and Mn, a different behavior was observed (**Figure 3.4**). These metals were observed to break through before chloride and bromide, assumed to be the advective front, after which the concentrations increase rapidly to concentrations greater than those measured in the influent FPW stock solution. For Mg and Ca, the sudden increase in concentration is rapid and short-lived, with concentrations spiking at a factor of approximately 3.60 and 2.60, respectively, returning to those found in the stock solution after approximately 1.80 pore volumes (**Figure 3.4**). This result is consistent with the FPW flowing through the fluvial sand dissolving minerals containing these elements. XRD analyses on the fluvial sand

identified the presence of carbonates (**Table A5**), and chemical analysis confirm the presence of these elements (**Table 3.2**). We propose that the mixing front between the simulated groundwater and the FPW entering the column dissolved carbonate minerals containing Mg and Ca, resulting in the behavior observed in our experiments.

For Ba, concentrations spike at a factor of over 17, then slowly drop after approximately 2 pore volumes (**Figure 3.4**). The concentration of Ba returns to those measured in the stock solution after approximately 20 pore volumes. Mn exhibits similar behavior to Ba. Mn concentrations spike at a factor between 13 and 25 over that of the stock solution and begins to decrease after approximately 1 to 2 pore volumes (**Figure 3.4**); however, the concentration of Mn remains elevated even after 125 pore volumes. Based on the study by Zhang et al. (2001), we suggest that Ba^{2+} is exchangeable within the sediment, and as a result of the highly saline FPW flowing through the column, Ba sequestered on the soil was displaced by other mono- and divalent cations, such as Na^+ , K^+ , Ca^{2+} , and Mg^{2+} . Manganese, in its divalent form, Mn^{2+} , is also known to be soluble, mobile, and exchangeable (Aubert and Pinta 1977), and may follow a similar behavior to Ba.

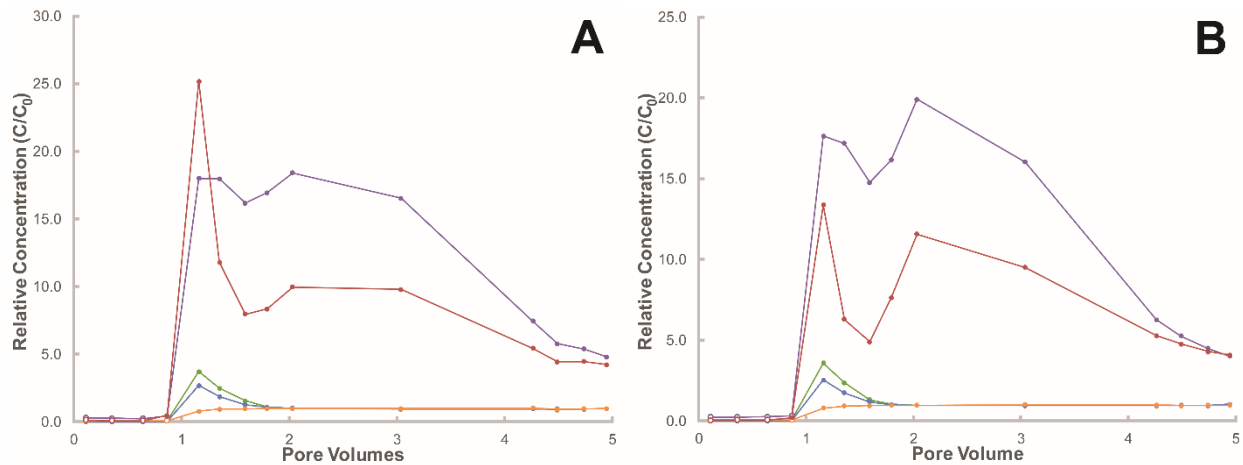


Figure 3.4: Breakthrough curves of some inorganics for **A)** column A; and **B)** column B. Colors denote different elements: orange = Br; green = Mg; blue = Ca; purple = Ba; and red = Mn. Empty points indicate measurement was below detection limit.

3.4.3.3 Trace metals

Nickel appears to steady increase in concentration with time, eventually plateauing at a relative concentration of unity after approximately 60 pore volumes (**Figure 3.5A and B**). Interestingly, after approximately 70 pore volumes the concentration of Ni in the effluent slightly exceeds the concentration in the stock solution by approximately 20%. Tsang and Lo (2006) observed a similar behavior in the binary Cu-Cd system, whereby the concentration of Cd, which sorbed weakly compared to Cu, was elevated in the competitive column experiments by approximately 10%. They argued that this behavior arose due to mobilization of Cd caused by displacement by Cu ions at sorption sites (Tsang and Lo 2006). Nickel has been observed to sorb to a lesser degree than Cu (Covelo et al. 2007; Tahervand and Jalali 2017; Elbana et al. 2018), therefore, Ni displacement caused by Cu (and possibly other metals in FPW solution) competing for sorption sites is likely.

Copper, likewise, increased over the course of the experiment, but never reaches the stock solution concentration within 125 pore volumes (**Figure 3.5A and B**). This is consistent with the overall higher sorption potential of Cu over other metals (Tsang and Lo 2006; Seo et al. 2008). Based on the K_d value obtained for Cu for FLUV in the batch experiments (**Table 3.5**), we would have expected a retardation factor of about 10. However, we observed stronger sorption in the column experiments (**Figure 3.5A and B**). This suggests that other processes other than sorption, possibly precipitation of Cu-bearing solids, may have occurred in the column experiments, further enhancing the Cu retention capacity of FLUV. Seo et al. (2008) argued that because their column experiments were conducted under anaerobic conditions, this promoted the precipitation of insoluble sulphide minerals (from reduced sulphate in solution). The batch experiments, on the other hand, were conducted under aerobic conditions, whereby the formation of sulphide minerals would not be favored (Seo et al. 2008). Seo et al. (2008) also observed a significant decrease in sorption of Cu due to competition with other metals in column experiments. They found that it took approximately 400 pore volumes for the advective front to pass for Cu under mono-element conditions, whereas it took approximately 100 pore volumes under multi-element conditions (Seo et al. 2008), also consistent with our findings.

Karthikeyan et al. (1999) performed batch sorption experiments to study the sorption and precipitation of Cu onto hydrous iron oxides (HFO) and hydrous aluminum oxides (HAO). For HFO, under alkaline conditions ($\text{pH} > 7.8$), new XRD peaks were observed, corresponding with the presence and likely precipitation of $\text{CuO}_{(s)}$ and $\text{Cu}(\text{OH})_{2(s)}$, and possibly hydrous Cu oxides (Karthikeyan et al. 1999). For HAO, under more acidic conditions ($\text{pH} > 5.6$), Cu removal was likely due to surface precipitation of a solid solution material, likely a mixed (Al, Cu) oxide ($\text{CuAl}_2\text{O}_{4(s)}$) (Karthikeyan et al. 1999). These results were successfully modeled with a surface

complexation model (Karthikeyan and Elliott 1999). We argue that it is likely that the enhanced retention of Cu observed in our column experiments is likely due to precipitation of Cu-bearing solids. Although we are unsure of the exact composition of these solids, we argue that Cu-carbonates, Cu-oxides, or Cu-hydroxides are more likely than Cu-sulphides in our system.

Interestingly, in both columns, sudden spikes in Ni and Cu (and possibly Zn) can be observed, with these elements in column B coincident with time (**Figure 3.5**). FLUV was observed to naturally contain as much as 6.4 mg/kg Ni, 2.5 mg/kg Cu, and 33.6 mg/kg Zn (**Table 3.2**). Several studies investigating the mobilization of metals due to de-icing salts (Amrhein et al. 1992; Norrström 2005), as well as a column study using hydraulic fracturing-derived wastewater (Oetjen et al. 2018), observed metal mobilization (including Cu and Zn). These studies proposed that the mechanism for the release of these metals was due to organic matter mobilization (Amrhein et al. 1992) or through colloid transport (Norrström 2005). Oetjen et al. (2018) further highlighted the importance of high salinity in the mobilization of the metals, with highly saline waters able to mobilize metals within the soil readily. Sang et al. (2014) conducted several column experiments to study the effect of FPW on colloid transport in the unsaturated zone. They observed that there was a marked increase in colloid remobilization in columns with FPW flowing, likely due to sorption of surfactants onto the colloid, promoting disaggregation and detachment, and cation exchange, whereby calcium bridges connecting colloids to sand surfaces break due to exchange with Na^+ , thereby releasing the colloids (Ouali and Pefferkorn 1994; Zhuang et al. 2010; Sang et al. 2014). Higher flow rates of FPW were also observed to further increase colloid remobilization (Sang et al. 2014). The authors argued that the release and infiltration of FPW could mobilize contaminants previously sequestered within the soil, releasing heavy metals, among others, and contaminate groundwater resources. The simultaneous spike in

Ni and Cu (\pm Zn) lends credence to the hypothesis that the sudden increase in concentration of these two metals is likely from mobilization of these elements from the sediment in the column, possibly through colloid transport. The numerous erratic spikes in Zn may be a result of the higher Zn content in the FLUV sediment, leading to several mobilization events within the column. Heterogeneities within the soil may also be responsible for the erratic release of pulses of Zn from the soil.

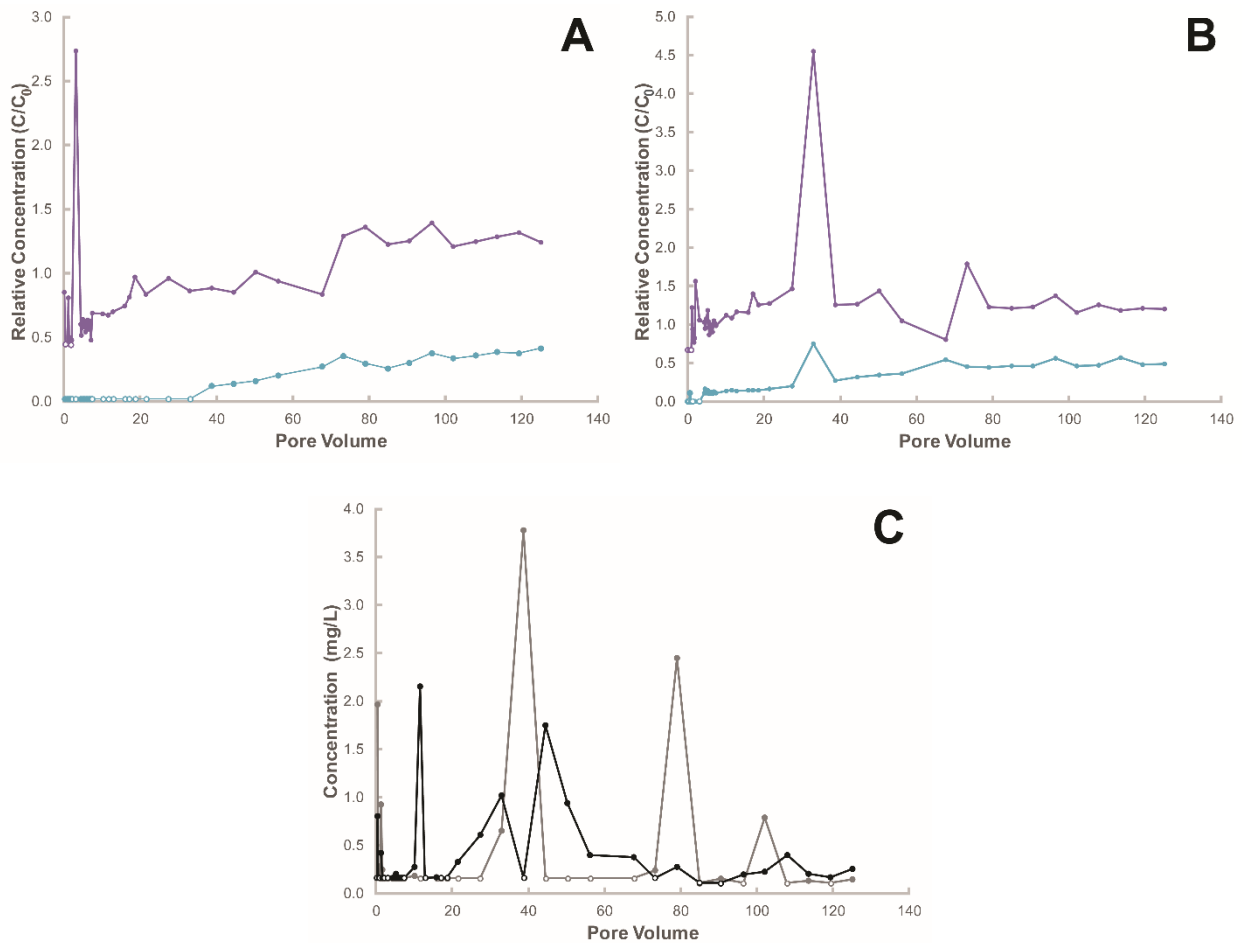


Figure 3.5: Breakthrough curves of some heavy metals for **A)** Ni (purple) and Cu (blue) for column A; **B)** Ni (purple) and Cu (blue) for column B; and **C)** Zn for column A (black) and B (grey). Empty points indicate measurement was below detection limit.

3.4.4 Column sorption of organic components

Ours is the first study to investigate the transport of field-collected FPW through saturated porous media. Oetjen et al. (2018) simulated the transport of hydraulic fracturing wastewater through a column of agricultural soil during rain events. The column was dry packed with the agricultural soil, classified as a mollisol, which was sieved to 0.1 cm. Spill events were simulated by pouring HF-derived wastewater at the top of the soil column, with flow induced by gravity alone. Effluent collected at the bottom of the column were analyzed for a number of organics, including PEGs ranging from PEG-10 and PEG-14, benzalkonium chlorides (BACs), and alkyl ethoxylates (AEOs). Of the 27 organic surfactants that were present and analyzed for in the wastewater samples, none were observed in the leachate (Oetjen et al. 2018). Oetjen et al. (2018) also determined that these organics were not broken down through biodegradation processes within the column, as no metabolites were detected in the leachate. They determined that the volume of wastewater used in their experiments, estimated to equal one year's worth of rainfall in volume, was insufficient to mobilize the surfactants (Oetjen et al. 2018). They concluded that their experiments suggested that migration of surfactants, including PEGs, should be minimal (Oetjen et al. 2018).

We found that PEGs were detectable almost immediately in the effluent from the columns, with the first sample taken after only one pore volume (PV) had passed through. Both columns behaved similarly with respect to the observed PEGs, suggesting that our duplicate results are valid (**Figure 3.6**). We also observed a systematic increase in sorption with increasing EO-units in the PEGs. Retardation factors estimated for PEG-6 were approximately 3.0, whereas retardation factors for PEG-11 were estimated to be approximately 55 (**Table 3.9**). This is consistent with the batch experiments above (see **Section 3.4.2.**), which was interpreted to be a

result of increasing hydrophobicity with increasing EO-units in the organic molecule. However, the magnitude of sorption was substantially less in the column experiments compared to the batch experiments. K_d' values, estimated from the retardation factor, were usually an order of magnitude less than K_d values determined from the batch sorption experiments (**Table 3.7**). This suggests that sorption of PEGs onto FLUV sediment is not instantaneous, and likely depressed due to kinetics factors. Sorption of PEGs usually involves a fast adsorption process on external sites, followed by slower internal diffusion processes (Noll 1992; McKay 1996; Chang et al. 2003).

In contrast to the Oetjen et al. (2018) study, our results suggest that PEGs are mobile in the subsurface. We speculate that the composition of the wastewater used in the Oetjen et al. (2018) study may be one factor that explains the variation in results. Unlike the high salinity FPW used in this study (TDS >140,000 mg/L), the wastewater utilized in the Oetjen et al. (2018) study had a considerably lower salinity (TDS <10,000 mg/L). Differences in soil composition and mineralogy may also explain the variation between the two studies. FLUV in our study is dominated by fine-grained quartz sand, with minor amounts of trace and accessory minerals, which include some clay minerals and carbonates (**Table A5**); the TOC of FLUV is also only a very small portion of the sediment (**Table A5**). In contrast, the agricultural soil used in the Oetjen et al. (2018) study is largely dominated by silt and sand but has a considerably larger soil organic carbon content (8.2 g/kg). The large percentage of organic carbon in the agricultural soil, combined with the overall low salinity of the wastewater, may explain why the PEG surfactants were not mobilized, nor detected in the leachate collected in the Oetjen et al. (2018) study.

Compound	Column A		Column B	
	R (-)	K _d ' (L/kg)	R (-)	K _d ' (L/kg)
PEG-6	2.80	0.42	3.00	0.46
PEG-7	3.20	0.51	4.00	0.70
PEG-9	20.00	4.45	24.00	5.34
PEG-11	54.00	12.40	56.00	12.76

Table 3.9: Retardation factors (R) and the calculated effective linear distribution coefficients (K_d') for the PEGs in the column experiments.

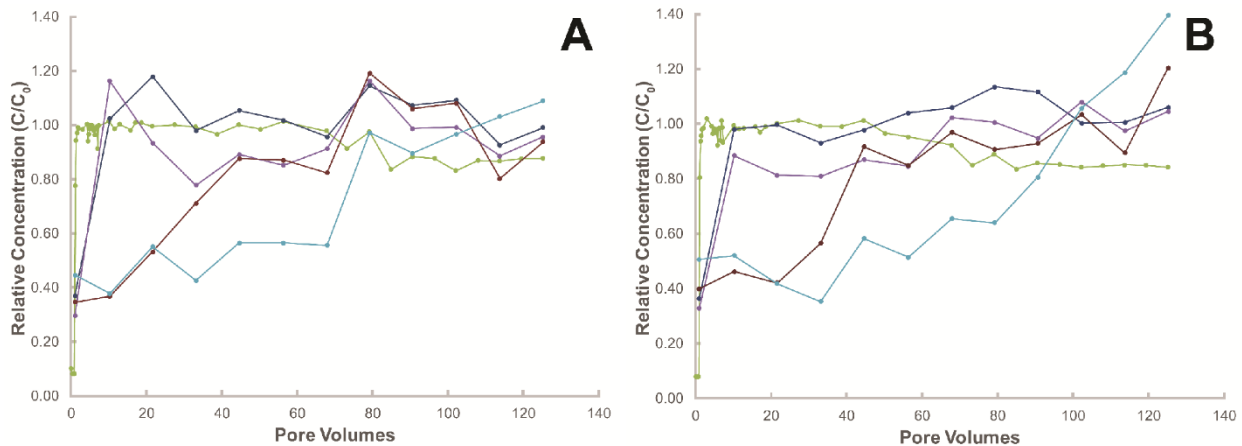


Figure 3.6: Breakthrough curves of PEGs for A) column A; and B) column B. Colors denote different compounds: green = Br; dark blue = PEG-6; purple = PEG-7; red = PEG-9; light blue = PEG-11.

3.5 Summary & Conclusions

With the increasing prevalence of hydraulic fracturing operations within Canada and throughout the world, an understanding of the risks posed by those operations to the surrounding environment is necessary to limit and mitigate potential impacts. Wastewater from these operations can contain high concentrations of salt, dissolved metals, organic compounds, and other potentially hazardous constituents. FPW may pose a serious threat to the soil and groundwater environments if spilt at the surface, and their impact to those systems needs to be addressed. To quantify the potential mobility of inorganic and organic constituents found within FPW, we conducted a series of both batch sorption and column transport experiments to

constrain their transport in the subsurface environment. FPW samples used in our experiments were collected from two different hydraulically fractured wells in the Duvernay Formation, near Fox Creek, AB. Soil and sediment samples from this same region were exposed to the FPW.

In our batch sorption experiments, we found that Sr K_d values were significantly depressed relative to published literature values, likely due to the negative impact ionic strength has on Sr sorption, as well as competition with other cations in solution (e.g. Na^+ , K^+ , Mg^{2+} , Ca^{2+}). The high salinity of the FPW, as well as competition with other dissolved cations, likely depressed Ni and Cu sorption as well. However, other inorganics, such as B and Li, were negligibly impacted by the high salinity of the FPW, or the presence of other dissolved constituents in solution. PEGs found within the FPW were also studied, with the degree of PEGs sorption increasing with the number of EO-units within the molecule. Sorption of PEGs were also found to be dependent not only of the organic matter content of the soil, but also the mineralogy of the clay minerals found within the soil.

Column transport experiments were conducted on the fluvial sand to access the impact of flow on sorption of compounds within the FPW. We found that dissolved inorganics such as Sr, B, Li, Na, and K exhibited significantly lower sorption than the batch experiments for the same sediment. We interpret these results to suggest that sorption is non-instantaneous, and that slow sorption processes, such as diffusion into internal sites and/or precipitation, were negated by flow. For other elements, such as Ca, Mg, Ba, and Mn, we observed an early spike in concentration above what was measured in the stock solution, coincident with the advective front, followed by a gradual decline back to stock solution concentrations. We interpret this behavior to be a result of carbonate dissolution as the FPW passed through the column, releasing Ca and Mg, combined with displacement of Ba and Mn from the soil surfaces due to the

prevalence of other cations, such as Na^+ and K^+ , in solution. The sorption of Cu was observed to be enhanced by flow. We suspect that additional processes, such as precipitation of Cu-bearing solid phases, were present within the column experiments, but not in the batch experiments. Exclusion of Ni, in favor of Cu, was also observed, resulting in increased Ni mobility. PEGs in solution followed a similar trend to what was observed in the batch experiments, with sorption increasing with increasing EO-units. However, overall sorption of the individual PEG compounds in the column experiments were significantly less than those observed in the batch experiments. We argue that flow within the column negated the slow sorption process, thereby reducing the overall ability for the sediment to retain the PEGs.

Our results from both the batch sorption and column transport experiments highlight the potential risk FPW may pose to soil and groundwater systems. Our results indicate that both dissolved metals and organic compounds are likely to be highly mobile in the subsurface, and that retention of these compounds, even in high organic matter, high clay content soils, is likely to be minimal. In alluvial aquifer systems dominated by quartz sand, the mobility of these constituents is even greater, although certain heavy trace metals (e.g. Cu) may be retained to a greater degree. Retardation factors are, in general, very small, and therefore, these compounds are able to travel great distances in a relatively short amount of time. Biodegradation of these constituents was not observed over the course of our experiments, likely due to the high salinity of the FPW, which further exacerbates the transport potential of these inorganic and organic compounds. Coupled with the known toxicity FPW poses to aquatic ecosystems (e.g. Blewett et al. 2017a, b; Folkerts et al. 2017a, b; He et al. 2017a, 2018), we argue that FPW may pose a threat to groundwater aquifers and aquatic ecosystems in the event of a surface spill.

Acknowledgements

This research was funded by a Collaborative Research and Development Grant from the Natural Sciences and Engineering Research Council of Canada (NSERC) (CRDPJ 469308-14) to D. Alessi and J. Martin, support from the Encana Corporation, and a Queen Elizabeth II Graduate Scholarship to S. Funk.

References

- Adeleye SA, Clay PG, Oladipo MOA (1994) Sorption of caesium, strontium and europium ions on clay minerals. *Journal of Materials Science* **29**: 954 – 958.
- Akiba K, Hashimoto H (1990) Distribution coefficient of strontium on variety of minerals and rocks. *Journal of Nuclear Science and Technology* **27**: 275 – 279.
- Alberta Environment and Parks (AEP) (2015) Soil remediation guidelines for boron: Environmental and human health. Land policy branch, policy and planning division. 146 pp.
- Alessi DS, Zolfaghari A, Kletke S, Gehman J, Allen DM, Goss GG (2017) Comparative analysis of hydraulic fracturing wastewater practices in unconventional shale development: Water sourcing, treatment and disposal practices. *Canadian Water Resources Journal* **42**: 105 – 121.
- Ames LL, Rai D (1978) Radionuclide interactions with soil and rock media. Volume 1: Processes influencing radionuclide mobility and retention, element chemistry and geochemistry, and conclusions and evaluation. EPA 520/6-78-007A, prepared for the U.S. Environmental Protection Agency by the Pacific Northwest Laboratory, Richland, Washington.
- Amrhein C, Strong JE, Mosher PA (1992) Effect of deicing salts on metal and organic matter mobilization in roadside soils. *Environmental Science and Technology* **26**: 703 – 709.
- Anderson MA, Bertsch PM (1988) The distribution of lithium in selected soils and surface waters of the southeastern U.S.A. *Applied Geochemistry* **3**: 205 – 212.

- Antoniadis V, Tsadilas CD, Ashworth DJ (2007) Monometal and competitive adsorption of heavy metals by sewage sludge-amended soil. *Chemosphere* **68**: 489 – 494.
- Arbuckle WB, Osman M (2000) Polyethylene glycol adsorption equilibrium on activated carbon. *Environmental Engineering Science* **17**: 147 – 158.
- Arora S, Chahal DS (2007) Comparison of kinetic models for boron adsorption in alluvium-derived soils of Punjab, India. *Communications in Soil Science and Plant Analysis* **38**: 523 – 532.
- Aubert H, Pinta M (1977) Manganese. In: *Developments in Soil Science*, Aubert H, Pinta M (editors). Volume 7: 43 – 53.
- Basta NT, Tabatabai MA (1992) Effect of cropping systems on adsorption of metals by soils: III. Competitive systems. *Soil Science* **153**: 331 – 337.
- Bergström L (2000) Leaching of agrochemicals in field lysimeters – A method to test mobility of chemicals in soil. In: Cornejo J, Jamet P, Lobnik F (eds.), *Pesticide/Soil Interactions: Some Current Research Methods*. INRA, Paris, p. 479.
- Bencala KE, Jackman AP, Kennedy VC, Avanzino RJ, Zellweger GW (1983) Kinetic analysis of strontium and potassium sorption onto sands and gravels in a natural channel. *Water Resources Research* **19**: 725 – 731.
- Berns AE, Flath A, Mehmood K, Hofmann D, Jacques D, Sauter M, Vereecken H, Engelhardt I (2018) Numerical and experimental investigations of cesium and strontium sorption and transport in agricultural soils. *Vadose Zone Journal* **17**: 170126. doi:10.2136/vzj2017.06.0126.
- Blewett TA, Delompre PLM, He Y, Folkerts EJ, Flynn SL, Alessi DS, Goss GG (2017a) Sublethal and reproductive effects of acute and chronic exposure to flowback and produced water from hydraulic

fracturing on the water flea *Daphnia magna*. *Environmental Science & Technology* **51**: 3032 – 3039.

Blewett TA, Weinrauch AM, Delompre PLM, Goss GG (2017b) The effects of hydraulic flowback and produced water on gill morphology, oxidative stress and antioxidant response in rainbow trout (*Oncorhynchus mykiss*). *Scientific Reports* **7**: 46582; doi: 10.1038/srep46582

Bremner JM (1996) Nitrogen Total. *In*: Sparks (ed.) *Method of soil analysis. Part 3: Chemical methods*. SSSA Book Ser. 5. SSSA, Madison, WI, p. 1085 – 1122.

Brownawell BJ, Chen H, Zhang W, Westall JC (1997) Sorption of nonionic surfactants on sediment materials. *Environmental Science & Technology* **31**: 1735 – 1741.

Brusseau ML (1994) Transport of reactive contaminants in heterogeneous porous media. *Reviews of Geophysics* **32**: 285 – 313.

Cameron RE (1992) Guide to site and soil description for hazardous waste site characterization. Volume 1: Metals. United States Environmental Protection Agency, EPA/600/4-91-029.

Carter KE, Hakala JA, Hammack RW (2013) Hydraulic fracturing and organic compounds: Uses, disposal and challenges. *In*: SPE Eastern Regional Meeting; Society of Petroleum Engineers: Pittsburgh, PA. DOI: <http://dx.doi.org/10.2118/165692-MS>.

Castanho GM, Regitano JB, Tornisiello VL, Abdalla AL (2009) Sorption and mobility of polyethylene glycol (PEG 4000) in tropical soils. *Toxicological and Environmental Chemistry* **91**: 1263 – 1271.

Cerqueira B, Covelo EF, Andrade L, Vega FA (2011a) The influence of soil properties on the individual and competitive sorption and desorption of Cu and Cd. *Geoderma* **162**: 20 – 26.

Cerqueira B, Covelo EF, Andrade L, Vega FA (2011b) Retention and mobility of copper and lead in soils as influenced by soil horizon properties. *Pedosphere* **21**: 603 – 614.

- Chang CF, Chang CY, Tsai WT, Wu SC (2000) Adsorption equilibrium of polyethylene glycol in electroplating solution on activated carbon. *Journal of Colloid and Interface Science* **232**: 207 – 209.
- Chang CY, Tsai WT, Ing CH, Chang CF (2003) Adsorption of polyethylene glycol (PEG) from aqueous solution onto hydrophobic zeolite. *Journal of Colloid and Interface Science* **260**: 273 – 279.
- Chen C-C, Hayes KF (1999) X-ray absorption spectroscopy investigation of aqueous Co(II) and Sr(II) sorption at clay-water interfaces. *Geochimica et Cosmochimica Acta* **63**: 3205 – 3215.
- Chen SS, Sun Y, Tsang DCW, Graham NJD, Ok YS, Feng Y, Li X-D (2017) Insights into the subsurface transport of As(V) and Se(VI) in produced water from hydraulic fracturing using soil samples from Qingshankou Formation, Songliao Basin, China. *Environmental Pollution* **223**: 449 – 456.
- Clegg F, Breen C, Khairuddin (2014) Synergistic and competitive aspects of the adsorption of poly(ethylene glycol) and poly(vinyl alcohol) onto Na-bentonite. *Journal of Physical Chemistry B* **118**: 13268 – 13278.
- Colborn T, Kwiatkowski C, Schultz K, Bachran M (2011) Natural gas operations from a public health perspective. *Human and Ecological Risk Assessment* **17**: 1039 – 1056.
- Communar G, Keren R, Li FH (2004) Deriving boron adsorption isotherms from soil column displacement experiments. *Soil Science Society of America Journal* **68**: 481 – 488.
- Costa JL, Prunty L (2006) Solute transport in fine sandy loam soil under different flow rates. *Agricultural Water Management* **83**: 111 – 118.
- Covelo EF, Vega FA, Andrade ML (2007) Competitive sorption and desorption of heavy metals by individual soil components. *Journal of Hazardous Materials* **140**: 308 – 315.

Davey BG, Wheeler RC (1980) Some aspects of the chemistry of lithium in soils. *Plant and Soil* **57**: 49 – 60.

DiGiulio DC, Jackson RB (2016) Impact to underground sources of drinking water and domestic wells from production well stimulation and completion practices in the pavilion, Wyoming, Field. *Environmental Science & Technology* **50**: 4524 – 4536.

Dişli E (2010) Batch and column experiments to support heavy metal (Cu, Zn, and Mn) transport modeling in alluvial sediments between the Mogan Lake and the Eymir Lake, Gölbaşı, Ankara. *Ground Water Monitoring & Remediation* **30**: 125 – 139.

Drollette BD, Hoelzer K, Warner NR, Darrah TH, Karatum O, O'Connor MP, Nelson RK, Fernandez LA, Reddy CM, Vengosh A, Jackson RB, Elsner M, Plata DL (2015) Elevated levels of diesel range organic compounds in groundwater near Marcellus gas operations are derived from surface activities. *Proceedings of the National Academy of Sciences of the United States of America* **112**: 13184 – 13189.

Elbana TA, Selim HM, Akrami N, Newman A, Shaheen SM, Rinklebe J (2018) Freundlich sorption parameters for cadmium, copper, nickel, lead, and zinc for different soils: Influence of kinetics. *Geoderma* **324**: 80 – 88.

Fike WB (2001) Sorption of cadmium, copper, lead, and zinc as influenced by ionic strength, pH, and selected soil components. Doctor of Philosophy Thesis. Virginia Polytechnic Institute and State University.

Folkerts EJ, Blewett TA, He Y, Goss GG (2017a) Cardio-respirometry disruption in zebrafish (*Danio rerio*) embryos exposed to hydraulic fracturing flowback and produced water. *Environmental Pollution* **231**: 1477 – 1487.

- Folkerts EJ, Blewett TA, He Y, Goss GG (2017b) Alterations to juvenile zebrafish (*Danio rerio*) swim performance after acute embryonic exposure to sub-lethal exposures of hydraulic fracturing flowback and produced water. *Aquatic Toxicology* **193**: 50 – 59.
- Funk SP, Hnatyshin D, Alessi DS (2017) HYDROSCAPE: A new versatile software program for evaluating contaminant transport in groundwater. *Software X* **6**: 261 – 266.
- Gajdos L, Pietrelli L, Ciccarello A, Derco J (2007) *Polish Journal of Environmental Studies* **16**: 385 – 388.
- Gehman J, Thompson DY, Alessi DS, Allen DM, Goss GG (2016) Comparative analysis of hydraulic fracturing wastewater practices in unconventional shale development: Newspaper coverage of stakeholder concerns and social license to operate. *Sustainability* **8**: 1 – 23; doi:10.3390/su8090912
- Goldberg S (1997) Reactions of boron with soils. *Plant and Soil* **193**: 35 – 48.
- Goldberg S (1999) Reanalysis of boron adsorption on soils and soil minerals using the constant capacitance model. *Soil Science Society of America Journal* **63**: 823 – 829.
- Goldberg S, Forster HS, Heick EL (1993) Boron adsorption mechanisms on oxides, clay minerals, and soils inferred from ionic strength effects. *Soil Science Society of America Journal* **57**: 704 – 708.
- Gupta UC, Jame YW, Campbell CA, Leyshon AJ, Nicholaichuk W (1985) Boron toxicity and deficiency: A review. *Canadian Journal of Soil Science* **65**: 381 – 409.
- He Y, Folkerts EJ, Zhang Y, Martin JW, Alessi DS, Goss GG (2017a) Effects on biotransformation, oxidative stress, and endocrine disruption on rainbow trout (*Oncorhynchus mykiss*) exposed to hydraulic fracturing flowback and produced water. *Environmental Science & Technology* **51**: 940 – 947.

- He Y, Flynn SL, Folkerts EJ, Zhang Y, Ruan D, Alessi DS, Martin JW, Goss GG (2017b) Chemical and toxicological characterization of hydraulic fracturing flowback and produced water. *Water Research* **114**: 78 – 87.
- He Y, Zhang Y, Martin JW, Alessi DS, Giesy JP, Goss GG (2018) *In vitro* assessment of endocrine disrupting potential of organic fractions extracted from hydraulic fracturing flowback and produced water (HF-FPW). *Environment International* **121**: 824 – 831.
- Hendershot WH, Duquette M (1986) A Simple Barium Chloride Method for Determining Cation Exchange Capacity and Exchangeable Cations 1. *Soil Science Society of America Journal* **50(3)**: 605 – 608.
- Hofmann A, van Beinum W, Meeussen JCL, Kretzschmar R (2005) Sorption kinetics of strontium in porous hydrous ferric oxide aggregates II. Comparison of experimental results and model predictions. *Journal of Colloid and Interface Science* **283**: 29 – 40.
- Hooda PS (2010) Trace elements in soils. In: Hooda PS, editor. Chichester, United Kingdom: John Wiley & Sons Ltd., p. 3.
- Hückel E (1924) Zur Theorie der Elektrolyte. In: *Schriftleitung der »Naturwissenschaften«* (eds) *Ergebnisse der Exakten Naturwissenschaften*. Springer, Berlin, Heidelberg.
- Huo L, Qian T, Hao J, Zhao D (2013) Sorption and retardation of strontium in saturated Chinese loess: Experimental results and model analysis. *Journal of Environmental Radioactivity* **116**: 19 – 27.
- Janik LJ, Forrester ST, Soriano-Disla JM, Kirby JK, McLaughlin MJ (2015) GEMAS: Prediction of soil-solution phase partitioning coefficients (K_d) for oxoanions and boric acid in soils using mid-infrared diffuse reflectance spectroscopy. *Environmental Toxicology and Chemistry* **34**: 235 – 246.

- Juo ASR, Barber SA (1970) The retention of strontium by soils as influenced by pH, organic matter and saturated cations. *Soil Science* **109**: 143 – 148.
- Kalra YP (1995) Determination of pH of soils by different methods: collaborative study. *Journal of AOAC International* **78(2)**: 310 – 324.
- Karthikeyan KG, Elliott HA, Chorover J (1999) Role of surface precipitation in copper sorption by the hydrous oxides of iron and aluminum. *Journal of Colloid and Interface Science* **209**: 72 – 78.
- Karthikeyan KG, Elliott HA (1999) Surface complexation modeling of copper sorption by hydrous oxides of iron and aluminum. *Journal of Colloid and Interface Science* **220**: 88 – 95.
- Keren R, Gast RG, Bar-Yosef B (1981) pH-dependent boron adsorption by Na-montmorillonite. *Soil Science Society of America Journal* **45**: 45 – 48.
- Keren R, Mezuman U (1981) Boron adsorption by clay minerals using a phenomenological equation. *Clays and Clay Minerals* **29**: 198 – 204.
- Keren R, O'Connor GA (1982) Effect of exchangeable ions and ionic strength on boron adsorption by montmorillonite and illite. *Clays and Clay Minerals* **30**: 341 – 346.
- Keren R, O'Connor GA (1983) Strontium adsorption by noncalcareous soils – Exchangeable ions and solution composition effects. *Soil Science* **135**: 308 – 315.
- King GE (2012) Hydraulic fracturing 101: What every representative, environmentalist, regulator, reporter, investor, university researcher, neighbor, and engineer should know about hydraulic fracturing risk. *Journal of Petroleum Technology* **64**: 34 – 42.
- Krishnasamy R (1996) Kinetics of boron adsorption in soils. *Journal of Indian Society of Soils* **44**: 783 – 785.

- Lefevre R, Sardin M, Schweich D (1993) Migration of strontium in clayey and calcareous sandy soil: Precipitation and ion exchange. *Journal of Contaminant Hydrology* **13**: 215 – 229.
- Lewis J, Sjöstrom J (2010) Optimizing the experimental design of soil columns in saturated and unsaturated transport experiments. *Journal of Contaminant Hydrology* **115**: 1 – 13.
- Liao L, Selim HM (2009) Competitive sorption of nickel and cadmium in different soils. *Soil Science* **174**: 549 – 555.
- Liu D-C, Hsu C-N, Chuang C-L (1995) Ion-exchange and sorption kinetics of cesium and strontium in soils. *Applied Radiation and Isotopes* **9**: 839 – 846.
- Mahmood-ul-Hassan M, Akhtar MS, Nabi G (2006) Boron and zinc sorption and transport in calcareous soils. *Soil and Environment* **25**: 17 – 27.
- Manz KE, Haerr G, Lucchesi J, Carter KE (2016) Adsorption of hydraulic fracturing fluid components 2-butoxyethanol and furfural onto granulated activated carbon and shale rock. *Chemosphere* **164**: 585 – 592.
- Mattigod SV, Gibali AS, Page AL (1979) Effect of ionic strength and ion pair formation on the adsorption of nickel by kaolinite. *Clays and Clay Minerals* **27**: 411 – 416.
- McHenry JR (1958) Ion exchange properties of strontium in calcareous soil. *Soil Science Society of America Proceedings* **22**: 514 – 518.
- McKay G (1996) Use of adsorbents for the removal of pollutants from wastewater. In: McKay G (editor), CRC Press: p. 208.
- McLaughlin MC, Borch T, Blotvogel J (2016) Spills of hydraulic fracturing chemicals on agricultural topsoil: Biodegradation, sorption, and co-contaminant interactions. *Environmental Science & Technology* **50**: 6071 – 6078.

- Mellis EV, da Cruz MCP, Casagrande JC (2004) Nickel adsorption by soils in relation to pH, organic matter, and iron oxides. *Scientia Agricola* **61**: 190 – 195.
- Misono M, Ochiai E, Saito Y, Yoneda Y (1967) A new dual parameter scale for the strength of Lewis acids and bases with the evaluation of their softness. *Journal of Inorganic and Nuclear Chemistry* **29**: 2685 – 2691.
- Nelson DW, Sommers LE (1996) Total carbon, organic carbon and organic matter. *In*: Sparks (ed.) *Method of soil analysis. Part 3: Chemical methods*. SSSA Book Ser. 5. SSSA, Madison, WI, p. 961 – 1010.
- Noll KE (1992) Adsorption technology for air and water pollution control. *In*: Noll KE (editor), Lewis Publishers: p. 376.
- Norrström AC (2005) Metal mobility by de-icing salt from an infiltration trench for highway runoff. *Applied Geochemistry* **20**: 1907 – 1919.
- Oetjen K, Blotevogel J, Borch T, Ranville JF, Higgins CP (2018) Simulation of a hydraulic fracturing wastewater surface spill on agricultural soil. *Science of the Total Environment* **645**: 229 – 234.
- Oliveira IB, Demond AH, Salehzadeh A (1996) Packing of sands for the production of homogeneous porous media. *Soil Science Society of America Journal* **60**: 49 – 53.
- Ouali L, Pefferkorn E (1994) Fragmentation of colloidal aggregates induced by polymer adsorption. *Journal of Colloid and Interface Science* **168**: 315 – 322.
- Patterson RJ, Spoel (1981) Laboratory measurements of the strontium distribution coefficient K_d^{Sr} for sediment from a shallow sand aquifer. *Water Resources Research* **17**: 513 – 520.
- Powell BA, Miller T, Kaplan DI (2015) On the influence of ionic strength on radium and strontium sorption to sandy loam soils. *Journal of the South Carolina Academy of Science* **131**: 13 – 18.

- Prout WE (1958) Adsorption of radioactive wastes by Savannah River Plant soil. *Soil Science* **84**: 13 – 17.
- Ramachandran V, D'Souza SF (2013) Adsorption of nickel by Indian soils. *Journal of Soil Science and Plant Nutrition* **13**: 165 – 173.
- Randtke SJ, Jepsen CP (1982) Effects of salts on activated carbon adsorption of fulvic acids. *Journal – American Water Works Association* **74**: 84 – 93.
- Reddy MR, Dunn SJ (1986) Distribution coefficients for nickel and zinc in soils. *Environmental Pollution (Series B)* **11**: 303 – 313.
- Relyea JF (1982) Theoretical and experimental considerations for the use of the column method for determining retardation factors. *Radioactive Waste Management and the Nuclear Fuel Cycle* **3**: 151 – 166.
- Rhodes DW (1957) The effect of pH on the uptake of radioactive isotopes from solution by soil. *Soil Science Society of America Proceedings* **21**: 389 – 392.
- Rivard C, Lavoie D, Lefebvre R, Séjourné S, Lamontagne C, Duchesne M (2014) An overview of Canadian shale gas production and environmental concerns. *International Journal of Coal Geology* **126**: 64 – 76.
- Rogers JD, Burke TL, Osborn SG, Ryan JN (2015) A framework for identifying organic compounds of concern in hydraulic fracturing fluids based on their mobility and persistence in groundwater. *Environmental Science & Technology Letters* **2**: 158 – 164.
- Roy WR, Krapac IG, Chou SFJ, Griffin RA (1992) Batch-type procedures for estimating soil adsorption of chemicals. EPA/530/SW-87/006-F, April 1992.

- Ryan J, Miyamoto S, Stroehlein JL (1977) Relation of solute and sorbed boron to the boron hazard in irrigation water. *Plant and Soil* **47**: 253 – 256.
- Saha PK (2012) Sorption and transport modeling of copper in sandy soil. MSc Thesis.
- Saha PK, Badruzzaman ABM (2014) An experimental investigation of sorption of copper on sandy soil by laboratory batch and column experiments. *International Journal of Environment and Waste Management* **13**: 160 – 178.
- Sajih M, Bryan ND, Livens FR, Vaughan DJ, Descostes M, Phrommavanh V, Nos J, Morris K (2014) Adsorption of radium and barium on goethite and ferrihydrite: A kinetic and surface complexation modelling study. *Geochimica et Cosmochimica Acta* **146**: 150 – 163.
- Sang W, Stoof CR, Zhang W, Morales VL, Gao B, Kay RW, Liu L, Zhang Y, Steenhuis TS (2014) Effect of hydrofracking fluid on colloid transport in the unsaturated zone. *Environmental Science & Technology* **48**: 8266 – 8274.
- Seo DC, Yu K, Delaune RD (2008) Comparison of monometal and multimetal adsorption in Mississippi River alluvial wetland sediment: Batch and column experiments. *Chemosphere* **73**: 1757 – 1764.
- Serne RJ, LeGore VL (1996) Strontium-90 adsorption-desorption properties and sediment characterization at the 100 N-Area. PNL-10899, Pacific Northwest National Laboratory, Richland, Washington.
- Shaheen SM, Tsadilas CD, Mitsibonas T, Tzouvalekas M (2009) Distribution coefficient of copper in different soils from Egypt and Greece. *Communications in Soil Science and Plant Analysis* **40**: 214 – 226.

- Shaheen SM, Tsadilas CD, Rinklebe J (2013) A review of the distribution coefficients of trace elements in soil: Influence of sorption system, element characteristics, and soil colloidal properties. *Advances in Colloid and Interface Science* **201-202**: 43 – 56.
- Shimajima E, Sharma ML (1995) The influence of pore-water velocity on transport of sorptive and non-sorptive chemicals through an unsaturated sand. *Journal of Hydrology* **164**: 239 – 261.
- Sjolander SA, Clark J, Rizzo D, Turack J (2011) Water facts #31: Introduction to hydrofracturing. University Park, PA: Penn State College of Agricultural Sciences – Cooperative Extension.
http://www.shale-gas-information-platform.org/fileadmin/ship/dokumente/introduction_to_hydrofracturing-2.pdf
- Soares MR, Casagrande JC, Mouta ER (2011) Nickel adsorption by variable charge soils: Effect of pH and ionic strength. *Brazilian Archives of Biology and Technology* **54**: 207 – 220.
- Sparks DL (2000) New frontiers in elucidating the kinetics and mechanisms of metal and oxyanion sorption at the soil mineral/water interface. *Journal of Plant Nutrition and Soil Science* **163**: 563 – 570.
- Sposito G (1989) *The chemistry of soils*. New York: Oxford University Press.
- Streng DL, Peterson SR (1989) Chemical databases for the multimedia environmental pollutant assessment system. PNL-7145, Pacific Northwest Laboratory, Richland, Washington.
- Stuanes AO, Ogner G, Opem M (1984) Ammonium nitrate as extractant for soil exchangeable cations, exchangeable acidity and aluminum. *Communications in Soil Science and Plant Analysis* **15(7)**: 773 – 778.
- Su C, Suarez DL (1995) Coordination of adsorbed boron: A FTIR spectroscopic study. *Environmental Science and Technology* **29**: 302 – 311.

- Suzuki M, Kawai T, Kawazoe K (1976) Adsorption of poly(oxyethylene) of various molecular weights from aqueous solutions on activated carbon. *Journal of Chemical Engineering of Japan* **9**: 203 – 208.
- Tahervand S, Jalali M (2017) Sorption and desorption of potentially toxic metals (Cd, Cu, Ni and Zn) by soil amended with bentonite, calcite and zeolite as a function of pH. *Journal of Geochemical Exploration* **181**: 148 – 159.
- Tsang DCW, Lo IMC (2006) Competitive Cu and Cd sorption and transport in soils: A combined batch kinetics, column, and sequential extraction study. *Environmental Science and Technology* **40**: 6655 – 6661.
- United States Environmental Protection Agency (EPA) (1999) Understanding variation in partition coefficient, K_d , values. Volume II: Review of geochemistry and available K_d values for cadmium, cesium, chromium, lead, plutonium, radon, strontium, thorium, tritium (^3H), and uranium. EPA 402-R-99-004B.
- United States Environmental Protection Agency (2015). Review of state and industrial spill data: Characterization of hydraulic fracturing-related spills. Office of Research and Development, Washington, D.C., EPA/601/R-14/001.
- United States Environmental Protection Agency (2016). Hydraulic fracturing for oil and gas: Impacts from the hydraulic fracturing water cycle on drinking water resources in the United States. Office of Research and Development, Washington, D.C., EPA/600/R-16/236Fa.
- Usman ARA (2008) The relative adsorption selectivities of Pb, Cu, Zn, Cd and Ni by soils developed on shale in New Valley, Egypt. *Geoderma* **144**: 334 – 343.

- van Beinum W, Hofmann A, Meeussen JCL, Kretzschmar R (2005) Sorption kinetics of strontium in porous hydrous ferric oxide aggregates I. The Donnan diffusion model. *Journal of Colloid and Interface Science* **283**: 18 – 28.
- Vega FA, Covelo EF, Andrade ML (2008) A versatile parameter for comparing the capacities of soils for sorption and retention of heavy metals dumped individually or together: Results for cadmium, copper and lead in twenty soil horizons. *Journal of Colloid and Interface Science* **327**: 275 – 286.
- Vengosh A, Warner N, Jackson R, Darrah T (2013) The effects of shale gas exploration and hydraulic fracturing on the quality of water resources in the United States. *Procedia Earth and Planetary Sciences* **7**: 863 – 866.
- Vidic RD, Brantley SL, Vandenbossche JM, Yoxtheimer D, Abad JD (2013) Impact of shale gas development on regional water quality. *Science* **340**: 826.
- von Gunten K, Alam MS, Hubmann M, Ok YS, Konhauser KO, Alessi DS (2017) Modified sequential extraction for biochar and petroleum coke: Metal release potential and its environmental implications. *Bioresource technology* **236**: 106 – 110.
- Warner NR, Jackson RB, Darrah TH, Osborn SG, Down A, Zhao K, White A, Vengosh A (2012) Geochemical evidence for possible natural migration of Marcellus Formation brine to shallow aquifers in Pennsylvania. *Proceedings of the National Academy of Sciences of the United States of America* **109**: 11961 – 11966.
- Warner NR, Jackson RB, Darrah TH, Millot R, Kloppmann W, Vengosh A (2014) New tracers identify hydraulic fracturing fluids and accidental releases from oil and gas operations. *Environmental Science & Technology* **48**: 12552 – 12560.
- Yalamanchali RC (2012) How mobile is lithium in the soil-plant system?: Lithium, an emerging environmental contaminant, is mobile in the soil-plant system. MSc Thesis.

- Ye Z, Prigiobbe V (2018) Effect of ionic strength on barium transport in porous media. *Journal of Contaminant Hydrology* **209**: 24 – 32.
- Yu S, Mei H, Chen X, Tan X, Ahmad B, Alsaedi A, Hayat T, Wang X (2015) Impact of environmental conditions on the sorption behavior of radionuclide $^{90}\text{Sr}(\text{II})$ on Na-montmorillonite. *Journal of Molecular Liquids* **203**: 39 – 46.
- Zachara JM, Streile GP (1991) Use of batch and column methodologies to assess utility waste leaching and subsurface chemical attenuation. ERPI EN-7313, Project 2485-8 Interim Report, May 1991.
- Zhang F, Ou X, Ran C, Wu Y (2011) Influence of pH, ionic strength, and temperature on adsorption of lead, copper and zinc in natural soils. *Advanced Materials Research* **255-260**: 2810 – 2814.
- Zhang P-C, Brady PV, Arthur SE, Zhou W-Q, Sawyer D, Hesterberg DA (2001) Adsorption of barium(II) on montmorillonite: An EXAFS study. *Colloids and Surfaces A: Physicochemical and Engineering Aspects* **190**: 239 – 249.
- Zhao X, Urano K, Ogasawara S (1989) Adsorption of polyethylene glycol from aqueous solution on montmorillonite clays. *Colloid and Polymer Science* **267**: 899 – 906.
- Zhu B, Alva AK (1993) Differential adsorption of trace metals by soils as influenced by exchangeable cations and ionic strength. *Soil Science* **155**: 61 – 66.
- Zhuang J, Goeppert N, Tu C, McCarthy J, Perfect E, McKay L (2010) Colloid transport with wetting fronts: Interactive effects of solution surface tension and ionic strength. *Water Research* **44**: 1270 – 1278.

Chapter 4 – HYDROSCAPE: A new versatile software program for evaluating contaminant transport in groundwater³

4.1. Introduction

Modeling how contaminants are transported in the subsurface is an important aspect in contaminant hydrogeology due to its application in developing proper remediation strategies. The complexities associated with most contaminated sites may include geological heterogeneities, material variability, and spatial and temporal changes in both the source region and groundwater flow. Therefore, numerical simulations are often used to predict the fate and transport of contaminants in the subsurface. However, numerical simulations can be costly, require copious amounts of data, are time consuming to construct, and may be subject to errors such as numerical dispersion, oscillations, non-convergence, and truncation errors (Zheng and Bennett 1995). Analytical solutions to the advection-dispersion equation (ADE; equation 4.1), a partial differential equation that describes the transport of a solute through advection, dispersion, and diffusion, are therefore invaluable for rapid and inexpensive assessments of contaminant scenarios (Cecan and Schneiber 2008), determining the mechanisms for transport (Park and Zhan 2001) and verifying numerical codes (Cecan and Schneiber 2008).

$$R \frac{\partial C}{\partial t} = D_L \frac{\partial^2 C}{\partial x^2} + D_{TH} \frac{\partial^2 C}{\partial y^2} + D_{TV} \frac{\partial^2 C}{\partial z^2} - v \frac{\partial C}{\partial x} - \lambda C \quad (4.1)$$

Notation and terms are defined in **Table 4.1**.

³ A version of this chapter has been submitted to and published in *SoftwareX* as Funk S, Hnatyshin D, Alessi DS (2017) HYDROSCAPE: A new versatile software program for evaluating contaminant transport in groundwater. <https://doi.org/10.1016/j.softx.2017.10.001>

HYDROSCAPE uses an analytical solution to equation 4.1 (Karanovic et al. 2007; hereafter referred to as “the solution”), and packages it into an easy-to-use interactive graphical user interface (GUI) that produces high-quality outputs, includes a parameter estimator for inverse modeling, and allows the user to upload maps from Google Maps™. Furthermore, we have modified the solution to allow users to: 1) build a customizable source region; and 2) implement horizontal geological units, each having different hydraulic and transport parameters, within the domain (“simple geology”). These novel features allow hydrogeologists to simulate quickly more complex scenarios that would otherwise be impossible with conventional analytical solutions. As a screening-level tool, HYDROSCAPE is more versatile and more broadly applicable than other programs currently available (see below).

Following its development, we used HYDROSCAPE to simulate various spill scenarios of flowback and produced water (FPW) from hydraulic fracturing operations. HYDROSCAPE was utilized to test the differences in transport behavior of specific classes of contaminants found in FPW, depending on the source of the sorption data. Experimentally-derived results from **Chapter 2** and **Chapter 3**, along with published literature sources, were used. Ultimately, HYDROSCAPE may expedite the evaluation of remediation strategies for contaminated sites by hydrogeologists and environmental scientists. Additional details are provided in **Appendix C** and the User’s Manual (<https://www.eas.ualberta.ca/download/>).

4.2. Comparison with Related Programs

Windows-based software programs utilizing analytical solution to the ADE have been developed in the past and are briefly described below.

The FORTRAN-based computer program 3DADE and N3DADE were developed by the US Department of Agriculture (Leij and Bradford 1994), based on the solutions of Leij et al. (1991) and (1993). However, these programs come with the disclaimer “The code lacks the versatility to handle a wide variety of transport scenarios, whereas computational efficiency and user-friendliness were not a major concern during code development” (Leij and Bradford 1994).

The code for AT123D was developed based on the semi-analytical solutions in Yeh (1981). The AT123D models have been used to simulate 3D transport of dissolved contaminants (e.g. Sinton et al. 2000), with a variety of source region configurations to choose from, within semi-infinite or finite aquifers. The use of Green’s functions in AT123D allows for the user to choose from simple geometric sources, including point, line, plane, or prismatic sources, and allows for either semi-infinite or finite aquifers Yeh (1981). Improvements made in the numerical integration and infinite series schemes (Burnell et al. 2012) and the introduction of a GUI (Burnell et al. 2016) have subsequently improved the code (now called AT123D-AT).

Perhaps the most well-known analytical solution-based computer program is the Domenico (1987) family of software programs (i.e. BIOSCREEN and BIOCHLOR), which were developed by the US EPA (Environmental Protection Agency) for the simulation of either hydrocarbon-based contaminants (BIOSCREEN; Newell et al. 1996) or chlorinated solvents (BIOCHLOR; Aziz et al. 2000) through natural attenuation. The benefit of BIOSCREEN (and its improved BIOSCREEN-AT; Karanovic et al. 2007) and BIOCHLOR is that the code is readily available as an easy-to-use Microsoft Excel[®]-based program. Similar to BIOSCREEN, Neville (1998) developed ATRANS for a continuous patch source in a finite-thickness aquifer. Using the principle of superposition, ATRANS allows the user to create an arbitrary source function, whereas BIOSCREEN allows for a “layer cake” source region (Connor et al. 1994; discussed

more in **Section 4.4.4.1.**) Recently, an extension of ArcGIS called ArcNLET was developed for simulating nitrate load in groundwater (Rios et al. 2013). ArcNLET uses the Domenico (1987) solution to solve the transport module of the program. ArcNLET first solves the flow module using a digital elevation map (DEM) and a map of the distribution of hydraulic conductivities and porosities (Rios et al. 2013). Using some simplifying assumptions, particle tracking is used to generate a representation of the groundwater flow field (Rios et al. 2013). ArcNLET then solves the transport of nitrate by superimposing the plume onto the flow field such that the centerline of the plume conforms with the flow paths of the field (Rios et al. 2013). Comparisons with numerical simulations shows that the ArcNLET implementation is adequate for a screening-level tool (Rios et al. 2013).

Table 4.2 highlights some of the key features of the abovementioned programs and compares them to HYDROSCAPE. Most of the programs mentioned are largely constrained by the limitations and simplifications of the analytical solutions on which they are based (e.g. 3DADE/N3DADE and AT123D-AT). Other than BIOSCREEN (Newell et al. 1996) and ATRANS (Neville 1998), the analytical solutions used remain unaltered. However, a feature that most programs lack is the ability to simulate horizontal layers within the domain (i.e. simple geology). ArcNLET allows its users to simulate horizontal heterogeneity, whereas HYDROSCAPE allows for vertical heterogeneity; however, ArcNLET lacks the customizability of the source region (**Table 4.2**).

4.3. HYDROSCAPE Architecture

HYDROSCAPE is a MATLAB[®]-based program that uses a modified solution to the ADE to solve solute transport problems. To increase accessibility, HYDROSCAPE has been compiled into an executable file, allowing the user to run the program without MATLAB[®]. User-

friendliness, versatility and computational efficiency were of primary concern during the development of the code and interface (**Figure 4.1**). HYDROSCAPE was created to be used in two ways: 1) to solve a forward problem whereby parameters are known, and the user is interested in predicting the fate of the plume; or 2) to solve the inverse problem, whereby the user has some experimental or field data and wants to estimate what set(s) of parameters can reproduce the data (outlined in **Section 4.4.2**).

For the forward problem, users work through HYDROSCAPE's tab structure, inputting the requisite parameters in each tab (**Figure 4.1**). Each tab (and certain buttons) is color coded to emphasize what parameters are required to be inputted and accepted. HYDROSCAPE then produces a simulation for the user to review. Standard outputs include surface and contour maps in map and cross-sectional views, three-dimensional contour volumes, concentration profiles (along an arbitrary transect), and breakthrough curves, all of which can be animated. Multiple breakthrough curves and concentration profiles can be plotted together for comparison. HYDROSCAPE also calculates a variety of parameters associated with the plume (e.g. plume dimensions, mass, and volume). HYDROSCAPE allows the user to import and overlay a map by accessing Google Maps™, allowing for a quick assessment of the real-world extent of a plume (**Figure 4.1**).

For the inverse problem, users may select the "Parameter Estimator" feature in HYDROSCAPE. Users must input the patch source geometry, the free-solution diffusion coefficient, and "control points", known values of concentration at specified locations in space and time. The user is also required to put realistic upper and lower bounds on the estimated parameters (see **Table 4.3**). After all inputs are entered, HYDROSCAPE automatically finds

matching parameter sets that fit the given control points to within a user-defined tolerance (more details in **Section 4.4.2.**).

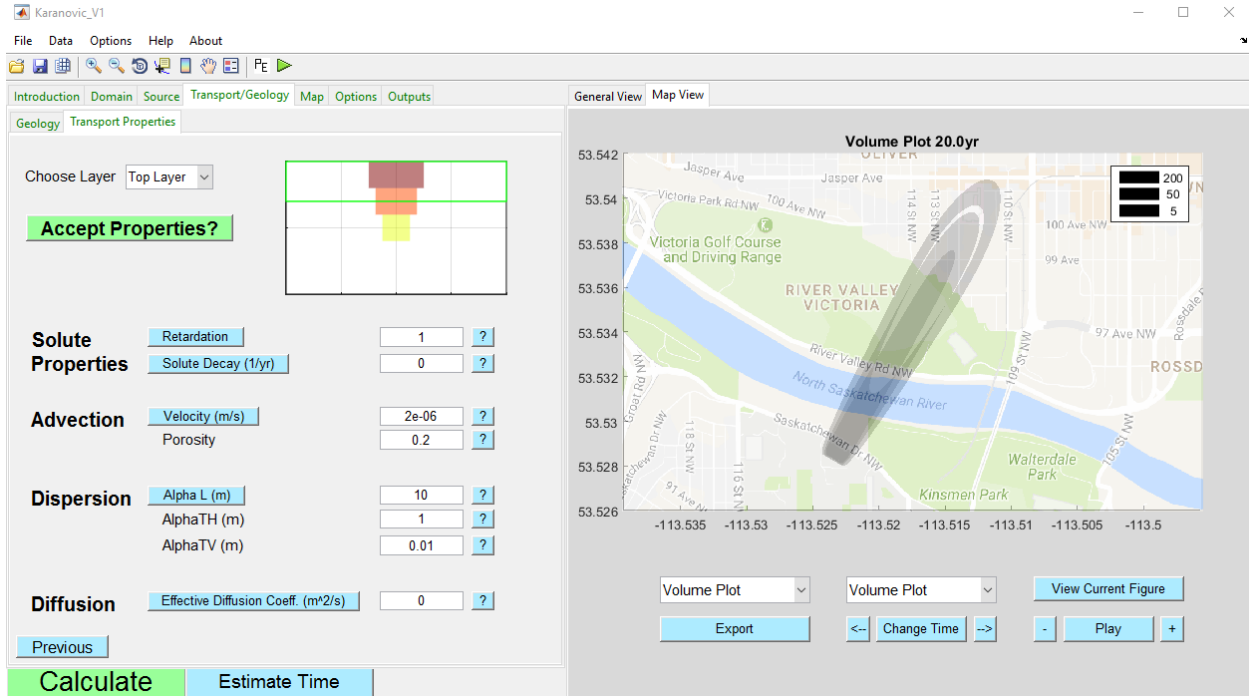


Figure 4.1: HYDROSCAPE’s graphical user interface (GUI) showcasing a user-defined source region and simple geology (left side) with a Google Maps™ output (right side). Figure not based on a real site.

4.4. Implementation

4.4.1. Advanced Features

HYDROSCAPE uses mathematical techniques to modify the solution to make it more versatile. These modifications allow the user to: 1) build a custom source region (arbitrary source function/geometry and spatial variations in source concentration); and 2) implement horizontal geological units within the domain.

4.4.1.1. User-Defined Sources

One of the major limitations of analytical solutions is that the user has very little control over the characterization of the source region. Most analytical solutions force the user to represent the source region with simple geometric shapes, such as points, lines, rectangular planes, or prisms, which have spatially uniform concentration distributions and simple source functions. This is rarely the case in reality; most source regions vary, both spatially (in shape and concentration) and temporally. With these limitations in mind, HYDROSCAPE aimed to loosen these constraints by allowing the user to customize the source region to fit any situation.

Source histories are known to fluctuate with time due to changes in loading histories, infiltration rate, properties of the source region and seasonal effects (e.g. Frind and Hokkanen 1987); therefore, being able to implement a dynamic source function is a key advantage when using HYDROSCAPE. The method used to create an arbitrary source function is similar to that outlined by Neville (1998), however, we used the logistic function, $L(t-t_0)$ (equation 4.2), rather than the Heaviside step function. This was done to allow for faster computations.

$$L(t-t_0) = \frac{1}{1 + \exp(-k(t-t_0))} \quad (4.2)$$

where k defines the sharpness of the step, and t_0 defines when the time change occurs.

If $S(x, y, z, t)$ is the solution to the ADE, then by using principle of superposition, we are able to construct an arbitrary source function in the following way:

$$S_{TOTAL}(x, y, z, t) = \text{Re} \left(\sum_{i=1}^n L_i(t-t_i) \Delta C_i S(x, y, z, t_i) \right) \quad (4.3)$$

where n defines how many steps in the source function there are, and ΔC_i defines the relative concentration change for that step.

Similarly, source regions rarely have simple geometries and uniform concentration distributions; by allowing the user to construct an arbitrary source geometry (shape) and implement spatial variability in source concentration (Connor et al. 1994), we allow for better physical characterization of the source region. This requires building a source region of rectangular tiles, with a different concentration assigned to each tile, and translating those tiles to the appropriate position. By applying the principle of superposition, the full source region can be calculated (**Figure 4.2**). This method is less restrictive than the “layer cake” method (Connor et al. 1994) used in BIOSCREEN; ultimately, the “layer cake” method (Connor et al. 1994) always results in a rectangular patch source, whereas our method can accommodate any source region shape.

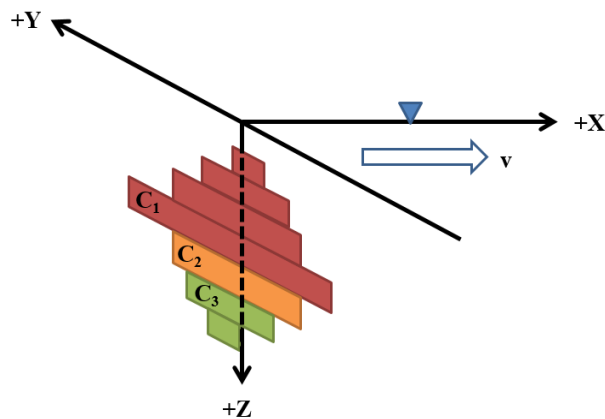


Figure 4.2: Schematic diagram illustrating how HYDROSCAPE constructs a source region of arbitrary shape and arbitrary concentration distribution. $C_1 \neq C_2 \neq C_3$.

4.4.1.2. Simple Geology

Layering in the subsurface can dramatically affect the transport of contaminants, however, typical analytical solutions do not explicitly solve for this additional complexity. Therefore, in HYDROSCAPE, we have designed a “simple geology” feature to allow for the construction of horizontal layers in the subsurface. By translating solutions vertically to the interface between layers (similar to the method outlined in **Section 4.4.1.1.**), applying a different set of parameters for each layer and then superimposing the solutions, we are able to achieve an approximation of horizontal bedding (**Figure 4.3**). HYDROSCAPE’s implementation of horizontal beds is purely heuristic (outlined further in **Section 4.5**) and is subject to non-trivial errors without careful consideration (also see **Appendix C**).

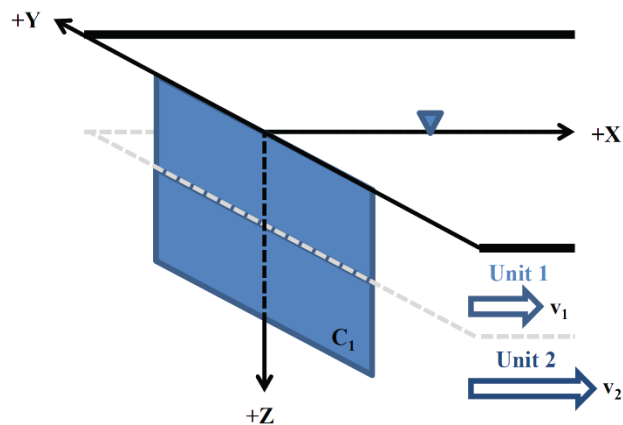


Figure 4.3: Schematic diagram illustrating how HYDROSCAPE implements simple geology. The algorithm splits the patch source into two different patch sources, with the lower patch source translated, each with a distinct set of transport and hydraulic parameters.

4.4.2. Parameter Estimation and Sensitivity Analysis

One of the advantages in using analytical solutions is that we can estimate field parameters related to contaminant movement in the subsurface relatively easily (Park and Zhan

2001). Hydrogeologists may have sparse information on the subsurface properties of a contaminated site, yet often still need to model the site. To aid users during the modeling phase of most contamination sites, HYDROSCAPE includes a parameter estimator algorithm, utilizing a brute-force algorithm to find the appropriate parameters for a particular scenario. A brute-force algorithm was chosen over more sophisticated techniques due to its algorithmic simplicity, high success rate in finding one or more parameter sets for the problem, if one exists, and computational efficiency (when applied to analytical solutions).

In the algorithm, HYDROSCAPE takes “control points” (see **Section 4.3**) and runs exclusionary simulations. The user must first place realistic upper and lower bounds on each parameter that is to be estimated. HYDROSCAPE then calculates the resultant concentration for each combination of parameters at the point in space and time for the first control point. The algorithm then compares the resultant concentration with the concentration specified at the first control point. Only those sets of parameters that match the concentration of the control point, to within a user-defined acceptable range, are kept. By using successive control points as filters, smaller sets of parameters are achieved.

The parameter estimator packaged with HYDROSCAPE can generally solve for all parameters within the solution (**Table 4.3**), but we only allow for a single patch source with a user-defined free-solution diffusion coefficient to reduce computational time and the number of non-unique sets. Due to the preset source geometry, HYDROSCAPE cannot estimate parameters for models using the advanced features mentioned in **Section 4.4.1**.

It is common for multiple sets of calibrated parameters (i.e. non-uniqueness) to be calculated by our parameter estimator. To evaluate the sensitivity of these parameters,

HYDROSCAPE has a built-in sensitivity analysis routine whereby HYDROSCAPE produces a breakthrough curve for each parameter combination. The results are plotted together to allow the user to quickly and easily evaluate the sensitivity of the solution.

4.5. Comparison with Numerical Simulations

To showcase the “simple geology” feature in HYDROSCAPE, we conceptualized a simple aquifer-aquitard example, whereby an overlying 30 m thick lower permeability layer ($K = 1.2 \times 10^{-6}$ m/s) is underlain by a semi-infinitely thick higher permeability unit ($K = 1.2 \times 10^{-5}$ m/s). The top boundary is taken to be an impermeable boundary. To demonstrate the customizability of the source region, the source region we conceptualized has a complex shape and concentration distribution (**Figure 4.4A** and **Table 4.4**) that is unable to be modeled with conventional analytical solutions; additionally, we imposed a dynamic source history in our simulation (**Figure 4.4B**). The solute is taken to be conservative ($R = 1, \lambda = 0$). To test the validity of HYDROSCAPE’s heuristic modeling of simple geology, we compared our results to numerical simulations produced by the finite-difference code MODFLOW-2005 (Harbaugh 2005) using MT3DMS (Zheng and Wang 1999) (together referred to as MODFLOW). For a proper comparison, identical sets of parameters and domains were used (**Table 4.5**). The numerical model was solved using an upstream finite difference (UFD) method; the model discretization (Δx) varied, finer near the source region and coarsening outward (**Table 4.5**), and was such that the Peclet number ($Pe_x = v\Delta x / D_L$) was ≤ 10 to minimize numerical dispersion yet produce reasonable computational times.

The plume shapes and concentration distributions predicted by HYDROSCAPE are comparable to those produced with MODFLOW (**Figure 4.5**). Distinctive features in the

simulations, such as “plume pinch-outs” (e.g. **Figure 4.5B**), were also reproduced to a high level of accuracy (also see **Appendix C**). Investigation of the breakthrough curves at representative depths (2.5 and 52.5 m) along the centerline profile shows that HYDROSCAPE typically produces concentrations lower than MODFLOW (**Figure 4.6**), but are similar in trend and magnitude. Differences between the two models are generally small (<20%) (see **Appendix C**). Similarly, the plume mass calculated by HYDROSCAPE (13,817 kg) is comparable to MODFLOW (13,596 kg).

The observed differences in predicted concentrations (relative to MODFLOW) from HYDROSCAPE may be a result of a number of factors. We speculate it may be due to the finite length in the MODFLOW patch source, is an inherent feature in the analytical solution, the discretization in MODFLOW, or is caused by numerical errors when solving the finite-difference equations using the UFD solver. Differences in breakthrough times are also speculated to be caused by the finite length in MODFLOW and resultant differences in the advective front. However, these discrepancies are unlikely, in our opinion, to be a result of the implementation of the novel features in HYDROSCAPE. Since the differences between the analytical and numerical simulations are small for much of the domain, and result in very similar plume shapes, sizes and mass, the advanced features in HYDROSCAPE are useful screening-level tools under the strict constraints that both: 1) the transverse vertical dispersivity, and 2) exchange by molecular diffusion between layers are negligible (see **Appendix C**).

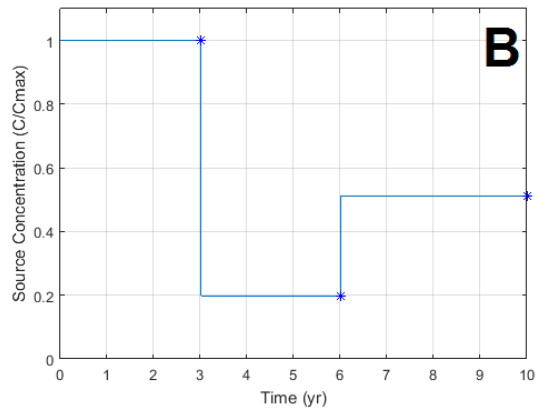
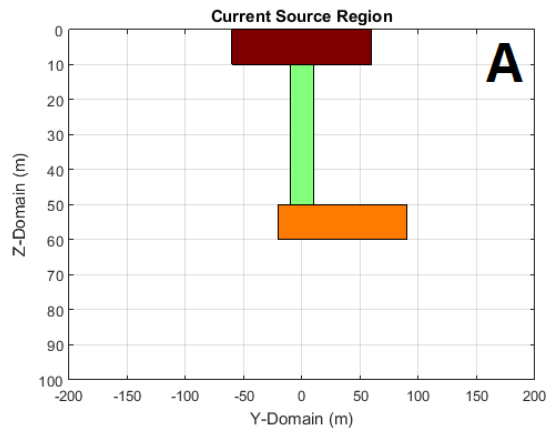


Figure 4.4: **A)** Source region geometry and concentration distribution. Inputs for the source regions are given in Table 4.4. **B)** The source function used.

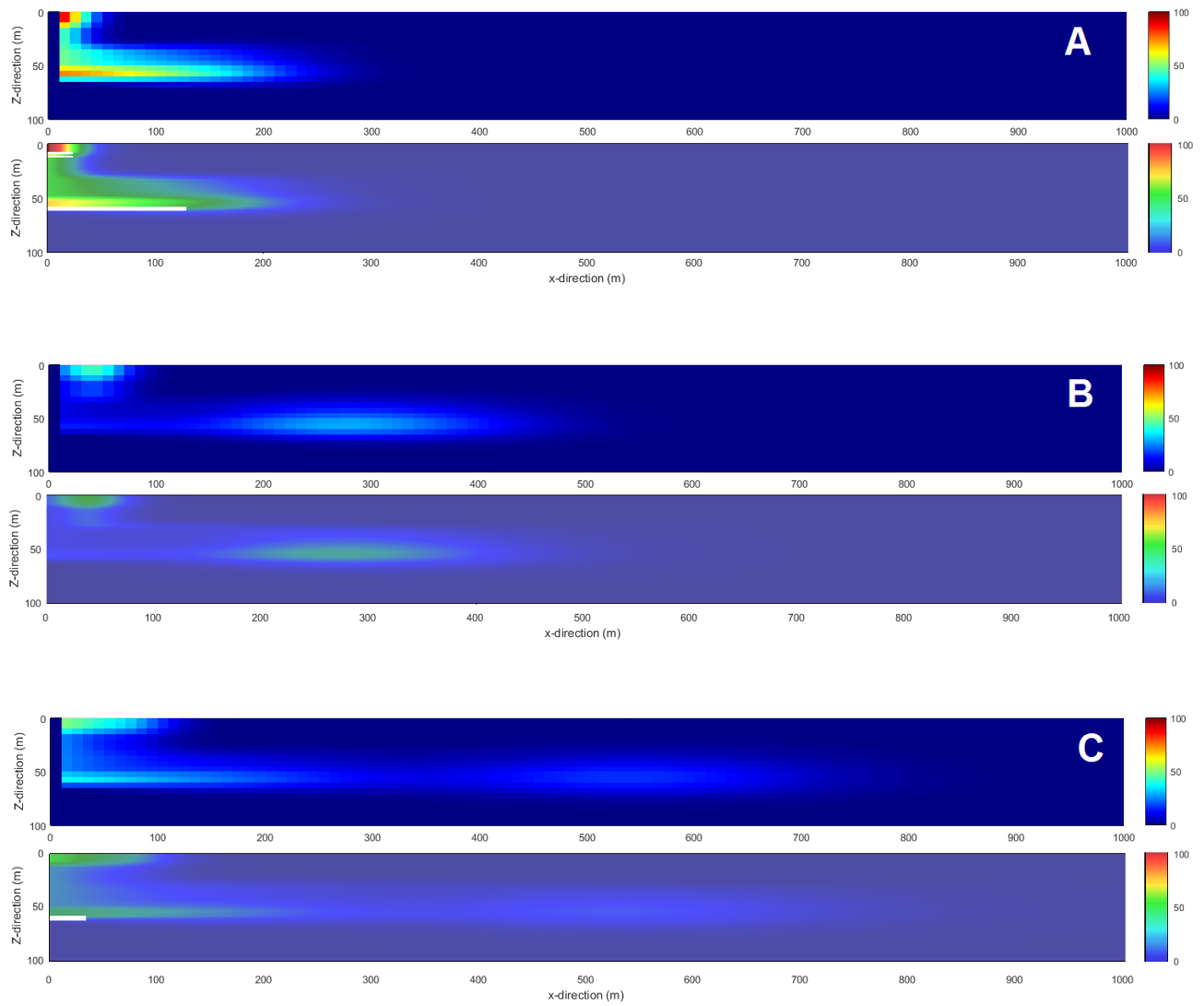


Figure 4.5: Comparison of HYDROSCAPE (top) and MODFLOW (bottom) in cross-section through the centerline after **A)** 3 years; **B)** 6 years; and **C)** 10 years. Color bar units are in mg/L.

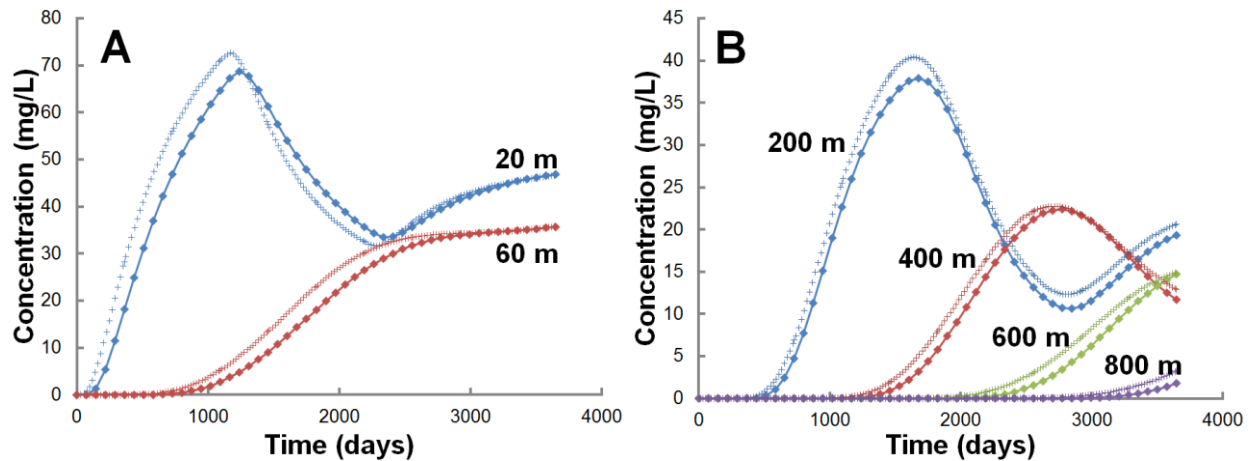


Figure 4.6: Comparison of breakthrough curves; **A)** within the aquitard screened at a depth of 2.5 m; **B)** within the aquifer screened at 52.5 m. Crosses denote MODFLOW; diamonds denote HYDROSCAPE.

4.6. Transport of FPW contaminants

To determine the potential transport and distribution of contaminants in flowback and produced water (FPW) in the subsurface, simple, first-order simulations were conducted using the analytical model within HYDROSCAPE. To use HYDROSCAPE, several simplifications and assumptions needed to be made. HYDROSCAPE requires the assumption that the aquifer is homogeneous, hydraulically isotropic, and fully saturated. The sorption reactions are also assumed to be accurately represented by a single constant retardation factor, and desorption is assumed to be negligible. The model also assumes that the properties (e.g. density, viscosity) of the fluid (i.e. the FPW) are negligibly different to fresh water. The total dissolved solid (TDS) of the FPWs studied were >140,000 mg/L, and specific gravity of the FPWs were >1.1. Therefore, the density (and possibly viscosity) effects the FPW may have on the subsurface groundwater system are not considered, and not modeled explicitly. Therefore, these simulations are not meant to accurately simulate an FPW spill. Rather, our goal with these simulations were threefold: (1) to illustrate the usefulness of HYDROSCAPE for modeling certain transport scenarios; (2) to illustrate the importance of considering co-contaminant interaction, in this case

applied to FPW spills; and (3) to demonstrate contaminant separation that may occur due to differences in sorption affinity of the constituents of FPW.

To that end, we will show the results from three different conceptual models for FPW leakage into the subsurface: the first scenario simulates the discrete input of FPW into an alluvial aquifer, the second scenario simulates continuous leakage of FPW into a sandy aquifer, and lastly, the third scenario simulates the continuous downward percolation of FPW through an organic-rich, clay-rich soil horizon. Results from **Chapter 2** and **Chapter 3** will be used in these simulations. Model parameters are provided in **Table 4.6**.

The first scenario, a discrete input of FPW into an alluvial aquifer, was based on spill data taken from US EPA (2015) and Gandhi (2017). In this scenario, a source function was utilized to represent the source as a continuous point source that lasted for 96 h, after which, the source concentration dropped to zero, simulating the cessation of the leakage. Four different classes of contaminants were chosen to be represented: conservative solutes (represented by Cl), divalent cations (represented by Sr), heavy metals (represented by Cu), and polyethylene glycols (PEGs) (represented by PEG-6 and PEG-11). The model assumes that the aquifer is fully saturated, and that sorption can be represented by a single retardation factor R . Further, each class of contaminants were simulated individually, after which the results from each simulation were superimposed. For the purposes of this simulation, the 3D model was represented as a pseudo-2D model, whereby the source region was assumed to be fully penetrating and dispersion in the transverse vertical direction was assumed to be negligible. Breakthrough curves were generated 50 m away from the source along the centerline. The results from simulations using parameters from the column experiments, the batch sorption experiments with fluvial sand, and literature values are given in **Figure 4.7**. Using the K_d values experimentally derived from our

column experiments in **Chapter 3 (Tables 3.5 and 3.7)**, after Cl appears, we observe a quick succession of Sr, followed by light organics (PEG-6), with decreasing peak concentrations with increasing time. These three classes of contaminants all peak and dissipate within a year (**Figure 4.7A**). Heavier organics (PEG-11) appear and peak after approximately 5 years, with a peak concentration an order of magnitude less than those observed with PEG-6 (**Figure 4.7A**). Lastly, the modeled heavy metals (Cu) appears last, peaking around a decade after the discrete input, with a peak concentration comparable with that observed in PEG-11 (**Figure 4.7A**). A slightly different sequence was observed using experimental results from our batch sorption experiments. Strontium is still the first contaminant to appear, but is observed to peak at a slightly later time compared to the previous simulation (**Figure 4.7B**); likewise, PEG-6 also appears next, at a later time, and is almost coincident with Cu (**Figure 4.7B**). Lastly, within a century, PEG-11 was never observed to peak. The last set of simulations that were run utilized representative values taken from published literature (Sr: US EPA 1999; PEGs: Zhao et al. 1989; Cu: Shaheen et al. 2009). These simulations showed the most deviation compared to the previous sets of experiments. After Cl appears, light organics (PEG-6), followed by heavier organics (PEG-11) appear soon after (**Figure 4.7C**). Strontium peaks around a decade after the input, with a peak concentration significantly less than those observed for the organics (**Figure 4.7C**). Copper is the last contaminant to breakthrough, peaking at around a half century after the initial input (**Figure 4.7C**). Differences in our model predictions between the column transport and batch sorption experiments highlight the importance of considering the impact flow may have on sorption processes. Likewise, the differences between using K_d values obtained from literature and our experimental results from FPW highlight the importance of considering co-contaminant interactions.

In the second scenario, the source region was replaced with a continuously leaking point source inputting mass into the same alluvial aquifer above. As above, four classes of contaminants were chosen to be simulated. Likewise, the same assumptions about the aquifer and sorption, as outlined above, were made here. Breakthrough curves were generated 200 m away from the source along the centerline. The results from simulations using parameters from the column experiments, the batch sorption experiments with fluvial sand, and literature values are given in **Figure 4.8**. Our results from the column transport experiments, as well as the simulations (**Figure 4.8A**), suggest that after Cl appears, Sr and light organics (PEG-6) would be among the first to breakthrough, within a year, with heavier organics subsequently appearing afterward, on the order of decades, with heavy metals breaking through last, taking almost a century (**Figure 4.8A**). However, using the results from our batch sorption experiments with FPW onto fluvial sand, we would predict something different entirely. Strontium would breakthrough in slightly more than a year, and heavy metals (Cu) and light organics (PEG-6) would breakthrough within several years (**Figure 4.8B**). Heavy organics (PEG-11) would not breakthrough within a millennium (**Figure 4.8B**). The results demonstrate the impact flow may have on sorption, and the variation in results one can obtain if not considered. Using K_d values obtained from published literature (US EPA 1999; Zhao et al. 1989; Shaheen et al. 2009) results in yet different observations. Using just literature values, we would predict organics (both PEG-6 and -11) to breakthrough shortly after Cl, within a year, with Sr taking a couple of decades, and heavy metals taking a century (**Figure 4.8C**). Some similarities can be seen between the simulations using column experiment data and the literature values, such as the Cu and PEG-6 trends, whereas for others, they are quite different, with Sr predicted to breakthrough much later, and PEG-11 predicted to breakthrough much earlier (**Figure 4.8C**).

In our third scenario, we simulated the continuous downward percolation of FPW through an organic-rich, clay-rich soil horizon. Five different classes of contaminants found in FPW were chosen: conservative solutes (represented by Cl), divalent cations (represented by Sr), aryl phosphates (represented by DPP), and PEGs (represented by PEG-6 and PEG-11). The sorption of heavy metals (e.g. Ni, Cu) from Sample 1 were not quantified in **Chapter 3** due to their lack of detection in the collected effluent and are therefore not included in this set of simulations. We assumed that the soil horizon was fully saturated for simplicity. As in the above simulations, sorption was assumed to be represented by a single retardation factor R. For the purposes of this simulation, the 3D model was reduced to a pseudo-1D model by having the patch source significantly greater than the thickness of the soil, with the FPW travelling through a 5 m thick soil layer. K_d values were taken for the moraine set of experiments (**Tables 3.5 and 3.7**). Further, while DPP was not quantified in the FPW batch sorption experiments in **Chapter 3**, we used the results from **Chapter 2** here, assuming the sorption of DPP would not be effected by co-contaminant interactions (**Table 2.1**). A sensitivity analysis was conducted to determine the influence of the longitudinal dispersivity (α_L) on the transport characteristics (**Figure 4.9**). Generally, using a higher α_L results in earlier breakthrough. The order in which contaminants appear is similar for both sets of simulations. We found that Cl appears first, generally less than a decade, followed by lighter organics (DPP and PEG-6), on the order of several decades depending on α_L , followed by Sr and heavier organics (PEG-11) (**Figure 4.9**). As above, these sets of simulations demonstrate the phenomena of contaminant separation.

The results from the simulations further demonstrate contaminant separation caused by sorption. McLaughlin et al. (2016) discussed possible implications for contaminant separation and the importance of considering co-contaminant interactions. They studied the sorption of

several organic compounds commonly found in hydraulic fracturing fluids, including biocides (glutaraldehyde; GA), surfactants (PEGs), and friction reducers (polyacrylamide; PAM), onto agricultural soil. A synthetic mixture of these compounds was made in a laboratory and experiments were conducted in aerobic batch reactors. They found that the biocides present in the fluid initially inhibited microbial degradation of organics, but due to rapid sorption and removal of GA onto the soil, the aqueous concentration of the biocide dropped to below effective limits, allowing biodegradation processes to occur. Further, McLaughlin et al. (2016) argued for the importance of considering co-contaminant effects when dealing with hydraulic fracturing fluids and other complex fluids, such as the impact surface-active agents (surfactants; e.g. PEGs) may have on increasing the mobility of other organic additives in the fluid or solubilizing metals present in the soil. Our results further highlight the importance of considering co-contaminant interactions, and contaminant separation, but also how flow may impact these abiotic processes, and how these processes may be altered in an anaerobic setting commonly found in saturated aquifers.

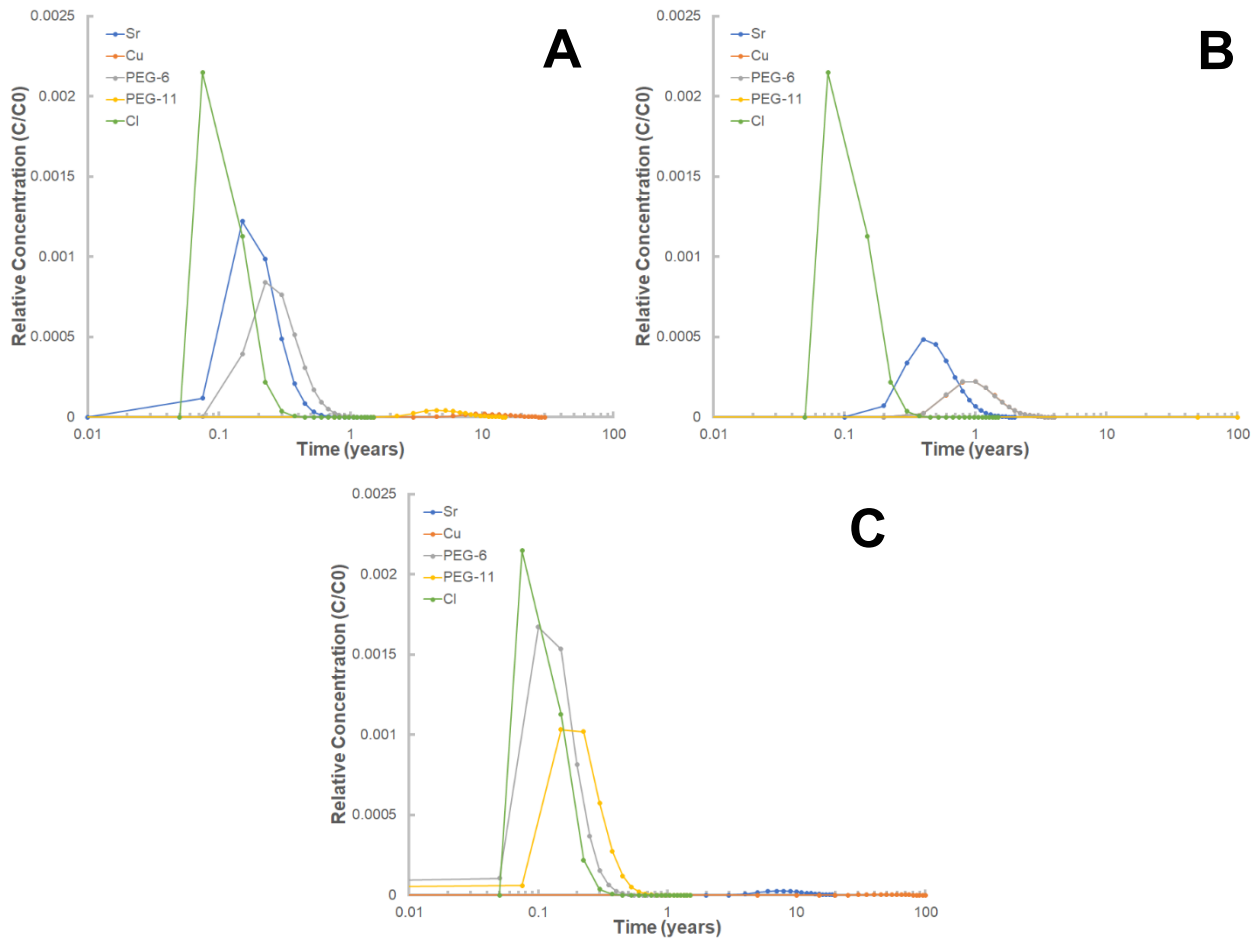


Figure 4.7: Comparison of breakthrough curves for discrete 3-D simulations taken 50 m away through fluvial sediment from the source with Cl (green), Sr (blue), Cu (orange), PEG-6 (grey), and PEG-11 (yellow) using K_d values from: **A)** column experiments; **B)** batch experiments; and **C)** literature values.

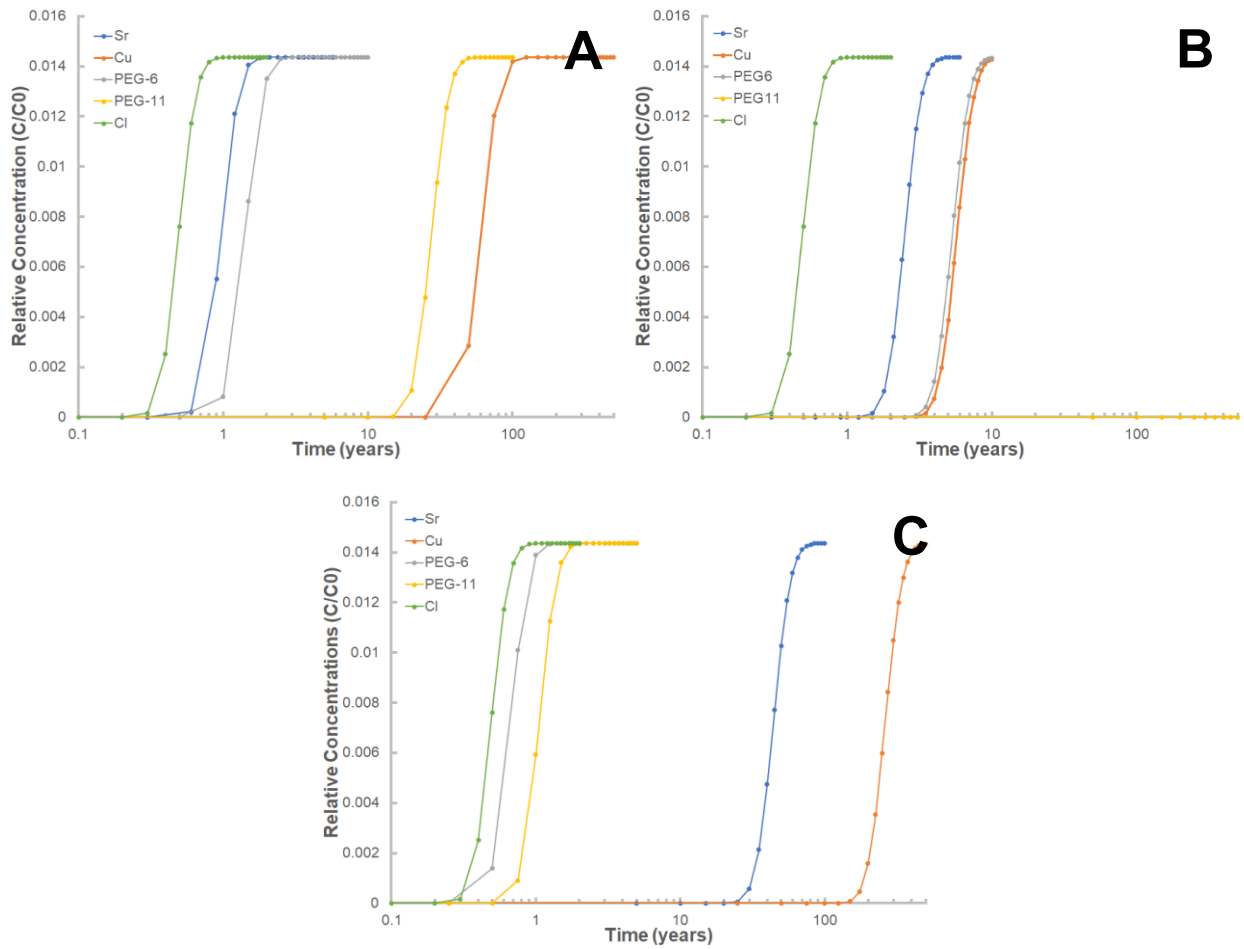


Figure 4.8: Comparison of breakthrough curves for 3-D simulations taken 200 m away through fluvial sediment from the source with Cl (green), Sr (blue), Cu (orange), PEG-6 (grey), and PEG-11 (yellow) using K_d values from: **A)** column experiments; **B)** batch experiments; and **C)** literature values.

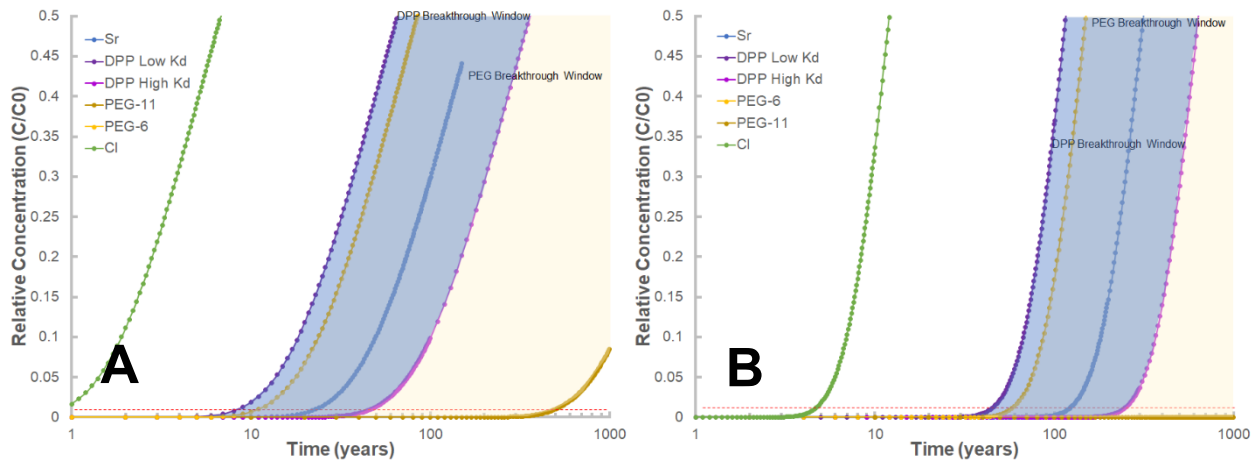


Figure 4.9: Comparison of breakthrough curves for 1-D simulations taken 5 m down through moraine soil with Cl (green), Sr (blue), DPP (purples), and PEGs (yellows). Light and dark variations of colors denote a range of K_d values used in the simulations; shaded area represents the time window whereby the compound may breakthrough. K_d values taken from batch experiments. Simulations: **A**) using an $\alpha_L = 5$ m; and **B**) using an $\alpha_L = 0.5$ m. Red dashed line denotes the 1% of source concentration.

4.7. Conclusions

HYDROSCAPE is a MATLAB[®]-based program with an easy-to-use, intuitive user interface that can be used to simulate a variety of transport scenarios. It allows the user to upload map overlays with Google Maps[™], allowing the user to visualize the plume in relation to the real-world. HYDROSCAPE also includes a simple parameter estimator algorithm and sensitivity analysis routine, allowing the user to conduct inverse modeling efficiently. HYDROSCAPE additionally modifies the Karanovic et al. (2007) solution, making it more versatile. These enhancements include: 1) custom source region (arbitrary user-defined source function/geometry and spatial variations in source concentration); and 2) simple geology. The novel “simple geology” feature is a heuristic approximation, subject to potential errors if not used carefully.

We show that although our implementation of simple geology is heuristic, the differences when compared to MODFLOW are small for much of the domain investigated, with plume shape, dimensions and mass being similar. Likewise, breakthrough curves and centerline concentration profiles (see **Appendix C**) produced by both these programs were comparable. We argue that HYDROSCAPE's implementation of simple geology, when compared to MODFLOW, is largely acceptable as a screening tool under certain constraints.

HYDROSCAPE is an effective tool in the simulation of various spill scenarios, including FPW as illustrated above. Those modeling exercises highlight the importance of considering source region history and co-contaminant interactions, as our results show that predictions of contaminant breakthrough order vary dramatically depending on whether the K_d values taken were from column experiments, batch experiments, or from published literature sources. The time at which certain contaminants appear at a receptor may vary by orders of magnitude, depending on the data source from which the K_d values are calculated.

In assessing remediation strategies for contaminated sites, HYDROSCAPE is a more useful and versatile tool than pre-existing similar programs currently being used (e.g. Newell et al. 1996, Aziz et al. 2000). The program acts as a bridge between expensive, resource intensive numerical simulations, and inexpensive, faster analytical solutions. HYDROSCAPE allows users to balance these two end-members, allowing for faster, more complex simulations, while keeping costs and computational time down. Video tutorials can be found on YouTube™ (<https://www.youtube.com/channel/UCI9GwvAA5kUMJC9fB-19aiA>). Additional solutions are planned to be added over time or at the request of the community.

Symbol	Units	Description
x, y, z	[L]	Spatial coordinates
t	[T]	Time
C	[M/L ³]	Concentration
D_L	[L ² /T]	Longitudinal dispersion coefficient
D_{TH}	[L ² /T]	Transverse horizontal dispersion coefficient
D_{TV}	[L ² /T]	Transverse vertical dispersion coefficient
v	[L/T]	Average linear groundwater velocity
λ	[1/T]	First-order decay constant (solute)
R	[-]	Retardation factor

Table 4.1: List of commonly used notation and symbols, along with their units, for the three-dimensional advection-dispersion equation (ADE).

Program	Reactions			Aquifer	Map Overlay	Customized Source Region		Heterogeneity	
	First-order Decay	Zeroth-order Rxn	Inst. Bio. Rxn	Finite Dim.		Shape/Conc.	Source Function	Vertical (Simple Geol.)	Horiz.
HYDROSCAPE	✓				✓	✓	✓	✓	
3DADE/N3DADE	✓	✓							
AT123D-AT	✓			✓	✓				
BIOSCREEN / BIOCHLOR	✓		✓			✓			
ATRANS	✓			✓			✓		
ArcNLET	✓				✓				✓

Table 4.2: Comparison of some key features of HYDROSCAPE to other programs that use analytical solutions to the ADE.

Symbol	Units	Description
C_0	[M/L ³]	Source concentration
W	[L]	Source width
H	[L]	Source thickness
α_L	[L]	Longitudinal dispersivity
α_{TH}	[L]	Transverse horizontal dispersivity
α_{TV}	[L]	Transverse vertical dispersivity
v	[L/T]	Average linear groundwater velocity
R	[-]	Retardation factor
λ	[1/T]	First-order decay constant (solute)
k_s	[1/T]	Source decay constant
τ	[-]	Tortuosity
D_0	[L ² /T]	Free-solution diffusion coefficient

Table 4.3: The list of the parameters that can be estimated in HYDROSCAPE.

Source Name	Source1	Source2	Source3
Source Position Y (m)	0	0	35
Source Position Z (m)	-5	-30	-55
Source Width (m)	120	20	110
Source Thickness (m)	10	40	10
Concentration (mg/L)	100	50	75

Table 4.4: List of inputs for each patch source

	HYD	MOD
X (m)	[0, 1000]	
Y (m)	[-300, 300]	
Z (m)	[0, 100]	
Time (days)	3650	
α_L (m)	10	
α_{TH} (m)	1	
α_{TV} (m)	0.1	
V_{aquitard} (m/s)	2×10^{-7}	-
V_{aquifer} (m/s)	2×10^{-6}	-
K_{aquitard} (m/s)	-	1.2×10^{-6}
K_{aquifer} (m/s)	-	1.2×10^{-5}
∇h (-)	-	0.05
Φ (-)	0.3	
ΔX_{source} (m)	-	2.5
ΔX_{far} (m)	-	10
Nodes	64	-

Table 4.5: List of parameters used in HYDROSCAPE (“HYD”) and MODFLOW (“MOD”) simulations.

Parameter	One-dimension	Three-dimension		
X (m)	[0, 5]	[0, 200]		
Y (m)	-	[-25, 25]		
Z (m)	-	[0, 1]		
Source Concentration	Relative	Relative		
Source Width (m)	-	0.5		
Source Thickness (m)	-	1		
ρ_b (g/cm ³)	1.56	1.56		
		Batch	Column	Literature
K _d (L/kg); Cl	0	0	0	0
K _d (L/kg); DPP	2 to 12	-	-	-
K _d (L/kg); Sr	5.80 [‡]	0.91	0.21	20 ^[1]
K _d (L/kg); PEGs	2.66 to 130.83	2.20 to 1644.80	0.42 to 12.40	0.075 to 0.25 ^[2]
K _d (L/kg); Cu	-	2.20	27.46 [§]	120 ^[3] *
λ (1/yr)	0	0	0	0
v (m/s)	1.2×10^{-8}	1.2×10^{-5}		
α_L (m)	0.5 to 5	5		
α_{TH} (m)	-	0.5		
Φ (-)	0.36	0.36		
D^* (m ² /s)	0	0		

Table 4.6: List of model parameters for both the 1D and 3D (pseudo-2D) simulations. Literature values taken or estimated from: [1] US EPA 1999; [2] Zhao et al. (1989); [3] Shaheen et al. (2009).

[‡] Estimated from batch sorption results from **Chapter 3** by fitting a trendline through the low concentration data for Sr.

[§] Estimated from column transport results from **Chapter 3** by estimating a retardation factor of 120 and calculating an effective K_d from that.

* Lower limit assumed.

Acknowledgements

This research was funded by a Discovery Grant from the Natural Sciences and Engineering Research Council of Canada (NSERC) to D. Alessi and an NSERC Postgraduate Scholarship Fund to S. Funk. We would also like to thank C. Mendoza and T. Ferré for their expertise and many helpful discussions. We would also like to thank an anonymous reviewer for their helpful suggestions for improving this manuscript.

References

- Aziz CE, Newell CJ, Gonzales JR, Haas PE, Clement TP, Sun Y (2000) BIOCHLOR Natural Attenuation Decision Support System, User's Manual Version 1.0. EPA/600/R-00/008, Washington, D.C.: U.S. EPA Office of Research and Development.
- Burnell DK, Lester BH, Mercer JW (2012) Improvements and corrections to AT123D code. *Groundwater* **50**: 943 – 953.
- Burnell DK, Cooper J, Xu J, Burden DS (2016) Graphical user interface for AT123D-AT solute transport model. *Groundwater* **54**: 313 – 314.
- Cecan L, Schneiber RA (2008) BIOSCREEN, AT123D and MODFLOW/MT3D: A comprehensive review of model results. *Proceedings of the Annual International Conference on Soils, Sediments, Water and Energy* **13**: Article 22.
- Connor, J.A., C.J. Newell, J.P. Nevin, and H.S. Rifai (1994) Guidelines for use of groundwater spreadsheet models in risk-based corrective action design. In *Proceedings of the NGWA Petroleum Hydrocarbons Conference*, Houston, TX, November 1994.
- Domenico PA (1987) An analytical model for multidimensional transport of a decaying contaminant species. *Journal of Hydrology* **91**: 49 – 58.

- Frind EO, Hokkanen GE (1987) Simulation of the Borden plume using the alternating direction Galerkin technique. *Water Resources Research* **23**: 918 – 930.
- Gandhi HR (2017) An accidental release of flowback water from storage system: A risk assessment study. M.A.Sc Thesis. University of British Columbia.
- Harbaugh AW (2005) MODFLOW-2005: The U.S. Geological Survey Modular Ground-Water Model – The Ground-Water Flow Process. USGS Techniques and Methods 6-A16.
- Karanovic M, Neville CJ, Andrews CB (2007) BIOSCREEN-AT: BIOSCREEN with an exact analytical solution. *Groundwater* **45**: 242 – 245.
- Leij FJ, Bradford SA (1994) 3DADE: A computer program for evaluating three-dimensional equilibrium solute transport in porous media. Research No. 134 US Salinity Laboratory, USDA, ARS, Riverside, CA.
- Leij FJ, Skaggs TH, van Genuchten MT (1991) Analytical solutions for solute transport in three-dimensional semi-infinite porous media. *Water Resources Research* **27**: 2719 – 2733.
- Leij FJ, Toride N, van Genuchten MT (1993) Analytical solutions for non-equilibrium solute transport in three-dimensional porous media. *Journal of Hydrology* **151**: 193 – 228.
- McLaughlin MC, Borch T, Blotvogel J (2016) Spills of hydraulic fracturing chemicals on agricultural topsoil: Biodegradation, sorption, and co-contaminant interactions. *Environmental Science & Technology* **50**: 6071 – 6078.
- Neville C, SS Papadopoulos & Associates Inc. (1998) ATRANS: Analytical solutions for three-dimensional solute transport from a patch source. Version 2. SS Papadopoulos & Associates Inc., Bethesda, Maryland.

- Newell CJ, McLeod RK, Gonzales JR (1996) BIOSCREEN Natural Attenuation Decision Support System, User's Manual Version 1.3. National Risk Management Research Laboratory, Office of Research and Development, US EPA.
- Park E, Zhan H (2001) Analytical solutions of contaminant transport from finite one-, two- and three-dimensional sources in a finite-thickness aquifer. *Journal of Contaminant Hydrolog* **53**: 41 – 61.
- Rios JF, Ye M, Wang L, Lee PZ, Davis H, Hicks R (2013) ArcNLET: A GIS-based software to simulate groundwater nitrate load from septic systems to surface water bodies. *Computers & Geosciences* **52**: 108 – 116.
- Shaheen SM, Tsadilas CD, Mitsibonas T, Tzouvalekas M (2009) Distribution coefficient of copper in different soils from Egypt and Greece. *Communications in Soil Science and Plant Analysis* **40**: 214 – 226.
- Sinton LW, Noonan RK, Finlay RK, Pang L, Close ME (2000) Transport and attenuation of bacteria and bacteriophages in an alluvial gravel aquifer. *New Zealand Journal of Marine and Freshwater Research* **24**: 175 – 186.
- United States Environmental Protection Agency (EPA) (1999) Understanding variation in partition coefficient, K_d , values. Volume II: Review of geochemistry and available K_d values for cadmium, cesium, chromium, lead, plutonium, radon, strontium, thorium, tritium (^3H), and uranium. EPA 402-R-99-004B.
- United States Environmental Protection Agency (2015). Review of state and industrial spill data: Characterization of hydraulic fracturing-related spills. Office of Research and Development, Washington, D.C., EPA/601/R-14/001.

Yeh GT (1981) AT123D: Analytical transient one-, two-, and three-dimensional simulation of waste transport in the aquifer system. ORNL-5602, Oak Ridge National Laboratory, Oak Ridge, Tennessee.

Zhao X, Urano K, Ogasawara S (1989) Adsorption of polyethylene glycol from aqueous solution on montmorillonite clays. *Colloid and Polymer Science* **267**: 899 – 906.

Zheng C, Bennett GD (1995) *Applied Contaminant Transport Modeling: Theory and Practice*. Van Nostrand Reinhold (now John Wiley & Sons), New York, 440 pp.

Zheng C, Wang PP (1999) MT3DMS: A modular three-dimensional multispecies transport model. DoD_3.50.A. Contract Report SERDP-99.

Chapter 5 – Conclusions & Future Directions

5.1. Conclusions

With increasing energy demands, hydraulic fracturing operations targeting tight, unconventional hydrocarbon formations (e.g. shales) have increased sharply (Vengosh et al. 2013). Because of this, there has been increased awareness and concern from stakeholders, as the public, and industry regarding the potential environmental risks that hydraulic fracturing operations and the storage, transport, and disposal of wastewater produced during those operations may pose (Gehman et al. 2016). The research in this dissertation aimed to constrain the potential impacts that specific compounds found within hydraulic fracturing-derived wastewater (called flowback and produced water; FPW), as well as the entire FPW itself, might pose to the environment and aquatic ecosystems.

Recently, samples of FPW derived from hydraulic fracturing of the Duvernay Formation, AB, were found to contain a previously unidentified class of aryl phosphates (including diphenyl phosphate (DPP), triphenyl phosphate (TPP), among others) (He et al. 2017). Aryl phosphates are used in a variety of other industries, and they can be found in flame retardants, plasticizers, lubricants, hydraulic fluids, and oxidizers. Many of these aryl phosphates break down into DPP (e.g. Muir and Grift 1981; Anderson et al. 1993). Therefore, it is important to determine the environmental fate and potential impacts of DPP if spilled in the near-surface environment, as DPP is an emerging contaminant in soil and groundwater systems. In **Chapter 2**, the sorption behavior of DPP onto various surficial sediments (clays and sandy materials) collected within the Fox Creek, AB region was constrained by conducting batch sorption experiments, as was the potential toxicity of DPP to a model aquatic organism. The sorption of DPP onto both clay-rich soils and sandy sediment was low as compared to other aryl phosphates (e.g. TPP: $\log K_{OC}$

~3.50; Anderson et al. 1993), with K_d values ranging from approximately 2 to 12 L/kg for clay-rich soil types (moraine, glaciolacustrine clay, stagnant moraine) and down to approximately 0.1 to 0.4 L/kg for sand-rich materials (HFO-coated sand, fluvial sand). An average $\log K_{OC}$ value $\sim 2.30 \pm 0.43$ (one sigma) was calculated from our results. Within the tested pH range (~ 5 to 9), most of the materials tested showed no significant pH-dependence on the degree of DPP sorption and neither Freundlich nor Langmuir equations were used or required to fit the data. Rather, it appears sorption of DPP onto the tested soil types seem to be dominated by soil f_{OC} . With one exception, experiments using the moraine seem to indicate that sorption of DPP onto the clay-rich, organic-rich soil decreases with increasing pH. I hypothesize that because the moraine was dominated by clays, specifically kaolinite with a point zero charge (PZC) of ~ 4.0 (Schroth and Sposito 1997), which become increasingly more negative with increasing pH, this may result in a repulsion of the deprotonated DPP molecule, resulting in less sorption at higher pH. Therefore, the transport of DPP in groundwater would be rapid due to its low degree of sorption to surficial materials. The acute 96 h-LC₅₀ of DPP on zebrafish embryos was determined to be $\sim 50 \pm 7.1$ mg/L. Su et al. (2014) studied the toxic effects of DPP and TPP on chicken embryonic hepatocytes and found that DPP had less cytotoxic effects than TPP but altered more gene transcripts. Together with our study, it may be possible for DPP to pose an environmental risk to aquatic ecosystems if released into the environment, but further studies on how DPP interacts in the soil and groundwater environment, as well as its toxicity on aquatic organisms, would need to be undertaken.

An extension of the above study, in **Chapter 3**, batch sorption and column transport experiments were performed to determine the sorption characteristics of the inorganic (dissolved metals) and organic (primarily compounds used in the original hydraulic fracturing fluid)

constituents found within a real FPW sample collected from hydraulic fracturing operations near Fox Creek, AB, to assess its potential impact to the soil and groundwater environments if split at the surface. In total, 24 different metals and 4 different organic constituents were investigated in our study. In our batch sorption experiments, the Sr sorption K_d values were observed to be significantly depressed relative to published literature values, likely due to the negative impact ionic strength has on Sr sorption (e.g. Keren and O'Connor 1983; Chen and Hayes 1999; Powell et al. 2015; Yu et al. 2015), as well as competition with other cations in solution (e.g. Na^+ , K^+ , Mg^{2+} , Ca^{2+} , etc.) (e.g. Keren and O'Connor 1983; Chen and Hayes 1999; Powell et al. 2015). The high salinity of FPW (e.g. Mattigod et al. 1979; Soares et al. 2011; Zhang et al. 2011; Saha and Badruzzaman 2014), as well as competition with other dissolved cations (e.g. Basta and Tabatabai 1992; Tsang and Lo 2006; Antoniadis et al. 2007; Covelo et al. 2007; Usman 2008; Liao and Selim 2009; Dişli 2010), likely depressed Ni and Cu sorption as well. However, other metals, such as B and Li, were negligibly impacted by the high salinity of the FPW, or the presence of other dissolved constituents in solution. For boron, this is likely due to the mechanism by which boron sorbs onto soils; boron sorbs onto clay minerals or, if present, carbonates, via ligand exchange (Goldberg et al. 1993; Goldberg 1997). This form of chemisorption is less dependent on variables such as ionic strength and competition with other dissolved metals. In addition to the suite of metals investigated, four different PEGs with different ethylene oxide (EO) numbers found within the FPW were also studied. The sorption of PEGs was observed to be dependent on the number of EO-units within the molecule, with sorption increasing as EO-units increased. Sorption of PEGs were also found to be dependent not only on the organic matter content of the soil, but also the mineralogy of the clays found within the soil, with 2:1 clays (e.g. chlorite) sorbing PEGs more strongly than 1:1 clays (e.g. kaolinite).

Column transport experiments were conducted on the fluvial sand to assess the impact of flow on sorption of compounds within the FPW. Some dissolved metals, such as Sr, B, Li, Na, and K, exhibited significantly lower sorption than the batch experiments for the same sediment. I interpret these results to suggest that sorption is non-instantaneous, and that slow sorption processes, such as diffusion into internal sites and/or precipitation, were negated by flow (e.g. Krishnasamy 1996; Sparks 2000; Arora and Chahal 2007). For other elements, such as Ca, Mg, Ba, and Mn, sudden spikes in concentration above what was measured in the stock solution were observed, coincident with the advective front, followed by a gradual decline back to stock solution concentrations. It is possible that this behavior is the result of carbonate dissolution as the FPW passed through the column, releasing Ca and Mg, combined with displacement of Ba (Zhang et al. 2001) and Mn (Aubert and Pinta 1977) from the soil surfaces due to the prevalence of other cations, such as Na^+ and K^+ , in solution. Sorption of Cu was observed to be enhanced by flow. Additional processes, such as precipitation of Cu-bearing solids (possibly carbonates), were suspected to be present in the column experiments, but not in the batch experiments, due to the anaerobic conditions found within the column (Seo et al. 2008). Exclusion of Ni, in favor of Cu, at sorption sites were also observed, resulting in Ni concentrations in the effluent to be greater than those measured in the stock solution (Tsang and Lo 2006). PEGs in solution followed a similar trend to what was observed in the batch experiments, with sorption increasing with increasing EO-units. However, overall sorption of the individual PEG compounds in the column experiments were significantly less than those observed in the batch experiments. I argue that flow within the column negated slow sorption process, thereby reducing the overall ability for the sediment to retain the PEGs (e.g. Noll et al. 1992; McKay 1996; Chang et al. 2003).

Our results are in stark contrast to Oetjen et al. (2018), who simulated the transport of hydraulic fracturing wastewater through a column of agricultural soil during rain events. Spill events were simulated by pouring HF-derived wastewater at the top of the soil column, with flow induced by gravity alone. They concluded that their experiments suggested that migration of surfactants, including PEGs (with EO-numbers between 10 and 14), should be minimal (Oetjen et al. 2018). However, our results suggest that PEGs (with EO-numbers between 6 and 11) are mobile in the subsurface. I speculate that the composition of the wastewater used in the Oetjen et al. (2018) study (TDS <10,000 mg/L) compared to the FPW in our study (TDS >140,000 mg/L), as well as variations in soil composition, mineralogy, or organic matter content may be factors that explain the differences in results.

Understanding how contaminants such as those in hydraulic fracturing FPW are transported in the subsurface is a major problem in hydrogeology. In recent years, with increases in computer power, numerical modeling has increased in popularity. In **Chapter 4**, I developed a new software program called HYDROSCAPE (Funk et al. 2017). HYDROSCAPE uses a three-dimensional analytical solution to the advection-dispersion equation (ADE) (Karanovic et al. 2007) to solve contaminant transport problems in porous media. HYDROSCAPE is an easy-to-use program that produces high-quality outputs such as contour maps of the plume, breakthrough curves, concentration profiles and videos of the plume's progression. Unlike other programs that use analytical solutions, HYDROSCAPE utilizes novel mathematical techniques to circumnavigate some of the limitations of the solutions. These new features allow the user to: 1) build a fully customized source region, and 2) implement horizontal layers, with different hydraulic conductivities, within the domain. By allowing the domain to be heterogeneous and the source region to vary in shape, concentration and time, more complexity is possible in these

models and they are then more applicable to real-world settings. Comparisons with an identical numerical model (MODFLOW with MT3DMS) demonstrates that our implementation for horizontal layering is a close approximation. Additionally, HYDROSCAPE also allows the user to place the plume into real-world regional context by importing maps from Google Maps™. This visualization allows the user to evaluate how the plume evolves relative to real-world boundaries and objects. While some limitations still exist within the models, namely that vertical dispersion and diffusion between layers is negligible, HYDROSCAPE represents a bridge between simple models using analytical solutions and complex numerical simulations and may be a valuable tool for hydrogeologists in the future.

Using HYDROSCAPE, three simple analytical models to simulate leakage of FPW into the subsurface (US EPA 2015; Gandhi 2017). In both of our pseudo-2D simulations in a saturated alluvial aquifer, the predicted contaminant distributions vary considerably depending on whether the sorption data came from our column or batch experiments from **Chapter 3**, or if they were taken from literature values, highlighting the impact of co-contaminant interactions and the importance of flow on sorption. Further, in our pseudo-1D simulations, contaminant separation caused by differential sorption was also observed in an organics-rich, clay-rich medium. The impact this may have on other processes, such as biodegradation, although not modeled in our simulations, may be an important consideration going forward. Our results demonstrate the importance of considering transient and co-contaminant effects when modeling the transport of FPW, as well as contaminant separation (McLaughlin et al. 2016).

5.2. Future Directions

The experiments conducted in this study represent is a key step forward in our understanding of the potential risks that hydraulic fracturing operations, and its waste products

such as FPW pose on the environment, specifically to aquatic ecosystems. Following on the insights gained from the experiments in this dissertation, more work on the environmental risk potential aryl phosphates and flowback and produced water pose is needed. Below, I will outline some of the key directions that future research should explore. These suggestions will focus mainly on the transport aspects of the contaminants rather than their toxicity, as that is beyond the scope of this discussion.

Much, if not all, of the batch sorption and column transport experiments conducted within this study were conducted assuming abiotic conditions. Sorption was considered the sole natural attenuation process in these experiments. However, the potential for biotic degradation of both aryl phosphates and FPW was not assessed and could be an important attenuation pathway. Diphenyl phosphate (DPP) was the aryl phosphate studied in **Chapter 2**, and was chosen because it was present in the FPW sample studied in He et al. (2017), but also because DPP is soluble in water. It remains unclear if DPP, or the full FPW, could undergo further degradation, through biological means. For these experiments, batch sorption experiments could be conducted on DPP and the FPW using the same surficial sediment from Fox Creek, AB, but could be either inoculated with microbes, or the soil could be amended with a carbon source (e.g. acetate, lactate, molasses) to simulate growth of indigenous microbes already present in the soil. These experiments could then be compared with the experiments outlined in **Chapter 2 and Chapter 3**, under the assumption that everything else is identical, any differences in the concentrations (assumed to be lower in biotic experiments when compared to abiotic ones) could be attributed to biodegradation. With the addition of microbial community analysis, along with an analysis of the breakdown products of the organic compounds found in FPW, would be valuable in pinpointing which microbes are involved in the biodegradation process, and constraining the

breakdown pathways. In addition to these experiments, parallel time-series experiments could also be conducted to constrain the first-order decay constant for DPP degradation. This would allow better modeling of DPP transport in groundwater (as our models assumed $\lambda = 0 \text{ yr}^{-1}$).

Similarly, DPP was just one aryl phosphate that was studied because of the lack of information available pertinent to its environmental fate and transport. However, He et al. (2017) identified many other aryl phosphates, including bis(2,4-di-tert-butylphenyl) phosphate and tris(2,4-di-tert-butylphenyl) phosphate. These two organophosphates, likewise, have little available information regarding their sorption onto soil or sediment. Batch sorption experiments could be conducted on these aryl phosphates as well, to constrain their transport in groundwater environments. One potential difficulty with working with these compounds would be the relatively low (<1 mg/L?) water solubility of these compounds. This would make analyzing these organophosphates difficult, but it may be possible to employ similar low detection limit and high precision analytical methods as those outlined in **Chapter 2**.

Column experiments with DPP were not conducted in this study. Conducting these would be a crucial step forward to determine the applicability of the K_d values obtained from our equilibrium batch sorption experiments (Funk et al. 2019). Column experiments using the same surficial sediments collected from Fox Creek, AB, used in our experiments, could be conducted using DPP. Breakthrough curves could be obtained and a retardation factor (R) determined, and therefore effective K_d , could be calculated. These effective K_d values obtained from the column experiments could then be compared with those obtained in **Chapter 2**. It would be important to determine if flow (and by extension, transient processes) significantly impacts sorption in a groundwater environment.

In **Chapter 3**, many mechanisms were proposed to explain the results from the FPW batch sorption and column transport experiments. However, for many of the metals investigated, there is a lack of experimental studies that are conducted at field-relevant conditions (primarily at realistic solution ionic strength values). Rather, studies conducted at lower ionic strengths were extrapolated to conditions similar to those found in FPW, and conclusions were drawn from there. Our study offers for the first time testable, experimental results to determine the multitude of mechanisms found in the transport of both dissolved metals and organics in FPW within the subsurface. Further investigations into these mechanisms for retention should be conducted. For example, the effect of high ionic strength, like those found in FPW, on the sorption of both metals (e.g. Sr, B, Li, Ni, Cu), under mono-element and multi-element conditions, and organics should be conducted. These experiments should also use different electrolyte compositions (e.g. NaCl vs. CaCl₂) to also address how the major elements that comprise FPW impact the sorption of potentially toxic trace elements of interest. One aspect of the FPW study that was not fully addressed was the effect of organics on metal sorption, and vice versa. Batch sorption experiments conducted in binary systems should be undertaken to address and constrain this effect. The impact of different types of organic compounds commonly found in hydraulic fracturing fluids, such as those used for surfactants, biocides, friction reducers, or those derived from the formation, such as polycyclic aromatic hydrocarbons, on metal sorption should be investigated.

Additional column experiments are also recommended. One proposed mechanism to explain the enhanced sorption of Cu (and possibly other chalcophile elements) observed in our experiments is via precipitation of Cu-bearing minerals (likely sulphides), because the experiments were performed under anaerobic conditions. Column experiments could be

performed to address this mechanism whereby either a simplified synthetic fluid or FPW is flowed through a column, and the sediment is later analyzed by XRD to determine if new minerals had precipitated from solution. Further, only one sediment type (fluvial sand) was tested in our study. A variety of soils, with a range of clay content, mineralogy, and organic matter, should be tested under flowing systems to determine how FPW behaves in those systems.

Beyond these relatively simple batch sorption and column transport experiments, experiments that more accurately replicate the natural environment could be conducted with the FPW samples. Infiltration experiments, not dissimilar to those performed by Oetjen et al. (2018), should be performed. For these infiltration experiments, soil cores, ideally from the Fox Creek, AB region, would need to be collected. These soil samples should be preserved as best as possible, with the soil moisture within remaining intact (it will likely be unsaturated). The experiment would involve placing the FPW at the “surface” of the soil column, which would be placed in a cylindrical container, and measurement points could be taken along the length of the column, measuring the concentration of dissolved inorganics (metals), organics, and TOC/TN, as well as changes to the microbial community, as a function of depth. These infiltration experiments would provide important constraints of a surface FPW spill in the region of operations, and would allow for direct comparison with Oetjen et al. (2018).

Lastly, the experiments conducted in this study, and the suggestions for future directions above, have focused on contaminant transport and their potential natural attenuation in the environment. However, aspects of potential remediation methods for treating either DPP, aryl phosphates, or the FPW itself, have not been addressed. The knowledge from this dissertation, along with the information gained from the studies discussed in “Future Directions” above, forms the basis for exploring possible remediation options in the case of an FPW spill.

Investigations should be geared towards the applicability and successfulness of these remedial methods, such as soil amendments, chemical oxidizers, or reactive barriers, to name a few.

References

- Anderson C, Wischer D, Schmieder A, Spiteller M (1993) Fate of triphenyl phosphate in soil. *Chemosphere* **27**: 869 – 879.
- Antoniadis V, Tsadilas CD, Ashworth DJ (2007) Monometal and competitive adsorption of heavy metals by sewage sludge-amended soil. *Chemosphere* **68**: 489 – 494.
- Arora S, Chahal DS (2007) Comparison of kinetic models for boron adsorption in alluvium-derived soils of Punjab, India. *Communications in Soil Science and Plant Analysis* **38**: 523 – 532.
- Aubert H, Pinta M (1977) Manganese. In: *Developments in Soil Science*, Aubert H, Pinta M (editors). Volume 7: 43 – 53.
- Basta NT, Tabatabai MA (1992) Effect of cropping systems on adsorption of metals by soils: III. Competitive systems. *Soil Science* **153**: 331 – 337.
- Chang CY, Tsai WT, Ing CH, Chang CF (2003) Adsorption of polyethylene glycol (PEG) from aqueous solution onto hydrophobic zeolite. *Journal of Colloid and Interface Science* **260**: 273 – 279.
- Chen C-C, Hayes KF (1999) X-ray absorption spectroscopy investigation of aqueous Co(II) and Sr(II) sorption at clay-water interfaces. *Geochimica et Cosmochimica Acta* **63**: 3205 – 3215.
- Covelo EF, Vega FA, Andrade ML (2007) Competitive sorption and desorption of heavy metals by individual soil components. *Journal of Hazardous Materials* **140**: 308 – 315.
- Dişli E (2010) Batch and column experiments to support heavy metal (Cu, Zn, and Mn) transport modeling in alluvial sediments between the Mogan Lake and the Eymir Lake, Gölbaşı, Ankara. *Ground Water Monitoring & Remediation* **30**: 125 – 139.

- Funk SP, Hnatyshin D, Alessi DS (2017) HYDROSCAPE: A new versatile software program for evaluating contaminant transport in groundwater. *Software X* **6**: 261 – 266.
- Funk SP, Duffin L, He Y, McMullen C, Sun C, Utting N, Martin JW, Goss GG, Alessi DS (2019) Assessment of impacts of diphenyl phosphate on groundwater and near-surface environments: Sorption and toxicity. *Journal of Contaminant Hydrology* **221**: 50 – 57.
- Gandhi HR (2017) An accidental release of flowback water from storage system: A risk assessment study. M.A.Sc Thesis. University of British Columbia.
- Gehman J, Thompson DY, Alessi DS, Allen DM, Goss GG (2016) Comparative analysis of hydraulic fracturing wastewater practices in unconventional shale development: Newspaper coverage of stakeholder concerns and social license to operate. *Sustainability* **8**: 1 – 23; doi:10.3390/su8090912
- Goldberg S (1997) Reactions of boron with soils. *Plant and Soil* **193**: 35 – 48.
- Goldberg S, Forster HS, Heick EL (1993) Boron adsorption mechanisms on oxides, clay minerals, and soils inferred from ionic strength effects. *Soil Science Society of America Journal* **57**: 704 – 708.
- He Y, Flynn SL, Folkerts EJ, Zhang Y, Ruan D, Alessi DS, Martin JW, Goss GG (2017) Chemical and toxicological characterization of hydraulic fracturing flowback and produced water. *Water Research* **114**: 78 – 87.
- Karanovic M, Neville CJ, Andrews CB (2007) BIOSCREEN-AT: BIOSCREEN with an exact analytical solution. *Ground Water* **45**: 242 – 245.
- Keren R, O'Connor GA (1983) Strontium adsorption by noncalcareous soils – Exchangeable ions and solution composition effects. *Soil Science* **135**: 308 – 315.
- Krishnasamy R (1996) Kinetics of boron adsorption in soils. *Journal of Indian Society of Soils* **44**: 783 – 785.

- Liao L, Selim HM (2009) Competitive sorption of nickel and cadmium in different soils. *Soil Science* **174**: 549 – 555.
- Mattigod SV, Gibali AS, Page AL (1979) Effect of ionic strength and ion pair formation on the adsorption of nickel by kaolinite. *Clays and Clay Minerals* **27**: 411 – 416.
- McKay G (1996) Use of adsorbents for the removal of pollutants from wastewater. In: McKay G (editor), CRC Press: p. 208.
- McLaughlin MC, Borch T, Blotvogel J (2016) Spills of hydraulic fracturing chemicals on agricultural topsoil: Biodegradation, sorption, and co-contaminant interactions. *Environmental Science & Technology* **50**: 6071 – 6078.
- Muir DCG, Grift NP (1981) Environmental dynamics of phosphate esters II: Uptake and bioaccumulation of 2-ethylhexyl diphenyl phosphate and diphenyl phosphate by fish. *Chemosphere* **10**: 847 – 855.
- Noll KE (1992) Adsorption technology for air and water pollution control. In: Noll KE (editor), Lewis Publishers: p. 376.
- Oetjen K, Blotvogel J, Borch T, Ranville JF, Higgins CP (2018) Simulation of a hydraulic fracturing wastewater surface spill on agricultural soil. *Science of the Total Environment* **645**: 229 – 234.
- Powell BA, Miller T, Kaplan DI (2015) On the influence of ionic strength on radium and strontium sorption to sandy loam soils. *Journal of the South Carolina Academy of Science* **131**: 13 – 18.
- Saha PK, Badruzzaman ABM (2014) An experimental investigation of sorption of copper on sandy soil by laboratory batch and column experiments. *International Journal of Environment and Waste Management* **13**: 160 – 178.
- Schroth BK, Sposito G (1997) Surface charge properties of kaolinite. *Clays and Clay Minerals* **45**: 85 – 91.

- Seo DC, Yu K, Delaune RD (2008) Comparison of monometal and multimetal adsorption in Mississippi River alluvial wetland sediment: Batch and column experiments. *Chemosphere* **73**: 1757 – 1764.
- Soares MR, Casagrande JC, Mouta ER (2011) Nickel adsorption by variable charge soils: Effect of pH and ionic strength. *Brazilian Archives of Biology and Technology* **54**: 207 – 220.
- Sparks DL (2000) New frontiers in elucidating the kinetics and mechanisms of metal and oxyanion sorption at the soil mineral/water interface. *Journal of Plant Nutrition and Soil Science* **163**: 563 – 570.
- Su G, Crump D, Letcher RJ, Kennedy SW (2014) Rapid in vitro metabolism of the flame retardant triphenyl phosphate and effects on cytotoxicity and mRNA expression in chicken embryonic hepatocytes. *Environmental Science & Technology* **48**: 13511 – 13519.
- Tsang DCW, Lo IMC (2006) Competitive Cu and Cd sorption and transport in soils: A combined batch kinetics, column, and sequential extraction study. *Environmental Science and Technology* **40**: 6655 – 6661.
- US Environmental Protection Agency (EPA) (2015) Review of state and industry spill data: Characterization of hydraulic fracturing-related spills. EPA/601/R-14/001.
- Usman ARA (2008) The relative adsorption selectivities of Pb, Cu, Zn, Cd and Ni by soils developed on shale in New Valley, Egypt. *Geoderma* **144**: 334 – 343.
- Vengosh A, Warner N, Jackson R, Darrah T (2013) The effects of shale gas exploration and hydraulic fracturing on the quality of water resources in the United States. *Procedia Earth and Planetary Sciences* **7**: 863 – 866.

Yu S, Mei H, Chen X, Tan X, Ahmad B, Alsaedi A, Hayat T, Wang X (2015) Impact of environmental conditions on the sorption behavior of radionuclide $^{90}\text{Sr}(\text{II})$ on Na-montmorillonite. *Journal of Molecular Liquids* **203**: 39 – 46.

Zhang F, Ou X, Ran C, Wu Y (2011) Influence of pH, ionic strength, and temperature on adsorption of lead, copper and zinc in natural soils. *Advanced Materials Research* **255-260**: 2810 – 2814.

Zhang P-C, Brady PV, Arthur SE, Zhou W-Q, Sawyer D, Hesterberg DA (2001) Adsorption of barium(II) on montmorillonite: An EXAFS study. *Colloids and Surfaces A: Physicochemical and Engineering Aspects* **190**: 239 – 249.

Appendix A

Appendix A provides additional results from the characterization of the surficial materials collected from the Fox Creek region used in **Chapter 2 and Chapter 3**, the method of producing the HFO-coated sand used in **Chapter 2 and Chapter 3**, an outline of the method and results from kinetic and degradation experiments conducted on DPP, a discussion on how properties of DPP compare to other aryl phosphates, and additional details regarding the zebrafish embryo assays.

Name	Acronym
diphenyl phosphate	DPP
2-ethylhexyl diphenyl phosphate	EHDP
cresyl diphenyl phosphate	CDP
isodecyl diphenyl phosphate	IDDP
nonylphenyl diphenyl phosphate	NPDP
4-cumylphenyl diphenyl phosphate	CPDP
isopropylphenyl diphenyl phosphate	IPDP
tertbutylphenyl diphenyl phosphate	TBDP
triphenyl phosphate	TPP

Table A1: List of common aryl phosphates and their acronym

Constituent	Concentration (mg/L)
HCO ₃ ⁻	563
CO ₃ ²⁻	<1
SO ₄ ²⁻	28
Cl ⁻	<0.3
F ⁻	<0.02
NO ₂ ⁻ + NO ₃ ⁻	<0.02
Ca ²⁺ (extractable)	64.9
Fe ²⁺ (extractable)	0.952
Mg ²⁺ (extractable)	12.4
K ⁺	5.12
Na ²⁺	114
Silica	11.5
TDS	506 (calc)
pH	7.43

Table A2: Representative chemical analysis (inorganics) of a shallow groundwater sample taken from GIC 9486162 (7-20-62-21 W5). Total anions = 9.82 meq/L; total cations = 9.33 meq/L, yielding a charge balance error (CBE) of -2.58%. Method for “extractable” is given in **Appendix A**.

Sample	FLUV	MOR	STGM	GLC
% Passing 1000 μm	100.0%	N/A	N/A	N/A
% Passing 707 μm	99.9%	N/A	N/A	N/A
% Passing 420 μm	93.6%	N/A	N/A	N/A
% Passing 250 μm	41.2%	91.4%	96.3%	96.3%
% Passing 150 μm	19.1%	65.9%	94.1%	94.7%
% Passing 106 μm	13.7%	55.7%	92.6%	92.6%
% Passing 75 μm	11.7%	49.4%	89.5%	91.0%
% Passing 45 μm	9.7%	40.0%	75.3%	78.4%
Sand to Fines Ratio (SFR)	10.43	1.50	0.33	0.28

Table A3: Results of grain-size distribution for the collected soil and sediment types from the Fox Creek area, AB using the sieve method. Sand-to-fines ratio was calculated by difference. N/A = Not available.

Sample	MOR	GLC	STGM
Sample Intensity (Kcnts/s)	97	88	96
% Passing through 45 μm	99.5%	99.6%	98.0%
% Passing through 22 μm	91.8%	90.7%	72.0%
% Passing through 10 μm	78.0%	78.4%	46.2%
% Passing through 5 μm	62.6%	69.5%	32.4%
% Passing through 2 μm	42.1%	56.5%	19.5%

Table A4: Results of grain-size distribution for the collected soil and sediment types from the Fox Creek area, AB using the sedigraph method. A specific gravity of 2.65 g/cm³, liquid density of 0.99 g/cm³, liquid viscosity of 0.72 mPa s, baseline of 142 Kcnts/s were used.

	GLC	STGM	MOR	FLUV
Quartz	✓	✓	✓	✓
Orthoclase	✓	✓		
Sanidine				✓
Albite	✓	✓		✓
Muscovite	✓	✓	✓	✓
Clinchlore		✓		
Chlorite-serpentine	✓			
Kaolinite			✓	✓
Pyrite		✓		
Carbonates				✓
Soil Analyses				
TN (w/w%)	0.16	0.06	0.30	0.02
TC (w/w%)	1.79	0.69	8.93	0.44
TOC (w/w%)	1.64	0.66	8.92	0.23

Table A5: Table of minerals identified for glaciolacustrine clay (GLC), moraine (MOR), stagnant moraine (STGM), and fluvial sand (FLUV) by XRD. TN = total nitrogen, TC = total carbon, TOC = total organic carbon.

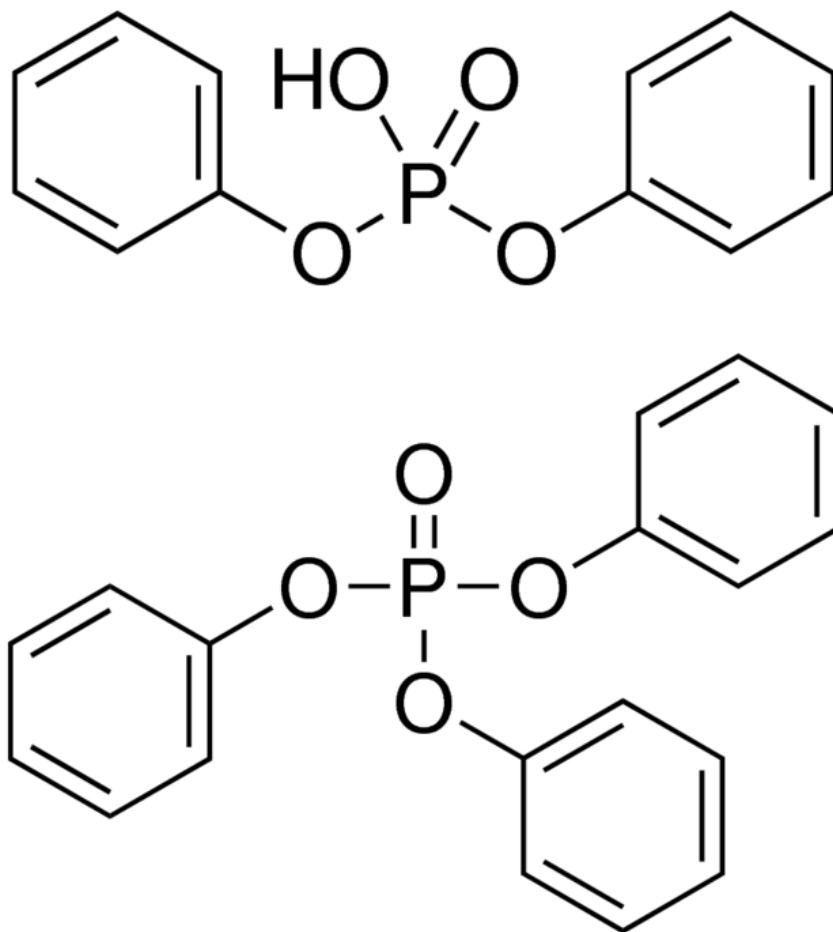


Figure A1: Above: Molecular structure of diphenyl phosphate (DPP); below: Molecular structure of triphenyl phosphate (TPP). Figures from Sigma-Aldrich.

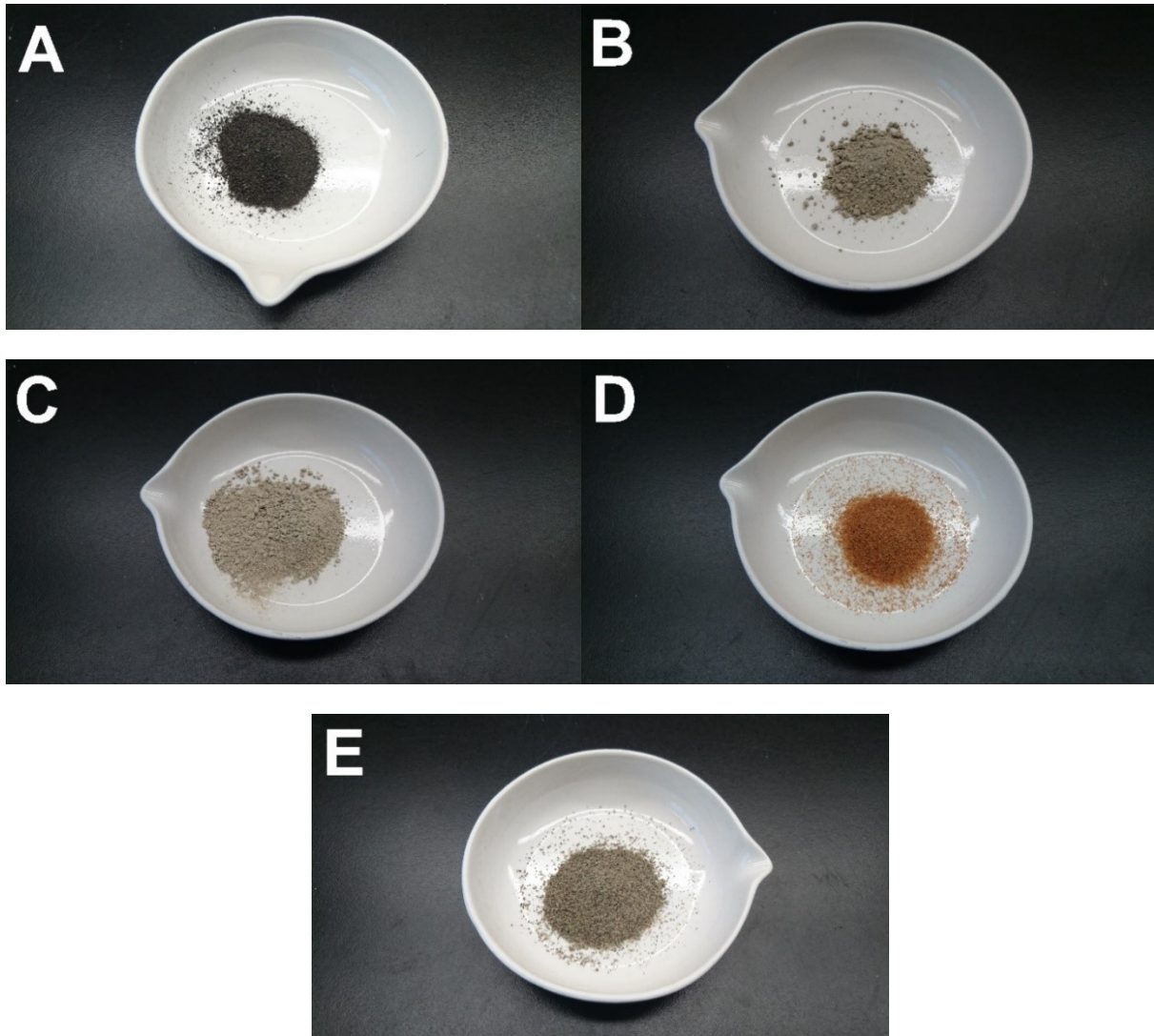


Figure A2: Photographs of the soil samples for **A)** moraine; **B)** glaciolacustrine clay; **C)** stagnant moraine; **D)** HFO-coated sand; **E)** fluvial sand.

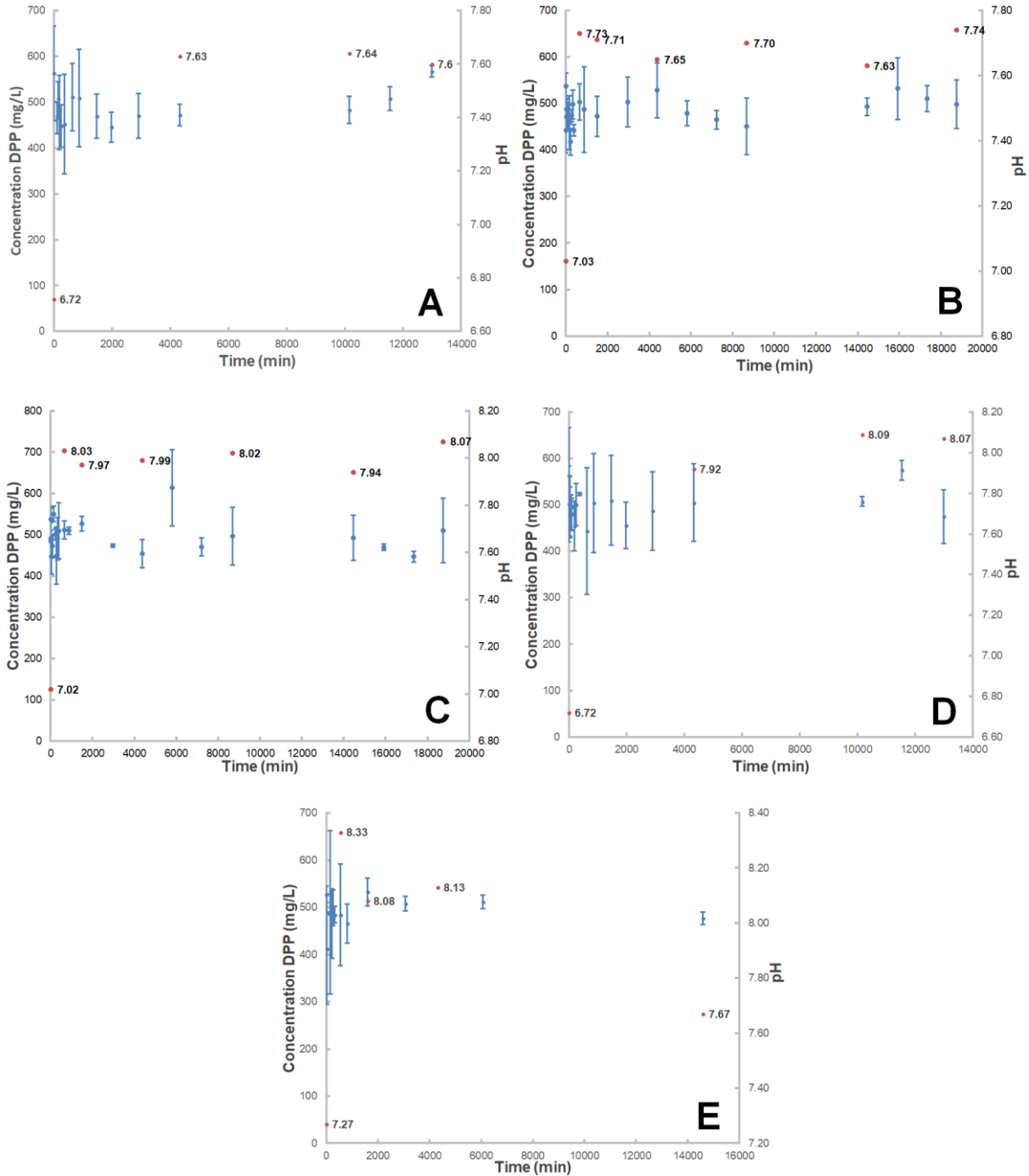


Figure A3: Results from the time-series kinetic experiments for **A)** moraine; **B)** glaciolacustrine clay; **C)** stagnant moraine; **D)** HFO-coated sand; **E)** fluvial sand. The concentration of DPP in solution is plotted against time; also plotted is the pH of the solution against time.

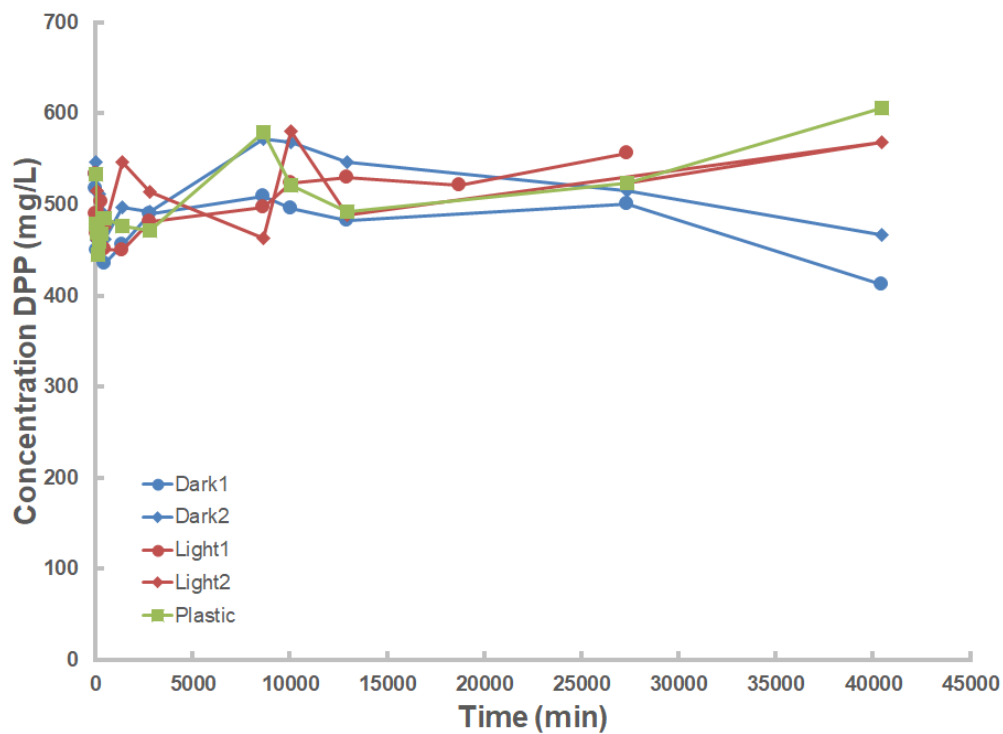


Figure A4: Control experiments to determine potential DPP loss pathways. Dark1 and Dark2 are replicates of DPP in glass media bottles wrapped in aluminum foil; Light1 and Light2 are replicates of DPP in glass media bottles exposed to sunlight. Plastic is a solution of DPP in a polypropylene bottle.

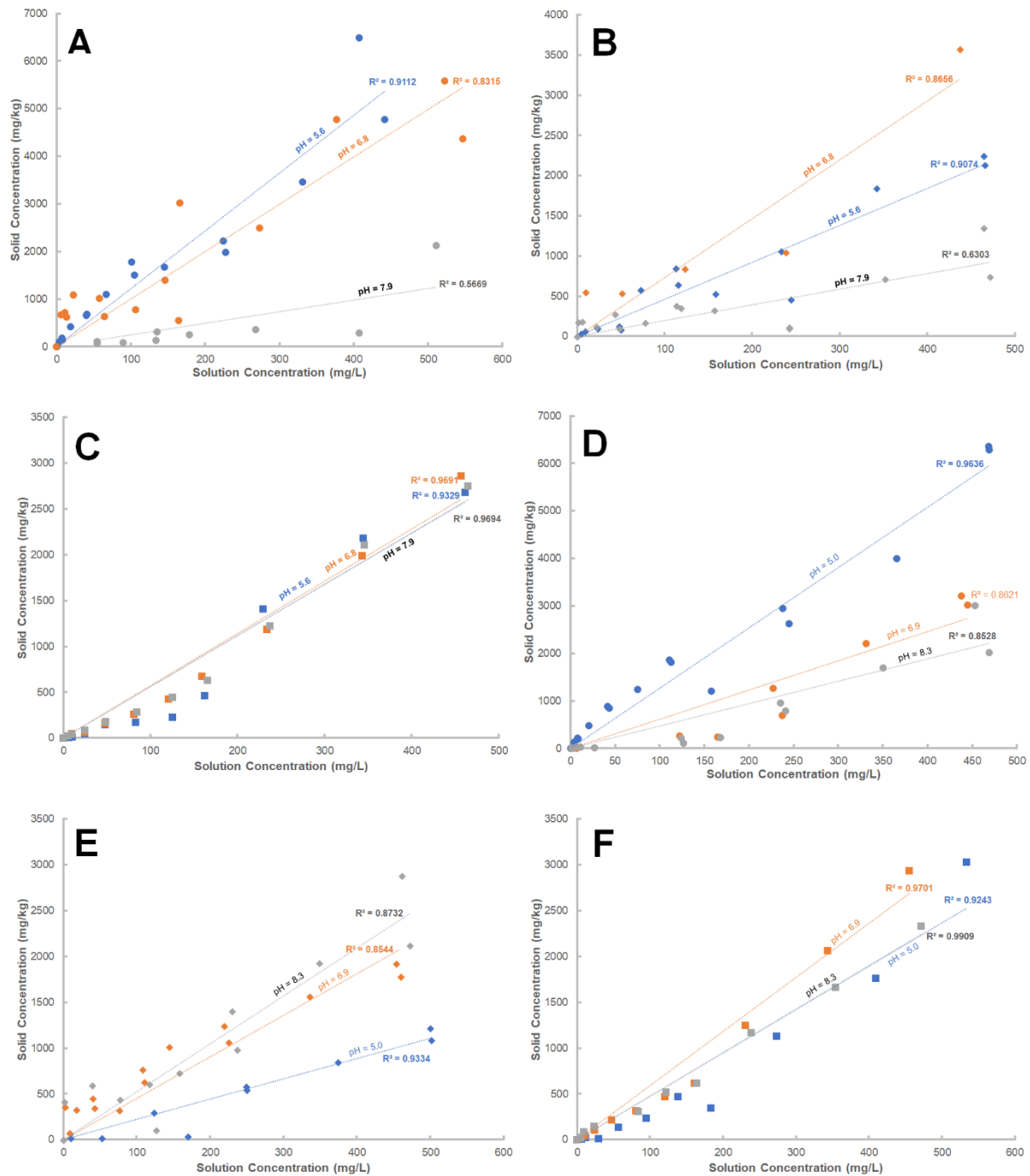


Figure A5: Sorption isotherms from A) moraine using MS/MS; B) moraine using TOC; C) moraine using TP; D) glaciolacustrine clay using MS/MS; E) glaciolacustrine clay using TOC; F) glaciolacustrine clay using TP. Blue represent experiments conducted at low pH (5.6 for MOR or 5.0 for GLC), orange represent middle pH (6.8 for MOR or 6.9 for GLC), and grey represent high pH (7.9 for MOR or 8.3 for GLC). R^2 are also give for each line.

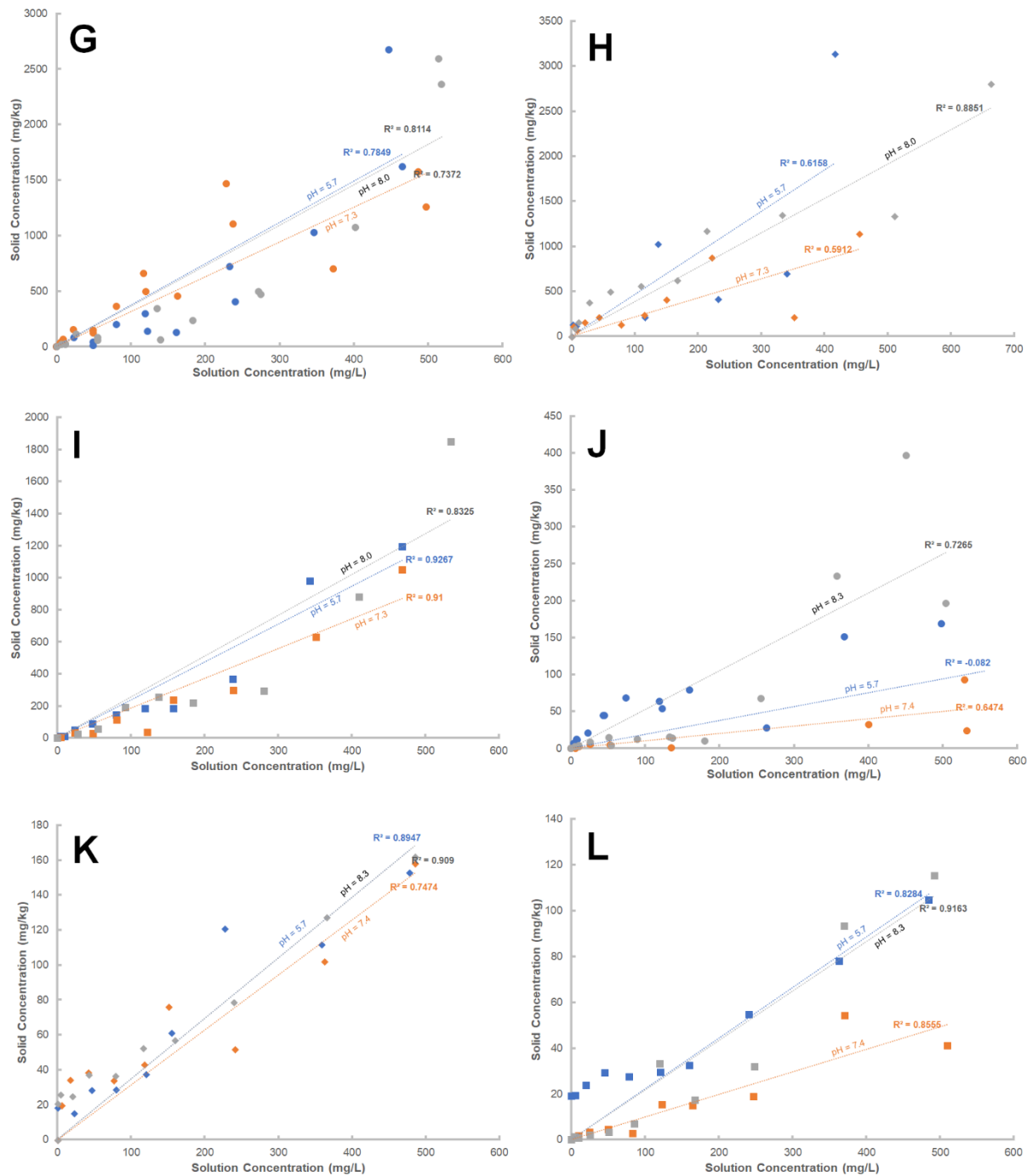


Figure A5 con't: Sorption isotherms from **G)** stagnant moraine using MS/MS; **H)** stagnant moraine using TOC; **I)** stagnant moraine using TP; **J)** HFO-coated sand using MS/MS; **K)** HFO-coated sand using TOC; **L)** HFO-coated sand using TP. Blue represent experiments conducted at low pH (5.7 for STGM and HFO), orange represent middle pH (7.3 for STGM or 7.4 for HFO), and grey represent high pH (8.0 for STGM or 8.3 for HFO). R² are also give for each line.

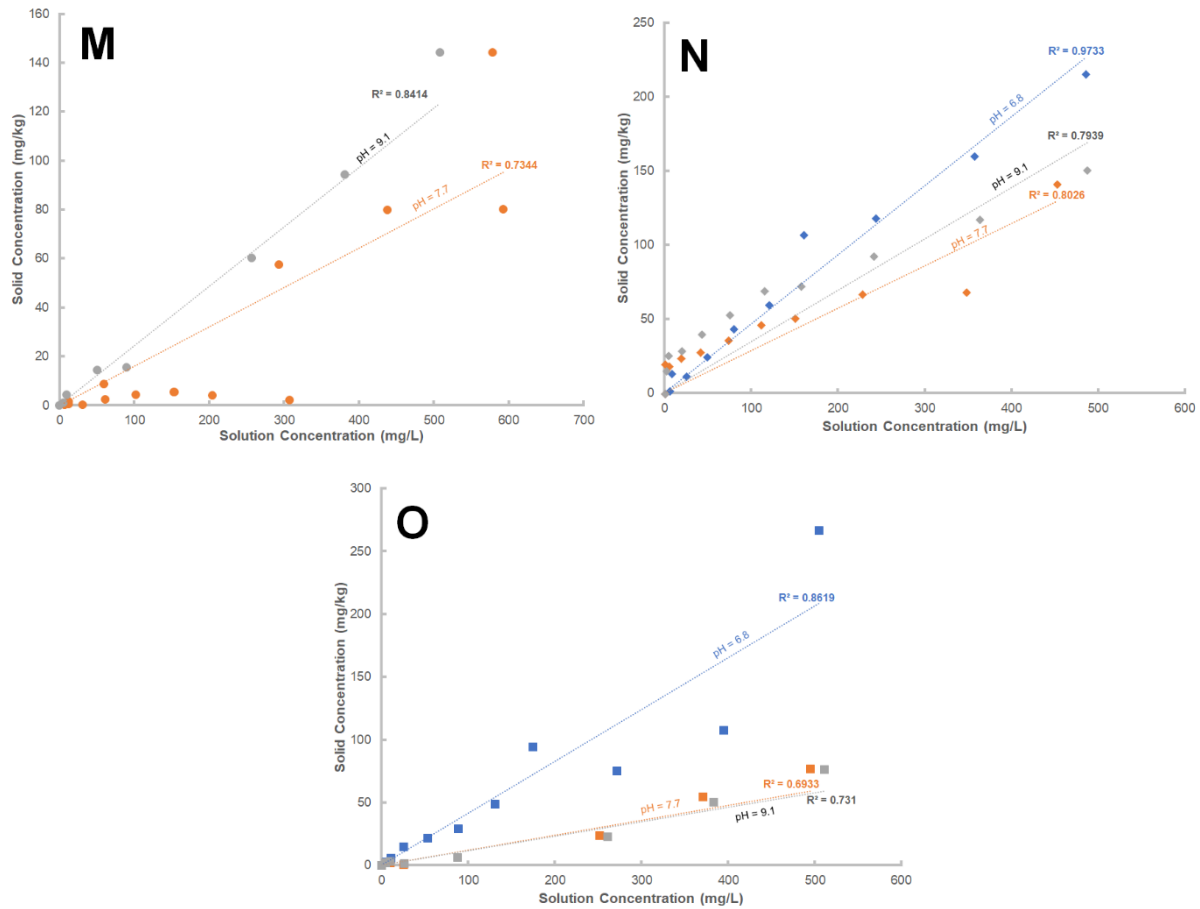


Figure A5 con't: Sorption isotherms from **M**) fluvial sand using MS/MS; **N**) fluvial sand using TOC; **O**) fluvial sand using TP. Blue represent experiments conducted at $\text{pH} \approx 6.8$, orange represent $\text{pH} \approx 7.7$, and grey represent $\text{pH} \approx 9.1$. R^2 are also give for each line.

Method for determining chemical composition of groundwater: In Table A2, the composition of a representative sample of groundwater from the Fox Creek area is given. For Fe, Ca and Mg specifically, an “extractable” method was used whereby 1% HNO₃ (v/v) was added to the tubes containing the sample and allowed to soak for 16 h. This allowed for the breakdown of colloidal materials and desorption of metals from suspended solids without the digestion of crystalline materials (sediment). For groundwater samples that contained a portion of sediment, a “total” digestion was done, which involved the same method described above, but after which, a microwave digestion was also conducted.

Production of Hydrous Ferric Oxide (HFO)-coated sand: The procedure for making HFO-coated sand was similar to that reported by Lo et al. (1997). Briefly, a silica sand (mesh 50 - 100) was placed inside polypropylene bottles and mixed with 2 L of 1 M HCl at a 1:4 solid:liquid ratio for 48 h. Afterward, the acid-washed sand was rinsed repeatedly with distilled water until all the HCl had been removed, as determined by measuring the pH of the water. The acid-washed sand was then placed on a Pyrex glass tray and left to dry at ambient conditions for 72 h. The dried sand was then mixed with 1 L of ferric nitrate solution (~80 g/L), after which approximately 50 mL of 10 M NaOH and 25 mL of 1 M NaOH was added such that the pH was 6.5±0.1. The sand-solution mixture was then placed in a plastic container and shaken vigorously for 48 h to thoroughly coat the sand with HFO. The sand-solution mixture was then placed into a glass beaker and dried in an oven at 110°C for 36 h. The HFO-coated sand was then rinsed repeatedly with distilled water again until the water ran clear. The rinsed HFO-coated sand was then placed back in the oven at 110°C for 24 h to fully dry, and finally, the HFO-coated sand was stored in sealed polypropylene bottles until use.

Kinetics Experiments Method: To determine the rate at which DPP sorbed onto the studied materials, a series of kinetics experiments were undertaken. Just prior to the experiment, stock solution of DPP at a concentration of approximately 500 mg/L, the highest concentration in our study, was prepared in an electrolyte solution containing ~1500 mg/L Na⁺, ~500 mg/L HCO₃⁻ and ~1000 mg/L Cl⁻ (simulated groundwater composition). For sandy materials (HFO-coated sand and fluvial sand), a solids-to-solution mass ratio of 1:10 was used, with approximately 25 g of solid material (precisely weighed) in the container; for finer-grained material (moraine, stagnant moraine and glaciolacustrine clay), a solids-to-solution mass ratio of 1:100 was used, with approximately 2.5 g of solid material (precisely weighed) in the container. Large volume (>200 mL) experiments were used such that aliquots of solution (~2 mL) could be taken over time without greatly affecting the overall solids-to-solution ratio. Experiments were run at pH between 6.5 and 7.5, and at room temperature (~22 ± 2°C). To start a kinetics experiment, a polypropylene bottle containing our solution (DPP and simulated groundwater) plus sediment was wrapped in aluminum foil to prevent photodegradation and then placed on a shaker. At regular intervals (approximately 10 min, 30 min, 1 h, 2 h, 4 h, 8 h, 24 h, then each 24 h after that) during the experiment, 2 mL aliquots were removed using a syringe and filtered through a 0.2 µm nylon membrane (Agilent Technologies) to remove the sediment in solution. The filtered solution was then placed in an amber vial and stored in the dark at 4°C before analysis. The vials were kept for no longer than a week before analysis using tandem-mass spectrometry (MS/MS). See **Figure A3** for results.

Degradation and Solubility Study Methods: To determine whether DPP degrades due to photolysis or hydrolysis during the course of the experiments, a series of duplicate control experiments were conducted. Just prior to the experiment, the DPP stock solution (approximately

500 mg/L) was prepared in an electrolyte solution containing Na^+ , HCO_3^- and $\sim \text{Cl}^-$.

Approximately 100 mL of stock solution was placed into four glass bottles (Pyrex), two of which were wrapped in aluminum foil to prevent photodegradation. The study was conducted at conditions identical to those of the batch sorption and kinetics experiments: pH between 6.5 and 7.5 and at room temperature ($\sim 22 \pm 2^\circ\text{C}$). At set times over the course of the study, 1.5 mL aliquots of solution were removed using a plastic pipette and stored in amber vials at 4°C before analysis. The vials were kept for no longer than a week before the MS/MS analyses were conducted.

A parallel control study was conducted whereby 100 mL of the same stock solution noted above was placed in a plastic container made of the same material used in the batch sorption experiments. This container was not covered in aluminum foil. This sub-study was conducted to see if DPP reacted differently when the solution was stored in a polypropylene plastic container rather than in glass bottles. The polypropylene container was placed alongside the four glass bottles, under the same conditions mentioned above.

Because the solubility of DPP in water is not well-known, a study of its solubility in water was undertaken. To do so, powdered DPP was added to a glass bottle that was then filled with ~ 50 mL deionized water. With each successive bottle, more DPP powder was added, but the volume of water used was the same. Each bottle was shaken until all the powder had dissolved.

Comparison with other aryl phosphates: The solubility of DPP in water (see **above** for Methods) is considerably higher than that of other related aryl phosphates: reported by the Estimation Program Interface (EPI) Suite to be 513.03 mg/L (US EPA 2012). We found that the

solubility of DPP in water was significantly higher than the reported value, in excess of 7500 mg/L. Saeger et al. (1979) determined the water solubility of several aryl phosphates, including TPP and a number that include the DPP-moiety. Of those studied, the reported water solubility for cresyl diphenyl phosphate (CDP) was the highest at 2.6 mg/L, with isodecyl diphenyl phosphate (IDDP) the lowest at 0.011 mg/L. Mayer et al. (1981) studied nonylphenyl diphenyl phosphate (NPDP) and 4-cumylphenyl diphenyl phosphate (CPDP) and found low water solubility (0.8 and 0.06 mg/L, respectively). The observed water solubility for DPP is at least three orders of magnitude greater than that of TPP, one potential parent product (Saeger et al. 1979), suggesting that DPP is significantly less hydrophobic than any other aryl phosphates, likely due to the hydroxyl-group within the DPP structure. The elevated solubility and lower hydrophobicity of DPP relative to other aryl phosphates likely means it is more readily mobilized in soils, sediments and aquifers. The increased mobility and higher water solubility of DPP may result in greater potential impacts to the environment, especially around industrial areas where aryl phosphates are used.

Our hydrolysis and photodegradation control studies (see **above** for Methods) revealed DPP to be more stable than other related aryl phosphates. Comparing the results for the DPP solutions kept in glass bottles out in the open (ambient light) to those kept in a plastic bottle wrapped in aluminum foil (dark), we observed no noticeable drop in concentration over the 28-day duration of the experiment (**Figure A4**). This indicates that no noticeable hydrolysis or other abiotic decay processes occurred over the span of the experiments. Likewise, comparisons of the measured concentrations in the glass bottles kept in the dark and those out in the open also indicate that photolysis is not a significant decay process (**Figure A4**). The plastic containers

used do not measurably affect the reactivity or degradability of DPP, nor do they sorb appreciable amounts of DPP (**Figure A4**).

Our results are in stark contrast to those for other aryl phosphates. Boethling and Cooper (1985) reported that hydrolysis was likely the most important abiotic transformation or degradation mechanism for aryl phosphates in the environment. They noted that hydrolysis occurred by a stepwise release of aryl or alkyl alcohols and acids. They also noted that aryl phosphates appear to hydrolyze more readily and rapidly under alkaline conditions but can still occur under acidic conditions (Great Lakes Chemical Corp. 2002). This is consistent with the results of Howard and Deo (1979) and Mayer et al. (1981), both of whom studied the hydrolysis of TPP. Although the hydrolysis of other aryl phosphates, including those with the DPP-moiety, has not been extensively studied, Boethling and Cooper (1985) speculated that the presence of methyl, butyl, isopropyl, nonyl, and cumyl groups as phenyl substitutes should lower the rate of hydrolysis, making them more persistent in the environment. Our study suggests that DPP may be the most refractory of the aryl phosphates. This is consistent with findings of Howard and Deo (1979), who similarly found that the rate of hydrolysis for DPP under both acidic and alkaline conditions was extremely slow. David and Seiber (1999a) also found that DPP was not susceptible to hydrolysis.

Ishikawa et al. (1992) studied the photochemical behavior of a number of organic phosphate esters, including TPP. They found that TPP underwent rapid photodegradation, with an estimated pseudo-first-order rate constant of $>40 \text{ h}^{-1}$ at pH of 3 and 10. By contrast, Brooke et al. (2009) predicted that organic phosphate esters are unlikely to undergo appreciable photodegradation. In this regard, DPP is similar to other aryl phosphates, as no noticeable photodegradation occurred over the span of this study.

Because DPP is a major degradation product of TPP and other aryl phosphates with the DPP-moiety (Howard and Deo 1979; Muir and Grift 1981; Anderson et al. 1993), we speculate that DPP may be an environmentally persistent contaminant. For example, Rodil et al. (2012) studied several emerging pollutants, including a number of organophosphates, within sewage, surface water and drinking water in Galicia, NW Spain. DPP, TPP and EHDP were some of the aryl phosphates studied. EHDP was never detected, whereas TPP was identified in only one sample. DPP was identified in all wastewater samples, in about half of the surface water samples, and in over 60% of the drinking water samples collected, with concentrations ranging from >0.0001 to ~ 10 $\mu\text{g/L}$ (Rodil et al. 2012). Although this is the only reported occurrence of DPP in the environment, we speculate that at other sites where TPP and other aryl phosphates with the DPP-moiety were identified, DPP would likely be present because the parent compounds are readily degradable and are used in common materials (Saeger et al. 1979; Boethling and Cooper 1985).

Zebrafish Husbandry: Adult zebrafish were cultured in the aquatic facility in the Department of Biological Sciences, University of Alberta following standardized animal use protocol 00001334. Embryos were obtained from matured fish bred from one male and two female fish, placed in one breeding aquarium. Fertilized embryos from three breeding aquaria were collected, rinsed, pooled, randomly selected and placed into exposure beakers to initiate the exposure.

Dilution Water for Zebrafish Embryo Assays: Dilution water was prepared with nano-pure water (PURELAB Flex, ELGA LabWater) and reagent grade salts (Sigma-Aldrich), which was prepared in 20 L batches containing 1.92 g of NaHCO_3 , 1.2 g of $\text{CaSO}_4 \cdot 2\text{H}_2\text{O}$, 1.2 g of MgSO_4 , and 0.08 g of KCl. The dilution water was kept at $25 \pm 1^\circ\text{C}$ and aerated prior to use.

Propagation of Errors: The measurement of various quantities is often uncertain to a degree. Multiple measurements, each with their individual uncertainties, are often required to be combined into a final result, with a combined uncertainty associated with it. The combination of uncertainties, or propagation of errors, depends on the situation. Here, we will briefly discuss the methods of error propagation relevant to this dissertation.

Often, quantities need to be added or subtracted together to obtain the result. For example, if quantities X and Y are to be added, and Z is to be subtracted to yield the result A , and each have an associated uncertainty, δX and δY , then:

$$A = X + Y - Z \quad (\text{A1})$$

And the uncertainty in A , denoted δA , is given by:

$$\delta A = \sqrt{(\delta X)^2 + (\delta Y)^2 + (\delta Z)^2} \quad (\text{A2})$$

For quantities for which the result is obtained by multiplication of a constant, it can be shown that the uncertainty in the result A , δA , is the uncertainty of the measured quantity multiplied by the absolute value of the constant, shown here:

$$A = cX \quad (\text{A3})$$

$$\delta A = |c|\delta X \quad (\text{A4})$$

For quantities that need to be multiplied or divided, a different propagation method is required. For this case, the quantities X and Y are multiplied, and divided by Z . Then A is given by:

$$A = \frac{XY}{Z} \quad (\text{A5})$$

Therefore, the uncertainty in A, is given by:

$$\delta A = |A| \sqrt{\left(\frac{\delta X}{X}\right)^2 + \left(\frac{\delta Y}{Y}\right)^2 + \left(\frac{\delta Z}{Z}\right)^2} \quad (\text{A6})$$

Lastly, if the result is dependant on the polynomial function of X to the n^{th} degree, where n can be either positive, negative, or non-interger, the result is given by:

$$A = X^n \quad (\text{A7})$$

The uncertainty in A for this case is given by:

$$\delta A = |n| \frac{\delta X}{|X|} |A| \quad (\text{A8})$$

References:

Anderson C, Wischer D, Schmieder A, Spiteller M (1993) Fate of triphenyl phosphate in soil.

Chemosphere **27**: 869 – 879.

Boethling RS, Cooper JC (1985) Environmental fate and effects of triaryl and tri-alkyl/aryl phosphates esters. Residue Reviews **94**: 49 – 99.

Brooke DN, Crookes MJ, Quarteman P, Burns J (2009) An overview of the environmental risk evaluation reports for aryl phosphate esters. Environment Agency, Rio House, Waterside Drive, Aztec West, Almondsbury, Bristol, UK.

David MD, Seiber JN (1999a) Accelerated hydrolysis of industrial organophosphates in water and soil using sodium perborate. Environmental Pollution **105**: 121 – 128.

Great Lakes Chemical Corporation (2002) Technical information and safety data sheet for Reofos TPP.

- Howard PH, Deo PG (1979) Degradation of aryl phosphates in aquatic environments. *Bulletin of Environmental Contamination and Toxicology* **22**: 337 – 344.
- Ishikawa S, Uchimura Y, Baba K, Eguchi Y, Kido K (1992) Photochemical behavior of organic phosphate esters in aqueous solutions irradiated with a mercury lamp. *Bulletin of Environmental Contamination and Toxicology* **49**: 368 – 374.
- Lo S-L, Jeng H-T, Lai C-H (1997) Characteristics and adsorption properties of iron-coated sand. *Water Science & Technology* **35**: 63 – 70.
- Mayer FL, Adams WJ, Finley MT, Michael PR, Mehrle PM, Saeger VW (1981) Phosphate ester hydraulic fluids: An aquatic environmental assessment of Pydrauls 50E and 115E. *Aquatic Toxicology and Hazard Assessment: 4th Conference, ASTM STP 737, American Society for Testing and Materials*: 103 – 123.
- Muir DCG, Grift NP (1981) Environmental dynamics of phosphate esters II: Uptake and bioaccumulation of 2-ethylhexyl phosphate and diphenyl phosphate by fish. *Chemosphere* **10**: 847 – 855.
- Rodil R, Quintana JB, Concha-Graña E, López-Mahía P, Muniategui-Lorenzo S, Prada-Rodríguez D (2012) Emerging pollutants in sewage, surface and drinking water in Galicia (NW Spain). *Chemosphere* **86**: 1040 – 1049.
- Saeger VW, Hicks O, Kaley RG, Michael PR, Mieure JP, Tucker ES (1979) Environmental fate of selected phosphate esters. *Environmental Science & Technology* **13**: 840 – 844.
- US Environmental Protection Agency (2012) Estimation Program Interface Suite™ for Microsoft® Windows, v4.11. United States Environmental Protection Agency, Washington, DC, USA.

Appendix B

Appendix B provides additional details regarding the ICP-MS/MS analyses conducted in **Chapter 3**, the raw analytical data from the ICP-MS/MS (inorganics) and HPLC-Orbitrap-MS (organics) for the batch sorption and column transport experiments in **Chapter 3**, and a discussion on Freundlich and Langmuir isotherms.

Element	Q1 → Q2	Gas	Element	Q1 → Q2	Gas
Li	7 → 7	-	Fe	56 → 56	He
B	11 → 11	-	Ni	60 → 60	He
Na	23 → 23	He	Cu	63 → 63	He
Mg	24 → 24	He	Zn	66 → 66	He
Al	27 → 27	He	As	75 → 91	O2
Si	28 → 28	H2	Br	79 → 79	He
P	31 → 47	O2	Sr	88 → 88	He
S	32 → 48	O2	Mo	95 → 95	He
K	39 → 39	He	Cd	114 → 114	-
Ca	40 → 40	H2	Ba	137 → 137	-
Cr	52 → 52	He	Pb	208 → 208	-
Mn	55 → 55	He	U	238 → 238	-

Table B1: Measured elements, MS/MS masses, and used collision/reaction gases.

Time (min)	In-Line SPE				Valve	Analytical C18 Column			
	Flow (mL/min)	Gradient	A%	B%		Flow (mL/min)	Gradient	A%	B%
0.00	2	Step	100	0		0.6	Step	99	1
3.00	0.1	Step	5	95	Switch	0.8	Step	100	
6.00	0.1	Step	0	100		0.6	Step	95	5
6.50	0.1	Step	0	100		0.6	Ramp	1	99
33.00	0.5	Step	100	0		0.6	Step	99	1

Table B2: Analytical details for the HPLC-Orbitrap-MS.

Oxide	GLC	MOR	FLUV
Na ₂ O	0.7%	0.2%	0.7%
MgO	0.3%	0.1%	0.0%
Al ₂ O ₃	3.8%	3.7%	1.9%
SiO ₂	64.6%	63.9%	49.7%
K ₂ O	1.6%	0.8%	1.3%
P ₂ O ₅	0.1%	0.1%	0.1%
CaO	0.1%	0.3%	0.0%
MnO	0.0%	0.0%	0.0%
Fe ₂ O ₃	3.3%	2.2%	1.4%

Table B3: Weight percent oxides for the three different soil types used in this study.

Sample	Lithium			Boron			Sodium			Magnesium		
	Conc.	Error	D.L.	Conc.	Error	D.L.	Conc.	Error	D.L.	Conc.	Error	D.L.
1/1 MOR	30.0	0.155	3.49	58.6	0.501	6.85	35400	120	1440	613	4.11	78.1
1/2 MOR	15.7	0.0630	1.51	31.9	0.373	2.96	22900	103	622	276	3.34	33.7
1/4 MOR	7.56	0.0442	0.786	15.8	0.220	1.54	7990	100	324	154	1.40	17.6
1/10 MOR	2.91	0.0638	0.405	6.58	0.0942	0.795	3500	24.7	167	73.7	0.190	9.06
MOR BLANK	BDL		0.413	BDL		0.811	143	1.27	171	9.61	0.383	9.25
1/1 GLC	34.1	0.164	3.27	65.3	0.433	6.43	33400	241	1350	590	6.31	73.3
1/2 GLC	14.9	0.0797	1.50	30.1	0.293	2.94	15000	164	620	281	3.13	33.5
1/4 GLC	8.52	0.0143	0.787	17.9	0.246	1.55	7740	72.2	325	158	0.739	17.6
1/10 GLC	2.96	0.0330	0.382	6.68	0.0270	0.750	3420	12.8	158	80.8	0.680	8.56
GLC BLANK	BDL		0.389	BDL		0.763	152	0.222	160	9.39	0.053	8.71
1/1 FLUV	34.0	0.102	3.26	66.1	1.09	6.41	33100	126	1350	581	2.93	73.1
1/2 FLUV	15.8	0.0735	1.50	31.7	0.291	2.95	15300	90.1	621	267	1.30	33.6
1/4 FLUV	8.25	0.0681	0.788	16.4	0.166	1.55	7840	125	325	143	1.95	17.7
1/10 FLUV	3.50	0.0085	0.405	6.94	0.103	0.796	3420	13.4	167	64.0	1.03	9.08
FLUV BLANK	BDL		0.412	BDL		0.808	172	1.30	170	13.2	0.225	9.22
FPW Plastic	34.2	0.285	3.24	69.1	0.375	6.36	47900.0	534	87.1	558	3.84	72.5
FPW Glass	34.0	0.243	3.20	69.3	0.772	6.29	46700.0	552	86.2	556	12.9	71.8

Table B4: ICP-MS/MS results from the batch experiments with Sample 1. Units are in mg/L. D.L. = detection limit. BDL = below detection limit.

Sample	Aluminum			Silicon			Phosphorous			Sulphur		
	Conc.	Error	D.L.	Conc.	Error	D.L.	Conc.	Error	D.L.	Conc.	Error	D.L.
1/1 MOR	BDL		0.443	BDL		130	BDL		0.159	70.5	1.69	28.0
1/2 MOR	BDL		0.191	BDL		56.1	BDL		0.0687	33.6	0.592	12.1
1/4 MOR	BDL		0.100	BDL		29.3	BDL		0.0358	18.6	0.622	6.30
1/10 MOR	BDL		0.0514	BDL		15.1	0.0191	0.00660	0.0184	7.92	0.608	3.24
MOR BLANK	1.57	0.0429	0.0524	BDL		15.4	0.102	0.0199	0.0188	BDL		3.31
1/1 GLC	BDL		0.416	BDL		122	0.206	0.141	0.149	77.0	1.84	26.2
1/2 GLC	BDL		0.190	BDL		55.7	BDL		0.0681	34.7	1.43	12.0
1/4 GLC	BDL		0.100	BDL		29.3	0.0924	0.0245	0.0359	17.6	0.672	6.31
1/10 GLC	0.0672	0.0144	0.0485	BDL		14.2	0.0631	0.00826	0.0174	8.44	0.210	3.06
GLC BLANK	2.28	0.194	0.0494	BDL		14.5	0.125	0.0504	0.0177	BDL		3.12
1/1 FLUV	BDL		0.414	BDL		121	BDL		0.149	77.6	0.772	26.1
1/2 FLUV	BDL		0.191	BDL		55.9	BDL		0.0684	36.7	0.397	12.0
1/4 FLUV	BDL		0.100	BDL		29.3	BDL		0.0359	18.5	0.401	6.32
1/10 FLUV	BDL		0.0515	BDL		15.1	BDL		0.0185	8.30	0.0283	3.25
FLUV BLANK	0.0716	0.00656	0.0523	BDL		15.3	BDL		0.0188	BDL		3.30
FPW Plastic	BDL		0.411	BDL		121	BDL		0.148	75.5	3.29	25.9
FPW Glass	BDL		0.407	BDL		119	BDL		0.146	71.9	0.432	25.7

Table B4 con't: ICP-MS/MS results from the batch experiments with Sample 1. Units are in mg/L. D.L. = detection limit. BDL = below detection limit.

Sample	Potassium			Calcium			Chromium			Manganese		
	Conc.	Error	D.L.	Conc.	Error	D.L.	Conc.	Error	D.L.	Conc.	Error	D.L.
1/1 MOR	1240	17.8	146	7090	44.9	95.7	BDL		2.29	9.01	0.0613	2.43
1/2 MOR	637	3.74	63.0	3290	42.6	41.3	BDL		0.987	4.44	0.0597	1.05
1/4 MOR	308	2.49	32.9	1720	12.9	21.6	BDL		0.515	2.82	0.0365	0.548
1/10 MOR	128	0.952	16.9	692	5.90	11.1	BDL		0.265	1.28	0.00721	0.282
MOR BLANK	BDL		17.3	17.9	1.12	11.3	BDL		0.271	0.419	0.0404	0.288
1/1 GLC	1320	6.92	137	7150	52.7	89.8	BDL		2.15	10.1	0.0845	2.28
1/2 GLC	583	9.85	62.6	3310	51.8	41.0	BDL		0.980	5.72	0.0349	1.04
1/4 GLC	326	1.92	32.9	1700	16.6	21.6	BDL		0.516	3.52	0.0467	0.548
1/10 GLC	118	0.502	16.0	701	7.91	10.5	BDL		0.250	2.55	0.0084	0.266
GLC BLANK	BDL		16.3	15.7	0.14	10.7	BDL		0.255	0.529	0.0128	0.271
1/1 FLUV	1320	6.65	136	7300	40.4	89.5	BDL		2.14	9.50	0.0162	2.27
1/2 FLUV	608	7.69	62.8	3380	54.0	41.2	BDL		0.984	4.93	0.0387	1.05
1/4 FLUV	314	5.90	33.0	1790	11.6	21.6	BDL		0.517	3.55	0.0686	0.549
1/10 FLUV	133	1.19	17.0	785	8.66	11.1	BDL		0.266	1.61	0.0180	0.282
FLUV BLANK	17.9	0.212	17.2	79.0	0.616	11.3	BDL		0.270	0.472	0.00300	0.287
FPW Plastic	1340	9.23	135	7170	48.6	88.8	BDL		2.12	8.77	0.224	2.26
FPW Glass	1330	4.69	134	7080	21.3	87.9	BDL		2.10	8.77	0.0959	2.23

Table B4 con't: ICP-MS/MS results from the batch experiments with Sample 1. Units are in mg/L. D.L. = detection limit. BDL = below detection limit.

Sample	Iron			Nickel			Copper			Zinc		
	Conc.	Error	D.L.	Conc.	Error	D.L.	Conc.	Error	D.L.	Conc.	Error	D.L.
1/1 MOR	BDL		1.82	BDL		2.06	BDL		1.80	BDL		3.84
1/2 MOR	BDL		0.784	BDL		0.890	BDL		0.778	BDL		1.66
1/4 MOR	BDL		0.409	BDL		0.465	BDL		0.406	BDL		0.866
1/10 MOR	BDL		0.211	BDL		0.239	BDL		0.209	BDL		0.446
MOR BLANK	1.43	0.195	0.215	BDL		0.244	BDL		0.213	BDL		0.455
1/1 GLC	BDL		1.70	BDL		1.94	BDL		1.69	BDL		3.60
1/2 GLC	1.14	0.0242	0.778	BDL		0.884	BDL		0.772	BDL		1.65
1/4 GLC	BDL		0.410	BDL		0.465	BDL		0.406	BDL		0.866
1/10 GLC	BDL		0.199	BDL		0.226	BDL		0.197	BDL		0.421
GLC BLANK	2.59	0.0190	0.202	BDL		0.230	BDL		0.201	BDL		0.428
1/1 FLUV	BDL		1.70	BDL		1.93	1.93	0.0313	1.68	BDL		3.59
1/2 FLUV	BDL		0.781	BDL		0.887	0.846	0.0232	0.775	BDL		1.65
1/4 FLUV	BDL		0.410	BDL		0.466	0.434	0.00178	0.407	BDL		0.868
1/10 FLUV	BDL		0.211	BDL		0.240	0.212	0.00802	0.209	BDL		0.446
FLUV BLANK	BDL		0.214	BDL		0.243	BDL		0.213	BDL		0.453
FPW Plastic	6.75	0.0312	1.69	BDL		1.91	2.61	0.0228	1.67	BDL		3.56
FPW Glass	10.6	0.0559	1.67	BDL		1.89	2.64	0.0676	1.65	3.70	0.0972	3.53

Table B4 con't: ICP-MS/MS results from the batch experiments with Sample 1. Units are in mg/L. D.L. = detection limit. BDL = below detection limit.

Sample	Arsenic			Bromide			Strontium			Molybdenum		
	Conc.	Error	D.L.	Conc.	Error	D.L.	Conc.	Error	D.L.	Conc.	Error	D.L.
1/1 MOR	BDL		0.0500	168	3.65	5.60	620	8.21	5.05	0.263	0.0164	0.0490
1/2 MOR	BDL		0.0216	79.5	1.40	2.42	262	1.84	2.18	0.0605	0.00222	0.0212
1/4 MOR	BDL		0.0113	41.4	0.0623	1.26	120	1.19	1.14	0.0198	0.00150	0.0111
1/10 MOR	BDL		0.00581	17.1	0.232	0.650	35.8	0.125	0.586	0.00773	0.00104	0.00569
MOR BLANK	BDL		0.00592	BDL		0.663	BDL		0.597	0.00621	0.000174	0.00581
1/1 GLC	BDL		0.0470	165	0.481	5.26	632	1.16	4.74	BDL		0.0460
1/2 GLC	BDL		0.0214	77.8	0.875	2.40	295	3.23	2.16	BDL		0.0210
1/4 GLC	BDL		0.0113	39.9	0.974	1.26	147	1.67	1.14	BDL		0.0111
1/10 GLC	BDL		0.00548	16.3	0.167	0.614	52.4	0.456	0.553	BDL		0.00537
GLC BLANK	BDL		0.00558	BDL		0.624	BDL		0.562	BDL		0.00547
1/1 FLUV	BDL		0.0468	167	1.36	5.24	660	1.73	4.72	BDL		0.0459
1/2 FLUV	BDL		0.0215	77.1	0.311	2.41	298	2.73	2.17	BDL		0.0211
1/4 FLUV	BDL		0.0113	40.2	0.235	1.27	157	1.72	1.14	BDL		0.0111
1/10 FLUV	BDL		0.00581	16.6	0.166	0.651	60.7	0.898	0.586	BDL		0.00570
FLUV BLANK	BDL		0.00591	BDL		0.661	BDL		0.596	BDL		0.00579
FPW Plastic	BDL		0.0464	164	0.610	5.20	661	3.46	4.68	BDL		0.0455
FPW Glass	BDL		0.0460	164	1.85	5.14	661	15.4	4.64	BDL		0.0451

Table B4 con't: ICP-MS/MS results from the batch experiments with Sample 1. Units are in mg/L. D.L. = detection limit. BDL = below detection limit.

Sample	Cadmium			Barium			Lead			Uranium		
	Conc.	Error	D.L.	Conc.	Error	D.L.	Conc.	Error	D.L.	Conc.	Error	D.L.
1/1 MOR	BDL		0.0496	27.6	0.174	2.81	1.28	0.0279	1.26	BDL		1.20
1/2 MOR	BDL		0.0214	16.3	0.239	1.21	0.546	0.00776	0.545	0.518	0.0257	0.516
1/4 MOR	BDL		0.0112	11.3	0.154	0.634	BDL		0.285	0.270	0.0158	0.269
1/10 MOR	BDL		0.00576	5.59	0.0264	0.326	BDL		0.147	0.141	0.00317	0.139
MOR BLANK	BDL		0.00587	0.439	0.00784	0.333	0.150	0.00273	0.149	0.142	0.00514	0.142
1/1 GLC	BDL		0.0466	9.15	0.101	2.64	1.19	0.0441	1.19	BDL		1.12
1/2 GLC	BDL		0.0213	5.27	0.0658	1.20	BDL		0.541	0.516	0.0136	0.512
1/4 GLC	BDL		0.0112	3.62	0.0293	0.634	BDL		0.285	0.275	0.00693	0.270
1/10 GLC	BDL		0.00543	2.02	0.0225	0.308	BDL		0.138	0.134	0.00554	0.131
GLC BLANK	BDL		0.00553	0.354	0.0152	0.313	0.142	0.00201	0.141	0.135	0.0102	0.133
1/1 FLUV	BDL		0.0464	9.26	0.287	2.63	1.19	0.0158	1.18	BDL		1.12
1/2 FLUV	BDL		0.0213	6.06	0.0780	1.21	BDL		0.543	0.516	0.0304	0.514
1/4 FLUV	BDL		0.0112	4.79	0.0742	0.635	BDL		0.285	0.274	0.00855	0.270
1/10 FLUV	BDL		0.00576	3.07	0.0522	0.327	BDL		0.147	0.144	0.000617	0.139
FLUV BLANK	BDL		0.00585	0.679	0.0310	0.332	0.149	0.00331	0.149	0.143	0.00253	0.141
FPW Plastic	BDL		0.0460	5.41	0.0428	2.61	1.35	0.0154	1.17	BDL	0.0601	1.11
FPW Glass	BDL		0.0456	5.67	0.0855	2.58	1.86	0.00577	1.16	BDL	0.0836	1.10

Table B4 con't: ICP-MS/MS results from the batch experiments with Sample 1. Units are in mg/L. D.L. = detection limit. BDL = below detection limit.

Sample	Lithium		Boron		Sodium		Magnesium		Aluminum		Silicon	
	Conc.	Error	Conc.	Error	Conc.	Error	Conc.	Error	Conc.	Error	Conc.	Error
1/1 MOR	40.3	0.27	82.2	2.6	56924	330	744	5.5	BDL	BDL	BDL	BDL
1/2 MOR	21.4	0.11	44.7	1.5	26909	156	428	1.2	BDL	BDL	BDL	BDL
1/4 MOR	10.7	0.072	22.7	0.23	14283	127	237	0.98	BDL	BDL	BDL	BDL
1/10 MOR	3.91	0.028	8.8	0.063	5746	59	108	0.91	0.0337	0.0013	BDL	BDL
1/20 MOR	1.76	0.01	4.49	0.048	3141	13	59.7	0.29	0.0271	0.00064	BDL	BDL
MOR BLANK	BDL	BDL	BDL	BDL	75.3	0.41	1.88	0.028	2.21	0.035	2.97	0.047
1/1 GLC	42.8	0.28	79.3	1.1	55657	378	794	4.0	BDL	BDL	BDL	BDL
1/2 GLC	24.3	0.22	48.4	1.7	26034	171	482	5.9	BDL	BDL	BDL	BDL
1/4 GLC	12.5	0.21	25.7	1.1	12853	66	278	5.6	BDL	BDL	BDL	BDL
1/10 GLC	4.18	0.013	9.25	0.10	6019	38	120	0.28	0.0597	0.0018	BDL	BDL
1/20 GLC	1.96	0.010	4.82	0.061	3308	18	72.1	0.53	0.0298	0.00052	BDL	BDL
GLC BLANK	BDL	BDL	BDL	BDL	97.4	0.53	1.86	0.040	1.80	0.048	3.35	0.072
1/1 FLUV	45.3	0.23	88.2	2.3	55684	188	768	7.1	BDL	BDL	BDL	BDL
1/2 FLUV	27.9	0.30	57.7	1.4	26052	316	486	4.0	BDL	BDL	BDL	BDL
1/4 FLUV	12.2	0.11	24.5	0.60	14693	64	216	1.6	BDL	BDL	BDL	BDL
1/10 FLUV	4.97	0.027	10.0	0.41	5914	36	93.7	0.58	0.153	0.0014	8.42	0.065
1/20 FLUV	2.44	0.007	4.88	0.067	3179	30	50.1	0.22	0.0276	0.00084	BDL	BDL
FLUV BLANK	BDL	BDL	BDL	BDL	321	0.88	18.1	0.21	0.0671	0.0016	15.0	0.17
FPW Stock	44.8	0.23	91.1	2.1	50524	217	752	3.4	BDL	BDL	BDL	BDL

Table B5: ICP-MS/MS results from the batch experiments with Sample 2. BDL = below detection limit. Detection limits (mg/L) for

Li = 0.00052, B = 0.11, Na = 0.19, Mg = 0.22, Al = 0.0032, Si = 0.32.

Sample	Phosphorous		Sulphur		Potassium		Calcium		Chromium		Manganese	
	Conc.	Error	Conc.	Error	Conc.	Error	Conc.	Error	Conc.	Error	Conc.	Error
1/1 MOR	BDL	BDL	72.9	3.8	1969	13	8203	127	BDL	BDL	7.47	0.16
1/2 MOR	BDL	BDL	38.5	1.9	994	4.4	4338	20	BDL	BDL	4.57	0.11
1/4 MOR	BDL	BDL	19.8	0.84	493	3.9	2255	17	BDL	BDL	2.86	0.077
1/10 MOR	BDL	BDL	7.86	0.30	188	0.70	865	4.3	BDL	BDL	1.30	0.028
1/20 MOR	0.00719	0.0043	4.26	0.10	96.5	0.58	407	3.4	BDL	BDL	0.686	0.024
MOR BLANK	0.171	0.040	0.68	0.048	BDL	BDL	13.6	0.23	BDL	BDL	0.0658	0.0036
1/1 GLC	BDL	BDL	74.3	3.0	1892	7.1	8312	62	BDL	BDL	8.75	0.25
1/2 GLC	BDL	BDL	42.3	0.73	1021	11	4836	41	BDL	BDL	6.33	0.14
1/4 GLC	BDL	BDL	21.8	1.2	506	7.7	2513	25	BDL	BDL	4.29	0.027
1/10 GLC	0.0586	0.023	9.03	0.38	175	0.94	865	24	BDL	BDL	3.73	0.037
1/20 GLC	0.209	0.051	5.14	0.18	86.2	0.29	434	1.2	BDL	BDL	2.39	0.013
GLC BLANK	0.159	0.041	0.96	0.08	BDL	BDL	8.24	0.041	BDL	BDL	0.189	0.0053
1/1 FLUV	BDL	BDL	72.2	0.87	2005	13	8488	69	BDL	BDL	6.47	0.30
1/2 FLUV	BDL	BDL	42.2	0.70	1140	6.0	5032	49	BDL	BDL	4.00	0.11
1/4 FLUV	BDL	BDL	20.9	1.4	501	2.7	2370	13	BDL	BDL	1.88	0.066
1/10 FLUV	BDL	BDL	8.56	0.21	201	1.2	973	6.3	BDL	BDL	1.01	0.027
1/20 FLUV	BDL	BDL	5.14	0.19	97.6	0.46	519	3.2	BDL	BDL	0.688	0.0053
FLUV BLANK	BDL	BDL	2.24	0.08	12.7	0.03	193	1.5	BDL	BDL	0.323	0.0084
FPW Stock	BDL	BDL	73.4	2.6	2003	15	8224	54	BDL	BDL	6.07	0.11

Table B5 con't: ICP-MS/MS results from the batch experiments with Sample 2. BDL = below detection limit. Detection limits

(mg/L) for P = 0.00052, S = 0.06, K = 0.98, Ca = 0.95, Cr = 0.00033, Mn = 0.00052.

Sample	Iron		Nickel		Copper		Zinc		Arsenic		Bromide	
	Conc.	Error	Conc.	Error	Conc.	Error	Conc.	Error	Conc.	Error	Conc.	Error
1/1 MOR	BDL	BDL	0.380	0.0074	BDL	BDL	BDL	BDL	BDL	BDL	260	2.5
1/2 MOR	BDL	BDL	0.202	0.0063	BDL	BDL	BDL	BDL	BDL	BDL	133	1.3
1/4 MOR	BDL	BDL	0.106	0.0024	BDL	BDL	BDL	BDL	BDL	BDL	67.4	0.20
1/10 MOR	BDL	BDL	0.042	0.00086	BDL	BDL	0.371	0.0069	BDL	BDL	26.2	0.15
1/20 MOR	0.0481	0.0029	0.023	0.00087	0.00255	0.000081	0.177	0.0023	BDL	BDL	13.3	0.13
MOR BLANK	1.49	0.074	0.031	0.0012	BDL	BDL	0.662	0.012	0.00285	0.0021	0.607	0.088
1/1 GLC	BDL	BDL	0.444	0.015	BDL	BDL	BDL	BDL	BDL	BDL	225	3.5
1/2 GLC	BDL	BDL	0.274	0.0053	BDL	BDL	BDL	BDL	BDL	BDL	131	1.2
1/4 GLC	BDL	BDL	0.142	0.0037	BDL	BDL	BDL	BDL	BDL	BDL	69.0	1.3
1/10 GLC	BDL	BDL	0.054	0.0026	0.00973	0.00026	0.642	0.014	BDL	BDL	26.3	0.092
1/20 GLC	0.0846	0.0017	0.029	0.00062	0.00528	0.00019	0.332	0.0043	BDL	BDL	13.7	0.13
GLC BLANK	1.88	0.015	0.011	0.00058	BDL	BDL	0.415	0.0089	0.00384	0.0033	0.334	0.059
1/1 FLUV	BDL	BDL	1.18	0.030	BDL	BDL	BDL	BDL	BDL	BDL	226	2.9
1/2 FLUV	BDL	BDL	0.646	0.0070	0.0355	0.0016	0.965	0.026	0.0232	0.023	136	1.4
1/4 FLUV	BDL	BDL	0.211	0.0065	0.0204	0.00035	0.389	0.021	BDL	BDL	62.2	0.36
1/10 FLUV	BDL	BDL	0.067	0.0030	0.0124	0.00047	0.269	0.0065	BDL	BDL	25.7	0.20
1/20 FLUV	BDL	BDL	0.030	0.00022	0.00668	0.00033	0.132	0.0027	BDL	BDL	12.8	0.054
FLUV BLANK	BDL	BDL	BDL	BDL	BDL	BDL	0.531	0.0075	BDL	BDL	1.36	0.19
FPW Stock	3.75	0.070	2.18	0.02	BDL	BDL	BDL	BDL	BDL	BDL	224	3.6

Table B5 con't: ICP-MS/MS results from the batch experiments with Sample 2. BDL = below detection limit. Detection limits

(mg/L) for Fe = 0.010, Ni = 0.00052, Cu = 0.00051, Zn = 0.034, As = 0.00051, Br = 0.094.

Sample	Strontium		Molybenium		Cadmium		Barium		Lead	
	Conc.	Error	Conc.	Error	Conc.	Error	Conc.	Error	Conc.	Error
1/1 MOR	805	6.5	1.51	0.24	0.0343	0.0019	44.0	0.44	BDL	BDL
1/2 MOR	396	1.4	0.504	0.078	0.0231	0.0028	32.1	0.69	BDL	BDL
1/4 MOR	177	0.71	0.138	0.021	0.0139	0.00088	20.9	0.086	BDL	BDL
1/10 MOR	45.0	0.25	0.038	0.0063	BDL	BDL	9.29	0.050	BDL	BDL
1/20 MOR	14.7	0.11	0.0139	0.0015	BDL	BDL	4.50	0.027	0.00311	0.00019
MOR BLANK	BDL	BDL	0.0118	0.0015	BDL	BDL	0.0925	0.0015	0.00519	0.00016
1/1 GLC	859	3.9	0.0737	0.015	BDL	BDL	14.7	0.15	BDL	BDL
1/2 GLC	488	3.9	0.0335	0.0034	BDL	BDL	10.5	0.13	BDL	BDL
1/4 GLC	248	5.4	0.0156	0.0013	BDL	BDL	6.96	0.17	BDL	BDL
1/10 GLC	77.4	0.59	0.0122	0.00089	0.0112	0.0017	2.81	0.010	0.00841	0.0012
1/20 GLC	32.2	0.14	0.00343	0.00035	BDL	BDL	1.41	0.013	BDL	BDL
GLC BLANK	BDL	BDL	0.00330	0.00040	BDL	BDL	BDL	BDL	BDL	BDL
1/1 FLUV	887	4.5	BDL	BDL	BDL	BDL	14.8	0.20	BDL	BDL
1/2 FLUV	542	3.6	BDL	BDL	BDL	BDL	12.3	0.16	BDL	BDL
1/4 FLUV	228	1.8	0.0114	0.0028	BDL	BDL	7.52	0.11	BDL	BDL
1/10 FLUV	87.3	0.22	0.00615	0.00072	BDL	BDL	5.11	0.021	BDL	BDL
1/20 FLUV	38.2	0.13	0.00410	0.00026	0.00272	0.00038	3.25	0.016	BDL	BDL
FLUV BLANK	0.652	0.0043	0.00907	0.00087	BDL	BDL	0.911	0.0077	BDL	BDL
FPW Stock	873	2.9	BDL	BDL	BDL	BDL	8.80	0.10	0.0978	0.0031

Table B5 con't: ICP-MS/MS results from the batch experiments with Sample 2. BDL = below detection limit. Detection limits (mg/L) for Sr = 0.049, Mo = 0.00051, Cd = 0.00051, Ba = 0.00051, and Pb = 0.00051.

Sample	Bulk PEG	PEG-6	PEG-7	PEG-9	PEG-11
FLUV 1:10	1.83E+08	2.34E+07	2.46E+07	1.12E+06	1.72E+05
FLUV 1:4	4.65E+08	6.39E+07	6.67E+07	1.63E+06	3.23E+05
FLUV 1:2	1E+09	1.13E+08	1.14E+08	2.32E+06	3.73E+05
FLUV 1:1	1.06E+09	1.71E+08	1.19E+08	2.39E+06	3.87E+05
GLC 1:10	2.42E+08	1.02E+07	2.04E+07	5.14E+06	3.80E+05
GLC 1:4	5.61E+08	4.53E+07	6.72E+07	5.97E+06	4.66E+05
GLC 1:2	1.22E+09	1.11E+08	1.30E+08	7.51E+06	4.89E+05
GLC1:1	1.55E+09	1.65E+08	1.38E+08	1.67E+07	1.65E+06
MOR 1:10	3.64E+08	2.23E+07	3.98E+07	1.43E+07	1.88E+06
MOR 1:4	1.05E+09	7.30E+07	1.20E+08	6.91E+07	8.02E+06
MOR 1:2	1.92E+09	1.27E+08	2.27E+08	1.17E+08	8.71E+06
MOR 1:1	2.72E+09	2.13E+08	3.38E+08	1.23E+08	1.68E+07
FPW stock	5.36E+09	2.62E+08	4.54E+08	4.70E+08	2.14E+08

Table B6: HPLC-Orbitrap-MS peak areas (representing concentrations) of various PEGs in the batch experiments for Sample 1. The FPW stock solution was also measured.

Sample	Lithium			Boron			Sodium			Magnesium			Aluminum		Silicon			Phosphorous		Sulphur				
	Conc.	Error	D.L.	Conc.	Error	D.L.	Conc.	Error	D.L.	Conc.	Error	D.L.	Conc.	Error	D.L.	Conc.	Error	D.L.	Conc.	Error	D.L.			
FPW Stock 1	6.75	0.0644	0.308	14.7	0.0342	0.469	5870	30.3	67.8	116	2.08	3.70	BDL		0.0544	2.55	0.116	0.00809	BDL		0.00811	22.5	0.311	0.829
FPW Stock 2	7.55	0.0621	0.307	14.9	0.0510	0.468	5730	68.7	72.4	118	2.30	3.69	BDL		0.0542	1.91	0.057	0.00807	BDL		0.00808	22.4	0.922	0.827
FPW Stock 3	7.65	0.0158	0.308	15.1	0.1032	0.469	5720	19.7	72.2	118	1.73	3.70	BDL		0.0544	2.50	0.114	0.00809	BDL		0.00810	23.9	0.199	0.829
FPW Stock 4	7.66	0.0534	0.0854	15.1	0.138	1.50	5800	36.8	83.5	114	2.06	16.8	BDL		0.0794	1.90	0.0360	0.401	0.0133	0.00577	0.00954	23.0	0.131	6.58
GW Stock	BDL		0.312	BDL		0.475	97.5	1.078	69.6	5.02	0.306	3.75	BDL		0.0552	1.83	0.109	0.00820	BDL		0.00822	BDL		0.841
1A	BDL		0.314	BDL		0.479	99.4	1.50	69.7	6.60	0.287	3.77	BDL		0.0555	2.14	0.102	0.00826	0.0165	0.0108	0.00827	BDL		0.846
2A	BDL		0.315	BDL		0.480	99.0	1.66	69.9	5.17	0.117	3.78	BDL		0.0557	2.25	0.053	0.00828	0.0135	0.0135	0.00829	BDL		0.848
3A	BDL		0.314	BDL		0.479	99.5	0.763	69.6	5.13	0.262	3.78	BDL		0.0556	2.27	0.115	0.00827	BDL		0.00828	BDL		0.847
4A	BDL		0.313	BDL		0.477	165	1.37	69.4	10.0	0.339	3.76	BDL		0.0554	2.27	0.117	0.00824	0.0174	0.0114	0.00825	BDL		0.844
6A	2.54	0.00160	0.309	BDL		0.470	2390	11.79	68.7	441	3.89	3.71	BDL		0.0546	2.42	0.065	0.00811	0.0212	0.0166	0.00813	BDL		0.831
7A	5.70	0.02403	0.310	3.59	0.0536	0.473	4550	33.7	69.1	292	4.55	3.73	BDL		0.0548	2.62	0.047	0.00815	BDL		0.00817	22.5	0.486	0.835
8A	6.65	0.07653	0.310	9.53	0.1928	0.473	5560	40.7	69.1	183	4.22	3.73	BDL		0.0549	2.73	0.057	0.00817	BDL		0.00818	22.8	0.999	0.837
9A	6.86	0.03348	0.310	12.1	0.0702	0.472	5930	7.96	68.6	129	2.34	3.72	BDL		0.0548	2.73	0.205	0.00814	0.0132	0.0132	0.00816	22.9	0.765	0.835
10A	6.77	0.07796	0.309	12.6	0.1752	0.471	5760	84.2	68.2	120	1.44	3.71	BDL		0.0546	2.83	0.070	0.00812	0.0177	0.0170	0.00814	BDL		0.832
11A	6.87	0.03642	0.308	13.7	0.0455	0.469	5810	43.0	68.1	112	2.05	3.70	BDL		0.0544	2.52	0.126	0.00809	BDL		0.00811	22.7	0.474	0.829
12A	7.02	0.10560	0.313	14.4	0.2105	0.478	5970	58.9	79.6	116	1.82	3.76	BDL		0.0554	2.33	0.095	0.00824	BDL		0.00825	23.1	0.859	0.844
14A	6.92	0.12249	0.308	14.1	0.1314	0.469	5550	113.4	68.4	104	2.51	3.70	BDL		0.0544	2.53	0.163	0.00809	BDL		0.00811	22.4	0.166	0.829
15A	6.79	0.06647	0.312	13.9	0.1202	0.476	5750	67.5	69.4	113	2.21	3.75	BDL		0.0552	2.44	0.134	0.00821	BDL		0.00823	22.9	0.105	0.841
16A	7.45	0.05735	0.312	15.1	0.2391	0.475	5730	68.7	69.3	116	3.19	3.75	BDL		0.0551	2.20	0.061	0.00820	BDL		0.00821	23.6	0.657	0.840
17A	6.93	0.03566	0.313	14.2	0.1756	0.477	5860	57.5	69.9	116	2.86	3.76	BDL		0.0554	2.24	0.121	0.00824	BDL		0.00825	23.0	0.801	0.844
18A	6.95	0.11175	0.312	14.3	0.0806	0.475	6000	19.1	69.1	116	1.020	3.75	BDL		0.0552	2.11	0.095	0.00820	BDL		0.00822	23.0	0.180	0.840
19A	6.77	0.12494	0.312	13.8	0.2325	0.475	5790	91.9	69.2	115	1.66	3.75	BDL		0.0551	2.15	0.103	0.00820	BDL		0.00822	22.7	0.520	0.840
20A	6.95	0.11163	0.312	14.3	0.1814	0.476	5770	58.0	69.5	116	1.06	3.75	BDL		0.0552	2.18	0.070	0.00821	BDL		0.00822	22.4	0.649	0.841
21A	7.03	0.06395	0.310	14.3	0.0732	0.473	5771	39.8	69.1	115	2.98	3.73	0.0634	0.0126	0.0549	2.23	0.052	0.00816	BDL		0.00817	23.0	0.720	0.836
22A	7.07	0.02142	0.310	14.5	0.0950	0.473	5810	49.3	69.1	111	2.84	3.73	BDL		0.0549	2.26	0.030	0.00816	BDL		0.00818	23.0	0.443	0.836
23A	6.78	0.04351	0.310	14.0	0.1350	0.473	5850	50.2	69.2	118	0.87	3.73	BDL		0.0549	2.17	0.193	0.00816	BDL		0.00818	23.2	0.778	0.836
25A	6.98	0.00773	0.309	14.1	0.1499	0.471	5910	84.2	68.8	117	2.52	3.71	BDL		0.0546	1.44	0.035	0.00812	BDL		0.00814	23.2	0.736	0.832
26A	6.96	0.08869	0.308	14.2	0.2154	0.470	5760	41.2	68.8	104	2.37	3.70	BDL		0.0545	2.18	0.028	0.00811	BDL		0.00812	23.0	0.308	0.831
27A	6.97	0.15175	0.310	14.1	0.0968	0.473	5760	73.0	69.1	119	1.58	3.73	BDL		0.0549	2.11	0.079	0.00816	BDL		0.00818	23.2	0.275	0.836
28A	7.03	0.11177	0.310	14.4	0.1667	0.473	5830	77.6	68.8	116	1.32	3.73	BDL		0.0548	2.05	0.137	0.00815	BDL		0.00817	23.3	0.341	0.835
30A	7.02	0.08310	0.310	14.4	0.0744	0.472	5790	80.5	68.9	117	2.52	3.72	0.0965	0.00774	0.0548	2.06	0.069	0.00814	BDL		0.00816	22.9	0.778	0.834
32A	6.95	0.10310	0.309	14.4	0.1632	0.472	5800	58.6	68.8	116	1.39	3.72	BDL		0.0547	2.10	0.024	0.00814	BDL		0.00815	22.8	1.39	0.834
34A	6.94	0.02473	0.311	14.3	0.1016	0.474	5850	17.4	69.2	114	2.08	3.74	BDL		0.0550	2.60	0.123	0.00818	BDL		0.00819	23.0	0.774	0.838
36A	6.92	0.08497	0.309	14.4	0.0443	0.472	6380	91.0	68.6	116	1.92	3.72	BDL		0.0547	2.36	0.042	0.00814	BDL		0.00815	22.3	0.517	0.834
37A	6.98	0.03789	0.309	14.4	0.2650	0.471	5980	54.0	68.2	118	3.58	3.72	BDL		0.0547	2.25	0.039	0.00813	BDL		0.00815	22.6	0.996	0.833
39A	7.09	0.01923	0.309	14.6	0.0621	0.471	5840	6.25	68.9	116	1.48	3.71	BDL		0.0546	2.43	0.210	0.00812	BDL		0.00813	22.6	0.635	0.832
42A	7.08	0.07162	0.312	14.7	0.2203	0.475	5840	33.7	71.9	117	1.11	3.75	BDL		0.0551	2.56	0.052	0.00820	BDL		0.00822	23.5	0.523	0.840
45A	7.20	0.15863	0.309	14.7	0.0660	0.471	5820	64.4	69.2	117	1.50	3.71	BDL		0.0546	2.68	0.111	0.00813	BDL		0.00814	23.0	0.325	0.833
47A	7.16	0.14574	0.310	15.0	0.0773	0.472	5800	34.2	72.9	118	0.875	3.72	0.389	0.0716	0.0548	3.07	0.244	0.00815	BDL		0.00817	23.7	0.094	0.835
50A	7.09	0.09461	0.310	14.6	0.3403	0.472	5890	35.5	72.9	116	2.11	3.72	BDL		0.0547	2.56	0.063	0.00814	BDL		0.00816	23.2	0.382	0.834
52A	7.60	0.0169	0.308	15.0	0.2671	0.470	5830	32.9	72.7	117	2.13	3.70	BDL		0.0545	2.95	0.128	0.00811	BDL		0.00812	22.9	0.080	0.831
54A	7.62	0.0399	0.308	15.1	0.1731	0.469	6010	54.6	72.3	119	1.64	3.70	BDL		0.0544	2.94	0.136	0.00809	0.0111	0.0111	0.00810	22.9	0.276	0.829
57A	7.57	0.0900	0.311	15.1	0.1259	0.474	5730	91.7	73.4	116	2.49	3.74	BDL		0.0550	3.19	0.083	0.00818	BDL		0.00820	24.1	0.442	0.839
60A	6.46	0.125	0.0858	13.6	0.268	1.51	5580	57.0	83.0	111	1.48	16.9	BDL		0.0797	2.52	0.0707	0.403	0.0310	0.00671	0.00958	22.8	0.591	6.61
63A	6.30	0.153	0.0864	13.3	0.141	1.52	5560	29.2	84.7	120	2.16	17.0	BDL		0.0803	2.41	0.120	0.406	BDL		0.00966	24.7	0.653	6.66
66A	6.16	0.155	0.0854	13.1	0.175	1.50	5600	38.9	83.7	96.7	1.25	16.8	BDL		0.0794	2.33	0.0584	0.401	BDL		0.00954	19.9	0.599	6.58
68A	6.32	0.156	0.0857	13.3	0.206	1.51	5650	33.6	84.2	108	2.32	16.9	BDL		0.0797	2.28	0.125	0.402	BDL		0.00958	22.6	0.848	6.60
70A	6.12	0.188	0.0850	13.0	0.0997	1.50	5700	34.4	83.5	109	2.22	16.8	BDL		0.0790	2.20	0.0805	0.399	BDL		0.00950	22.5	0.827	6.55
72A	6.51	0.0924	0.0853	13.6	0.0130	1.50	3810	27.0	83.3	103	2.26	16.8	BDL		0.0793	2.24	0.118	0.401	0.0205	0.0177	0.00954	21.3	0.488	6.58
74A	6.70	0.152	0.0853	13.9	0.240	1.50	5730	67.3	83.1	112	2.61	16.8	BDL		0.0793	2.27	0.0462	0.400	0.0137	0.00593	0.00954	22.8	0.365	6.58
77A	6.76	0.1049	0.0853	13.8	0.309	1.50	5690	43.2	83.3	110	1.82	16.8	BDL		0.0793	2.20	0.0159	0.400	BDL		0.00953	22.3	0.602	6.57
79A	7.59	0.0511	0.0858	15.5	0.241	1.51	5770	21.9	84.3	115	1.47	16.9	BDL		0.0798	2.19	0.0825	0.403	0.0186	0.0233	0.00959	23.1	0.185	6.61
81A	7.08	0.0520	0.0861																					

Sample	Chloride			Potassium			Calcium			Chromium			Manganese			Iron			Nickel			Copper		
	Conc.	Error	D.L.	Conc.	Error	D.L.	Conc.	Error	D.L.	Conc.	Error	D.L.	Conc.	Error	D.L.	Conc.	Error	D.L.	Conc.	Error	D.L.	Conc.	Error	D.L.
FPW Stock 1	13900	1080	29.6	308	3.92	0.00809	1610	18.5	16.7	BDL		0.113	1.33	0.0153	0.00825	BDL		0.00825	0.0318	0.00115	0.0210	0.192	0.00105	0.0194
FPW Stock 2	9120	97.1	31.6	283	3.29	0.00807	1460	21.7	16.7	BDL		0.113	0.991	0.00392	0.00823	BDL		0.00823	0.0307	0.00230	0.0210	0.181	0.00090	0.0194
FPW Stock 3	7100	359	31.5	287	3.11	0.00809	1520	19.3	16.7	BDL		0.113	1.27	0.0179	0.00825	BDL		0.00825	0.0307	0.00121	0.0210	0.148	0.00192	0.0194
FPW Stock 4	11400	1730	11132	300	4.31	16.8	1550	16.5	22.6	BDL		0.122	0.870	0.0115	0.0751	BDL		0.0973	0.0481	0.00272	0.0344	0.145	0.00307	0.0360
GW Stock	1060	173	30.4	BDL		0.00820	BDL		17.0	BDL		0.115	BDL		0.00837	BDL		0.00837	BDL		0.0213	BDL		0.0194
1A	2740	466	30.4	BDL		0.00826	BDL		17.1	BDL		0.116	0.171	0.00328	0.00842	0.0562	0.00232	0.00842	0.0409	0.00109	0.0215	0.0493	0.000989	0.0194
2A	1950	179	30.5	BDL		0.00828	BDL		17.1	BDL		0.116	0.131	0.00548	0.00844	BDL		0.00844	BDL		0.0215	BDL		0.0194
3A	BDL		30.4	BDL		0.00827	BDL		17.1	BDL		0.116	0.134	0.00198	0.00843	BDL		0.00843	BDL		0.0215	BDL		0.0194
4A	1650	250	30.3	BDL		0.00824	71.5	1.037	17.0	BDL		0.115	0.644	0.0140	0.00840	0.374	0.00706	0.00840	BDL		0.0214	BDL		0.0194
6A	9430	1340	30.0	21.3	0.395	0.00811	4340	47.0	16.8	BDL		0.114	33.5	0.592	0.00827	39.9	0.425	0.00827	0.0388	0.00146	0.0211	BDL		0.0194
7A	12800	520	30.2	22.8	0.674	0.00815	2990	48.3	16.9	BDL		0.114	15.7	0.311	0.00831	16.2	0.214	0.00831	0.0241	0.00053	0.0212	BDL		0.0194
8A	13100	892	30.1	35.0	0.168	0.00817	2030	20.3	16.9	BDL		0.114	10.59	0.1036	0.00833	8.06	0.122	0.00833	BDL		0.0212	BDL		0.0194
9A	17200	1010	30.0	64.3	1.71	0.00814	1760	26.4	16.8	BDL		0.114	11.1	0.227	0.00831	6.41	0.112	0.00831	BDL		0.0212	BDL		0.0194
10A	10100	1020	29.8	111	1.61	0.00812	1620	25.2	16.8	BDL		0.114	13.2	0.195	0.00828	5.91	0.0869	0.00828	0.0230	0.000423	0.0211	BDL		0.0194
11A	13500	1270	29.7	262	2.76	0.00809	1560	27.6	16.7	BDL		0.113	13.0	0.0604	0.00825	4.64	0.0648	0.00825	0.132	0.00151	0.0210	BDL		0.0194
12A	BDL		30.4	271	2.08	0.00824	1550	18.7	17.0	BDL		0.115	7.23	0.0749	0.00840	2.58	0.0375	0.00840	0.0291	0.000752	0.0214	BDL		0.0194
14A	10200	492	29.9	269	3.52	0.00809	1540	15.4	16.7	BDL		0.113	5.89	0.0840	0.00826	2.10	0.0244	0.00826	0.0248	0.001039	0.0211	BDL		0.0194
15A	11800	1020	30.3	261	2.87	0.00821	1510	17.9	17.0	BDL		0.115	5.92	0.1002	0.00837	2.12	0.0380	0.00837	0.0278	0.000552	0.0214	BDL		0.0194
16A	11300	1840	30.2	284	3.76	0.00820	1610	36.2	16.9	BDL		0.115	5.62	0.0874	0.00836	2.03	0.0375	0.00836	0.0308	0.000633	0.0213	BDL		0.0194
17A	10300	602	30.5	269	6.14	0.00824	1540	21.6	17.0	BDL		0.115	5.21	0.0786	0.00840	1.91	0.0292	0.00840	0.0294	0.000746	0.0214	BDL		0.0194
18A	110000	1650	30.2	271	3.14	0.00820	1560	22.9	17.0	BDL		0.115	4.91	0.0877	0.00836	1.79	0.0333	0.00836	0.0293	0.000793	0.0213	BDL		0.0194
19A	12000	1630	30.2	264	1.55	0.00820	1510	18.2	17.0	BDL		0.115	4.57	0.0403	0.00836	1.65	0.0269	0.00836	0.0261	0.000679	0.0213	BDL		0.0194
20A	11200	1170	30.3	271	5.06	0.00821	1550	20.8	17.0	BDL		0.115	4.37	0.0728	0.00837	1.58	0.0101	0.00837	0.0293	0.000986	0.0213	BDL		0.0194
21A	12000	982	30.2	275	3.07	0.00816	1550	12.5	16.9	BDL		0.114	4.09	0.0417	0.00832	1.50	0.0255	0.00832	0.0305	0.000343	0.0212	BDL		0.0194
22A	14500	983	30.1	275	7.07	0.00816	1560	28.5	16.9	BDL		0.114	3.78	0.0704	0.00832	1.38	0.0307	0.00832	0.0272	0.000607	0.0212	BDL		0.0194
23A	7970	177	30.2	269	2.03	0.00816	1480	33.4	16.9	BDL		0.114	3.46	0.0508	0.00832	0.228	0.00361	0.00832	0.0271	0.000705	0.0212	BDL		0.0194
25A	7920	177	30.0	274	3.97	0.00812	1530	14.9	16.8	BDL		0.114	3.63	0.0471	0.00828	1.33	0.0119	0.00828	0.0299	0.00126	0.0211	BDL		0.0194
26A	13000	290	30.0	272	3.00	0.00811	1550	21.5	16.8	BDL		0.114	3.11	0.0673	0.00827	1.09	0.0157	0.00827	0.0229	0.000513	0.0211	BDL		0.0194
27A	13900	2220	30.1	278	4.88	0.00816	1530	18.9	16.9	BDL		0.114	3.41	0.0886	0.00832	1.28	0.0205	0.00832	0.0331	0.00159	0.0212	BDL		0.0194
28A	14100	1740	30.0	274	1.93	0.00815	1560	28.7	16.9	BDL		0.114	2.54	0.0156	0.00831	0.824	0.0105	0.00831	0.0330	0.000850	0.0212	BDL		0.0194
30A	13800	1010	30.1	278	7.56	0.00814	1570	18.1	16.8	BDL		0.114	2.39	0.0473	0.00830	0.741	0.0221	0.00830	0.0324	0.000335	0.0212	BDL		0.0194
32A	12300	582	30.0	277	4.26	0.00814	1540	5.85	16.8	BDL		0.114	2.25	0.0553	0.00830	0.692	0.0180	0.00830	0.0337	0.00161	0.0212	BDL		0.0194
34A	14300	225	30.2	271	0.788	0.00818	1520	32.5	16.9	BDL		0.115	2.08	0.0071	0.00834	0.556	0.00248	0.00834	0.0357	0.00121	0.0213	BDL		0.0194
36A	13900	587	30.0	274	2.19	0.00814	1520	12.0	16.8	BDL		0.114	2.10	0.0436	0.00830	0.551	0.00929	0.00830	0.0391	0.000629	0.0212	BDL		0.0194
37A	17300	146	29.8	271	6.41	0.00813	1540	28.4	16.8	BDL		0.114	2.12	0.0397	0.00829	0.566	0.00927	0.00829	0.0466	0.00108	0.0211	BDL		0.0194
39A	10300	848	30.1	277	3.13	0.00812	1520	25.5	16.8	BDL		0.114	2.02	0.0290	0.00828	0.542	0.00917	0.00828	0.0403	0.00202	0.0211	BDL		0.0194
42A	11900	1200	31.4	278	3.26	0.00820	1540	18.4	17.0	BDL		0.115	1.95	0.00685	0.00836	0.582	0.00299	0.00836	0.0461	0.00229	0.0213	BDL		0.0194
45A	14200	1390	30.2	281	3.07	0.00813	1550	23.2	16.8	BDL		0.114	1.87	0.0137	0.00829	0.614	0.00607	0.00829	0.0414	0.000222	0.0211	BDL		0.0194
47A	10400	392	31.8	284	4.80	0.00815	1560	12.2	16.8	BDL		0.114	1.88	0.0379	0.00831	0.646	0.00892	0.00831	0.0425	0.000747	0.0212	0.0227	0.000162	0.0194
50A	9150	1910	31.8	276	3.34	0.00814	1530	19.1	16.8	BDL		0.114	1.78	0.0305	0.00830	0.589	0.00715	0.00830	0.0409	0.00381	0.0212	0.0263	0.00106	0.0194
52A	7740	647	31.7	287	5.04	0.00811	1530	28.8	16.8	BDL		0.114	1.71	0.0234	0.00827	0.550	0.0111	0.00827	0.0484	0.00267	0.0211	0.0305	0.00077	0.0194
54A	10400	784	31.6	288	3.02	0.00809	1520	31.1	16.7	BDL		0.113	1.68	0.0116	0.00825	0.440	0.00508	0.00825	0.0452	0.00143	0.0210	0.0391	0.00079	0.0194
57A	8030	896	32.0	285	4.03	0.00818	1530	24.6	16.9	BDL		0.115	1.54	0.0241	0.00835	0.343	0.00281	0.00835	0.0402	0.00190	0.0213	0.0400	0.00117	0.0194
60A	14601	2900	11071	304	4.61	16.9	1510	15.0	22.7	BDL		0.122	1.46	0.0225	0.0755	0.387	0.00266	0.0978	0.0622	0.00199	0.0346	0.0525	0.0294	0.0361
63A	14600	1590	11292	334	5.06	17.0	1500	17.7	22.9	BDL		0.123	1.59	0.0185	0.0760	0.366	0.00821	0.0985	0.0655	0.00115	0.0348	0.0437	0.00170	0.0364
66A	13800	792	11165	274	1.56	16.8	1510	22.6	22.6	BDL		0.122	1.40	0.0238	0.0751	0.307	0.00863	0.0973	0.0590	0.000982	0.0344	0.0382	0.00120	0.0360
68A	15500	914	11224	300	5.97	16.9	1520	21.4	22.7	BDL		0.122	1.47	0.0234	0.0754	0.256	0.000503	0.0977	0.0603	0.00264	0.0345	0.0445	0.00134	0.0361
70A	14500	400	11130	301	6.56	16.8	1550	24.1	22.5	BDL		0.121	1.46	0.0392	0.0748	0.205	0.00117	0.0969	0.0670	0.000446	0.0343	0.0555	0.00119	0.0358
72A	14500	3250	11109	278	2.75	16.8	1530	19.8	22.6	BDL		0.122	1.43	0.0207	0.0751	0.171	0.000737	0.0973	0.0582	0.00164	0.0344	0.0497	0.00265	0.0360
74A	17900	1630	11085	303	3.99	16.8	1540	23.4	22.6	BDL		0.122	1.44	0.0239	0.0751	0.171	0.00661	0.0973	0.0601	0.00176	0.0344	0.0531	0.000689	0.0360
77A	14400	4090	11113	300	3.21	16.8	1520	6.52	22.6	BDL		0.121	1.45	0.0245	0.0750	0.156	0.00511							

Sample	Zinc			Arsenic			Bromide			Strontium			Molybdenum			Cadmium			Barium			Lead		
	Conc.	Error	D.L.	Conc.	Error	D.L.	Conc.	Error	D.L.	Conc.	Error	D.L.	Conc.	Error	D.L.	Conc.	Error	D.L.	Conc.	Error	D.L.	Conc.	Error	D.L.
FPW Stock 1	0.182	0.00396	0.160	BDL		1.93	37.4	1.025	2.95	132	2.09	6.53	0.0867	0.00310	0.00811	BDL		0.00812	1.18	0.0294	0.266	BDL		0.00814
FPW Stock 2	BDL		0.160	BDL		1.93	36.4	0.359	2.94	136	0.522	6.51	BDL		0.00809	BDL		0.00810	1.22	0.00748	0.266	BDL		0.00811
FPW Stock 3	0.245	0.00481	0.160	BDL		1.93	37.3	0.827	2.95	140	1.53	6.53	BDL		0.00811	BDL		0.00812	3.91	0.0979	0.266	BDL		0.00814
FPW Stock 4	BDL		0.109	BDL		0.00969	32.4	0.801	0.927	124	3.21	0.943	0.112	0.0218	0.110	BDL	0.00124	0.0397	3.78	0.0797	0.301	BDL		0.00939
GW Stock	BDL		0.163	BDL		1.96	3.75	0.298	2.99	BDL		6.62	0.0453	0.00137	0.00823	BDL		0.00823	0.294	0.0189	0.270	BDL		0.00825
1A	BDL		0.164	BDL		1.97	3.76	0.108	3.01	BDL		6.67	0.0596	0.00145	0.00828	#####	#####	0.00829	0.344	0.0150	0.272	0.0318	0.000512	0.00831
2A	0.802	0.0207	0.164	BDL		1.98	BDL		3.02	BDL		6.68	0.0201	0.00184	0.00830	BDL		0.00831	0.312	0.0158	0.273	BDL		0.00833
3A	BDL		0.164	BDL		1.98	BDL		3.02	BDL		6.68	0.0146	0.00110	0.00829	BDL		0.00830	0.310	0.0148	0.272	BDL		0.00832
4A	BDL		0.163	BDL		1.97	BDL		3.01	BDL		6.65	0.0148	0.00017	0.00826	BDL		0.00827	0.525	0.01034	0.271	BDL		0.00828
6A	0.419	0.00809	0.161	BDL		1.94	29.1	1.21	2.96	12.4	0.167	6.55	BDL		0.00814	BDL		0.00815	21.9	0.213	0.267	BDL		0.00816
7A	BDL		0.162	BDL		1.95	35.3	0.258	2.98	13.1	0.238	6.58	BDL		0.00818	BDL		0.00818	21.9	0.607	0.268	BDL		0.00820
8A	BDL		0.162	BDL		1.95	36.4	1.33	2.98	29.5	0.451	6.59	0.0156	0.00081	0.00819	BDL		0.00820	19.7	0.446	0.269	BDL		0.00821
9A	BDL		0.161	BDL		1.95	37.1	1.31	2.97	55.4	0.427	6.58	BDL		0.00817	BDL		0.00818	20.6	0.467	0.268	BDL		0.00819
10A	BDL		0.161	BDL		1.94	37.0	0.464	2.96	88.4	0.698	6.56	BDL		0.00814	BDL		0.00815	22.4	0.297	0.267	BDL		0.00817
11A	BDL		0.160	BDL		1.93	36.8	0.311	2.95	131	1.41	6.53	BDL		0.00811	BDL		0.00812	20.1	0.262	0.266	BDL		0.00814
12A	BDL		0.163	BDL		1.97	37.5	0.697	3.01	135	1.50	6.65	BDL		0.00826	BDL		0.00827	9.06	0.110	0.271	BDL		0.00829
14A	BDL		0.160	BDL		1.93	35.2	0.465	2.95	124	1.40	6.54	BDL		0.00812	BDL		0.00813	7.03	0.123	0.267	BDL		0.00814
15A	BDL		0.163	BDL		1.96	36.1	0.933	3.00	132	1.39	6.63	BDL		0.00824	BDL		0.00824	6.56	0.0704	0.270	BDL		0.00826
16A	0.205	0.00494	0.162	BDL		1.96	36.9	0.698	2.99	136	2.49	6.62	BDL		0.00822	BDL		0.00823	5.83	0.149	0.270	BDL		0.00825
17A	BDL		0.163	BDL		1.97	37.4	0.694	3.01	136	2.36	6.65	BDL		0.00826	BDL		0.00827	5.07	0.0884	0.271	BDL		0.00829
18A	BDL		0.163	BDL		1.96	36.9	0.767	2.99	133	2.27	6.62	BDL		0.00823	BDL		0.00823	4.51	0.0472	0.270	BDL		0.00825
19A	BDL		0.163	BDL		1.96	37.3	1.57	2.99	135	2.03	6.62	BDL		0.00822	BDL		0.00823	4.03	0.0345	0.270	BDL		0.00825
20A	BDL		0.163	BDL		1.96	36.9	1.12	3.00	132	2.33	6.63	BDL		0.00823	BDL		0.00824	3.65	0.0676	0.270	BDL		0.00826
21A	BDL		0.162	BDL		1.95	36.6	1.22	2.98	134	2.30	6.59	BDL		0.00818	BDL		0.00819	3.28	0.0607	0.269	BDL		0.00821
22A	BDL		0.162	BDL		1.95	36.0	0.418	2.98	130	2.05	6.59	BDL		0.00818	BDL		0.00819	2.94	0.0975	0.269	BDL		0.00821
23A	BDL		0.162	BDL		1.95	36.8	1.31	2.98	134	1.87	6.59	BDL		0.00818	BDL		0.00819	2.83	0.0470	0.269	BDL		0.00821
25A	BDL		0.161	BDL		1.94	37.1	1.004	2.96	133	3.04	6.56	BDL		0.00815	BDL		0.00816	2.62	0.0455	0.267	BDL		0.00817
26A	BDL		0.161	BDL		1.94	34.1	0.499	2.96	124	3.14	6.54	BDL		0.00813	BDL		0.00814	2.28	0.0448	0.267	BDL		0.00815
27A	0.279	0.00995	0.162	BDL		1.95	37.3	0.543	2.98	136	1.54	6.59	BDL		0.00819	BDL		0.00819	2.35	0.0162	0.269	BDL		0.00821
28A	2.15	0.0232	0.162	BDL		1.95	37.9	1.13	2.97	133	2.34	6.58	BDL		0.00818	BDL		0.00818	1.64	0.0174	0.268	0.0192	0.000112	0.00820
30A	BDL		0.161	BDL		1.94	36.8	1.28	2.97	134	3.41	6.57	BDL		0.00817	BDL		0.00817	1.53	0.0375	0.268	BDL		0.00819
32A	0.165	0.00086	0.161	BDL		1.94	37.5	1.000	2.97	137	2.89	6.57	BDL		0.00816	BDL		0.00817	1.49	0.0422	0.268	BDL		0.00819
34A	BDL		0.162	BDL		1.95	36.7	0.347	2.98	135	3.27	6.60	BDL		0.00820	BDL		0.00821	1.37	0.0119	0.269	BDL		0.00822
36A	BDL		0.161	BDL		1.94	37.7	0.564	2.97	138	2.46	6.57	BDL		0.00816	BDL		0.00817	1.39	0.0119	0.268	BDL		0.00819
37A	0.323	0.00637	0.161	BDL		1.94	37.7	1.07	2.97	135	2.56	6.56	BDL		0.00815	BDL		0.00816	1.37	0.0298	0.268	BDL		0.00818
39A	0.608	0.0148	0.161	BDL		1.94	37.2	1.19	2.96	136	1.60	6.55	BDL		0.00814	BDL		0.00815	1.34	0.0160	0.267	BDL		0.00817
42A	1.02	0.0183	0.163	BDL		1.96	37.4	0.673	2.99	135	3.03	6.62	BDL		0.00822	BDL		0.00823	1.33	0.0176	0.270	BDL		0.00825
45A	BDL		0.161	BDL		1.94	37.2	1.06	2.97	136	3.29	6.56	BDL		0.00815	BDL		0.00816	1.30	0.0218	0.268	BDL		0.00817
47A	1.75	0.04502	0.162	BDL		1.95	36.1	0.708	2.97	135	0.576	6.58	BDL		0.00817	BDL		0.00818	1.30	0.0158	0.268	BDL		0.00820
50A	0.937	0.00764	0.161	BDL		1.94	37.4	0.827	2.97	136	1.39	6.57	BDL		0.00816	BDL		0.00817	1.26	0.0182	0.268	BDL		0.00819
52A	0.401	0.0142	0.161	BDL		1.94	36.8	0.736	2.96	138	3.37	6.55	BDL		0.00813	BDL		0.00814	1.28	0.0255	0.267	BDL		0.00815
54A	0.376	0.00500	0.160	BDL		1.93	37.9	0.285	2.95	138	1.92	6.53	BDL		0.00811	BDL		0.00812	1.27	0.0164	0.266	BDL		0.00814
57A	BDL		0.162	BDL		1.95	36.5	0.887	2.99	138	2.73	6.61	BDL		0.00821	BDL		0.00822	2.73	0.0549	0.269	BDL		0.00823
60A	0.273	0.00783	0.110	BDL		0.00974	34.1	0.648	0.932	127	0.528	0.948	0.145	0.00625	0.110	0.0410	0.00531	0.0399	3.75	0.0378	0.303	BDL		0.00943
63A	BDL		0.110	BDL		0.00981	36.4	1.013	0.939	136	1.30	0.955	0.127	0.0129	0.111	0.0410	0.00396	0.0402	4.07	0.0921	0.305	BDL		0.00950
66A	BDL		0.109	BDL		0.00969	31.2	1.22	0.927	119	1.37	0.943	0.119	0.00887	0.110	0.0413	0.00273	0.0397	3.43	0.0899	0.302	BDL		0.00939
68A	0.197	0.00828	0.109	BDL		0.00973	32.9	1.69	0.931	126	2.45	0.947	0.115	0.00360	0.110	0.0405	0.00119	0.0398	3.75	0.0708	0.303	BDL		0.00942
70A	0.223	0.00548	0.109	BDL		0.00965	32.7	1.16	0.923	125	1.76	0.939	0.112	0.0111	0.109	0.0403	0.00160	0.0395	3.79	0.0352	0.300	BDL		0.00935
72A	0.399	0.00658	0.109	BDL		0.00969	31.0	0.929	0.927	121	1.60	0.943	0.112	0.00827	0.110	0.0403	0.00092	0.0397	3.58	0.123	0.301	0.843	0.0130	0.00939
74A	0.205	0.00245	0.109	BDL		0.00969	32.4	0.621	0.927	126	2.42	0.943	0.111	0.00763	0.110	0.0407	0.00223	0.0397	3.77	0.0592	0.301	BDL		0.00938
77A	0.168	0.00786	0.109	BDL		0.00968	32.3	1.35	0.926	124	1.13	0.942	0.112	0.00139	0.110	0.0403	0.00138	0.0396	3.81	0.0869	0.301	BDL		0.00938
79A	0.251	0.00146	0.110	BDL		0.00974	32.7	0.246	0.932	125	2.13	0.948	0.112	0.0129	0.110	0.0405	0.00189	0.0399	3.83	0.0910	0.303	BDL		0.00943
81A	0.121	0.00197	0.110	BDL		0.00977	32.7	0.285	0.935	125	1.73	0.951	0.111	0.00322	0.111	0.0402	0.00066	0.0400	3.84	0.0659	0.304	BDL		0.00946

Table B7 con't: ICP-MS/MS results from column A. FPW stock solutions and synthetic groundwater were also measured. Units are

in mg/L. D.L. = detection limit. BDL = below detection limit. Uranium was measured, but all measurements were BDL.

Sample	Lithium			Boron			Sodium			Magnesium			Aluminum			Silicon			Phosphorous			Sulphur		
	Conc.	Error	D.L.	Conc.	Error	D.L.	Conc.	Error	D.L.	Conc.	Error	D.L.	Conc.	Error	D.L.	Conc.	Error	D.L.	Conc.	Error	D.L.	Conc.	Error	D.L.
1B	BDL		0.310	BDL		0.472	99.4	1.156	69.1	4.99	0.376	3.72	BDL		0.0548	2.72	0.067	0.00815	BDL		0.00817	BDL		0.835
2B	BDL		0.311	BDL		0.473	95.2	1.73	68.9	5.07	0.279	3.73	BDL		0.0549	2.36	0.058	0.00817	BDL		0.00818	BDL		0.837
3B	BDL		0.308	BDL		0.470	92.3	1.63	68.0	5.07	0.225	3.70	BDL		0.0545	2.47	0.039	0.00810	BDL		0.00812	BDL		0.830
4B	BDL		0.312	BDL		0.475	129	0.334	69.0	7.32	0.166	3.75	BDL		0.0551	2.43	0.098	0.00820	BDL		0.00821	BDL		0.840
6B	2.82	0.0152	0.303	BDL		0.462	2430	27.2	67.7	424	9.81	3.64	0.247	0.00191	0.0536	3.05	0.075	0.00797	0.02	0.0101	0.00799	BDL		0.817
7B	5.98	0.0699	0.304	4.19	0.0616	0.464	4810	44.8	67.5	281	7.13	3.66	BDL		0.0538	2.97	0.060	0.00800	BDL		0.00802	22.5	0.285	0.820
8B	6.84	0.0706	0.303	10.65	0.1724	0.462	5610	78.4	67.4	156	21.20	3.64	BDL		0.0536	3.03	0.142	0.00796	BDL		0.00798	25.8	0.557	0.816
9B	6.76	0.0720	0.302	11.8	0.1951	0.460	5710	120.5	66.8	123	3.18	3.63	BDL		0.0534	3.10	0.094	0.00794	BDL		0.00796	22.9	0.383	0.814
10B	6.93	0.0417	0.305	12.9	0.1212	0.466	5710	77.5	67.6	116	1.003	3.67	BDL		0.0540	3.00	0.119	0.00803	BDL		0.00805	22.4	0.294	0.823
11B	7.03	0.0870	0.303	13.6	0.1355	0.462	5740	97.6	67.0	114	0.686	3.64	BDL		0.0536	2.71	0.074	0.00797	BDL		0.00798	22.6	0.753	0.816
12B	6.99	0.0936	0.304	13.9	0.1864	0.463	5680	113.8	67.4	116	2.12	3.65	BDL		0.0537	2.33	0.060	0.00798	BDL		0.00800	23.7	0.733	0.818
14B	7.18	0.1365	0.303	14.4	0.1712	0.463	5710	50.6	67.2	112	1.74	3.65	BDL		0.0537	2.26	0.052	0.00798	BDL		0.00800	22.4	0.683	0.818
15B	6.93	0.0895	0.304	14.0	0.2584	0.463	5790	71.8	67.6	112	2.13	3.65	BDL		0.0537	2.30	0.060	0.00799	BDL		0.00800	22.4	0.143	0.818
16B	7.85	0.0914	0.305	15.5	0.0784	0.465	5760	24.0	67.9	115	1.024	3.66	BDL		0.0539	2.29	0.084	0.00802	BDL		0.00803	22.7	0.308	0.821
17B	6.98	0.0743	0.305	14.1	0.0492	0.464	5760	40.3	67.6	112	0.641	3.66	BDL		0.0539	2.25	0.082	0.00801	BDL		0.00802	22.7	0.689	0.821
18B	7.24	0.1166	0.303	14.5	0.1917	0.463	6430	41.6	66.9	113	1.11	3.65	BDL		0.0537	2.35	0.066	0.00798	BDL		0.00800	23.1	0.059	0.818
19B	7.30	0.1359	0.305	14.5	0.2221	0.464	5740	75.5	68.0	110	1.19	3.66	BDL		0.0539	2.29	0.071	0.00801	BDL		0.00803	22.9	0.467	0.821
20B	7.23	0.1045	0.304	14.5	0.2690	0.464	5700	108.8	67.6	107	2.39	3.65	BDL		0.0538	2.34	0.058	0.00800	BDL		0.00801	22.9	0.402	0.819
21B	7.15	0.1161	0.305	14.4	0.0454	0.464	5740	42.8	68.3	115	1.22	3.66	BDL		0.0539	2.21	0.046	0.00801	BDL		0.00803	22.3	0.393	0.821
22B	7.08	0.0926	0.305	14.2	0.2155	0.465	5600	44.0	68.0	113	2.30	3.67	BDL		0.0540	2.22	0.100	0.00802	BDL		0.00804	22.3	0.520	0.822
23B	7.53	0.0464	0.305	14.9	0.2141	0.465	5760	65.3	68.0	110	1.71	3.67	BDL		0.0540	2.35	0.188	0.00803	BDL		0.00804	22.4	0.976	0.822
25B	7.09	0.0155	0.304	14.0	0.0356	0.463	5630	60.5	67.8	115	1.64	3.65	BDL		0.0537	2.10	0.143	0.00799	BDL		0.00800	22.9	0.026	0.819
26B	7.11	0.0209	0.305	14.0	0.4064	0.465	5590	23.4	67.8	116	1.84	3.66	BDL		0.0539	2.32	0.060	0.00802	BDL		0.00804	22.8	1.052	0.822
27B	7.13	0.0595	0.305	14.1	0.1286	0.465	5720	47.2	67.9	109	2.45	3.66	BDL		0.0539	2.30	0.065	0.00802	BDL		0.00803	22.6	0.826	0.821
28B	7.25	0.0791	0.304	14.5	0.0956	0.464	5700	46.9	68.4	115	2.14	3.66	BDL		0.0538	2.17	0.085	0.00800	BDL		0.00802	22.7	0.707	0.820
30B	7.08	0.1180	0.304	14.3	0.0980	0.464	5700	75.4	67.7	115	2.49	3.66	BDL		0.0538	2.22	0.064	0.00800	BDL		0.00802	22.1	0.562	0.820
32B	7.26	0.1159	0.307	14.6	0.2015	0.468	5800	34.8	68.6	117	1.96	3.69	BDL		0.0543	2.26	0.076	0.00808	BDL		0.00810	22.8	0.554	0.828
34B	7.34	0.0727	0.304	14.8	0.0239	0.464	5770	65.5	67.8	115	2.80	3.66	BDL		0.0538	2.35	0.063	0.00801	BDL		0.00802	22.4	0.637	0.820
36B	7.16	0.1249	0.305	14.4	0.2945	0.465	5720	58.7	67.7	114	1.93	3.67	BDL		0.0540	2.54	0.132	0.00802	BDL		0.00804	22.5	1.23	0.822
37B	7.39	0.0956	0.302	14.7	0.0967	0.460	5710	49.6	67.0	117	2.48	3.63	BDL		0.0534	2.40	0.170	0.00794	BDL		0.00795	22.4	0.268	0.813
39B	7.31	0.0644	0.303	14.7	0.0432	0.463	5690	48.2	67.3	116	2.12	3.65	BDL		0.0537	2.54	0.011	0.00798	BDL		0.00800	22.6	0.421	0.818
42B	7.27	0.1666	0.303	14.6	0.1060	0.462	5830	71.2	69.8	122	1.22	3.64	BDL		0.0536	2.57	0.021	0.00797	BDL		0.00798	22.6	0.479	0.816
45B	7.58	0.0897	0.303	14.9	0.1353	0.462	5780	26.6	71.9	117	1.47	3.64	0.170	0.0245	0.0536	2.70	0.151	0.00797	0.105	0.0489	0.00798	23.8	0.207	0.816
47B	7.48	0.0311	0.302	14.9	0.1064	0.461	5790	45.7	70.8	117	2.39	3.63	BDL		0.0535	2.77	0.131	0.00795	BDL		0.00797	22.2	0.990	0.815
50B	7.52	0.1599	0.303	15.0	0.0567	0.462	5610	98.0	71.4	116	2.36	3.64	BDL		0.0536	2.92	0.215	0.00797	BDL		0.00799	22.9	0.629	0.817
52B	7.30	0.0255	0.301	14.9	0.2016	0.459	5710	10.12	70.8	114	0.745	3.62	BDL		0.0532	2.90	0.152	0.00791	BDL		0.00793	22.5	0.380	0.811
54B	7.39	0.0320	0.303	14.8	0.1368	0.462	5820	13.7	71.2	107	2.38	3.64	BDL		0.0536	2.72	0.134	0.00797	BDL		0.00798	22.0	0.172	0.816
57B	7.27	0.0874	0.303	14.5	0.3053	0.462	5550	54.2	71.5	112	1.28	3.65	BDL		0.0536	3.15	0.021	0.00798	BDL		0.00799	23.2	0.390	0.817
60B	7.13	0.1056	0.0840	14.5	0.0327	1.48	5480	32.1	82.2	112	2.28	16.6	BDL		0.0781	2.64	0.134	0.394	BDL		0.00939	22.8	0.514	6.47
63B	7.29	0.0481	0.0841	14.8	0.150	1.48	5690	30.5	82.6	114	1.37	16.6	BDL		0.0782	2.44	0.116	0.395	0.0139	0.0160	0.00939	23.4	0.200	6.48
66B	7.27	0.183	0.0836	14.5	0.079	1.47	5670	34.2	82.1	113	1.68	16.5	BDL		0.0777	2.20	0.163	0.392	0.0222	0.0111	0.00934	23.0	0.652	6.44
68B	7.38	0.0250	0.0836	14.9	0.172	1.47	5550	35.0	81.8	112	2.26	16.5	BDL		0.0777	2.22	0.0713	0.392	BDL		0.00934	21.7	2.83	6.44
70B	7.43	0.0287	0.0835	14.9	0.386	1.47	5530	17.5	81.5	112	0.68	16.5	BDL		0.0776	2.25	0.0495	0.392	BDL		0.00933	22.9	0.652	6.43
72B	7.13	0.134	0.0837	14.2	0.0213	1.47	5660	41.1	81.5	114	1.67	16.5	BDL		0.0778	2.40	0.178	0.393	0.0220	0.0220	0.00935	23.3	0.717	6.45
74B	7.44	0.121	0.0840	14.8	0.0442	1.48	6250	55.5	82.1	111	1.27	16.6	BDL		0.0781	2.26	0.114	0.394	BDL		0.00939	23.3	0.825	6.47
77B	7.54	0.0697	0.0838	15.3	0.201	1.47	5670	34.1	81.6	112	1.14	16.5	BDL		0.0779	2.16	0.0568	0.393	0.0176	0.0162	0.00936	23.1	0.202	6.46
79B	7.46	0.184	0.0846	15.0	0.235	1.49	5570	72.9	82.9	113	1.47	16.7	0.1559	0.034374	0.0786	2.36	0.0791	0.397	0.0136	0.0117	0.00945	22.3	1.22	6.52
81B	7.41	0.130	0.0837	14.8	0.271	1.47	5060	42.3	81.5	112	1.77	16.5	BDL		0.0778	2.24	0.0702	0.393	BDL		0.00935	22.9	0.891	6.45

Table B8: ICP-MS/MS results from column B. Units are in mg/L. D.L. = detection limit. BDL = below detection limit.

Sample	Chloride			Potassium			Calcium			Chromium			Manganese			Iron			Nickel			Copper		
	Conc.	Error	D.L.	Conc.	Error	D.L.	Conc.	Error	D.L.	Conc.	Error	D.L.	Conc.	Error	D.L.	Conc.	Error	D.L.	Conc.	Error	D.L.	Conc.	Error	D.L.
1B	BDL		30.1	BDL		0.00815	BDL		16.8	BDL		0.114	0.0842	0.00182	0.00831	BDL		0.00831	BDL		0.0212	BDL		0.0194
2B	BDL		30.1	BDL		0.00817	BDL		16.9	BDL		0.114	0.0994	0.00294	0.00833	BDL		0.00833	BDL		0.0212	BDL		0.0194
3B	BDL		29.7	BDL		0.00810	BDL		16.7	BDL		0.114	0.112	0.00397	0.00826	BDL		0.00826	BDL		0.0211	0.0213	0.000158	0.0194
4B	BDL		30.1	BDL		0.00820	38.2	0.530	16.9	BDL		0.115	0.280	0.00399	0.00836	BDL		0.00836	BDL		0.0213	BDL		0.0194
6B	5900	854	29.5	20.3	0.184	0.00797	4090	87.7	16.5	BDL		0.112	17.8	0.148	0.00813	9.46	0.0716	0.00813	0.0389	0.001025	0.0207	BDL		0.0194
7B	9540	790	29.5	26.9	0.489	0.00800	2810	28.5	16.5	BDL		0.112	8.37	0.107	0.00816	3.68	0.0592	0.00816	0.0299	0.001055	0.0208	BDL		0.0194
8B	7060	1800	29.4	26.6	0.174	0.00796	1900	21.8	16.5	BDL		0.112	6.52	0.0923	0.00812	2.23	0.0235	0.00812	0.0245	0.00116	0.0207	BDL		0.0194
9B	11000	2170	29.2	53.2	0.616	0.00794	1630	26.3	16.4	BDL		0.111	10.13	0.115	0.00810	1.98	0.0200	0.00810	0.0261	0.000317	0.0207	BDL		0.0194
10B	9340	1800	29.5	149	0.723	0.00803	1560	18.6	16.6	BDL		0.113	15.4	0.266	0.00819	2.08	0.0186	0.00819	0.0498	0.00130	0.0209	BDL		0.0194
11B	11200	1270	29.3	270	3.66	0.00797	1530	6.16	16.5	BDL		0.112	12.6	0.1042	0.00812	1.27	0.0243	0.00812	0.0336	0.000762	0.0207	BDL		0.0194
12B	10200	626	29.4	271	1.27	0.00798	1520	17.9	16.5	BDL		0.112	7.01	0.0772	0.00814	0.69	0.00594	0.00814	0.0327	0.000520	0.0208	0.0206	0.00036	0.0194
14B	8920	286	29.3	279	1.98	0.00798	1560	28.8	16.5	BDL		0.112	6.33	0.133	0.00814	0.58	0.0157	0.00814	0.0301	0.000450	0.0208	0.0308	0.00176	0.0194
15B	10500	1140	29.5	279	2.96	0.00799	1530	25.4	16.5	BDL		0.112	5.72	0.0932	0.00814	0.49	0.0132	0.00814	0.0305	0.000284	0.0208	0.0205	0.00045	0.0194
16B	11100	1240	29.6	301	3.50	0.00802	1670	49.7	16.6	BDL		0.112	5.44	0.0541	0.00818	0.50	0.00441	0.00818	0.0344	0.00173	0.0208	0.0213	0.00010	0.0194
17B	10500	867	29.5	280	2.15	0.00801	1520	11.8	16.6	BDL		0.112	5.01	0.0235	0.00817	0.44	0.00633	0.00817	0.0376	0.001056	0.0208	0.0278	0.00035	0.0194
18B	8540	1400	29.2	281	2.84	0.00798	1540	17.8	16.5	BDL		0.112	4.79	0.0233	0.00814	0.42	0.00338	0.00814	0.0332	0.001024	0.0208	0.0202	0.00058	0.0194
19B	10400	936	29.7	282	2.16	0.00801	1550	13.1	16.6	BDL		0.112	4.38	0.0534	0.00817	0.36	0.00696	0.00817	0.0277	0.000824	0.0208	0.0202	0.00067	0.0194
20B	10200	535	29.5	276	4.16	0.00800	1530	25.5	16.5	BDL		0.112	3.99	0.0970	0.00816	0.32	0.00602	0.00816	0.0297	0.000441	0.0208	0.0213	0.00112	0.0194
21B	7770	183	29.8	279	2.48	0.00801	1510	15.9	16.6	BDL		0.112	4.12	0.0531	0.00817	0.34	0.00527	0.00817	0.0315	0.00112	0.0208	0.0226	0.00063	0.0194
22B	9290	710	29.7	275	5.65	0.00802	1490	23.7	16.6	BDL		0.112	3.87	0.0588	0.00818	0.35	0.00254	0.00818	0.0316	0.00222	0.0209	0.0218	0.00041	0.0194
23B	9490	113	29.7	287	7.69	0.00803	1590	19.4	16.6	BDL		0.112	3.62	0.0587	0.00818	0.27	0.00907	0.00818	0.0287	0.00111	0.0209	0.0202	0.00062	0.0194
25B	8840	230	29.6	276	2.23	0.00799	1530	25.1	16.5	BDL		0.112	3.56	0.0499	0.00815	0.31	0.00488	0.00815	0.0333	0.00127	0.0208	0.0246	0.00102	0.0194
26B	12500	2070	29.6	280	3.16	0.00802	1530	22.5	16.6	BDL		0.112	3.49	0.0384	0.00818	0.26	0.00132	0.00818	0.0326	0.00136	0.0209	0.0227	0.00028	0.0194
27B	10400	1010	29.6	275	5.34	0.00802	1510	17.1	16.6	BDL		0.112	3.16	0.0533	0.00817	0.22	0.00257	0.00817	0.0313	0.000526	0.0208	0.0219	0.00049	0.0194
28B	10800	997	29.8	279	2.40	0.00800	1540	9.17	16.5	BDL		0.112	2.56	0.0562	0.00816	0.13	0.00102	0.00816	0.0356	0.000278	0.0208	0.0262	0.00086	0.0194
30B	8240	1250	29.5	274	3.58	0.00800	1510	29.8	16.5	BDL		0.112	2.42	0.0513	0.00816	0.10	0.00214	0.00816	0.0345	0.000401	0.0208	0.0272	0.00120	0.0194
32B	6390	731	29.9	280	1.08	0.00808	1520	24.2	16.7	BDL		0.113	2.35	0.0272	0.00824	0.08	0.00107	0.00824	0.0372	0.00156	0.0210	0.0266	0.00089	0.0194
34B	8620	70.7	29.6	284	2.81	0.00801	1550	22.1	16.6	BDL		0.112	2.16	0.00973	0.00817	0.06	0.00135	0.00817	0.0367	0.00131	0.0208	0.0280	0.00028	0.0194
36B	8290	480	29.6	274	3.55	0.00802	1470	9.55	16.6	BDL		0.112	2.12	0.0376	0.00818	0.05	0.000511	0.00818	0.0447	0.00240	0.0209	0.0280	0.00044	0.0194
37B	11200	338	29.2	279	3.93	0.00794	1520	27.9	16.4	BDL		0.111	2.11	0.00990	0.00810	0.07	0.00163	0.00810	0.0399	0.000230	0.0206	0.0277	0.00150	0.0194
39B	8680	550	29.4	279	3.85	0.00798	1510	29.9	16.5	BDL		0.112	2.06	0.0265	0.00814	0.07	0.000428	0.00814	0.0404	0.00119	0.0208	0.0317	0.00072	0.0194
42B	12100	621	30.5	275	0.423	0.00797	1500	19.6	16.5	BDL		0.112	2.08	0.0128	0.00813	0.08	0.000614	0.00813	0.0465	0.000533	0.0207	0.0390	0.00081	0.0194
45B	11700	579	31.4	283	3.05	0.00797	1530	19.4	16.5	BDL		0.112	2.01	0.0139	0.00812	0.17	0.00452	0.00812	0.1448	0.00212	0.0207	0.1447	0.00210	0.0194
47B	8130	524	30.9	284	1.82	0.00795	1520	27.1	16.4	BDL		0.111	1.89	0.0332	0.00811	0.04	0.00168	0.00811	0.0400	0.000919	0.0207	0.0517	0.00073	0.0194
50B	7250	651	31.2	286	1.40	0.00797	1520	17.9	16.5	BDL		0.112	1.84	0.0207	0.00813	0.04	0.000648	0.00813	0.0403	0.00142	0.0207	0.0609	0.00152	0.0194
52B	6630	266	30.9	280	0.906	0.00791	1510	12.3	16.4	BDL		0.111	1.80	0.00477	0.00807	0.12	0.00181	0.00807	0.0457	0.000289	0.0206	0.0670	0.00197	0.0194
54B	10700	1130	31.1	281	4.13	0.00797	1490	19.3	16.5	BDL		0.112	1.57	0.0194	0.00813	BDL		0.00813	0.0334	0.00118	0.0207	0.0697	0.00204	0.0194
57B	7000	939	31.2	270	0.215	0.00798	1480	19.3	16.5	BDL		0.112	1.77	0.0283	0.00813	BDL		0.00813	0.0386	0.000731	0.0207	0.0810	0.00207	0.0194
60B	12800	1500	10964	295	7.98	16.6	1510	0.640	22.2	BDL		0.120	1.69	0.0475	0.0739	BDL		0.0957	0.0862	0.00198	0.0339	0.0672	0.00114	0.0354
63B	16200	2300	11011	298	4.11	16.6	1530	29.5	22.3	BDL		0.120	1.63	0.0213	0.0740	BDL		0.0958	0.0590	0.00301	0.0339	0.0655	0.00142	0.0354
66B	15400	521	10953	302	2.81	16.5	1440	17.1	22.1	BDL		0.119	1.68	0.0142	0.0735	BDL		0.0953	0.0583	0.00210	0.0337	0.0683	0.00253	0.0352
68B	14800	1160	10905	295	4.08	16.5	1520	30.1	22.1	BDL		0.119	1.61	0.0108	0.0736	BDL		0.0953	0.0590	0.00195	0.0337	0.0681	0.00106	0.0352
70B	13200	556	10865	298	6.29	16.5	1530	27.7	22.1	BDL		0.119	1.56	0.0272	0.0734	BDL		0.0951	0.0659	0.00224	0.0337	0.0829	0.00153	0.0352
72B	13800	1850	10873	298	4.21	16.5	1530	17.8	22.2	BDL		0.119	1.58	0.0222	0.0736	BDL		0.0954	0.0557	0.00211	0.0337	0.0680	0.00199	0.0353
74B	13600	2390	10943	292	2.18	16.6	1520	21.1	22.3	BDL		0.120	1.50	0.0143	0.0739	BDL		0.0958	0.0604	0.000379	0.0339	0.0696	0.00113	0.0354
77B	13700	1260	10880	297	6.34	16.5	1520	8.64	22.2	BDL		0.119	1.55	0.0196	0.0737	BDL		0.0955	0.0570	0.00130	0.0338	0.0847	0.00329	0.0353
79B	11400	1950	11060	301	5.63	16.7	1520	20.7	22.4	BDL		0.120	1.49	0.0125	0.0744	BDL		0.0964	0.0581	0.00113	0.0341	0.0711	0.00208	0.0356
81B	15300	2640	10874	299	7.99	16.5	1510	13.5	22.2	BDL		0.119	1.40	0.0233	0.0736	BDL		0.0953	0.0579	0.00260	0.0337	0.0728	0.00158	0.0353

Table B8 con't: ICP-MS/MS results from column B. Units are in mg/L. D.L. = detection limit. BDL = below detection limit.

Sample	Zinc			Arsenic			Bromide			Strontium			Molybdenum			Cadmium			Barium			Lead		
	Conc.	Error	D.L.	Conc.	Error	D.L.	Conc.	Error	D.L.	Conc.	Error	D.L.	Conc.	Error	D.L.	Conc.	Error	D.L.	Conc.	Error	D.L.	Conc.	Error	D.L.
1B	BDL		0.162	BDL		1.95	BDL		2.97	BDL		6.58	BDL		0.00817	BDL		0.00818	0.299	0.0252	0.268	BDL		0.00820
2B	1.97	0.02679	0.162	BDL		1.95	BDL		2.98	BDL		6.59	BDL		0.00819	BDL		0.00820	0.307	0.0118	0.269	BDL		0.00821
3B	BDL		0.161	BDL		1.94	BDL		2.96	BDL		6.54	BDL		0.00813	BDL		0.00813	0.313	0.0259	0.267	BDL		0.00815
4B	0.283	0.00754	0.162	BDL		1.96	BDL		2.99	BDL		6.62	BDL		0.00822	BDL		0.00823	0.391	0.00821	0.270	BDL		0.00824
6B	BDL		0.158	BDL		1.90	30.1	0.197	2.91	12.3	0.127	6.44	BDL		0.00799	BDL		0.00800	21.5	0.293	0.262	BDL		0.00802
7B	0.929	0.00783	0.159	BDL		1.91	35.1	0.110	2.92	9.8	0.163	6.46	BDL		0.00803	BDL		0.00803	20.9	0.370	0.263	BDL		0.00805
8B	0.249	0.00764	0.158	BDL		1.90	35.8	0.216	2.91	20.3	0.240	6.43	BDL		0.00799	BDL		0.00799	17.9	0.247	0.262	BDL		0.00801
9B	BDL		0.157	BDL		1.90	36.6	0.890	2.90	60.9	0.529	6.41	BDL		0.00796	BDL		0.00797	19.6	0.190	0.261	BDL		0.00799
10B	BDL		0.159	BDL		1.92	36.8	0.683	2.93	103.7	0.571	6.49	BDL		0.00806	BDL		0.00806	24.2	0.411	0.264	BDL		0.00808
11B	BDL		0.158	BDL		1.90	38.1	0.237	2.91	133	2.38	6.43	BDL		0.00799	BDL		0.00800	19.5	0.233	0.262	BDL		0.00801
12B	BDL		0.158	BDL		1.91	37.1	0.634	2.91	132	3.04	6.45	BDL		0.00801	BDL		0.00801	7.62	0.124	0.263	BDL		0.00803
14B	BDL		0.158	BDL		1.91	36.0	1.37	2.91	133	1.35	6.44	BDL		0.00800	BDL		0.00801	6.40	0.0466	0.263	BDL		0.00803
15B	BDL		0.158	BDL		1.91	36.2	0.199	2.91	131	0.691	6.45	BDL		0.00801	BDL		0.00802	5.46	0.0469	0.263	BDL		0.00803
16B	BDL		0.159	BDL		1.91	36.7	0.434	2.93	135	2.04	6.47	BDL		0.00804	BDL		0.00805	4.89	0.0826	0.264	BDL		0.00806
17B	BDL		0.159	BDL		1.91	36.5	1.45	2.92	134	1.10	6.47	BDL		0.00803	BDL		0.00804	4.31	0.0344	0.264	0.00929	0.000112	0.00806
18B	BDL		0.158	BDL		1.91	36.2	0.515	2.91	133	3.38	6.44	BDL		0.00800	BDL		0.00801	3.94	0.0373	0.263	BDL		0.00803
19B	BDL		0.159	BDL		1.91	36.2	1.33	2.92	132	2.74	6.47	BDL		0.00803	BDL		0.00804	3.45	0.0383	0.264	BDL		0.00806
20B	BDL		0.159	BDL		1.91	34.5	0.882	2.92	126	2.33	6.46	BDL		0.00802	BDL		0.00803	2.99	0.0818	0.263	BDL		0.00804
21B	BDL		0.159	BDL		1.91	36.8	0.905	2.92	135	3.02	6.47	BDL		0.00804	BDL		0.00804	2.96	0.0549	0.264	BDL		0.00806
22B	BDL		0.159	BDL		1.92	36.8	0.964	2.93	135	2.63	6.48	BDL		0.00805	BDL		0.00805	2.76	0.0410	0.264	BDL		0.00807
23B	BDL		0.159	BDL		1.92	35.1	0.456	2.93	128	2.01	6.48	BDL		0.00805	BDL		0.00806	2.51	0.0769	0.264	BDL		0.00807
25B	BDL		0.158	BDL		1.91	37.9	0.889	2.92	140	1.47	6.45	BDL		0.00801	BDL		0.00802	2.43	0.0405	0.263	BDL		0.00804
26B	BDL		0.159	BDL		1.92	36.9	0.546	2.93	138	2.50	6.48	BDL		0.00804	BDL		0.00805	2.32	0.0270	0.264	BDL		0.00807
27B	BDL		0.159	BDL		1.91	34.9	0.452	2.93	128	1.60	6.47	BDL		0.00804	BDL		0.00805	2.10	0.0484	0.264	BDL		0.00806
28B	0.181	0.00262	0.159	BDL		1.91	37.2	0.878	2.92	137	0.985	6.46	BDL		0.00802	BDL		0.00803	1.65	0.0610	0.263	BDL		0.00805
30B	BDL		0.159	BDL		1.91	36.7	0.240	2.92	134	1.77	6.46	BDL		0.00803	BDL		0.00803	1.51	0.0331	0.263	BDL		0.00805
32B	BDL		0.160	BDL		1.93	36.8	0.239	2.95	137	3.17	6.52	BDL		0.00810	BDL		0.00811	1.46	0.0197	0.266	BDL		0.00813
34B	BDL		0.159	BDL		1.91	37.0	1.08	2.92	137	1.20	6.46	BDL		0.00803	BDL		0.00804	1.37	0.0336	0.264	BDL		0.00805
36B	BDL		0.159	BDL		1.92	36.3	0.211	2.93	134	1.051	6.48	BDL		0.00805	BDL		0.00805	1.36	0.0265	0.264	BDL		0.00807
37B	BDL		0.157	BDL		1.90	37.0	0.620	2.90	137	1.72	6.41	BDL		0.00796	BDL		0.00797	1.36	0.0458	0.261	BDL		0.00799
39B	BDL		0.158	BDL		1.91	37.4	1.31	2.91	136	1.48	6.44	BDL		0.00800	BDL		0.00801	1.32	0.0296	0.263	BDL		0.00803
42B	BDL		0.158	BDL		1.90	37.8	0.966	2.91	141	1.29	6.43	BDL		0.00799	BDL		0.00800	1.35	0.0153	0.262	BDL		0.00801
45B	0.648	0.00280	0.158	BDL		1.90	37.1	0.770	2.91	136	1.41	6.43	BDL		0.00799	BDL		0.00800	1.37	0.0287	0.262	BDL		0.00801
47B	3.78	0.0618	0.158	BDL		1.90	37.0	0.667	2.90	135	1.22	6.42	BDL		0.00797	BDL		0.00798	1.28	0.0265	0.262	BDL		0.00800
50B	BDL		0.158	BDL		1.90	37.9	0.541	2.91	137	1.31	6.44	BDL		0.00800	BDL		0.00800	1.26	0.00925	0.262	BDL		0.00802
52B	BDL		0.157	BDL		1.89	36.1	0.896	2.89	133	1.67	6.39	BDL		0.00794	BDL		0.00794	1.26	0.0175	0.261	BDL		0.00796
54B	BDL		0.158	BDL		1.90	35.6	0.568	2.91	132	2.55	6.43	BDL		0.00799	BDL		0.00800	1.19	0.0227	0.262	BDL		0.00801
57B	BDL		0.158	BDL		1.91	34.4	0.973	2.91	132	1.80	6.44	BDL		0.00800	BDL		0.00801	2.84	0.0315	0.263	BDL		0.00802
60B	0.239	0.00537	0.107	BDL		0.00954	31.7	0.404	0.912	124	3.05	0.928	BDL		0.108	BDL	0.00122	0.0391	3.68	0.0991	0.297	BDL		0.00924
63B	2.45	0.06400	0.107	BDL		0.00954	33.2	0.822	0.913	124	2.22	0.929	BDL		0.108	0.0391	0.00091	0.0391	3.74	0.0692	0.297	BDL		0.00924
66B	BDL		0.107	BDL		0.00949	31.2	0.607	0.908	123	2.07	0.923	BDL		0.107	BDL	0.00128	0.0389	3.80	0.0441	0.295	BDL		0.00919
68B	0.152	0.00599	0.107	BDL		0.00949	31.9	0.855	0.908	123	2.42	0.924	BDL		0.107	0.0389	0.00395	0.0389	3.74	0.0882	0.295	BDL		0.00920
70B	BDL		0.107	BDL		0.00948	31.8	0.330	0.907	123	2.06	0.922	BDL		0.107	BDL	0.00268	0.0388	3.79	0.0587	0.295	BDL		0.00918
72B	0.790	0.0158	0.107	BDL		0.00950	31.4	2.00	0.909	121	2.46	0.924	BDL		0.108	BDL	0.00182	0.0389	3.81	0.0350	0.296	BDL		0.00920
74B	BDL		0.107	BDL		0.00954	31.6	0.381	0.913	122	1.85	0.928	0.108	0.0170	0.108	BDL	0.00128	0.0391	3.74	0.0470	0.297	BDL		0.00924
77B	0.129	0.00239	0.107	BDL		0.00951	31.7	0.427	0.910	122	1.69	0.926	BDL		0.108	0.0391	0.00855	0.0390	3.79	0.00832	0.296	BDL		0.00921
79B	BDL		0.108	BDL		0.00960	31.7	0.346	0.919	122	2.80	0.934	BDL		0.109	BDL	0.00434	0.0393	3.81	0.0521	0.299	BDL		0.00930
81B	0.142	0.00162	0.107	BDL		0.00950	31.4	0.514	0.909	121	2.81	0.924	0.108	0.0241	0.107	BDL	0.00380	0.0389	3.78	0.0574	0.295	BDL		0.00920

Table B8 con't: ICP-MS/MS results from column B. Units are in mg/L. D.L. = detection limit. BDL = below detection limit. Uranium was also measured, but all measurements were BDL.

Sample	PEG-6	PEG-7	PEG-9	PEG-11	Bulk PEG
Column A					
5A	1.94E+05	8.37E+05	2.80E+06	2.23E+06	---
29A	5.39E+05	3.29E+06	2.98E+06	1.89E+06	---
40A	6.21E+05	2.64E+06	4.31E+06	2.75E+06	---
46A	5.16E+05	2.20E+06	5.76E+06	2.13E+06	---
51A	5.55E+05	2.52E+06	7.09E+06	2.82E+06	---
55A	5.36E+05	2.41E+06	7.05E+06	2.82E+06	---
58A	4.62E+05	2.07E+06	5.29E+06	2.14E+06	---
64A	5.53E+05	2.64E+06	7.65E+06	3.74E+06	---
69A	5.18E+05	2.24E+06	6.80E+06	3.45E+06	---
73A	5.27E+05	2.25E+06	6.93E+06	3.72E+06	---
78A	4.47E+05	2.01E+06	5.15E+06	3.97E+06	---
82A	4.78E+05	2.17E+06	6.02E+06	3.89E+06	---
Column B					
5B	1.92E+05	9.29E+05	3.23E+06	2.53E+06	---
29B	5.16E+05	2.50E+06	3.73E+06	2.60E+06	---
40B	5.25E+05	2.30E+06	3.40E+06	2.09E+06	---
46B	4.90E+05	2.29E+06	4.57E+06	1.76E+06	---
51B	5.15E+05	2.46E+06	7.42E+06	2.91E+06	---
55B	5.48E+05	2.39E+06	6.86E+06	2.57E+06	---
58B	5.11E+05	2.32E+06	6.22E+06	2.52E+06	---
64B	5.48E+05	2.28E+06	5.82E+06	2.46E+06	---
69B	5.39E+05	2.15E+06	5.96E+06	3.10E+06	---
73B	4.84E+05	2.45E+06	6.63E+06	4.07E+06	---
78B	4.85E+05	2.21E+06	5.74E+06	4.57E+06	---
82B	5.12E+05	2.37E+06	7.73E+06	4.37E+06	---
Stock Solutions					
FPW Stock 1	5.27E+05	2.83E+06	8.10E+06	5.00E+06	8.93E+07
FPW Stock 2	4.72E+05	2.06E+06	5.17E+06	3.16E+06	7.63E+07
FPW Stock 3	4.59E+05	2.12E+06	5.16E+06	3.10E+06	7.56E+07
FPW Stock 4	4.83E+05	2.27E+06	6.42E+06	3.85E+06	7.53E+07

Table B9: HPLC-Orbitrap-MS peak areas (representing concentrations) for various PEGs for both columns A and B. Measurements of FPW stock solutions were also made.

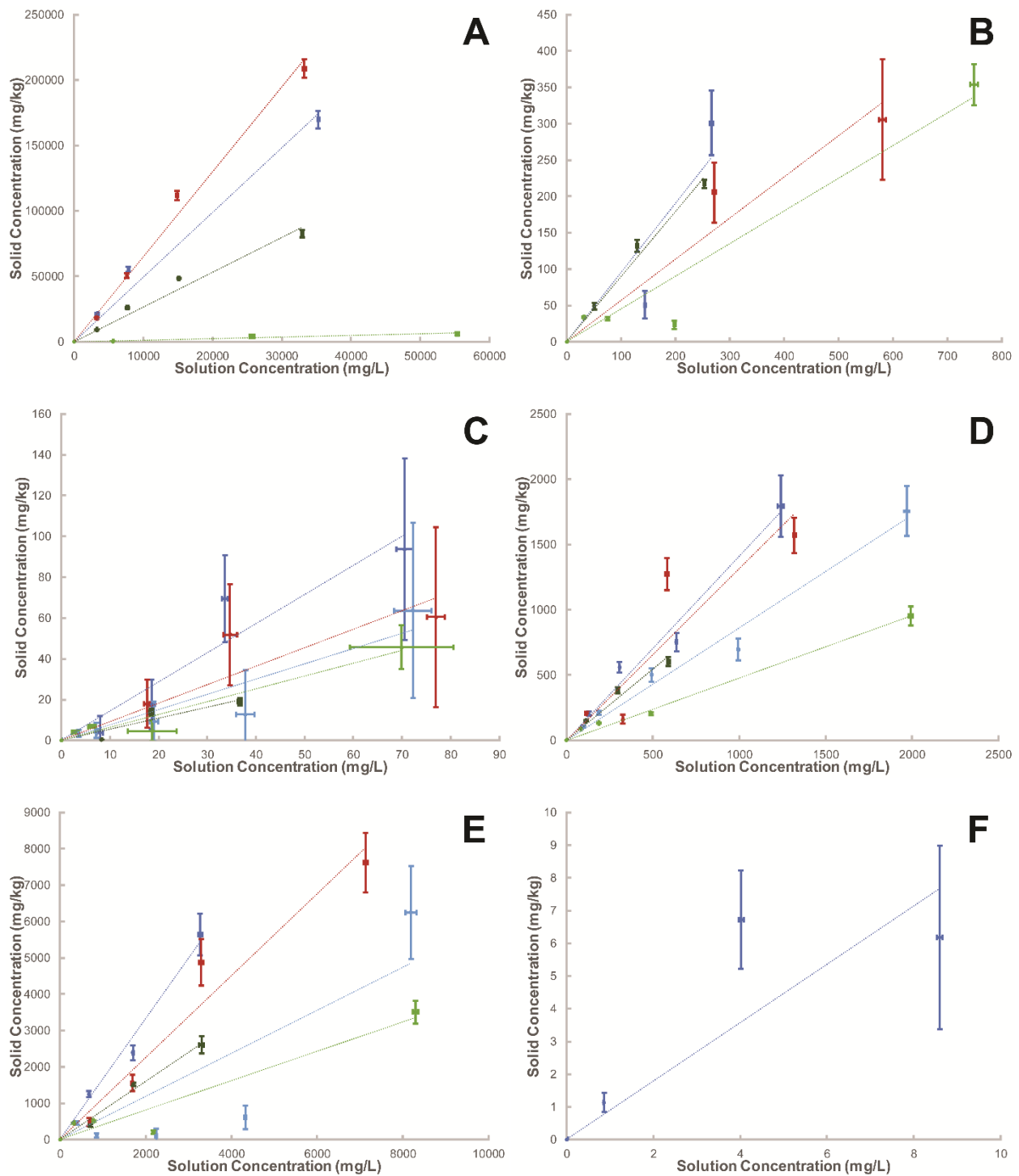


Figure B1: Isotherms for A) Na; B) Mg; C) S; D) K; E) Ca; and F) Mn. Errors were calculated by propagating both analytical and measurement errors. Dark variations denote Sample 1 experiments; light variations denote Sample 2 experiments.

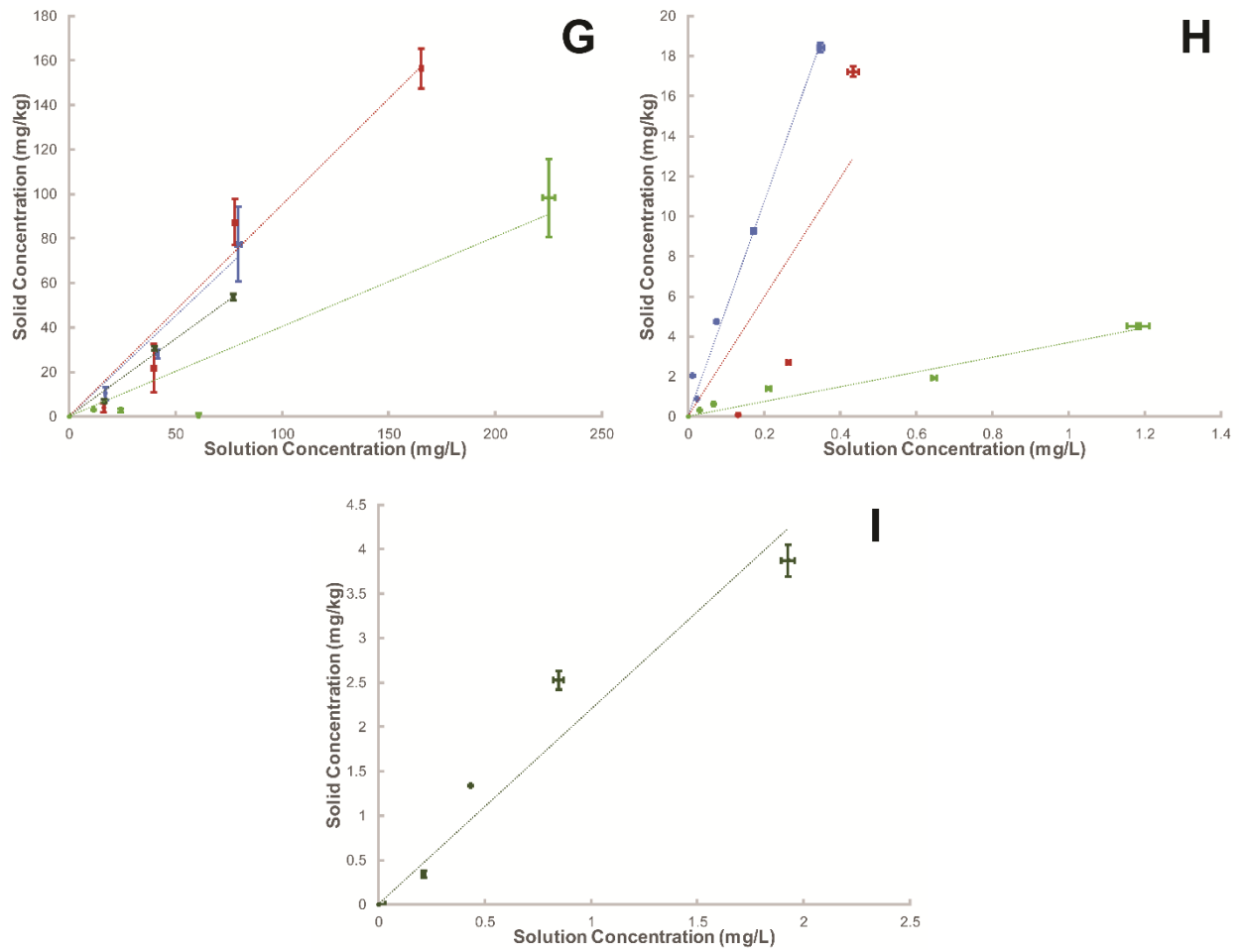


Figure B1 con't: Isotherms for **G)** Br; **H)** Ni; and **I)** Cu. Errors were calculated by propagating both analytical and measurement errors. Dark variations denote Sample 1 experiments; light variations denote Sample 2 experiments.

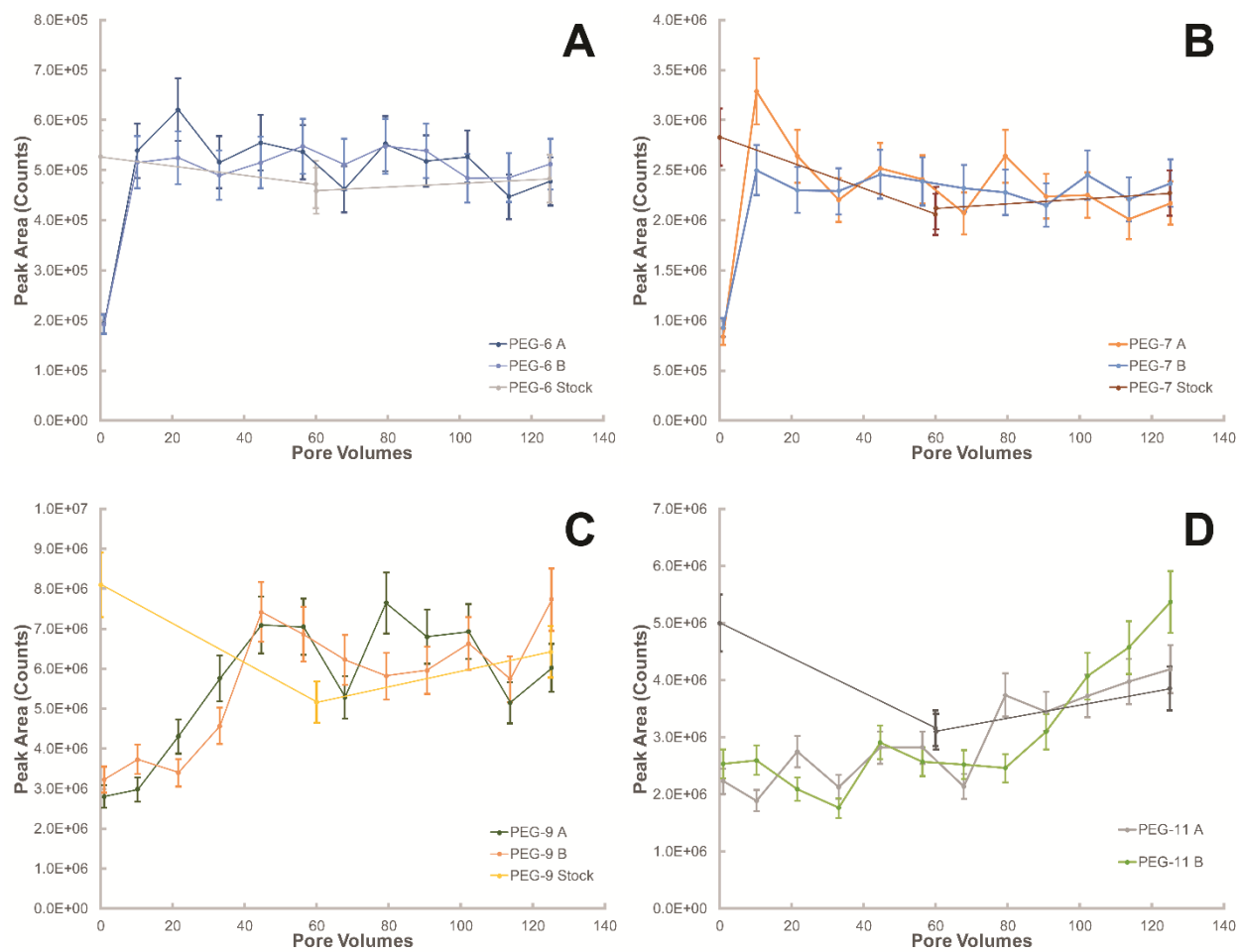


Figure B2: Breakthrough curves of peak area (representing concentration) vs. pore volumes for **A)** PEG-6; **B)** PEG-7; **C)** PEG-9; and **D)** PEG-11. Both columns A and B, along with the stock solution concentrations, are plotted. Error bars were estimated to be $\pm 10\%$.

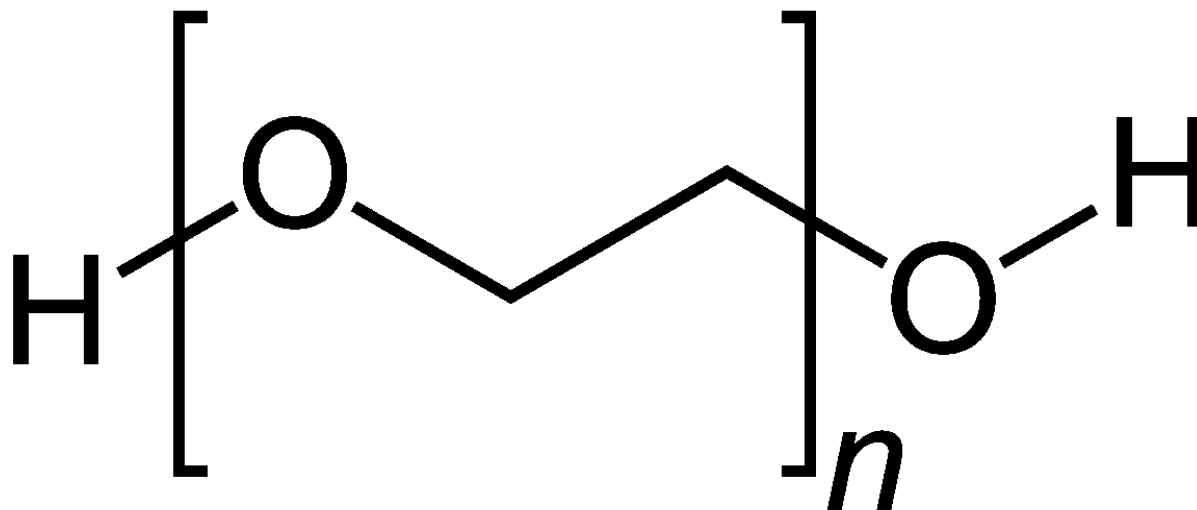


Figure B3: Molecular structure of a polyethylene glycol (PEG), where n represents the ethylene oxide (EO) number. Figures from Wikipedia.

Freundlich and Langmuir Isotherms: Sorption isotherms are graphical representations that describe the mass of solute remaining in solution compared with the mass of solute sorbed onto a solid material. In cases where the sorption isotherm is non-linear and cannot be described by a simple linear distribution coefficient (K_d), the data is typically fit with either Freundlich or Langmuir isotherms (Roy et al. 1992).

The Freundlich isotherm is an empirical expression first described by Freundlich (1909), and is given here in Equation B1:

$$C_S = K_F C^{1/n} \quad (\text{B1})$$

where C_S is the solid concentration [M/M], C is the solution concentration [M/L³], and K_F and n are constants. Sorption data was then fit to this equation by first linearizing Equation B1 into the form:

$$\log C_S = \log K_F + \frac{1}{n} \log C \quad (\text{B2})$$

In this form, $\log C$ and $\log C_S$ can be plotted together to form a straight line from which the slope and y-intercept can be used to derive the two constants K_F and n . Although the equation was purely empirical, some authors have suggested that K_F may be related to the affinity of the solid material, and the exponential term may be an indicator of intensity of sorption (e.g. Suffet and McGuire 1980).

An alternative expression that has been used to describe the sorption of solutes onto solid media is the Langmuir expression, which was first derived in Langmuir (1918). The Langmuir equation is given here in Equation B3:

$$C_S = \frac{K_L M C}{1 + K_L C} \quad (\text{B3})$$

where K_L and M are constants. M has been interpreted to indicate the maximum sorption capacity of the solid medium, whereas others have interpreted K_L to be related to the bonding energy between the solute and the solid medium (e.g. Harter and Baker 1977; Veith and Sposito 1977; Barrow 1978; Sposito 1982).

As with the Freundlich equation, the Langmuir expression can be linearized as well. There are two popular methods of linearization, both of which will be described here. The first is known as the “traditional linear Langmuir equation”, and is given in B4:

$$\frac{C}{C_S} = \frac{1}{K_L M} + \frac{C}{M} \quad (\text{B4})$$

Plotting C against $\frac{C}{C_S}$ should yield a straight line, from which the slope and y-intercept can be used to derive K_L and M . The second is known as the “double-reciprocal Langmuir equation”, which has been noted to be more suitable for data with equilibrium concentrations skewed toward the lower end of the spectrum. The double-reciprocal Langmuir equation is given below in equation B5:

$$\frac{1}{C_S} = \frac{1}{K_L M C} + \frac{1}{M} \quad (\text{B5})$$

From Equation B5, plotting $\frac{1}{C}$ against $\frac{1}{C_S}$ gives us a straight line, from which the slope and y-intercept can be used to derive the two Langmuir constants. Both forms of linearization were utilized in this study, but we observed that generally, the double-reciprocal Langmuir equation performed better as our data tended to be skewed more toward the lower end of the concentration spectrum. This is reflected in the generally higher R^2 values.

References:

- Barrow NJ (1978) The description of phosphate adsorption curves. *Journal of Soil Science* **29**: 447 – 462.
- Freundlich H (1909) *Kapillarchemie: eine Darstellung der Chemie der Kolloide und Verwandter Gebiete*, Leipzig, Akademische Verlagsgesellschaft, 591 p.
- Harter RD, Baker DE (1977) Applications and misapplications of the Langmuir equation to soil adsorption phenomena. *Soil Society of America Journal* **41**: 1077 – 1080.
- Langmuir I (1918) The adsorption of gases on plane surfaces of glass, mica, and platinum. *Journal of the American Chemical Society* **40**: 1136 – 1403.
- Roy WR, Krapac IG, Chou SFJ, Griffin RA (1992) Batch-type procedures for estimating soil adsorption of chemicals. EPA/530/SW-87/006-F, April 1992.
- Sposito G (1982) On the use of the Langmuir equation in the interpretation of “adsorption” phenomena: II. The “two-surface” Langmuir equation. *Soil Science Society of America Journal* **46**: 1147 – 1152.
- Suffet IH, McGuire MJ (1980) *Activated carbon adsorption of organics from the aqueous phase*. Volume 1, Ann Arbor Science, Michigan, 508 p.
- Veith JA, Sposito G (1977) On the use of the Langmuir equation in the “adsorption” phenomena. *Soil Science Society of America Journal* **41**: 697 – 702.

Appendix C

Appendix C provides additional comparisons between HYDROSCAPE and MODFLOW not used in Chapter 4, and an illustrative comparison showing one of the limitations of HYDROSCAPE.

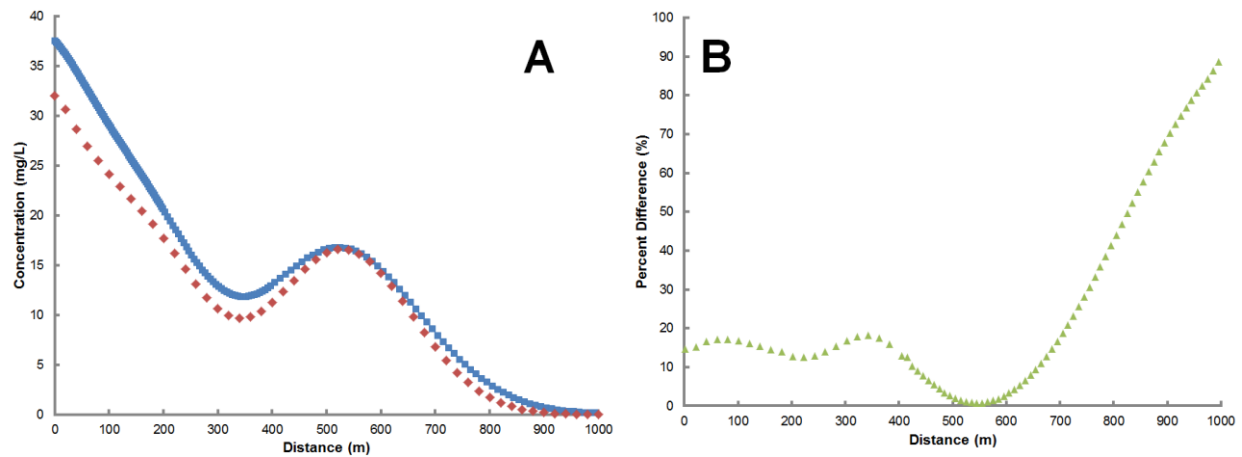


Figure C1: **A)** Centerline concentration profile (after 10 years) comparison between HYDROSCAPE (red diamonds) and MODFLOW (blue squares). **B)** Percent difference of centerline profile between HYDROSCAPE and MODFLOW.

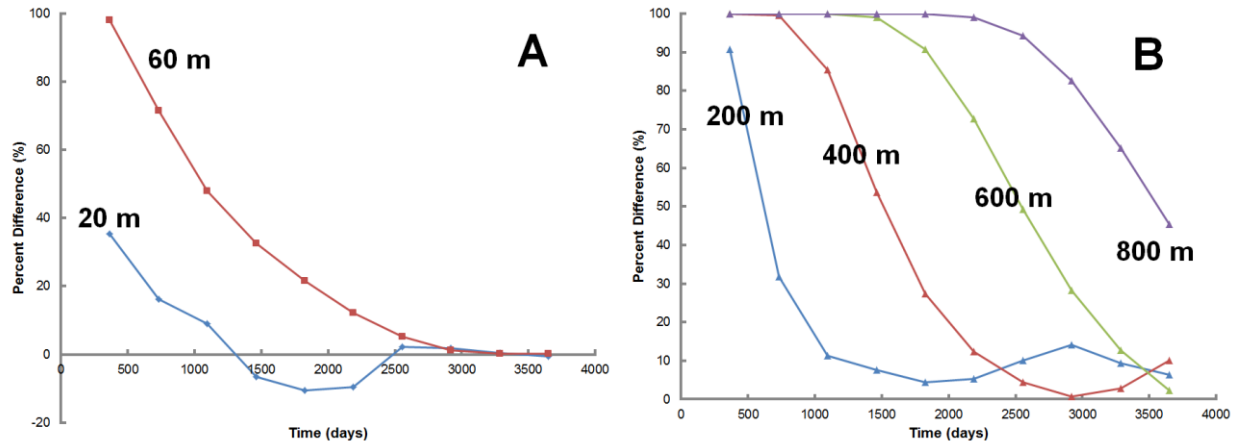


Figure C2: Percent difference of breakthrough curves between HYDROSCAPE and MODFLOW in **A)** the aquitard screened at a depth of 2.5 m; and **B)** the aquifer screened at a depth of 52.5 m.

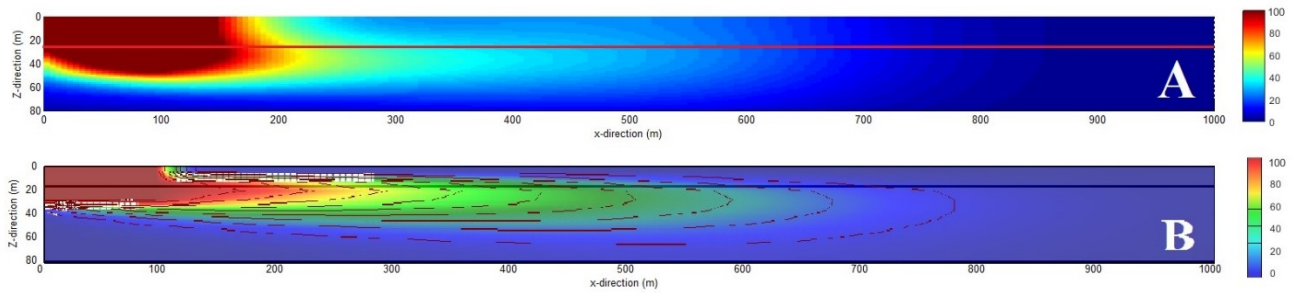


Figure C3: Comparison of HYDROSCAPE and MODFLOW in cross-section through the centerline. In this simulation, $\alpha_{TV} = 1$ m. All other parameters are identical between the two simulations.